ARTS Microwave Single Scattering Properties Database

Technical Report

CHALMERS

Universität Hamburg
DER FORSCHUNG | DER LEHRE | DER BILDUNG

Technical Report

Version 1.0
February 19, 2018

R. Ekelund (Chalmers)
M. Brath (UHH)
P. Eriksson (Chalmers)
J. Mendrok (Chalmers)

Cover picture: Examples on particle shapes (habits) to be included on the proposed database: six-bullet rosette, sector snowflake and an aggregate. The particle shape data have been created by our software toolkit for generating ice and snow particle shape data. This includes to generate the aggregate by a physically based model. The images have been rendered by the Blender open-source application.

Change record

Version	Date	(Major) Changes
0.9.2	2017-12-07	Database, technical report and readme document updated
1.0.0	2018-02-19	First official version released.

Contents

Abstract

A database of microwave single scattering properties has been generated. The aim is to support simulations of varying complexity, treating both passive and active observations. This is achieved by providing extinction, absorption and scattering matrix data with complete polarisation information, i.e. matching the full Stokes vector. Data are provided for three temperatures (190, 230 and 270 K) and 34 frequencies between 1 and 886 GHz. The frequencies are primarily selected to cover the channels found on existing operational microwave sensors, as well as the upcoming MWS, MWI and ICI instruments. Additional frequencies were included having common radar wavelengths and the ISMAR airborne instrument in mind. Data are at hand for a high number of particle shapes, organised into "habits". A habit is here defined as a series of particles of different sizes, roughly following a standard size-mass relationship ($m = \alpha D_{\max}^{\beta}$). Each habit is represented with at least 30 particle sizes.

The bulk of data are calculated assuming totally random orientation of the particles. For this orientation case, 34 ice hydrometeor habits are covered. The number of habits of single crystal type is 18, mainly modelled as plates, columns and bullet-rosettes. The remaining habits are intended to represent graupel, hail and particles of aggregate type. Mie calculations for ice and liquid spheres are included for comparison, while the remaining data have been produced using the discrete dipole approximation. To our best knowledge, this should constitute the most extensive database of its kind. Quite recently, *Ding et al.* (2016) presented a database that can be considered to be the first to provide a full coverage of the microwave region. That database is similar in terms of frequency and temperature coverage, but has considerably smaller coverage in terms of particle sizes and number of habits, particularly lacking complex aggregates.

Also, a second orientation case has been considered, azimuthally random orientation. The particles' minimum principal moment of inertia axis is here assumed to be aligned with respect to the horizon at a certain angle, the tilt angle, but to have no preference in azimuth angle. Despite large efforts to decrease both the calculation burden and the required storage space, this orientation case was found to provide huge practical obstacles and so far only a plate habit has been processed. Data for 10 tilt angles between 0° and 90° are provided and by post-processing it should be possible to derive scattering data for an arbitrary tilt angle distribution. These data have the same dense coverage in terms of frequency, temperature and size as the totally random data. They should provide a good basis for studying how to further optimise these calculations and practically incorporate such data into radiative transfer software.

MATLAB and Python functions to read and manipulate the data are provided, as well as code to make use of the database together with RTTOV-SCATT. Planned extensions of the database is to include data of melting particles.

1. Introduction

The aim of this document is to describe the scattering database developed inside the study, as well as the associated interfaces. The main steps of the database creation are outlined below, while theory and a detailed description of the database content are found in the following chapters.

1.1. Generation of the database

The database was created in several steps. The first step involves particle modelling and generation of shape data that can be used as input to the scattering calculations. A wide range of particle models has been incorporated, ranging from well-defined crystals to aggregates. Some particles are parametrised according to observations, while most of the aggregate particles were created by simulating stochastic processes. A part of these particle models has been developed by us, and are described in Section 3.2. Furthermore, external sources has been incorporated in one way or another, mainly from already existing databases such as the ones provided by *Liu* (2008), overviewed in Section 3.3.

The scattering data are calculated using the discrete dipole approximation (DDA, more information available in Section 4.1)), using the third-party software ADDA (*Yurkin and Hoekstra*, 2011). The DDA method requires that the particle is discretised onto a point grid, where each point represents a dipole in the scattering simulation. These dipole grids are in the future referred to as shape data. The computations are relatively demanding, and since the number of dimensions are large (frequency, temperature, size, habit), a high computational capacity is required. Also, each scattering case must be calculated over a set of incoming radiation angles and particle orientations, which are then integrated over in order to produce averaged scattering properties, further increasing the computation time. Depending on the orientation type calculated, different integration schemes are used. For totally random orientation, ADDAs internal orientation averaging routine is used, while for azimuthally preferred orientation an internally developed scheme has been developed, described in the Appendix 4.1.3.

In the final step, the raw DDA output data are converted to the chosen database format and structure (see Section 6). The main idea adopted is storing the scattering data in netCDF files, located in a folder structure. Interfaces in MATLAB and Python have been developed as well (see Chapter 7), in order to improve the database usability. The interfaces support displaying and extraction of data, among other features. However, the netCDF format is self-explanatory enough to allow for direct access if desired.

2. Theory background

2.1. Radiative transfer

Depending on the measurements to simulate, the optical properties of the atmosphere must be described to a varying degree. The most detailed description is required for simulations of passive observations when the complete polarisation state is of interest. The radiative transfer equation (RTE) to solve for such cases is:

$$\begin{aligned}\frac{\mathrm{d}\mathbf{I}(\nu,\mathbf{r},\hat{\mathbf{n}})}{\mathrm{d}s} = & -\mathbf{K}(\nu,\mathbf{r},\hat{\mathbf{n}})\mathbf{I}(\nu,\mathbf{r},\hat{\mathbf{n}}) + \mathbf{a}(\nu,\mathbf{r},\hat{\mathbf{n}})B(\nu,\mathbf{r}) \\ & + \textstyle\int_{4\pi} \mathbf{Z}(\nu,\mathbf{r},\hat{\mathbf{n}},\hat{\mathbf{n}}')\mathbf{I}(\nu,\mathbf{r},\hat{\mathbf{n}}')\mathrm{d}\hat{\mathbf{n}}',\end{aligned} \tag{2.1}$$

where $\mathbf{I}$ is the Stokes vector of the radiance, ν is the frequency, $\mathbf{r}$ is the atmospheric position, $\hat{\mathbf{n}}$ is the propagation direction, s is the distance along $\hat{\mathbf{n}}$, $\mathbf{K}$ is the extinction matrix, $\mathbf{a}$ is the absorption vector, B is the Planck function and $\mathbf{Z}$ is the scattering matrix. See *Mishchenko et al.* (2002) for details regarding the assumptions for this equation and definitions of the involved quantities. $\mathbf{Z}$ is frequently denoted as the phase matrix, but scattering matrix (e.g. *Bohren and Huffman*, 1998) is clearly a more descriptive name.

In the general case, $\mathbf{I}$ is a vector of length four, $\mathbf{K}$ and $\mathbf{Z}$ are matrices of size [4,4] and $\mathbf{a}$ is a vector of size [4], where $\mathbf{K}$ and $\mathbf{a}$ are dependent on direction of propagation, while $\mathbf{Z}$ is a function of both incident and scattered radiation directions $\hat{\mathbf{n}}$' and $\hat{\mathbf{n}}$, respectively. Following the energy conservation principle, $\mathbf{K}$, $\mathbf{Z}$ and $\mathbf{a}$ are related to each other by

$$\mathbf{K}_{i1} = \int_{4\pi} \mathbf{Z}_{i1}\,\mathrm{d}\hat{\mathbf{n}}' + \mathbf{a}_i. \tag{2.2}$$

where $\mathbf{K}_{i1}$ is the $(i,1)$ element of the $\mathbf{K}$ matrix etc.

In many situations it is possible to simplify Eq. (2.1) by considering fewer elements of the Stokes vector. This includes the case of "scalar radiative transfer" where the effective length of $\mathbf{I}$ is one. The optical properties to apply for these different simplifications are obtained as single elements, for the scalar case, or combinations of elements of the complete $\mathbf{K}$, $\mathbf{a}$ and $\mathbf{Z}$. The scalar versions of $\mathbf{K}$, $\mathbf{a}$, and $\mathbf{Z}$ are often denoted as extinction coefficient (β_e), absorption coefficient (β_a) and phase function (P), respectively. Following Eq. (2.2), the norm of the phase function as applied in the RTE given by Eq. (2.1) has to fulfil

$$\int_{4\pi} \mathbf{Z}_{11}\,\mathrm{d}\hat{\mathbf{n}}' = \beta_\mathrm{s} \equiv \beta_\mathrm{e} - \beta_\mathrm{a}, \tag{2.3}$$

where β_s is the scattering coefficient. On the other hand, for scalar radiative transfer the standard choice is to operate with a normalised phase function. The function P is

then normalised such that $\int P \, \mathrm{d}\hat{\mathbf{n}}' = 4\pi$, that is,

$$P = 4\pi \mathbf{Z}_{11} / \beta_\mathrm{s}. \tag{2.4}$$

Some radiative transfer tools do not operate with the full angular description of the optical properties, but with simplified quantities such as the single scattering albedo and the asymmetry parameter. These parameters are, as far as we are aware, only used in scalar radiative transfer and when only macroscopically isotropic and mirror symmetric particles, e.g. spheres or totally randomly oriented particles, are present. In the latter case, $\mathbf{K}$ and $\mathbf{a}$ are independent of propagation direction, and $\mathbf{Z}$ reduces to a function of scattering angle Θ, the angle between the incident and scattered direction. The single scattering albedo ω_0, describing the fraction of the incident radiation that is scattered compared to the total attenuation, is defined as

$$\omega_0 = \frac{\beta_\mathrm{s}}{\beta_\mathrm{e}} = \int_{4\pi} \mathbf{Z}_{11} \, \mathrm{d}\hat{\mathbf{n}}' \; / \; \mathbf{K}_{11}. \tag{2.5}$$

Purely scattering media, hence, have a single scattering albedo of 1.0, while $\omega_0 = 0.0$ indicates a purely absorbing medium.

Asymmetry parameter g is a measure on the balance between forward ($\Theta < 90°$) and backward scattering ($\Theta > 90°$), and is defined as

$$g = \frac{1}{2} \int_{-1}^{1} \mu P(\mu) \, \mathrm{d}\mu, \tag{2.6}$$

where $\mu = cos(\Theta)$. Isotropic scattering results in $g = 0$. Values of g above zero correspond to a domination of forward scattering.

It shall be noted that ω_0 and g can be derived from $\mathbf{K}$, $\mathbf{a}$ and $\mathbf{Z}$, i.e. no additional data are required to handle simplified or alternative versions of Eq. (2.1).

The main quantity required to simulate radar measurements is backscattering. The backscattering coefficient, for arbitrary polarisation, can be derived from $\mathbf{Z}$. The backscattering is essentially the scattering matrix value for the backward direction ($\hat{\mathbf{n}} = -\hat{\mathbf{n}}'$), that is backscattering is given by $\mathbf{Z}(-\hat{\mathbf{n}}, \hat{\mathbf{n}}')$. In the special case of macroscopically isotropic and mirror symmetric particles, the scalar backscattering coefficient can be given as

$$\beta_\mathrm{bac} = \mathbf{Z}_{11}(\Theta = \pi). \tag{2.7}$$

The remaining part of radar simulations is to include the (two-way) extinction. This is done by the same $\mathbf{K}$ as found in Eq. (2.1). Accordingly, radar simulations can be handled with the same set of optical properties as used in simulations of passive observations, and $\mathbf{K}$ and $\mathbf{Z}$ suffice to exhaustively describe all required parameters.

In summary, only absorption vector $\mathbf{a}$, extinction matrix $\mathbf{K}$ and scattering matrix $\mathbf{Z}$ are needed to describe the optical properties of particles in a general and complete manner[1].

[1] To be exact, $\mathbf{K}$ and $\mathbf{Z}$ suffice for a complete description as indicated by Eq. (2.2). However, deriving $\mathbf{a}$ from the other two is tedious and prone to numerical discretisation issues of the scattering matrix integral. Hence, it is common to provide all three parameters explicitly.

These quantities can together be denoted as the single scattering properties (SSP). Also, the term optical properties will be used as a common name on these quantities.

The single scattering properties of individual particles are determined by the complex refractive index of the particle material, the size of the particle in relation to the wavelength of the radiation and the particle shape. Refractive index is a frequency (or wavelength) dependent parameter. As size matters in relation to the radiation's wavelength, it is commonly expressed by the size parameter $x = f(r, \lambda)$. For further discussion of size measures see Section 2.5.

2.2. Relation of single particle to bulk single scattering properties

In reality, hydrometeors never occur as monodispersions, i.e. as particles of a single size, shape, and habit. That is, $\mathbf{K}$, $\mathbf{a}$ and $\mathbf{Z}$ as applied in Eq. (2.1) are the single scattering properties of a mixture of particles, a particle bulk. For the rest of this section, bulk properties will be denoted as $\langle\mathbf{K}\rangle$, $\langle\mathbf{a}\rangle$, and $\langle\mathbf{Z}\rangle$.

Assuming independent scattering[2], single scattering properties are additive, that is

$$\langle\mathbf{K}\rangle = \sum_{n=1}^{N} \mathbf{K}_n, \tag{2.8}$$

where $\langle\mathbf{K}\rangle$ is the bulk extinction matrix and $\mathbf{K}_n$ denotes the extinction matrix of individual, single particle n. Bulk absorption vector $\langle\mathbf{a}\rangle$ and bulk scattering matrix $\langle\mathbf{Z}\rangle$ are defined likewise.

It is common to categorise the particles into "habits", e.g. according to hydrometeor type (and possibly other "material" types like aerosols, Rayleigh scatterers etc.), and characterise each category separately further by certain distributions, e.g. regarding size, shape, habit. Those distributions, specifically regarding particle size, are often described by continuous distribution functions, hence

$$\langle\mathbf{K}\rangle = \sum_{h=1}^{H} \int_0^\infty N_h(r)\, \mathbf{K}_h(r)\, \mathrm{d}r, \tag{2.9}$$

where h denotes the habit, $\mathbf{K}_h(r)$ the extinction matrix of a category h particle of size r and $N_h(r)$ its corresponding number density (unit: per volume (air) per (particle) size unit). N is called the particle size distribution. As example, the integral of N:

$$\int N(r)\, \mathrm{d}r \tag{2.10}$$

gives the total number of particles (per volume unit) of the habit of concern. Note that r can refer to any size measure. Size distributions are typically expressed by a

[2]Particles can be considered independent scatterers if (a) each particle is in the far-field zone of all other particles and (b) scattering by the individual particles is incoherent.

few functional forms like gamma, modified-gamma, exponential, and log-normal distributions. *Petty and Huang* (2011) give an excellent presentation of that and how these distributions relate to each other.

2.3. Particle orientation

Particle orientation refers to how the particles' main axes are oriented with respect to the local horizon and the azimuthal reference. If the particle possesses spherical symmetry there is effectively no particle orientation, because it does not matter from which side the particle with spherical symmetry is viewed or how it is rotated – it will always look the same. As the particles considered in this study do not have a spherical symmetry they can have an orientation.

In general, the orientation of a particle in a three dimensional space can be described by a set of three parameters. The three Euler angles are one such parameter set. The Euler angles define the orientation of the particle (coordinate) system relative to a fixed coordinate system, hereafter called laboratory system. The particle system is the coordinate system that is attached to the particle. This means, if a particle is rotated, the particle system is rotated the same way. The laboratory system stays under the rotation of the particle whereas the particle system changes its orientation. But both systems have the same origin. In this study, the Euler angles according to the "zyz′"-notation are used, which is also used within ADDA to describe the particle orientation. The particle is first rotated by angle α over the laboratory Z-axis, then the particle is rotated by angle β over the particle Y-axis (y′) and last the particle is rotated by angle γ over the particle Z-axis (z′), see also Fig. 2.1. It holds,

$$\alpha \in [0,\, 2\pi] \tag{2.11}$$

$$\beta \in [0,\, \pi] \tag{2.12}$$

$$\gamma \in [0,\, 2\pi]\ . \tag{2.13}$$

These rotations are described by three orthogonal rotation matrices, see Appendix A.3 for details. It is important to know that the order of the rotation must not be changed, because the combination of rotations is not commutative.

Additional to the Euler angles, the orientation of the non-rotated particle is needed. As there is no absolute coordinate system, the orientation of the non-rotated particle is in general arbitrary. Therefore, we define that the non-rotated particle lies with its center of gravity at the origin of the laboratory system and all particle rotations will be relative to the origin of the laboratory system. The non-rotated particle is defined to have its principal moments of inertia axes aligned along the Cartesian coordinate axes, with the maximum inertia axis along the z-axis and the smallest along the x-axis (see Appendix A.1).

Within this study, we are interested not in the orientation of a single particle but of the orientation of an ensemble of particles. Generally, ensembles of orientations are

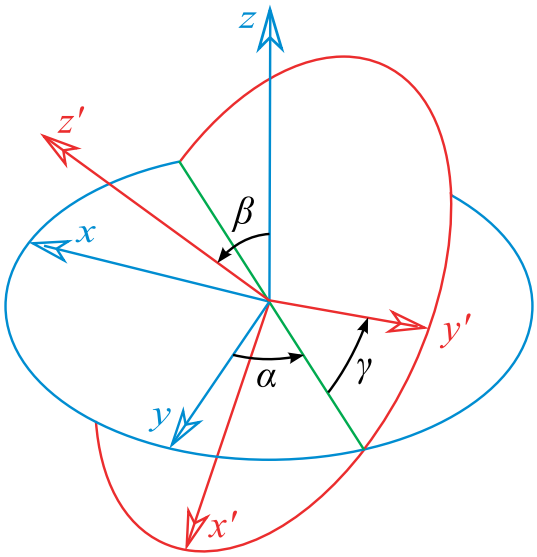

Figure 2.1.: Euler angles. Drawing is taken from *Yurkin and Hoekstra* (2014) and slightly modified.

described by averaging the SSP over the three Euler angles, such that for example for the scattering matrix $\mathbf{Z}_{\text{eo}}$ of an ensemble of orientated particles holds

$$\mathbf{Z}_{\text{eo}}\left(\theta_i, \phi_i, \theta_s, \phi_s\right) = \int_0^{2\pi}\int_0^{\pi}\int_0^{2\pi} p_\alpha(\alpha)\, p_\beta(\beta)\, p_\gamma(\gamma)\; \mathbf{Z}\left(\theta_i, \phi_i, \theta_s, \phi_s, \alpha, \beta, \gamma\right) \sin\beta \,\mathrm{d}\alpha \,\mathrm{d}\beta \,\mathrm{d}\gamma \tag{2.14}$$

with θ_i the incidence polar angle, ϕ_i the incidence azimuth angle, θ_s the scattering polar angle and ϕ_s the scattering azimuth angle. p_j are probability density functions describing the distribution of particle orientation.

Here, we distinguish between two basic states of particle orientation:

- totally random
- azimuthally random

The two orientations will be described in the next subsections and are shown in Fig. 2.2.

2.3.1. Totally random orientation

Totally randomly oriented particles are defined as the orientation average over the three Euler angles, in which the Euler angles are uniformly distributed. That is,

$$p_\alpha\left(\alpha\right) = p_\gamma\left(\gamma\right) = \frac{1}{2\pi} \tag{2.15}$$

$$p_\beta\left(\beta\right) = \frac{1}{\pi}\,. \tag{2.16}$$

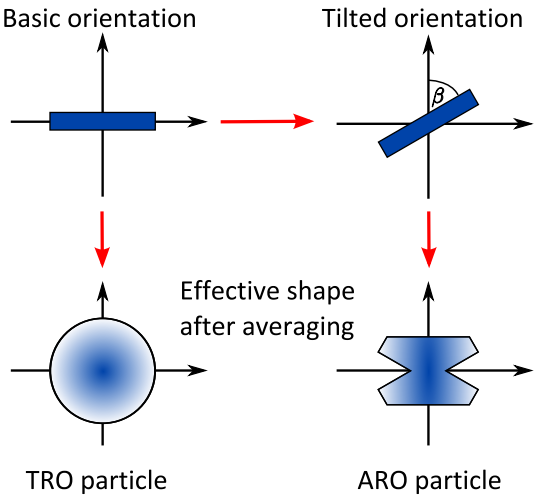

Figure 2.2.: Schematic of the difference between totally random (TRO) and azimuthally random orientation (ARO).

Due to this averaging, totally randomly oriented particles have effectively a spherical symmetry. This implies that the scattering matrix of totally randomly oriented particles depends only, like the scattering matrix of spheres, on the scattering angle Θ, i.e.

$$\mathbf{Z}_{\mathrm{ro}}(\Theta) = \mathbf{Z}_{\mathrm{ro}}(\theta_i, \phi_i, \theta_s, \phi_s), \tag{2.17}$$

and $\mathbf{K}_{\mathrm{ro}}$ and $\mathbf{a}_{\mathrm{ro}}$ will have no angular dependency.

For totally randomly oriented particles, averaging the scattering matrix over all particle orientations at one incidence angle is equivalent to averaging the scattering matrix of one particle orientation over all incidence angles. The resulting scattering matrix exhibits spherical symmetry. Therefore, it is sufficient to calculate the scattering matrix only for one incidence angle as in the work of *Liu* (2008) and *Hong et al.* (2009).

2.3.2. Azimuthally random orientation

Azimuthally randomly oriented particles with a specific orientation to the horizon, also referred to as tilt or canting, are defined as the orientation average over α and γ, in which α and γ are uniformly distributed. For the scattering matrix $\mathbf{Z}_{\mathrm{ao}}$ of azimuthally randomly oriented particles it, hence, holds

$$\mathbf{Z}_{\mathrm{ao}}(\theta_i, \phi_i, \theta_s, \phi_s, \beta) = \int_0^{2\pi}\int_0^{2\pi} p_\alpha(\alpha)\, p_\gamma(\gamma)\; \mathbf{Z}(\theta_i, \phi_i, \theta_s, \phi_s, \alpha, \beta, \gamma)\; \mathrm{d}\alpha\, \mathrm{d}\gamma \tag{2.18}$$

Due to the orientation averaging, the averaged scattering matrix depends in azimuth only on the difference between incident and scattered azimuth direction. Therefore, without any loss of generality, the azimuth incidence angle can be set to $\phi_i = 0$, and it holds

$$\mathbf{Z}_{\mathrm{ao}}\left(\theta_i, \theta_s, \Delta\phi\right) = \mathbf{Z}_{\mathrm{ao}}\left(\theta_i, \phi_i, \theta_s, \phi_s\right). \tag{2.19}$$

While the scattering matrix of totally randomly oriented particles depends only on the scattering angle Θ, the scattering matrix of azimuthally randomly oriented particles with a specific tilt orientation depends on the incidence polar angle θ_i, the scattering polar angle θ_s, the absolute difference of the incidence and scattering azimuth angles $\Delta\phi = \mathrm{abs}\left(\phi_i - \phi_s\right)$ and the tilt angle β or tilt angle distribution $p_\beta(\beta)$, see also Fig. 2.2.

For azimuthally randomly oriented particles with a specific orientation, the averaging equivalence shown for totally randomly oriented particles does not hold. The averaging only over α and γ results only in a rotational symmetry of the scattering matrix to the laboratory Z-axis. For the averaged scattering matrix it is not anymore equivalent if we rotate the particle by an angle β or if we change the polar incidence angle θ_i by $-\beta$, because changing β results in different averaged scattering matrix[3]. Due to fact that there is no more equivalence between the rotation of the body and the averaged scattering matrix, the calculation of scattering properties of azimuthally randomly oriented particles with a specific orientation has much higher computational cost than the calculation of scattering properties of totally randomly oriented particles. The orientation average of the extinction matrix of the different particles are analogue to the orientation averages of the scattering matrix.

2.4. Refractive index

Beside size and shape of hydrometeors, their single scattering properties are governed by the refractive indices of their forming material. Refractive index n is described as a complex number

$$n = n' + in'' = \sqrt{\varepsilon}, \tag{2.20}$$

with ε being the (complex) permittivity, where its real and imaginary parts primarily govern the scattering and absorption properties, respectively.

Refractive indices of both frozen and liquid water vary strongly with frequency and exhibit a significant temperature dependence in the electromagnetic region of interest here. These dependencies need to be considered and described sufficiently accurate, which can be done in form of parametric formulas or as a database or some other form of tabulated data.

2.4.1. Water ice

The parametrisation of ice refractive index in temperature and frequency by *Mätzler* (2006) provides the highest quality data over the full microwave region (up to about 1 THz) and Earth atmospheric temperatures and represents the current state-of-the-art. *Iwabuchi and Yang* (2011), which covers the full electromagnetic spectrum used for

[3] Assume, the particle rotates very fast around the laboratory Z-axis and the particle Z-axis to symbolize the orientational averaging and creating an effective solid of revolution. If we then change the angle β, this effective solid of revolution will have a different shape.

Earth observations, is essentially identical to the *Mätzler* (2006) model in the microwave to sub-millimetre spectral region. Though still in use, older models like *Warren* (1984) and *Ray* (1972) are found to not describe temperature dependence, particularly of the imaginary part of the refractive index, sufficiently accurate, which leads to errors in the derived absorption properties of frozen hydrometeors.

Accordingly, the parametrisation of *Mätzler* (2006) has been used to set the refractive index of ice. However, there is a slight inconsistency between the theoretical description in *Mätzler* (2006) and the MATLAB code applied. This MATLAB code was taken from *Mätzler* (2002). It was pointed out to us (*E. Clothiaux, personal communication*) that the MATLAB code applies the following expression for all temperatures

$$\varepsilon' = 3.1884 + 9.1 \cdot 10^{-4} \, (T - 273) \tag{2.21}$$

while in *Mätzler* (2006) it is said that the temperature dependency decreases below 240 K, but without specifying exactly what values to apply. Our interpretation of these comments is that the change is temperature dependency is limited, suggesting that the overall impact on the SSP is small compared to other uncertainties.

2.4.2. Liquid water

Ellison (2006) provided an empirically fitted Debye-relaxation model covering liquid water permittivity at 1 – 1000 GHz and 0 – 30 °C, which was extended to frequencies up to 25 THz and temperatures up to 100 °C by *Ellison* (2007). Based on microwave remote sensing measurements, *Turner et al.* (2016) derived a new liquid water dielectric model applicable also for supercooled water. Their extensive comparison with other models showed large deviations (several 10 to several 100% in absorption coefficient) at temperatures below 0 °C, and particularly at sub-millimetre frequencies, for all but the *Ellison* (2007) model.

While *Turner et al.* (2016) might be more reliable at lower temperatures, *Ellison* (2007) is the only model that covers the full frequency range targeted in this study. Furthermore considering that the liquid water hydrometeors of prior interest here, melting particles and rain, exhibit temperatures around the freezing point or above, the model of *Ellison* (2007) has been given preference.

2.5. Size and shape parameter definitions

A number of parameters related to particle shape and size are defined here for future reference. We have chosen to characterise the shape of a particle by its maximum diameter D_{max} and volume equivalent diameter D_{veq}. The maximum diameter is defined as the diameter of the particle's minimum bounding sphere. The volume equivalent diameter is the diameter of the (solid material) sphere with the same volume as the given particle (with the medium's phase unchanged), i.e.:

$$D_{\mathrm{veq}} = \left(\frac{6V}{\pi} \right)^3 , \tag{2.22}$$

where V is the volume of the particle. It holds that $D_{\text{veq}} \leq D_{\text{max}}$, with equality only for spheres. Furthermore, when considering a specific frequency, size parameter x is of importance as well. x describes the particle size compared to the wavelength of the radiation. We make use the definition that utilises D_{veq}:

$$x = \pi D_{\text{veq}}/\lambda, \tag{2.23}$$

where λ is the wavelength. The general behaviour of single scattering depends strongly on this variable. Therefore, it is common to make the distinction between particles where $x \ll 1$, $x \approx 1$, or $x \gg 1$, referred to as the Rayleigh, Mie, and geometric optics regimes, respectively.

The mass, m, of an individual particle is related to D_{veq} as

$$m = \frac{\rho\pi}{6} D_{\text{veq}}^3, \tag{2.24}$$

where ρ is the density (of solid ice etc.). The relationship between mass and D_{max} depends on the exact shape and can not be specified by a single expression. However, the general behaviour of the mass depending on the particle size for a given type or habit is commonly described by the mass-size relationship, which relates particle mass and maximum diameter by a power-law as

$$m = \alpha D_{\text{max}}^{\beta}, \tag{2.25}$$

where m is the particle mass, and α and β adjustable relationship coefficients. The β-coefficient relates to how the particle is growing with size, while α relates to how dense or porous the particle is. A sphere would have $\beta = 3$, while a plate that only grows along its edges has $\beta = 2$.

Aspect ratio (AR) provides a measure of the non-sphericity of a particle. It affects both the scattering properties and the particle orientation. Trying to express geometrical properties of a 3-dimensional (often irregular) structure by a two-number ratio, it is an inherently ambiguous and not clearly defined parameter. Accordingly, it is defined differently by different authors, and is also referred to as the axial ratio. However, aspect/axial ratio can in general be taken as the ratio between the maximum dimension and the dimension in a perpendicular direction. The definition mainly deviates in exactly how the perpendicular direction is found. Many in-situ measurements just obtain a two dimensional view of the particle and the AR can only be roughly estimated (as the size in the third dimension is not known). Our definition of AR will be linked to how the (non-rotated) particle is oriented with respect to the laboratory coordinate system (particle alignment is detailed in Appendix Bsection:initialPartAlign) defining AR as the ratio of the maximum length found in the X-Y-plane to that of the maximum length of the particle parallel to the Z-axis.

To summarise, for charactering a particle or a complete particle set, we consider:

- D_{veq}: The volume equivalent diameter.
- D_{max}: The maximum diameter.

- m: The mass.
- x: The size parameter.
- α and β: The mass-size relationship coefficients.
- AR: The aspect ratio.

3. Particle modelling

This chapter presents the sources and methods used in this study in order to generate shape data as input for the DDA calculations. In short, we made use of three different sources for shape data. Firstly, we used third-party shape data which can be used directly as DDA input. Secondly, third party shape models for which we are required to generate shape data by ourselves was utilized. Finally, we have also developed software and tools to generate shape data from scratch by ourselves. In specific, we chose to reuse the data models of *Liu* (2008) and *Hong et al.* (2009), which are partly based on observations and are established in the remote sensing community. Data from *Evans et al.* (2012) and *Tyynelä and Chandrasekar* (2014) have been used as well. The software developed by us was used mainly to generate larger particles such as aggregates, hail and graupel, which is still lacking in available databases at the relevant frequencies.

As mentioned in Chapter 2, all particles shall be parametrised according to the mass-size relationship described by the power law in Eq. 2.25. Each habit is thus characterised by an α and β coefficient. For aggregates, β are usually found to be close to 2, which can be compared to the values of the aggregates generated in this study (see Table 3.1), being in the range $\beta = 2.25 - 2.45$.

3.1. Software

Two software packages, the *Snowflake tool-kit* and *RimeCraft*, have been developed for the purpose of generating shape data and are described below.

3.1.1. The snowflake tool-kit

Shape data have mainly be generated using the internally developed snowflake-tool-kit (*Rathsman*, 2016). The tool-kit features capabilities to define crystal shapes, simulate aggregation and sample the shape data to ADDA dipole grids. Examples of particles generated are visualized in Fig 3.1. Specifics of the tool-kit capabilities follow below.

- Crystal representation: The tool-kit includes an internal format for representing crystal shapes, defining them as polygon meshes (see Fig 3.1 for examples). This makes it straightforward to represent not only simpler shapes such as hexagonals and bullets, but also aggregates of said crystals. The data are stored in separate files, which can be used as input for either dipole sampling or aggregate simulation.
- Dipole sampling: Functionality to sample either crystals or aggregates. This function can be used multiple times to create variants of one shape with different grid resolutions.

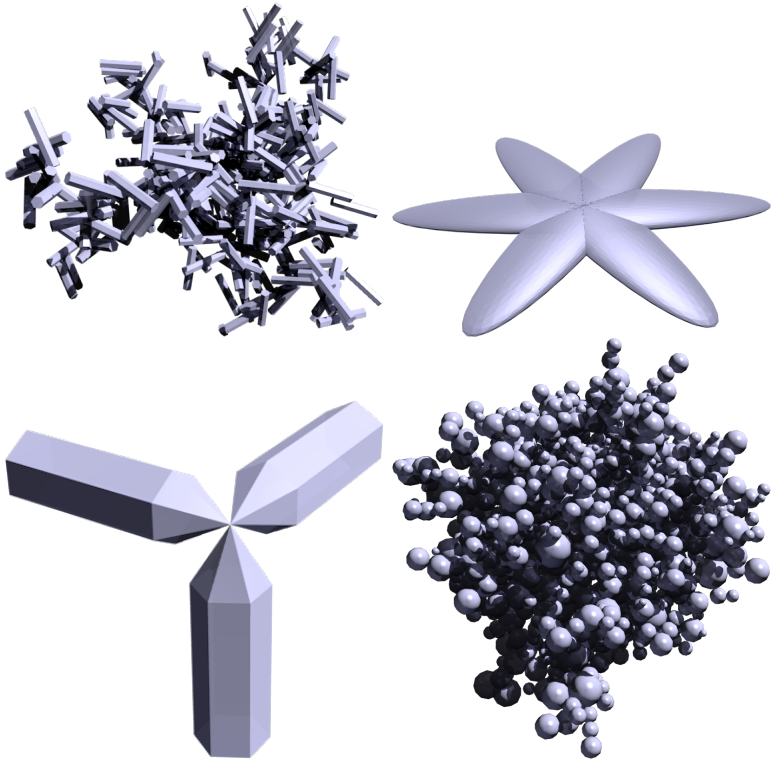

Figure 3.1.: Example particles generated using the snowflake tool-kit. (Top left) Column aggregate. (Top Right) Sector snowflake. (Bottom left) Bullet rosette. (Bottom right) Spherical graupel. Images are rendered using Blender.

- Aggregate simulation: Using crystal shapes as input, aggregation is simulated using a semi-physical model. In Fig 3.1 an example aggregate is shown (top left). The model could be considered to describe a small section in a cloud with a number of ice particles in it. A number of events can happen at each iteration, being the aggregation of two particles, growth of a new crystal, particle melting or fallout of the cloud. The likelihood of these events depend on a number of factors such as size, estimated fall speed and control parameters. Contrary to most aggregate models used in the field, this model allows for the aggregation of two aggregates. The aggregate sticking occurs at the faces of the particles, ant there are also control mechanisms to ensure that the building blocks the aggregate does not overlap with each other. Aggregation is modelled as if the two particles collide with each other at random angles and orientations. If an aggregation event does not result in a accepted aggregate, it is discarded. Available control parameters include:
  - Number of particles: Only a certain amount of particles can be allowed to populate the cloud at a given iteration. Consideration to memory has to be taken here.

  - Growth, melting and drop-out ratios: These parameters determine the relative likelihood of respective events.
  - Input crystals: Several options and features are available:
    * Usage of multiple crystal types at once, allowing for aggregates of plates and columns for example.
    * Probability density functions can be set for defined parameters of a given crystal type, such as length, width and overall size.
  - Overlap ratios: If desired, some overlap between the building blocks can be allowed. This is an option if denser aggregates are desired.
  - Number of retries: The likelihood that an aggregation event is accepted decreases as the morphologies become more complex. Thus, it may be desired to allow for a number of retries before the event is completely discarded.

- Graupel model: An alternative, more straight-forward aggregation simulator is also available. The main application is generating heavily rimed particles (see Section 5.2). The model describes a single aggregate particle, originally only a single crystal, on to which new spheres can aggregate onto. An example graupel is shown in Fig 3.1 (bottom right). Options and features available here are
  - Maximum diameter: This parameter controls the final size of the graupel. The simulation will not stop until the aggregate has reached the specified maximum dimension.
  - Fill ratio: This parameter controls the density of the output graupel. The fill ratio is defined as the particle volume divided by the minimum bounding sphere. Just as for the maximum diameter control parameter, it ensures that the simulation continues until the fill-ratio is achieved. If both the maximum diameter and fill ration options are used, then the simulation will continue until both conditions are met.
  - Angle distribution: Possibility to control the likelihood of incoming angles for the aggregation. This allows control over the overall shape of the aggregate. For example, conical graupels can be created using this option.
  - Penetration: Spheres can be allowed to penetrate through the aggregating particle (tunnelling is perhaps a better analogy, since no deformation on the aggregate is performed). Two input parameters control the behaviour, $\texttt{E}_0$ and `decay_distance`. The penetration depth is determined by its initial kinetic energy, chosen randomly by an uniform distribution $U(0, E_0)$. The sphere's energy is then dissipated exponentially (by a factor of 1/e at distance determined by `decay_distance`), until it stops. If there is no space for the sphere at its current position to exist without overlapping with the surrounding, it is progressively moved back along its track until finds space to exist in (which could effectively be at the surface of the aggregate, if it is already densely packed).

3.1.2. RimeCraft

A MATLAB package called RimeCraft, was developed as an additional source for simulating particle formation. The simulation process involves applying dipoles directly on the shape grid, and is mainly intended to mimic riming and to generate habits with specific parametrisations. By applying growth probability weights onto the grid coordinates and different types constraints, one can control the growth behaviour of the particle. One application is the generation of particles with specific mass-size relationships (Eq. 2.25), by letting the particle only grow outward in thin layers with specific fill-ratios. Another feature is simulation of melting.

To summarize, the main features are:

- Riming: A number of different riming schemes are available, based on either successively adding or removing dipoles. The dipoles can be added in an either random or deterministic way (or a combination of both). It is possible to use DDA shapes as input, for example to create rimed aggregates. Alternatively, predefined shapes such as columns or spheroids can be used as initiation particle. The output shape can thus be controlled by choice of input shape and different schemes to apply the dipoles.

  How to apply the dipoles is relatively flexible. In this study, an algorithm was designed with the goal of generating particles that closely follows predefined mass-size relationships (Eq. 2.25), taking coefficients α and β as input. The algorithm works by successively constricting the growth in spherical layers. At a given iteration, growth is only allowed in the current layer until the implied density has been achieved. At the next iteration, the growth continues in layer next outside. The algorithm proceeds until the desired size has been achieved. A set of particles with specific D_{max} or D_{veq} can be provided by removing successively removing outer layers of the large particle. Note that there is a randomness in how the dipoles are added. The likelihood of a dipole being added at a certain grid point is determined by the number and configuration of neighbouring dipoles already added, and the control parameters available to the user. This allows the user to influence textual details of the particle.

- Melting: Included are also routines to simulate and generate melting particles, strongly inspired by the algorithm presented by *Johnson et al.* (2016), using existing ice particle shape files as input. In short, the algorithm consist of two steps at each iteration. First, the ice grid coordinates with the smallest amount of neighbours are identified and assigned weights based on the radius from the center (to take the temperature gradient into account). A portion of the grid points with the highest weights are selected and converted to liquid. The liquid grid points are then allowed to move, in order to mimic surface tension. The iterations continue until the desired melting fraction is achieved. A column particle for example, would begin to melt at its tips, successively melt inwards and end up as a liquid sphere (if complete melting is simulated).

3.2. Chalmers particle models

A number of particle models used for this database have been developed internally using the software presented in Section 3.1. An overview of all habits is available in Table 5.1.

3.2.1. Aggregate generation

The aggregate simulator of the snowflake tool-kit (section 3.1.1) was used to create a number of aggregate habits. The constituent crystal used throughout was hexagonals of various axis ratios. The axis ratios used where 5 and 1 for column hexagonals, and 6 for plate hexagonals. The dimensions of each constituent crystal, length L and base diameter d, are not set with an exact fixed value, but are selected randomly from a Gamma distribution, using a standard variation of 25 %. Also varied is the constituent crystal maximum dimension, for which two values, 100 and 350 μm were chosen. The motivation for having two constituent crystal sizes is that the simulations could not provide large enough with only 100 μm crystals, hence habit versions with 350 μm crystals were created as well. The aggregate configurations considered in the database are presented in table 3.1.

Table 3.1.: Overview of aggregates produced internally using the Snowflake tool-kit.

Habit name	Id	Axis ratio (L/d)	Crystal $D_{\max}$ [μm]	α	β
Small Column Aggregate	17	6	100	0.14	2.45
Large Column Aggregate	18	6	350	0.25	2.43
Small Block Aggregate	21	1.25	100	0.21	2.33
Large Block Aggregate	22	1.25	350	0.35	2.27
Small Plate Aggregate	19	0.2	100	0.077	2.25
Large Plate aggregate	20	0.2	350	0.21	2.26

3.2.2. Bullet rosettes

Several bullet rosette habits have been created for this database, using the software presented in Section 3.1.1. In specific, the snowflake tool-kit internal shape format and dipole sampling routine was utilized. They vary in number and alignment of the bullet arms, as shown Fig. 3.2. To summarize, there are two habits with 3 bullets, one with perpendicular bullet alignment and one in which all bullets lie in a shared plane. Furthermore, in similar fashion there are 2 habits with 4 bullets, one in which all bullets lie in a shared plane and one in which one of the bullets has been flipped 90°. There is one habit that consist 5 bullets, for which only one bullet configuration is possible. Finally, there is one 6-bullet rosette that has been reconstructed from the database by *Hong et al.* (2009).

All of the habits are constructed in a similar fashion to the 6-bullet rosette in (see Fig. 3.2, bottom right). Firstly, the bullets are all designed as hexagonal columns with a tip at the end which connects the bullets. Secondly, the bullets of all habits grow in the

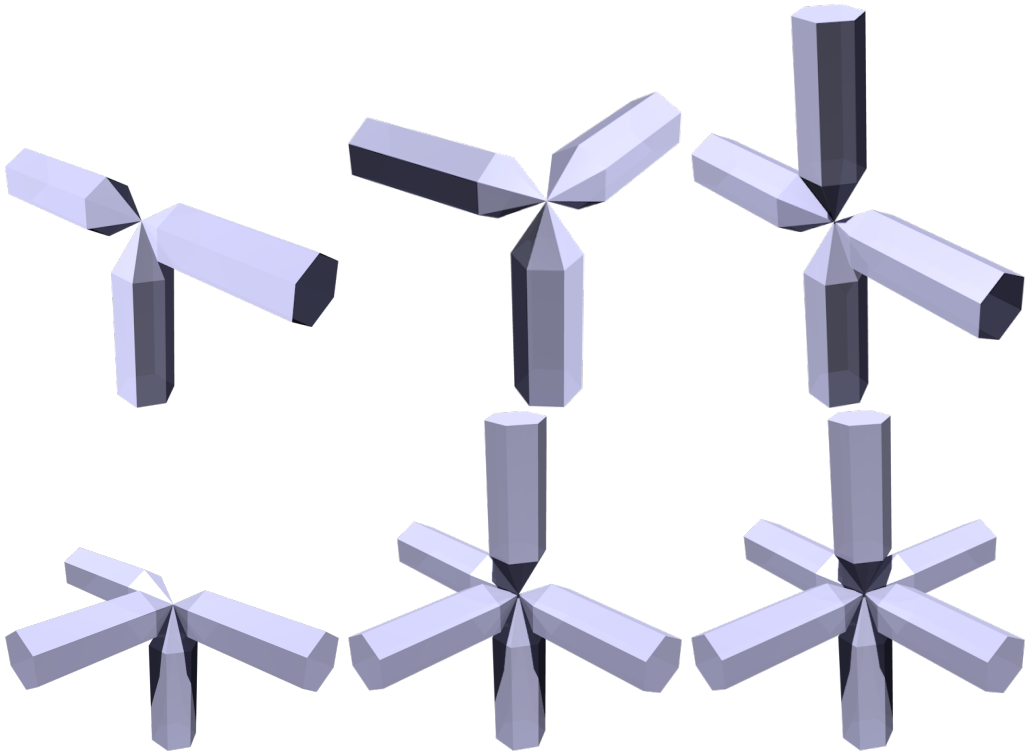

Figure 3.2.: Bullet rosettes included in the database. (Top left) Flat 3-bullet rosette, (top middle) perpendicular 3-bullet rosette, (top right) flat 4-bullet rosette, (bottom left) perpendicular 4-bullet rosette, (bottom middle) 5-bullet rosette, and (bottom right) 6-bullet rosette. Figures are rendered using Blender.

same manner, in the sense that a bullet of a given mass will have the same dimensions regardless of the habit considered. The growth of the bullets are taken from the bullet parametrisation in *Hong* (2007), which is based on the measurements listed in that paper.

3.2.3. Particles with pre-defined α and β

Using RimeCraft, a number of habits were generated that match the pre-defined mass-size relationships assumed by two models. The two considered models are GEM (Global Environmental Multiscale Model) and ICON (Icosahedral non-hydrostatic general circulation model). The GEM model was prepared for the EARTHCARE mission (*Côté et al.*, 1998) and the ICON model is a part of the German HD(CP)^2 project (`http://hdcp2.eu`). Both models have defined mass-size parametrisations for the following particle types (Table 3.2): cloud water, rain, cloud ice, snow, graupel and hail. However, cloud water and rain are in both models assumed to be liquid spheres, which is included in the database using Mie theory. Further, the cloud ice particles have settings indicating quasi-spherical solid particles, and it then seemed more reasonable to

represent these particles as spheroids than using RimeCraft. (Please note that the scattering properties for these spheroids were derived using DDA, to avoid limitations of the T-matrix method at large size parameters.)

Table 3.2.: Overview of particles produced using RimeCraft. Note that the α and β values reported here are the preset values used as input to RimeCraft. As such, these values differ somewhat to those reported in Tables 5.1/5.3, which were calculated post-simulation.

Habit name	Id	α	β	Initiation shape	Enclosure type
ICON Cloud Ice	27	1.59	2.56	-	-
ICON Hail	30	392	3.00	Single point	Sphere
ICON Snow	28	0.04	2.00	Semi 2D-cross	Flat cylinder
ICON Graupel	29	501	3.18	Point	Sphere
GEM Cloud Ice	31	440	3.00	-	-
GEM Hail	34	471	3.00	Single point	Sphere
GEM Snow	32	52.4	3.00	3D-cross	Sphere
GEM Graupel	33	209	3.00	Single point	Sphere

3.2.4. Miscellaneous

Habits that do not fit in above sections are covered here. As mentioned in Section 3.2.3, the ICON and cloud ice habits were not suitably modelled using RimeCraft. They were instead modelled as ellipsoids with parametrisations matching those in Table 3.2 (Id 27 and 31). This was done using the snowflake tool-kit internal shape format and dipole sampling routine. Furthermore, in order to model rain and liquid cloud particles, spherical liquid droplets are included in database using Mie theory (Section 4.2). Ice spheres has been included as well for convenience and completeness, using Mie theory as well.

3.3. Third party particle models

A number of third party habits have been included as well. They are divided into two groups, those that shape data in the ADDA format was available, and for those that shape data was re-created using models from literature.

3.3.1. External shape data

This section lists the habits for which explicit DDA shape data were available. Two sources were selected for inclusion in the end, though others were available. The sources are:

- *Evans et al.* (2012): One type of snowflake aggregate, with 95 sizes available from the source. We select a subset of 35 particles for our database. A problem with these shape data is that the dipole lengths are only as low as 32 μm, meaning

that the files are only valid up to 425 GHz considering the requirement dpl = 22 (see Section 4.1). Regardless of this, we chose to do calculations up to the max frequency (874 GHz). The user should keep in mind of this limit when using frequencies higher than 400 GHz.

  - Evans snow aggregate.

- *Tyynelä and Chandrasekar* (2014): Aggregates are generated using quasi-horizontal alignment where a Gaussian orientation distribution with a standard deviation of 2° was assumed. A large amount of shape data are available, but not of high enough dpl and sizes. After correspondence with Tyynelä a new shape dataset was created by him to solve this issue, resulting in the inclusion of one habit, describing aggregates of dendrites. A large number of shapes were provided (about 900), but only a subset of these are processed (35), in accordance with this size grid methodology used in this study (Section 5.6.3). To summarize, the following habit is included:

  - Tyynelä dendrite aggregate.

3.3.2. Recreated shape data

The shape data of the following habits were created using the Snowflake tool-kit described in Section 3.1.1, using particle models described in literature. Considered sources are:

- *Liu* (2008): The "Liu database" is limited in habits to idealized hexagonal crystals and two idealized snowflakes, albeit at relatively large size ranges. Note that the column and plate crystals all have values $\beta = 3$, which indicates that aspect ratios are fixed with respect to $D_{\max}$. This is not a realistic assumption, observations indicate values of β close to 2.5. More realistic mass-size relationships are observed for the bullet rosettes and snowflakes, with $\beta \approx 2.3$ and $\beta \approx 1.5$ respectively.

  See Fig. 3.3 for a rendering of the sector snowflake. Its mass-size relationship is based on measurements reported in *Heymsfield et al.* (2002) and *Heymsfield and Miloshevich* (2003). *Geer and Baordo* (2014) and *Eriksson et al.* (2015) argued for the sector snowflake as a good candidate for representing average scattering properties (up to 200 GHz).

  We have included a total of 6 habits from the Liu database, listed below:

  - Long, short and block columns.
  - Thick and thin plates.
  - Sector snowflake.

- *Hong et al.* (2009): The "Hong database" is, as the Liu database, limited to single crystal habits (we consider the bullet rosette a single crystal), with the exception of one aggregate. This aggregate model is an idealized representation, where 8 hexagonal columns of different sizes have been stuck together in a random fashion

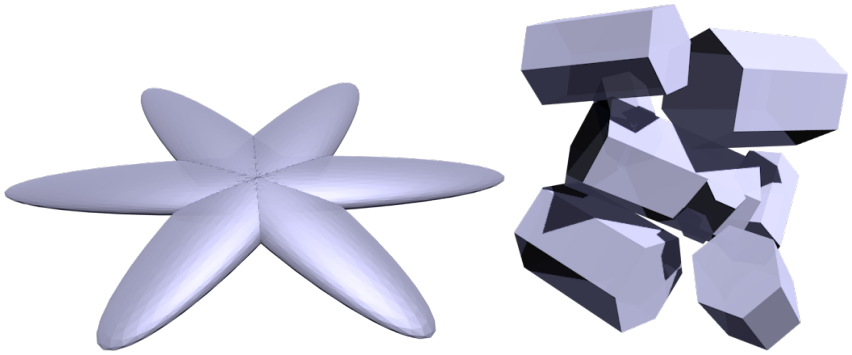

Figure 3.3.: (Left) Sector snowflake in *Liu* (2008) composed of three ellipsoids with a shared center. (Right) Aggregate in *Hong et al.* (2009), composed of eight hexagonal columns stuck together. Figures are rendered using Blender.

(see Fig. 3.3 for a visualization). The aggregate has β-value equal to 3, i.e. all three dimensions behave equally over all sizes, an unrealistic assumption as mentioned above. At sizes of $D_{max} \approx 2\,\text{mm}$ one might regard this particles as hail or a pellet, rather than something snowflake-like. The other habits demonstrate more realistic β values based on observations.

We have included a total of 4 habits from the Hong database. The column and plate habits are referred to as *Columns type 1* and *Plates type 1* in order to distinguish them from the columns and plates from the Liu database. Note that bullet rosette listed below is the same as the 6-bullet rosette discussed in Section 3.2.2. The included habits are listed below:

- Column type 1.
- Plate type 1.
- 6-Bullet rosette.
- 8-Column aggregate.

4. Scattering calculations

Two calculation approaches to derive scattering properties have been used, the Discrete Dipole Approximation (DDA, Section 4.1) and Mie theory (Section 4.2).

4.1. ADDA usage

For the generation of single scattering properties, we have chosen to mainly make use of DDA due its capability to treat particles of arbitrary shapes. In specific, we have used the Amsterdam DDA implementation (ADDA) (*Yurkin and Hoekstra*, 2011). It is well tested and has been used by several other relevant studies. It is fairly easy to use and also quite straightforward to set up parallel computations for calculations at clusters.

Another feature of ADDA is the possibility to automatically calculate scattering for random orientation, as opposed to running the program for several angles and integrating externally. If this option is activated, ADDA calculates and updates the orientation averaging after each calculation using Romberg integration, until the convergence criteria is met. For the configuration used in this study, this convergence occurs at a mean of 40 angles, and at a maximum of 250 angles. The advantage is thus that the number of orientations to process does not need to be specified in advance, and redundant calculations are avoided.

ADDA does not provide any built-in support for our second orientation case, azimuthally random. Hence a dedicated algorithm had to be developed to handle the averaging and required transformations. This algorithm is described in Section 4.1.3. Input and output data are discussed in Section 4.1.1 and 4.1.2 respectively.

4.1.1. Input

The required input is divided into variables and files. A selection of the most relevant parameters are available in Table 4.1 and all possible input files in Table 4.2. Note that, assuming a shape is specified, only two parameters are required to define a DDA grid, being the size parameter and the number of dipoles per wavelength. This means that only two of the parameters `dpl`, `lambda` and `eq_rad` need to be specified. The third parameter is given by the other two. It is critical that `dpl` is sufficiently large in order to resolve the wavelength. A common rule is

$$|n|kd < 0.5, \tag{4.1}$$

where n is the complex refractive index, k the wavenumber and d the dipole length. For ice this translates to a `dpl` of roughly 22 for ice at microwave and sub-millimetre

Table 4.1.: The most important command line parameters required by ADDA.

`dpl`	The number of dipoles per wavelength.
`lambda`	Wavelength.
`eq_rad`	The volume equivalent radius.
`eps`	Stopping criterion for the iterative solver.
`orient`	Specifies the orientation of the particle. Either fixed using Euler angles or specifying an `avg_params.dat`-file.
`prop`	Specifies propagation vector of the incident light.
`shape`	Specifies the shape. Can be either an ADDA predefined shape or a file.

Table 4.2.: Input files accepted by ADDA.

`avg_params.dat`	Specifies orientation averaging.
`scat_params.dat`	Specifies the scattering angle grid.
`Geometry file`	Describes the dipole grid of the input shape.

frequencies. In this study, `lambda` and `eq_rad` are given as input, because the input shape files are already created with a specific `dpl`.

A shape, or geometry, file describes the shape of the particle in an approximate manner on a grid of discrete coordinates, representing dipoles. This format is somewhat inflexible, since it fixes the dipole amount. This means that if a single geometry file is used for all frequencies, the minimum *dpl* condition will be exaggerated at lower frequencies, resulting in unnecessarily long computation times. Conversely, it may be the case that the dpl condition is not fulfilled for the highest considered frequencies. To avoid these problems, one should implement an adaptive shape grid, by keeping `dpl` constant at different frequencies. This is generally straightforward to implement when explicit shape definitions are available, from which the dipole grid can be sampled. For our internal shape data, such an adaptive grid has been adapted. For external shape data, we have been limited to either re-sampling existing shape grids or just make use of one grid per particle size (i.e. no adaptive grid at all).

The `eps` determines the convergence criteria by specifying the residual error, which is roughly the same as the actual electric field error. We have used a value of

$$\texttt{eps}_{\texttt{TRO}} = 10^{-2} \tag{4.2}$$

for totally random orientation. In general, this result in errors in the order of a few percent, when comparing to DDA solutions where high values of `eps` (about 10^{-6}) have been used. For azimuthally random orientation a value of

$$\texttt{eps}_{\texttt{AO}} = 10^{-3} \tag{4.3}$$

was used for all but the largest particles. For the ten largest sizes of habit 9 (see Table 5.5), a value of $\texttt{eps}_{\texttt{AO}} = 10^{-2}$ was used instead, due to the heavy computation costs.

Orientation of the particle can be specified in two ways. The simplest option is to specify a fixed orientation by the three Euler angles (see Section 2.3) directly into the command line. When orientation averaging is desired, one has to specify an input file, by default named `avg_params.dat`. The `avg_params`-file defines for which angle intervals the averaging shall be performed. One also has to set a convergence criteria for each angle. For totally random orientation a value of

$$\mathrm{eps}_{\mathrm{avg}} = 10^{-2} \tag{4.4}$$

was used for the β and γ angles. Averaging over the alpha angle is not needed, since it can be calculated analytically (by rotation of polarisation basis, assuming incident radiation always propagates along the z-axis). For azimuthally random orientation, `avg_params.dat` is not used. The averaging is performed using the method described in Section 4.1.3. In this case, the `scat_params`-file was used to fix the scattering angle resolution of the output Mueller and Amplitude matrices. The scattering grid was here set to an equidistant angle grid with 1° resolution.

4.1.2. Output

Possible output data from ADDA are specified in Table 4.3. The Mueller matrix is similar to the scattering phase matrix in that it relates the outgoing to incoming Stokes vector. It differs in that it is dimensionless, not normalised and defined with respect to the scattering reference frame. Depending on the specific calculation, either the `mueller` or `mueller_scatgrid` is the selected output. `mueller` is selected when the scattering is calculated in only one plane or for orientation averaging. Otherwise the more general, but larger `mueller_scatgrid` is given as an output. The differences between these two is that the former only gives the Mueller values over the zenith angle, while the later provides data over both zenith and azimuth. Section A.6 provides details on the conversion from Mueller to scattering matrix. `CrossSec` contains cross-sections. By default the extinction and absorption cross-sections are returned. The scattering cross-section is by definition the difference between the extinction and absorption cross-sections. However, ADDA can also calculate the scattering explicitly if desired, but not in the case when the internal averaging routine is used. An alternative output is the amplitude matrix, which contains information of the phase.

For both totally and azimuthally random orientation, the Mueller matrix output is used to retrieve the scattering matrix $\mathbf{Z}$. However, for the extinction matrix $\mathbf{K}$ and absorption vector $\mathbf{a}$ there are differences. The output amplitude matrix is used to calculate $\mathbf{K}$ for azimuthal orientation as described in the Appendix A.6, while the absorption vector is calculated using Eq. 2.2. For totally random orientation it holds that the diagonal elements $\mathbf{K}(i,i) = \beta_{\mathrm{e}}$ and $\mathbf{a}(1,1) = \beta_{\mathrm{a}}$ (remaining elements equals zero), hence it is enough to use the output cross-section values in `CrossSec`.

4.1.3. Calculation of azimuthally random particles

The treatment of azimuthally randomly oriented particles is different to that of the total randomly oriented particles. As mentioned, for azimuthally randomly oriented particles

Table 4.3.: ADDA output files.

`mueller`	Contains the Mueller matrix in one scattering plane angle.
`mueller_scatgrid`	Contains the Mueller matrix for the complete scattering grid.
`ampl`	Contains the amplitude matrix in one scattering plane.
`ampl_scatgrid`	Contains the amplitude matrix in one the complete scattering plane.
`CrossSec-X`	Contains cross-sections for incidence x-polarisation.
`CrossSec-Y`	Contains cross-sections for incidence y-polarisation.
`CrossSec`	Contains cross-sections for orientation averaged calculations.
`log`	Contains general log data and standard output.
`log_orient_avg`	Contains relevant log data when orientation averaging is used.

the orientation averaging of ADDA cannot be used. Instead a self developed averaging approach is being used, which involves integration over a set of DDA calculations at different angles, and transformation of reference frames. Details are found in Appendix A.

The methodology to calculate the scattering matrix in the case of one azimuthally randomly oriented particle can be summarised as:

1. DDA calculations: A set of DDA runs are performed over an icosahedral angle grid, demonstrated in Fig. 4.1. This type of grid ensures that the angle density is isotropic and increases the efficiency. Details are found in Appendix A.2. Symmetry considerations will reduce the number of actual DDA calculations needed. The result could be seen as a lookup table for the Mueller matrix $\mathbf{M}(\theta_i, \phi_i, \theta_s, \phi_s)$, defined over the incidence angle grid. Each Mueller matrix element $M_{ij}(\theta_i, \phi_i, \theta_s, \phi_s)$ is expanded as a spherical harmonics series over the scattering directions θ_s, ϕ_s (see Appendix A.4). The spherical harmonic series is truncated to the number of coefficients, when the mean square error between the series expansion and the original representation is less than 0.5% of the standard deviation of the M_{11} element over the scattered direction. Due to the spherical harmonics expansion the amount of data space for the Mueller lookup table can be reduced up to two orders of magnitude. The actual reduction depends on the scatterer's size and shape. For small particles the reduction is stronger than for large and complex particles.

2. Averaging: Azimuthally averaged Mueller matrices $\mathbf{M}(\theta_i, \theta_s, \phi_s, \beta)$ for a set of tilt angles β and polar incidence angles θ_i, are calculated by integrating the Mueller matrix over the incidence angle grid. The integration is accompanied by an interpolation scheme (see Appendix A.5).

3. Transformation: The averaged Mueller matrices are transformed to averaged scattering matrices. The Mueller matrix is related to incidence direction, while the scattering matrix is defined in the laboratory reference frame. Also, the polarization basis is related to the scattering direction for the Mueller matrix and to the incidence direction for the scattering matrix. Hence a transformation of coordinate systems are performed. More details are available in Appendix A.8. Furthermore,

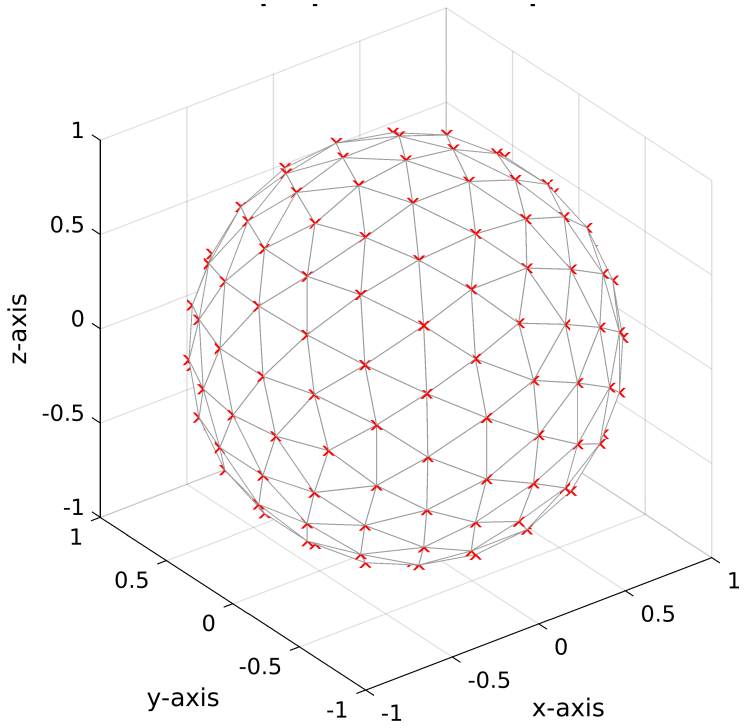

Figure 4.1.: Example of an icosphere grid with 162 vertices. Each gridpoint represent an incoming angle for which a DDA calculation is preformed. This type of configuration ensures that the grid density is isotropic, making the overall calculations more efficient (a standard polar grid would be inefficient since it yields an excessive amount of angles around the 'North and South poles").

each scattering matrix element $Z_{ij}(\theta_i, \phi_i, \theta_s, \phi_s)$ is also expanded as spherical harmonics series over the scattering directions θ_s, ϕ_s (see Appendix A.4). The spherical harmonic series is truncated to the number of coefficients, when the mean square error between the series expansion and the original representation is less than 1% of the standard deviation of the Z_{11} element over the scattered direction. The accuracy is slightly reduced compared to the Mueller matrices to reduce the amount of data for the scattering matrices.

As a result, we acquire a set of azimuthally averaged scattering matrices $\mathbf{Z}(\theta_i, \theta_s, \phi_s, \beta)$, for a set of tilt angles β and polar incidence angles θ_i with each scattering matrix element expanded in spherical harmonics. For the extinction matrix $\mathbf{K}$ the method is similar. The absorption vector $\mathbf{a}$ is calculated afterwards from the scattering matrix $\mathbf{Z}$ and the extinction matrix $\mathbf{K}$ using Eq. 2.2.

The advantage of the calculation method outlined above is that as long as step 1 has been performed, we can calculate the averaged matrices for any tilt and incidence angle using the Mueller matrix $\mathbf{M}(\theta_i, \theta_s, \phi_s, \beta)$ lookup table, i.e. it is not required to perform

any new DDA calculations for each new tilt/angle configuration. An angle grid of up to 2562 vertices (orientations) was be used, which is an order of magnitude larger compared to totally random orientation, and required a considerable amount of core hours. For the ten largest sizes of habit 9 (see Table 5.5), the amount of angles was reduced to 642, in order to accelerate the computations.

4.2. Mie theory

Two habits described by spheres are included in the database, liquid and solid water spheres, for the sake of convenience and due to the heavy computation costs. For calculations of the scattering properties of these habits, it is appropriate to make use of the well-known Mie theory which provides an exact solution. The implementation in MATLAB by *Mätzler* (2002) was used for this purpose, along with wrapper code provided by the Atmlab package[1].

Two functions are used, `mie` and `mie_12`, where the former calculates scalar quantities such scattering efficiencies and the later calculates the scattering amplitude functions. Table 4.4 gives an overview of the input and output of these functions. The efficiency parameters are normalized scattering quantities with respect to the particle cross-sectional area, for example in the case of extinction

$$Q_{ext} = \frac{C_{ext}}{\pi r^2}, \tag{4.5}$$

where r is the sphere radius. The S1 and S2 output variables describe the scattering amplitude matrix elements S_{11} and S_{22}. These elements describe the angular dependence of the plane-perpendicular and plane-parallel components of the scattered light relative to the incoming light (S_{12} element is zero, since there is no depolarization for spheres). The amplitude matrix is converted to scattering matrix $\mathbf{Z}$ using the wrapper code provided by Atmlab. Note that for the database, only the amplitude matrix, and the absorption and extinction efficiencies are actually used. Other parameters are derivable from this set of parameters.

4.3. Post processing

This section covers the post processing of the DDA output not covered elsewhere. This includes data checks and modifications to the DDA data.

4.3.1. Totally random orientation

A number of tests and modifications are performed on the totally random orientation DDA output in order to ensure quality. This is done in a number of steps outlined in Section 4.3.1.1 below. Furthermore, a number of validation analyses are presented in Section 4.3.1.2.

[1] http://www.radiativetransfer.org/tools/

Table 4.4.: The input and output of the `mie` and `mie_12` functions from the Mie code by *Mätzler* (2002).

`mie`	
`Input:`	
m	Complex refractive index n.
x	Size parameter x.
`Output:`	
qext	Extinction efficiency Q_{ext}.
qsca	Scattering efficiency Q_{sca}.
qabs	Absorption efficiency Q_{abs}.
qb	Backscattering efficiency Q_{bck}.
asy	Asymmetry parameter g
qratio	Q-ratio (ratio of backscattering to scattering cross-sections).
`mie_12`	
`Input:`	
m	Complex refractive index n.
x	Size parameter x.
u	Cosine of the scattering angle, $\cos(\Theta)$.
`Output:`	
S1	Scattering amplitude matrix element 11.
S2	Scattering amplitude matrix element 22.

4.3.1.1. Post processing and checks

As described above, the output of the ADDA calculations are the extinction cross-section β_e, absorption cross-section β_a and Mueller matrix $\mathbf{M}$. For each database entry, sanity checks and modifications are performed in the following order before being accepted into the database:

1. Basic sanity checks: The ADDA output extinction cross-section is tested for positivity, i.e. $\beta_\mathrm{e} > 0$. Furthermore, the output absorption cross-section is tested for
$$\frac{\beta_\mathrm{a}}{\beta_\mathrm{e}} \geq -0.01 \tag{4.6}$$
and
$$\frac{\beta_\mathrm{a} - \beta_\mathrm{e}}{\beta_\mathrm{e}} \leq 0.01. \tag{4.7}$$
This ensures that the absorption is positive and smaller than the extinction, with a tolerance of one percent. Such cases are due to numerical inaccuracy in the cases where the scattering is either relatively small or large compared to the extinction. These borderline cases are taken into account in the steps below. Cases that do not pass all of the tests here are discarded.

2. Scattering cross-section: For the TRO calculations, scattering cross-section is calculated by integration of the Mueller matrix as
$$\beta_\mathrm{s} = \frac{1}{k^2} \int_{4\pi} \mathbf{M}_{11} \, \mathrm{d}\hat{\mathbf{n}}'. \tag{4.8}$$
The reason for not using $\beta_\mathrm{s} = \beta_\mathrm{e} - \beta_\mathrm{a}$, is that the later function results in significantly inaccurate values for scattering in the Rayleigh regime, while the former provides reasonable values over all sizes (see Section 4.3.1.2 for a comparison to older scattering data).

3. Scattering matrix: The scattering cross-section is not stored explicitly in the database. Rather, it is stored implicitly by the scattering matrix, which is transformed from the Mueller matrix. For TRO, the transformation consists of a multiplication by a normalization factor, such that the integral of the first element of $\mathbf{Z}$ equals the scattering cross-section (Eq. 2.3).

4. Absorption vector: The absorption vector is equivalent to the absorption cross-section for TRO. In general, no transformation is used here, the output absorption is stored directly in the database. However, in some cases the absorption is slightly negative (cases with large negativity has already been discarded above). In those cases, the absorption value is discarded and calculated using $\beta'_\mathrm{a} = \beta_\mathrm{e} - \beta_\mathrm{s}$. This value is tested for
$$\frac{|\beta'_\mathrm{a} - \beta_\mathrm{a}|}{\beta_\mathrm{e}} \leq 0.01, \tag{4.9}$$
in order to make sure it does not deviate to much from the original value. If the test fails, the calculation is discarded.

5. Extinction matrix: Is equivalent to the extinction cross-section for TRO. We ensure that the scattering data adhere to the conservation of energy principle, i.e. $\beta_e = \beta_s + \beta_a$. This is done by discarding the ADDA output extinction cross-section, and setting the database value as $\beta'_e = \beta_s + \beta_a$. This approach ensures consistency and covers the cases where the output absorption is slightly larger than the extinction. We perform a final check to ensure that this value does not deviate to much from the original extinction value:

$$\frac{|\beta'_e - \beta_e|}{\beta_e} \leq 0.3. \tag{4.10}$$

The tolerance value is somewhat large, but it should be noted that only a small fraction of all data is above a 5 % difference (less than 0.5 % of all TRO data entries). Recalculating these case would have taken a significant amount of time. If the test fails, the calculation is discarded.

Cases that were discarded above are recalculated with the DDA accuracy increased. In specific, the convergence criterion is decreased by a factor 10 ($\texttt{eps}_{\texttt{TRO}} = 10^{-3}$). If this calculation also fails, then another calculation is performed with the Romberg integration accuracy increased in a similar fashion ($\texttt{eps}_{\texttt{avg}} = 10^{-3}$). If it is found that the calculation is still not accepted, the accuracy should be increased even more, however this has not been required so far.

4.3.1.2. Validation

For habits based on external sources, we can check agreement with calculations the previous databases. This is only possible for totally random orientation and mainly for the Hong and Liu databases. In order to compare with previous databases, interpolation to temperature, frequency and size grids used by those databases is required. In order to minimize the interpolation error, the frequencies and temperatures best matching between a given database and ARTS database are selected. Observed discrepancies will depend on differences in accuracy (DDA convergence criterion), orientation averaging, and interpolation error. Furthermore, there are some anomalies observed in both the Hong and Liu data, discussed below.

In Fig 4.2, 8-column aggregate extinction, absorption and cross-sections of the Hong and ARTS database are compared for five different frequencies (90, 183.3, 448, 664 and 874 GHz). In the top left panel, the extinction cross sections are seen to be well matched in magnitude at all sizes and frequencies. However the bottom left panel shows that the error is in the order of 7 % for small sizes and go up to 25 % for for 874 GHz. For the absorption, differences of over 25 % are observed. The back-scattering is closely matching at small to intermediate sizes, with larger deviations observed for large sizes, especially at the highest frequencies. The largest error observed is about 60 % (not shown). Overall, the calculations agree, but the matching is not perfect. As already mentioned, several factors influence the discrepancies involved. A fairly lax convergence criterion was used for this database, resulting in errors in the order of a few percent. What convergence

criterion was used for the Hong database is not known, and one should note that they used DDSCAT, a version older than the 2010 releases. Hence, there might be differences in solvers used, and it is also possible that DDSCAT accuracy has been improved since Hong's database was developed (this is the case for ADDA). Furthermore, even though the databases mass-size relation ship is almost perfectly matching (Fig 4.2, bottom right panel), the shape data files are not the same, hence further miss-match can be expected. Finally, the refractive index (by *Warren* (1984)) used in the Hong database is outdated, which the differences can be partly attributed to. For this comparison, a "fixed" version of the Hong database was used, where the absorption has been rescaled by a factor of $\mathrm{im}(n)/\mathrm{im}(n_0)$, where n_0 and n is the refractive index from *Warren* (1984) and *Mätzler* (2006), respectively. As such, it is hard to make any definite conclusions. Similar results are retrieved from comparison of the other Hong particles.

A similar comparison is done for the sector snowflake between the Liu and Arts database in Fig 4.3. Frequencies used are 5, 94, 183, 220 and 340 GHz. The extinction and absorption agree, with relative differences up to 17 %. The back-scattering agrees well except for the largest sizes, where the ARTS data seems to deviate upwards. The same tendency can be glimpsed for the Liu data, but it occurs at a higher size. The discrepancies could be explained by the fact that the Liu data demonstrate some anomalies regarding the mass-size relationship, seen in Fig 4.3, bottom right panel, where the difference in mass as a function of D_{max} has been plotted. The two databases do not perfectly agree, partly due to the Liu data being mapped on a coarser size grid, failing to catch some of the variation. At 4 mm in D_{max} there is a large deviation of almost 10 % in mass, for an unknown reason. A consequence of this is that the heaviest Liu particle has a smaller D_{max} compared to the ARTS particles, and conversely a smaller projected area. This could explain why the back-scattering is much lower for the Liu data. Similar results are retrieved for the other Liu particles.

Finally, comparisons to T-matrix calculations can be seen in Fig. 4.4 for five different frequencies (3, 31.5, 94.1, 175.3, 228 and 336.1 GHz). Here, DDA calculations of hexagonal long (axis ratio 4) and block (axis ratio 1) columns are compared to T-matrix calculations of equivalent cylinders. They are equivalent to the hexagonal columns in the sense that a DDA column and T-matrix column of equal mass have the same length and base area. As seen, the calculations agree well with each other, both in extinction and absorption. The long and block columns deviate about 3 % at smaller sizes. At larger sizes, there are fluctuations due to the hexagonal features having more impact. Results are similar when comparing crystals of other aspect ratios.

4.3.2. Azimuthally random orientation

4.3.2.1. Data checks

The calculation of the scattering properties for azimuthally random orientation was described Section 4.1.3. Two basic checks are done:

- For azimuthally random orientation must hold that for incidence angle of 0° and 180° the extinction matrix is diagonal with the diagonal elements being the same.

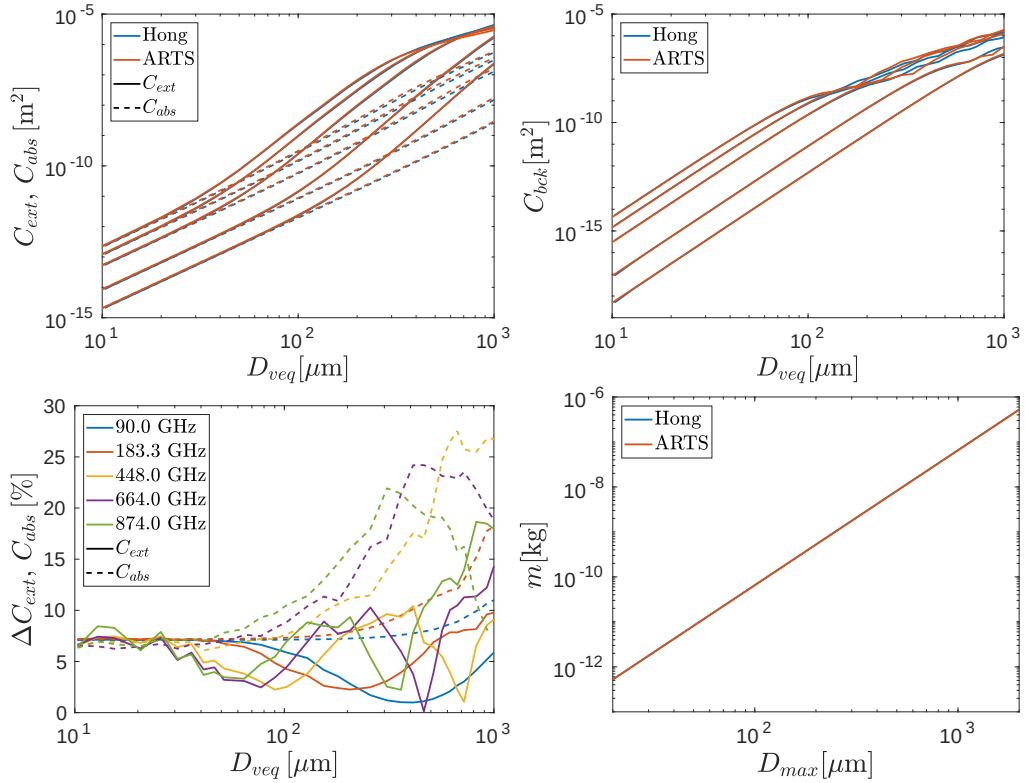

Figure 4.2.: Comparison of the 8-column aggregate. (Top left) Extinction (full lines) and absorption (dashed lines) cross-sections as a function of D_{veq} for the 8-column aggregate. The Hong database is in blue lines and the ARTS database is in red lines. 5 frequencies has been plotted: 90, 183.3, 448, 664 and 874 GHz, with increasing frequency from bottom to upper lines. (Top right) Similar to top left figure, but only back-scattering cross-sections are shown. (Bottom left) Relative differences of extinction (full lines) and absorption (dashed lines) cross-sections of the 8-column aggregate between the Hong and ARTS database for 5 different frequencies. The difference is calculated as $|\beta_{\text{Hong}} - \beta_{\text{ARTS}}|/\beta_{\text{Hong}}$. (Bottom right) Mass as a function of D_{max} for the Hong database (blue line) and the ARTS database (red line).

- Calculated cross-sections: $\beta_e = \beta_s + \beta_a$ (conservation of energy principle), see also Section 2.1 in Part II. The scattering cross section β_{sca} calculated by integrating the first matrix element of the scattering matrix $\mathbf{Z}$ over 4π must be smaller or equal the extinction cross section, so that the absorption cross section β_a cannot be negative. If this is not fulfilled, the scattering matrix $\mathbf{Z}$ is rescaled. This means the scattering matrix $\mathbf{Z}$ is multiplied with

$$f_{rescale} = 1 + \frac{\beta_e - \beta_s}{\beta_s}\,, \tag{4.11}$$

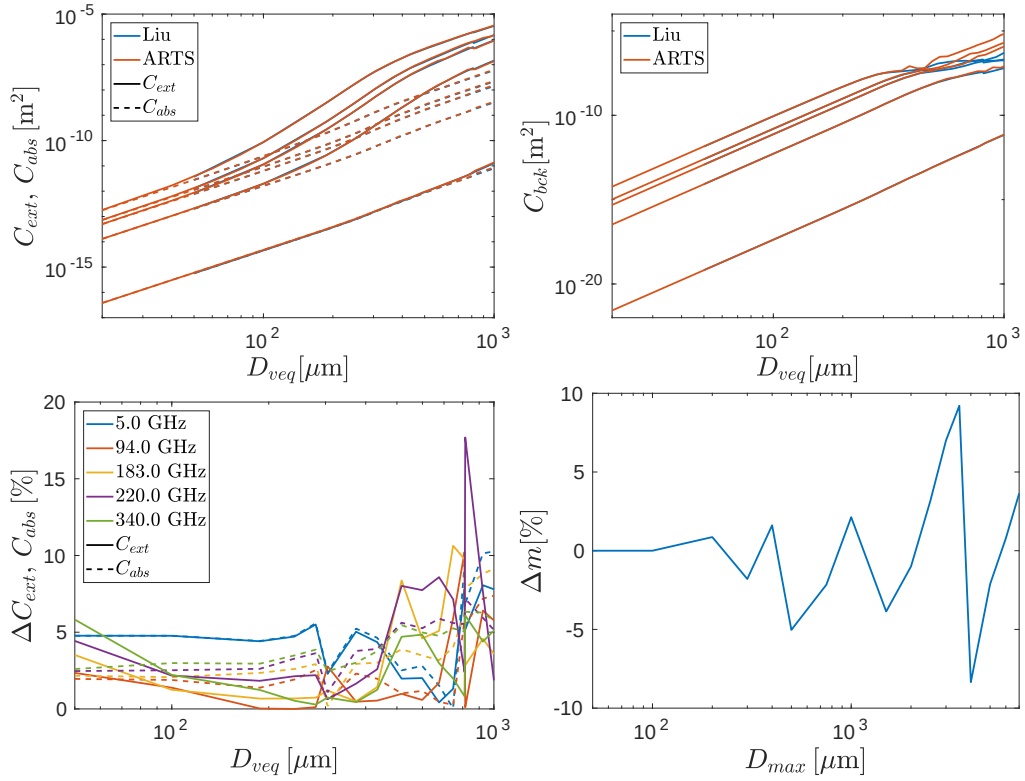

Figure 4.3.: Comparison of the sector snowflake. (Top left) Extinction (full lines) and absorption (dashed lines) cross-sections as a function of D_{veq} for the sector snowflake. The Liu database is in blue lines and the ARTS database is in red lines. 5 frequencies has been plotted: 5, 94, 183, 220 and 340 GHz, with increasing frequency from bottom to upper lines. (Top right) Similar to top left figure, but only back-scattering cross-sections are shown. (Bottom left) Relative differences of extinction (full lines) and absorption (dashed lines) cross-sections of the sector snowflake between the Liu and ARTS database for 5 different frequencies. The difference is calculated as $|\beta_{\text{Liu}} - \beta_{\text{ARTS}}|/\beta_{\text{Liu}}$. (Bottom right) The difference in mass between the Liu and ARTS database as a function of D_{max} for the sector snowflake. The difference is calculated as $(m_{\text{Liu}} - m_{\text{ARTS}})/m_{\text{Liu}}$.

so that the absorption cross section calculated from the extinction cross section and the rescaled scattering matrix is zero.

4.3.2.2. Validation

The idea behind the validation is to make a direct comparison of the results of our approach with the T-matrix method implemented in ARTS. The T-matrix method of ARTS is restricted in orientation and particle type. Therefore the test is restricted

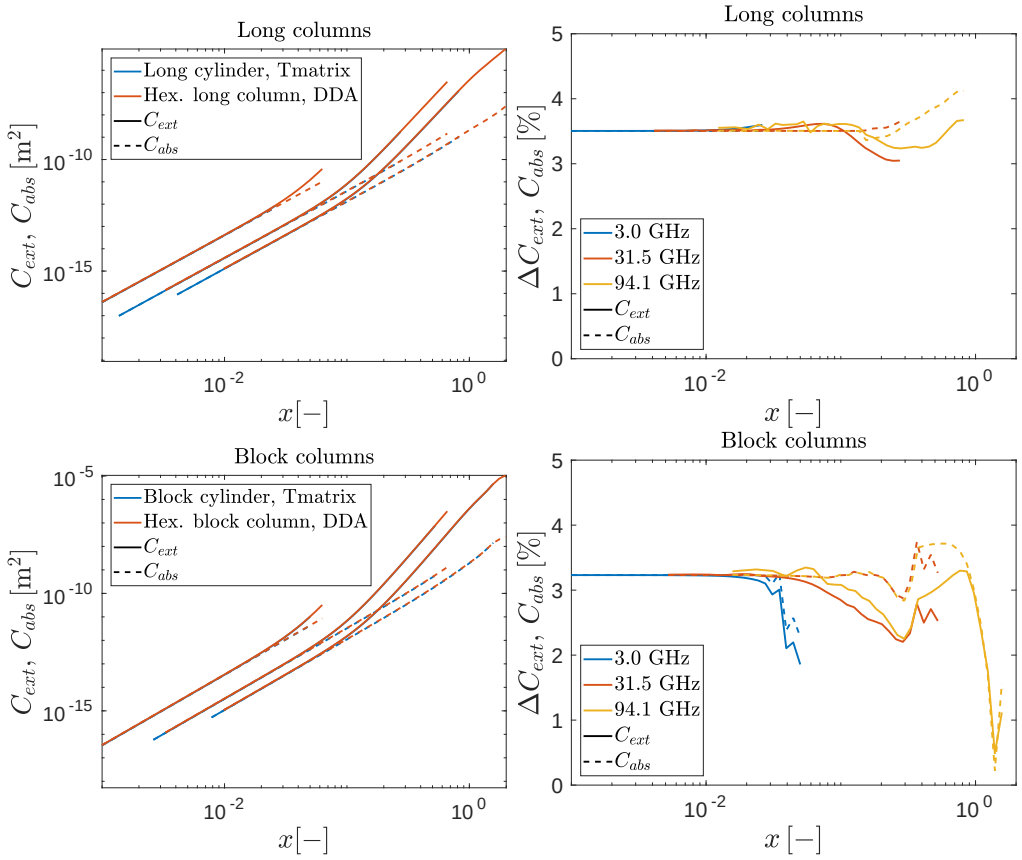

Figure 4.4.: Cross-section comparisons for DDA calculations of hexagonal columns, to T-matrix calculations of cylinders. The cylinders are designed to have equal mass and height compared to the hexagonal columns. Long columns (axis ratio 4) are represented in the top row and block columns (axis ratio 1) in the bottom row. The T-matrix calculations are in blue lines and the DDA calculations are in red lines. 3 frequencies has been plotted: 3, 31.5 and 94.1 GHz, with increasing frequency from bottom to upper lines. The left panels shows extinction (full lines) and absorption (dashed lines) cross-sections as a function of the size parameter x. The right panels show the relative difference in cross-sections for the T-matrix and DDA particles, as a function of size parameter x for 3 different frequencies. The differences are calculated as $|\beta_{\text{Tmat}} - \beta_{\text{DDA}}|/\beta_{\text{Tmat}}$.

to cases, which can be calculated with the ARTS T-matrix method. Furthermore no symmetries were used. For the test, the scattering properties of azimuthally randomly oriented prolate ellipsoids with an aspect ratio of 0.5, which lay with their longest axis parallel to the X-Y-plane, are calculated by our approach and are compared with results from T-matrix calculations. This equivalent to a β angle of 0°. Three different sizes were computed with the size parameters $x \in [0.1, 1, 5]$ at a frequency of 183 GHz. The

number of dipoles per wavelength within the DDA calculation was set by ADDA. For the comparison the scattering matrices were evaluated at a 1° resolution and the extinction matrices were evaluated for 37 incidence angles.

In Figs 4.5 – 4.7 the extinction matrices for the three different sizes are shown. The ADDA results are in a good agreement with the results of the T-matrix method. The difference of the diagonal elements are in the order of $1-2\%$. Only for $x = 5$ at $\theta_{inc} = 0°$ and $\theta_{inc} = 180°$ the difference is in the order of 5%. The difference of the $\mathbf{K}(1, 2)$- and the $\mathbf{K}(4, 3)$-element for $x = 0.1, 1$ are in same order as for the diagonal elements. The same holds for the $\mathbf{K}(2, 1)$ and the $\mathbf{K}(3, 4)$-element because $\mathbf{K}(2, 1) = \mathbf{K}(1, 2)$ and $\mathbf{K}(3, 4) = -\mathbf{K}(4, 3)$, see also Appendix A.6. For $x = 5$ the differences are larger in which the absolute values of the $\mathbf{K}(1, 2)$- and the $\mathbf{K}(4, 3)$-elements are two orders of magnitude than the diagonal elements. Hence, they are in the limit of the desired accuracy of a few percent. The off-diagonal blocks differ more, because the off-diagonal elements of the T-matrix method are set to zero by definition. But as the off-diagonal block elements are mostly at least three orders of magnitudes smaller than the diagonal elements, the difference of the off-diagonal block elements can be neglected within the desired accuracy. Only the $\mathbf{K}(4, 2)$- and the $\mathbf{K}(2, 4)$-element for $x = 0.1$ are only one to two orders of magnitude smaller than the diagonal-elements. This is due to the much coarser discretisation of the particle for $x = 0.1$ compared to the greater size parameters. This is not an issue, because in this test the discretisation was set by adda and within our used shape files the discretisation is finer. Therefore, the differences of the off-diagonal block elements can be neglected within the given accuracy and can be assumed to be zero, which they should be according to theory, see Appendix A.6.

The figures 4.8 and 4.9 show the scattering matrix for an azimuthally random oriented prolate ellipsoid for $x = 1$ as function of the scattering direction for an incidence angle of 30°. The agreement between the results of our approach and the T-matrix calculations are good. Except for the smaller stripy patterns in Fig. 4.8, which results from the truncated spherical harmonics, the agreement by eye is very good. In Fig. 4.10 the difference between our approach and T-matrix is shown. The local absolute differences are mostly $\ll 10\%$. Only at the poles ($\theta_s = 0°, 180°$) of the elements $\mathbf{Z}(2, 2)$, $\mathbf{Z}(2, 3)$, $\mathbf{Z}(3, 2)$, and $\mathbf{Z}(3, 3)$ they are larger. The stripy pattern and the larger deviations at the poles result from the truncation of the spherical harmonics. The relative rms deviation (averaged over the scattering direction) of each matrix element is shown on top of each subfigure. The deviations are $< 6\%$ except for the elements $\mathbf{Z}(1, 4)$ to $\mathbf{Z}(3, 4)$, $\mathbf{Z}(3, 1)$, and $\mathbf{Z}(4, 3)$. The deviations of these elements are larger because of the limited accuracy in our approach and because the absolute values of these elements are much lower than the other elements. Otherwise, their contribution relative to the other elements is small and we do not consider these deviations problematic. For larger size parameter x (not shown) the rms deviation of the off-diagonal-elements increases, because due to the limited accuracy and because the absolute values of the off diagonal elements of the scattering matrix decrease relative to the first element of the scattering matrix.

As within the given accuracy our approach is in good agreement with the T-matrix method, we conclude from this test that our approach is working and shows the right results. By setting a higher accuracy the differences locally and averaged can be reduced,

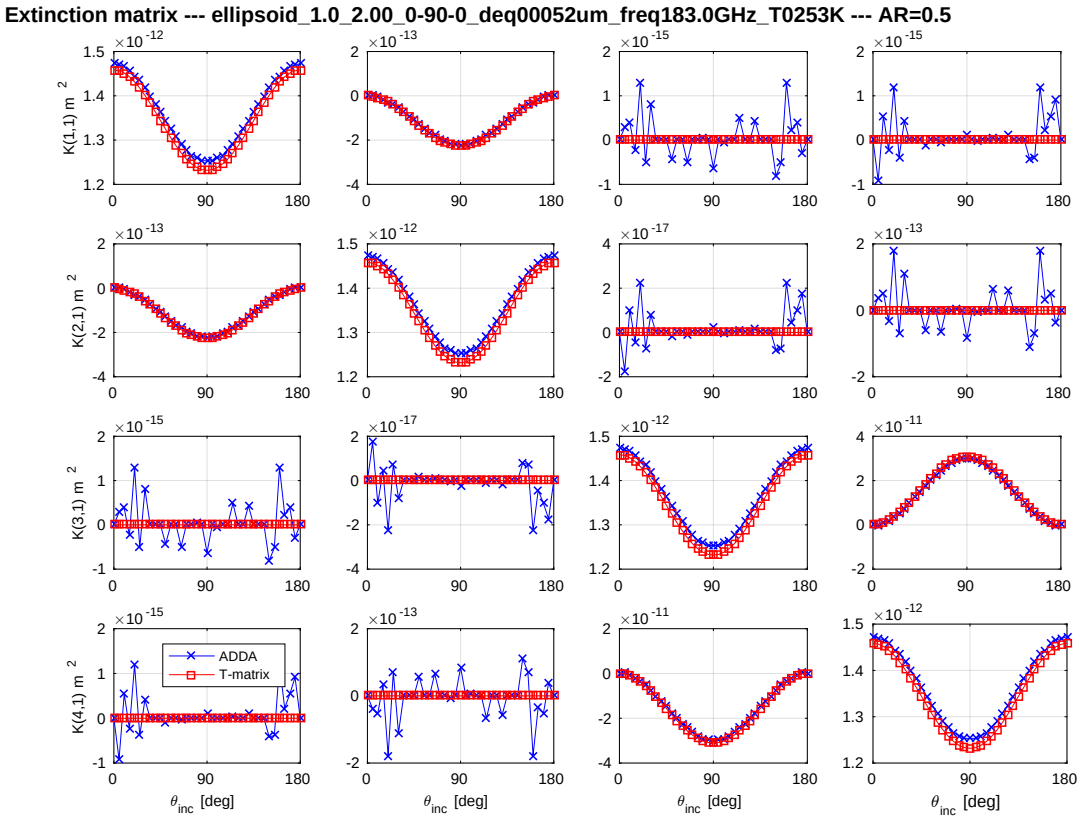

Figure 4.5.: Extinction matrix of azimuthally random oriented prolate ellipsoid with as an aspect ratio of 0.5 and a size parameter $x = 0.1$ as function of the incidence angle.

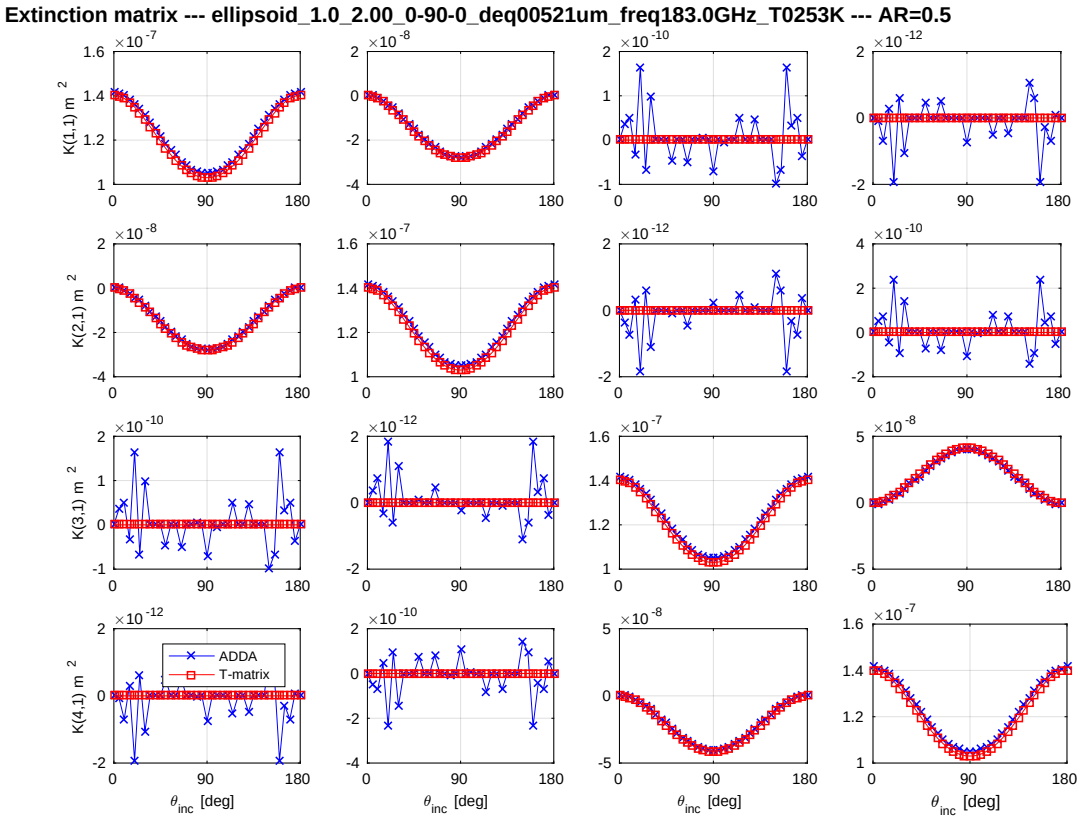

Figure 4.6.: Extinction matrix of azimuthally random oriented prolate ellipsoid with as an aspect ratio of 0.5 and a size parameter $x = 1$ as function of the incidence angle.

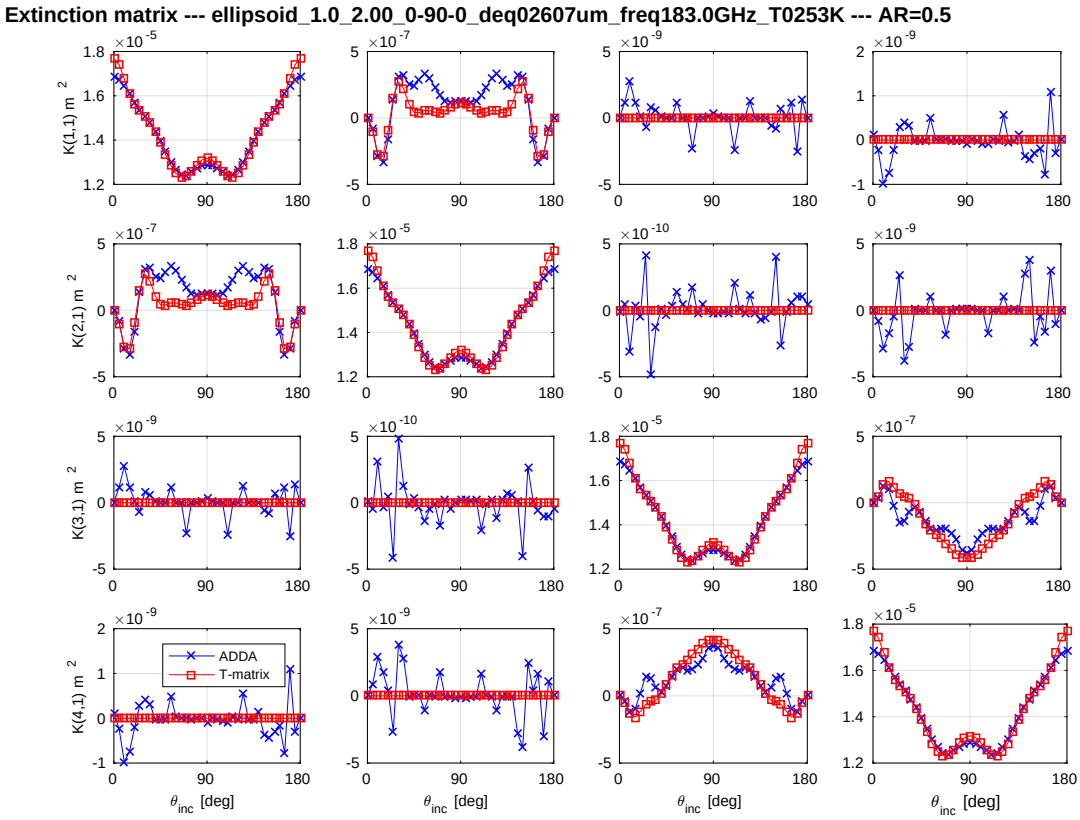

Figure 4.7.: Extinction matrix of azimuthally random oriented prolate ellipsoid with as an aspect ratio of 0.5 and a size parameter $x = 5$ as function of the incidence angle.

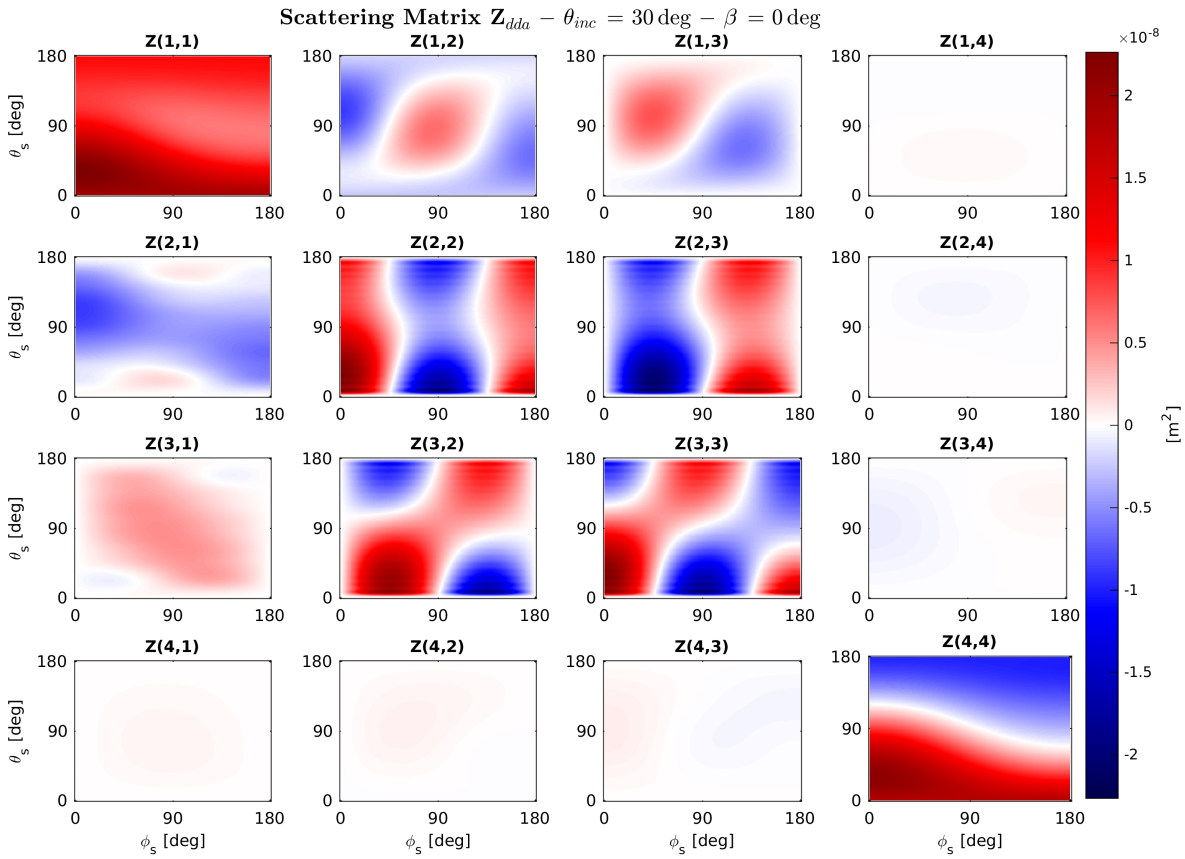

Figure 4.8.: Scattering matrix **Z** of an azimuthally randomly oriented prolate ellipsoid with an aspect ratio of 0.5 and size parameter $x = 1$ as function of the scattering direction for an incidence angle of 30° calculated using our approach.

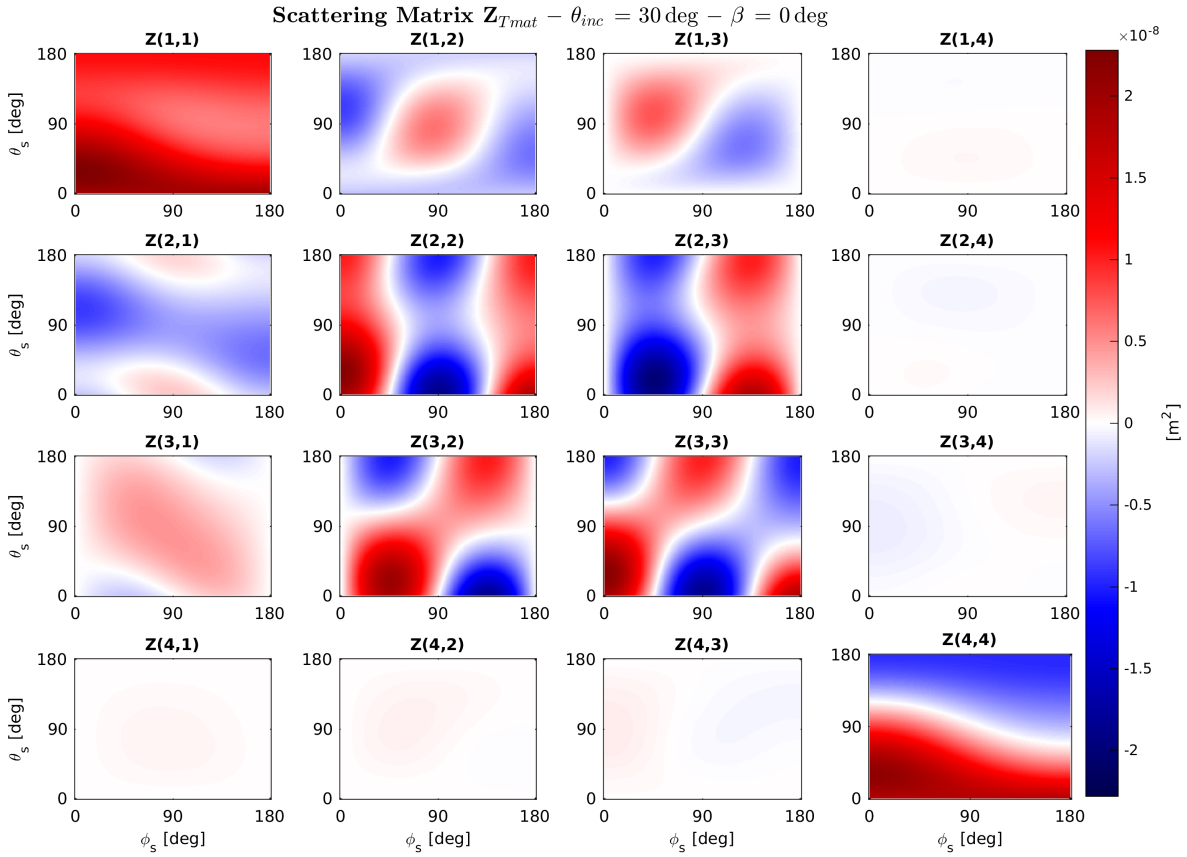

Figure 4.9.: Scattering matrix **Z** of an azimuthally randomly oriented prolate ellipsoid with an aspect ratio of 0.5 and size parameter $x = 1$ as function of the scattering direction for an incidence angle of 30° calculated using T-matrix.

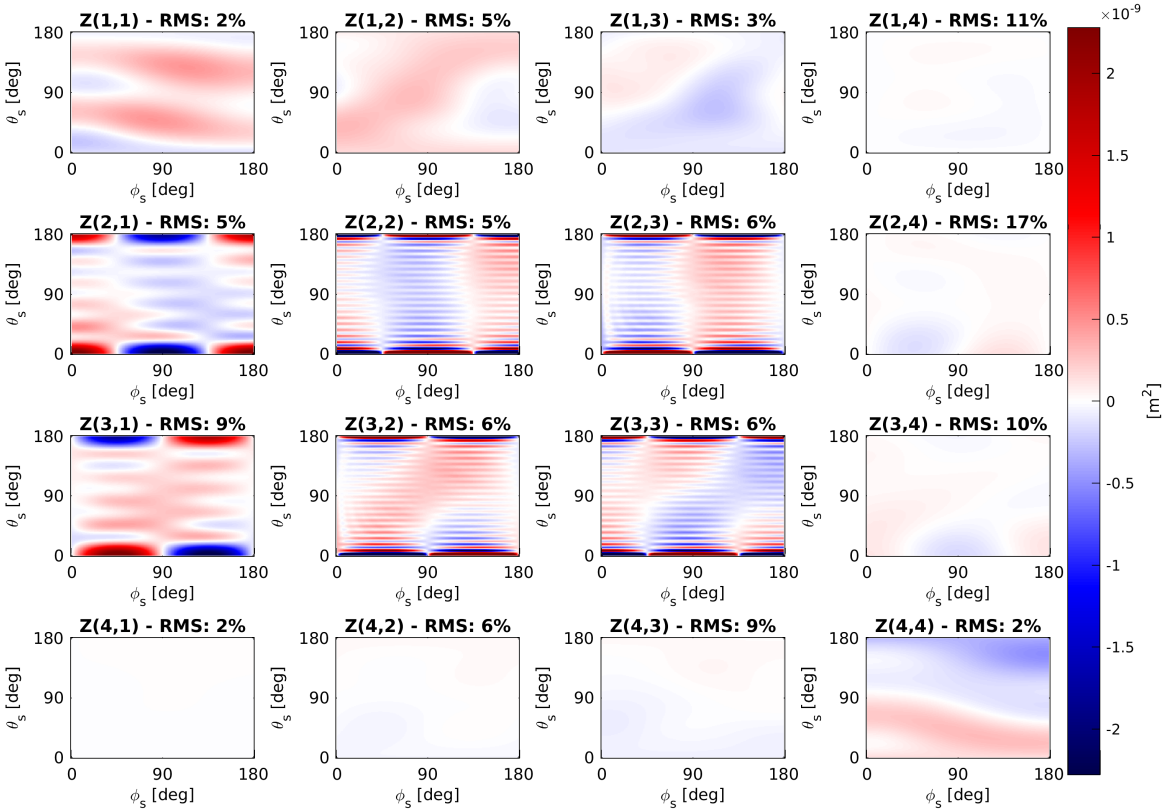

Figure 4.10.: Difference between the scattering matrices calculated by our approach (Fig. 4.8) and by T-matrix (Fig. 4.9 for an azimuthally randomly oriented prolate ellipsoid with an aspect ratio of 0.5 and size parameter $x = 1$ as function of the scattering direction for an incidence angle of 30°. The relative rms deviation (averaged over the scattering direction) of each matrix element is shown on top of each subfigure.

otherwise this would increase computation time and more important would increase the amount of data. Tests showed that increasing the accuracy by one order the amount of data increases by a factor of ten. With the given accuracy the database for just one habit of azimuthally randomly oriented particle has already a size of $\approx 130\,\mathrm{GB}$.

In Fig. 4.11, the (1, 1) and the (1, 2) elements of the extinction matrix are shown as example of an actual azimuthally randomly oriented particle of the database with size parameter $x = 1$ as function of the incidence angle for different β angles are shown. For $\beta = 0°$ the behaviour is similar to the extinction matrix elements shown in Fig. 4.5. Interesting, how the extinction matrix elements change with increasing β angle. Whereas the maximum of the (1, 1)-element for $\beta = 0°$ is at $\theta_{inc} = 0°$ and $\theta_{inc} = 180°$, the maximum for $\beta = 90°$ is at $\theta_{inc} = 90°$. This behaviour can be used as simple sanity check. For $\beta = 0°$ the effective particle in our example has its biggest cross section parallel to the x-y-plane and its smallest cross section parallel to the z-axis, therefore when looking from above or from below the extinction must be stronger than looking from aside. For $\beta = 90°$ the effective particle can be thought as a fast spinning coin around the z-axis. When looking from above or below on the spinning coin the background is less darkened compared to when looking from aside. As our database particle behaves like this, this gives us additional confidence about the quality of our results. Interesting, at incidence angle around 50° the influence of the orientation is small and only slightly different to the extinction of totally randomly orientation. This is interesting in view of sensors like the Ice Cloud Imager on board the upcoming satellite Metop-SG-B[2], which have an incidence angle of 53°. Though there is less influence of the orientation for the (1, 1) element, there is a strong influence for the (1, 2) element.

[2] https://directory.eoportal.org/web/eoportal/satellitemissions/m/metop-sg

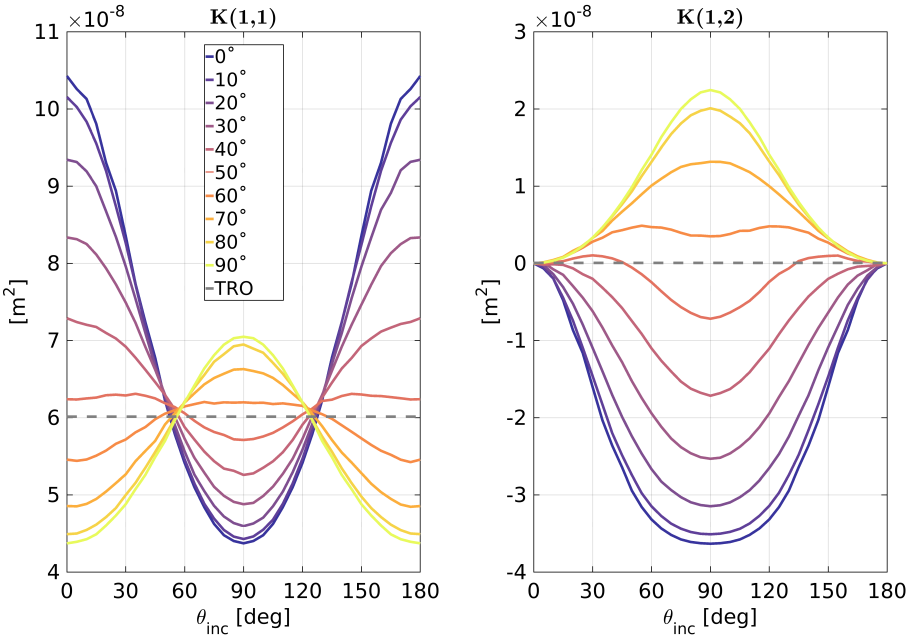

Figure 4.11.: The (1, 1) and the (1, 2) elements of the extinction matrix of an azimuthally randomly oriented hexagonal plate (Hong plate, Id 9) of the database with size parameter $x = 1$ as a function of the incidence angle for different β angles are shown for a frequency of 175 GHz. The different colors indicate the different β angles and the dashed grey line indicate the corresponding value for a totally randomly oriented particle.

5. Database specifications

An overview of the database specifications is given in Tables 5.1/5.3 and Table 5.5 for totally and azimuthally random orientation, respectively. In Table 5.2 and 5.4, figures of each habit are available. Detailed information on each habit is available in Appendix D. To summarize, scattering data are provided for 34 frequencies spanning from 1 GHz to 886.4 GHz. For frozen (liquid) hydrometeors, data is provided for three (five) temperatures from 190 to 270 K (230 to 310 K). Refractive index models used are *Mätzler* (2006) for ice and *Ellison* (2007) for liquid water. Currently, a total of 34 habits in totally random orientation are included as well as one habit additionally in azimuthally randomly orientation on 10 tilt angles over the range of 0-90°.

5.1. Scattering properties

As discussed in Section 2.1, only the scattering matrix ($\mathbf{Z}$), the absorption vector ($\mathbf{a}$) and the extinction matrix ($\mathbf{K}$) are required to fully characterise the single scattering properties in a general manner (including polarimetric data). Any other variable (backscattering coefficient, asymmetry parameter, etc.) can be calculated from these variables. Therefore, we have decided to only store $\mathbf{Z}$, $\mathbf{K}$ and $\mathbf{a}$ in the database. Routines for extracting other parameters, specifically such required by RTTOV, are provided by the database interfaces (see Chapter 7).

The scattering properties are defined on angular grids, both for incidence and scattered radiation (Table 5.6 specifies the general dependencies). For totally random and azimuthally random orientation, symmetries can be used to reduce the number of stored elements, both in terms of angular dimensions as well as in number of independent matrix and vector elements (for details see *Mishchenko et al.*, 2002). Table 5.7 displays the dimensions and number of elements of each of the scattering variables for the respective orientation type as they are stored in the database.

5.2. Habits

All habits included in the database are listed in Table 5.1. This database makes several distinctions between habits. At first, distinctions are made regarding the phase of the particle, i.e. if it is *ice*, *liquid* or *melting* (melting means both ice and liquid present). Ice particles are further distinguished regarding their aggregation type, i.e. whether the given particle is a *single crystal* or an *aggregate*. This is, e.g. important when considering what size range should be applied to the habit (more on this in Section 5.6). Furthermore, ice particles are divided into groups of *pristine* and *rimed* particles. Habits employing

Table 5.1.: Database specifications for totally random orientation. Continued in Table 5.3. Habits marked with * are calculated using Mie theory. The last column displays the software or source used to created the shape data of the given habit, with abbreviations being RSP (Recreated Shape Data), RC (RimeCraft), SFTK (SnowFlake Tool-Kit) and ESP (External Shape Data).

Source:	Chalmers University of Technology, University of Hamburg.
Products provided:	Scattering matrix **Z**, absorption vector **a**and extinction matrix **K**.
Orientation:	Totally random.
Frequencies [GHz]:	1, 1.4, 3, 5, 7, 9, 10, 10.65, 13.4, 15, 18.6, 24, 31.3, 31.5, 35.6, 50.1, 57.6, 88.8, 94.1, 115.3, 122.2, 164.1, 166.9, 175.3, 191.3, 228, 247.2, 314.2, 336.1, 439.3, 456.7, 657.3, 670.7, 862.4, 886.4
Temperatures (ice) [K]:	190, 230, 270
Temperatures (liquid) [K]:	230, 250, 270, 290, 310
Refractive index of ice:	*Mätzler* (2006, Eq.(5.30) for all temperatures)
Refractive index of water:	*Ellison* (2007)
Computational method:	DDA, software: ADDA (*Yurkin and Hoekstra*, 2011). Mie theory*, software: Matlab Mie code (*Mätzler*, 2002).

Habits	Id	$D_{\max}$ [μm]	D_{veq} [μm]	No. of sizes	α	β	Software used
Ice:							
Single crystals:							
Pristine:							
Plate type 1 (3.3.2)	9	13 – 10,000	10 – 2,596	45	0.76	2.48	RSP
Column type 1(3.3.2)	7	14 – 10,000	10 – 1,815	45	0.037	2.05	RSP
Thin Plate (3.3.2)	16	25 – 5,059	10 – 2,000	35	30	3.00	RSP
Thick Plate (3.3.2)	15	16 – 3,246	10 – 2,000	35	110	3.00	RSP
Block Column (3.3.2)	12	13 – 2,632	10 – 2,000	35	210	3.00	RSP
Short Column (3.3.2)	13	17 – 3,303	10 – 2,000	34	110	3.00	RSP
Long Column (3.3.2)	14	24 – 4,835	10 – 2,000	35	34	3.00	RSP
Sector Snowflake (3.3.2)	3	20 – 12,000	20 – 1,415	34	0.00081	1.44	RSP
Ice Sphere* (3.2.4)	24	1 – 50,000	1 – 50,000	200	480	3.00	Mie
ICON Cloud Ice (3.2.4)	27	13 – 10,000	10 – 2,929	45	1.6	2.56	RC
GEM Cloud Ice (3.2.4)	31	10 – 3,088	10 – 3,000	45	440	3.00	RC
6-Bullet Rosette (3.3.2)	6	16 – 10,000	10 – 2,371	45	0.48	2.42	RSP
5-Bullet Rosette (3.2.2)	2	17 – 10,000	10 – 2,231	45	0.4	2.43	SFTK
Perpendicular 4-Bullet Rosette (3.2.2)	10	18 – 10,000	10 – 2,071	45	0.32	2.43	SFTK
Flat 4-Bullet Rosette (3.2.2)	11	18 – 10,000	10 – 2,071	45	0.32	2.43	SFTK
Perpendicular 3-Bullet Rosette (3.2.2)	4	19 – 10,000	10 – 2,137	45	0.44	2.47	SFTK
Flat 3-Bullet Rosette (3.2.2)	5	20 – 10,000	10 – 1,882	45	0.2	2.43	SFTK

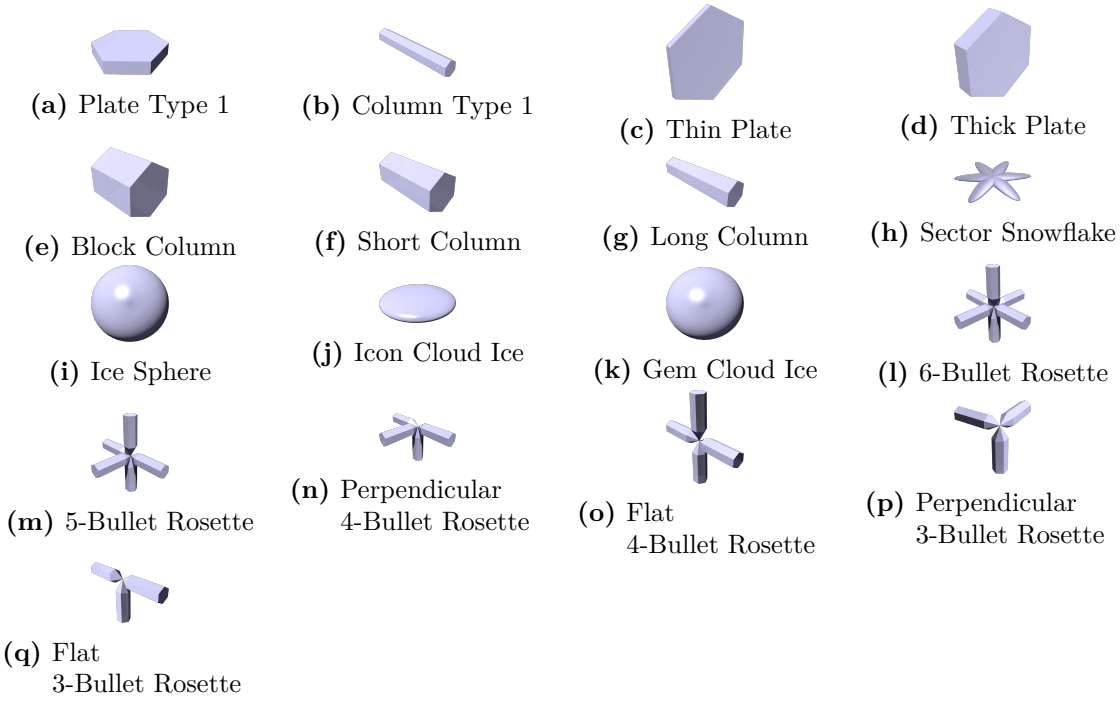

(a) Plate Type 1 **(b)** Column Type 1 **(c)** Thin Plate **(d)** Thick Plate

(e) Block Column **(f)** Short Column **(g)** Long Column **(h)** Sector Snowflake

(i) Ice Sphere **(j)** Icon Cloud Ice **(k)** Gem Cloud Ice **(l)** 6-Bullet Rosette

(m) 5-Bullet Rosette **(n)** Perpendicular 4-Bullet Rosette **(o)** Flat 4-Bullet Rosette **(p)** Perpendicular 3-Bullet Rosette

(q) Flat 3-Bullet Rosette

Table 5.2.: Single crystal habit figures.

different types of orientation, *totally random* and *azimuthally random* are essentially treated as different habits as well.

The database includes habits developed by us (Chalmers) and from third party sources. Some of the third party habits, mostly single crystals, could be re-created by us based on their specifications in literature. For several third-party aggregates, original shape data had to be used (see Section 3.3 for details and Section 5.6 for the effects on particle size gridding).

From the single crystals created by us, the 5-bullet rosettes have been designed so that the bullets follow the same mass-size relationship as the Hong bullet rosette, but with different arm configurations. The flat versions have all bullets lying in the same plane, while the perpendicular ones have one or multiple arms oriented perpendicular to that "base" plane. Also included as single crystals are the ICON and GEM cloud ice habits, modelled by spheroids, designed to follow specific preset mass-size relationships (see Section 3.2.3). Ice and liquid spheres have been included as well for completeness using Mie theory (Section 4.2).

Our aggregate habits have been generated using the snowflake tool-kit and RimeCraft. Six types of aggregates were generated using the snowflake tool-kit assuming constituent crystals being either hexagonal plate, block (column of aspect ratio 1.25) or column crystals. For each crystal assumption, there is a version with small and with large constituents, created using different scaling of the output particles (see Section 3.2.1). Furthermore, four habits were generated using RimeCraft assuming preset mass-size

Table 5.3.: Database specifications for totally random orientation continued. Habits marked with * are calculated using Mie theory.

Habits	Id	$D_{\max}$ [μm]	D_{veq} [μm]	No. of sizes	α	β	Software used
Aggregates:							
Pristine:							
Evans Snow Aggregate (3.3.1)	1	32 – 11,755	50 – 2,506	35	0.20	2.39	ESP
Tyynelä Dendrite Aggregate (3.3.1)	26	595 – 20,826	228 – 3,328	35	0.10	2.25	ESP
8-Column Aggregate (3.3.2)	8	19 – 9,714	10 – 5,000	39	65	3.00	RSP
Small Column Aggregate (3.2.1)	17	105 – 3,855	37 – 738	35	0.14	2.45	SFTK
Large Column Aggregate (3.2.1)	18	368 – 19,981	128 – 3,021	35	0.25	2.43	SFTK
Small Block Aggregate (3.2.1)	21	100 – 7,328	72 – 1,665	35	0.21	2.33	SFTK
Large Block Aggregate (3.2.1)	22	349 – 21,875	253 – 4,607	35	0.35	2.27	SFTK
Small Plate Aggregate (3.2.1)	19	99 – 7,054	53 – 1,376	35	0.077	2.25	SFTK
Large Plate Aggregate (3.2.1)	20	349 – 22,860	197 – 4,563	34	0.21	2.26	SFTK
ICON Hail (3.1.2)	30	120 – 5,349	94 – 5,000	35	380	2.99	RC
ICON Snow (3.1.2)	28	120 – 20,000	94 – 3,219	35	0.031	1.95	RC
GEM Hail (3.1.2)	29	120 – 5,031	94 – 5,000	35	540	3.02	RC
GEM Snow (3.1.2)	32	170 – 10,459	94 – 5,000	35	24	2.86	RC
Rimed:							
Spherical Graupel (3.2.1)	23	622 – 9,744	454 – 5,293	30	13	2.69	SFTK
ICON Graupel (3.1.2)	29	170 – 6,658	94 – 5,000	35	390	3.13	RC
GEM Graupel (3.1.2)	33	120 – 6,597	94 – 5,000	35	170	2.96	RC
Liquid:							
Single crystals:							
Pristine:							
Liquid Sphere* (3.2.4)	25	1 – 50,000	1 – 50,000	200	480	3.00	Mie

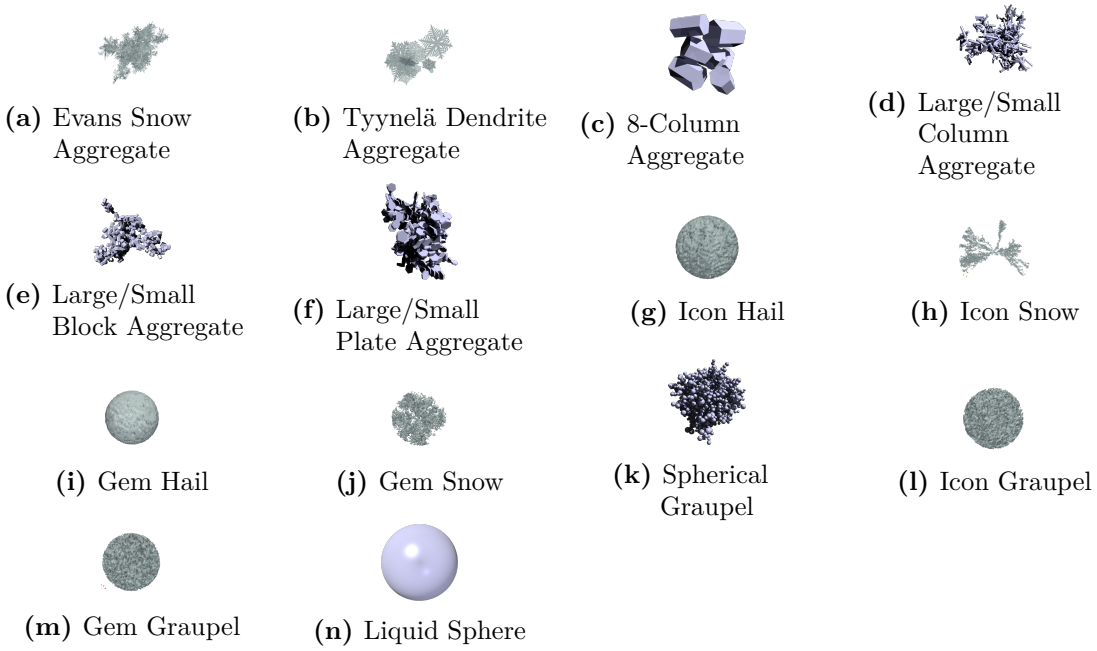

(a) Evans Snow Aggregate

(b) Tyynelä Dendrite Aggregate

(c) 8-Column Aggregate

(d) Large/Small Column Aggregate

(e) Large/Small Block Aggregate

(f) Large/Small Plate Aggregate

(g) Icon Hail

(h) Icon Snow

(i) Gem Hail

(j) Gem Snow

(k) Spherical Graupel

(l) Icon Graupel

(m) Gem Graupel

(n) Liquid Sphere

Table 5.4.: Aggregate habit figures. The liquid sphere has been included also.

relationships (see Section 3.2.3). These are the ICON hail and snow and the GEM hail and snow habits. While hail is technically not an aggregate, it has been included here because we consider hail to have roughly the same size characteristics as aggregates in general. Lastly, three habits that can be considered rimed have been included as well, being the spherical graupel (snowflake tool-kit) and the ICON and GEM graupel (RimeCraft) habits.

5.3. Orientation

Two different particle orientation cases are considered:

- Totally random: Every possible orientation is equally probable, i.e. the scattering properties are integrated over all angles. The particles have effectively a spherical symmetry.
- Azimuthally random: The particles have no preferred azimuthal orientation, but a specific orientation w.r.t. local horizon. A reference plane is defined for each particle, and the angle between this plane and the horizontal plane is denoted as the tilt angle.

More details about the orientations in general are available in Section 2.3 and about the calculation of SSP of azimuthally randomly oriented particles in Appendix A. Table 5.7 summarizes the angular grid dependencies and number of independent elements in the SSP matrices for each of the orientation types.

Table 5.5.: Database specifications for azimuthally random orientation.

Source:	Chalmers University of Technology, University of Hamburg.
Products provided:	Scattering matrix **Z**, absorption vector **a**and extinction matrix **K**.
Orientation:	Azimuthally random
Tilt angles [°]:	0, 10, 20, 30, 40, 50, 60, 70, 80, 90
Frequencies [GHz]:	1, 1.4, 3, 5, 7, 9, 10, 10.65, 13.4, 15, 18.6, 24, 31.3, 31.5, 35.6, 50.1, 57.6, 88.8, 94.1, 115.3, 122.2, 164.1, 166.9, 175.3, 191.3, 228, 247.2, 314.2, 336.1, 439.3, 456.7, 657.3, 670.7, 862.4, 886.4
Temperatures [°C]:	190, 230, 270
Refractive index of ice:	*Mätzler* (2006, Eq.(5.30) for all temperatures)
Computational method:	DDA, software: ADDA (*Yurkin and Hoekstra*, 2011).

Habits	Id	$D_{\max}$ [μm]	D_{veq} [μm]	No. of sizes	α	β	Software used
Ice:							
Single crystals:							
Pristine:							
Plates type 1 (3.3.2)	9	13 – 10,000	10 – 2,596	51	0.76	2.48	RSP

Totally random orientation SSP require the least resources in terms of storage and computational power, and are thus calculated for all habits considered. Azimuthally random orientation is so far only considered for one plate habit, the "Plate type 1".

5.3.1. Totally randomly oriented particles

Since totally randomly oriented particles effectively possess spherical symmetry, their extinction and absorption are independent of direction, i.e. only a single value is required (per frequency, temperature, and size). The angular dependence of the scattering matrix is fully described over a single angular grid in terms of the scattering angle. For the particles in the database, the scattering angle grid is not fixed, but varies, mainly with size parameter (higher size parameters result in more complicated scattering patterns, hence require a higher number of angle grid points to be properly described), ranging from 181 to 721 equidistant angles.

5.3.2. Azimuthally randomly oriented particles

Azimuthally randomly oriented particles have been calculated for tilt angles β with a 10° resolution. For particles symmetric to the x-y-plane, e.g. hexagonal plates as used here, only β between 0° and 90° are required, and SSP for larger β can be derived from their symmetry equivalents at $180° - \beta$.

As the azimuthally randomly oriented particles effectively possess cylindrical symmetry, extinction and absorption are only dependent on polar incidence angle, and the scattering matrices in addition to the incidence and scattered polar angles depend only

Table 5.6.: Database single scattering properties, and their dimensions, dependencies, and number of independent elements in the general case.

Variable	Symbol	Size	Dependencies	Indep. Elem.
Scattering matrix	$\mathbf{Z}$	[4,4]	ψ_{inc}, ω_{inc}, ψ_{sca}, ω_{sca}	16
Extinction matrix	$\mathbf{K}$	[4,4]	ψ_{inc}, ω_{inc}	7
Absorption vector	$\mathbf{a}$	[4]	ψ_{inc}, ω_{inc}	4
Incidence polar angle	ψ_{inc}	$N_{\psi_{inc}}$		
Incidence azimuthal angle	ω_{inc}	$N_{\omega_{inc}}$		
Scattering polar angle	ψ_{sca}	$N_{\psi_{sca}}$		
Scattering azimuthal angle	ω_{sca}	$N_{\omega_{sca}}$		

on the azimuth angle difference between incident and scattered direction, not the incident and scattered azimuths themselves.

In the database, SSP are provided with polar incidence angle ψ_{inc} ranging from 0° to 180° with a 5° spacing resulting in 37 incidence angles per tilt angle β. The scattering matrix elements $\mathbf{Z}_{ij}$ are expanded as spherical harmonics series with varying length per matrix element and particle, see Appendix A. By using the database interface, data for any desired scattering direction can be (re)derived.

5.4. Frequencies

The strategy regarding frequencies is to cover each channel/band by two frequencies placed at each end of the channel/band (see Fig. 5.1 for an illustration of frequency coverage). The used frequencies with associated instrument and channel Id are reported in Table 5.8. A total of 22 frequencies have been selected to cover MWS, MWI and ICI. Additional frequencies have been included facilitating current and envisioned near-future data assimilation channels (i.e. with RTTOV in mind, suggested by A. Geer), standard (ground-based and satellite) radar frequencies as well as ISMAR and IceCube. In total, the database covers 34 frequencies.

Table 5.7.: Dependencies and number of independent elements as stored in the database in case of totally randomly (TRO) and azimuthally randomly (ARO) oriented particles. Θ denotes the scattering angle (see Eq. A.51), and $\Delta\omega = \mathrm{abs}\,(\omega_{inc} - \omega_{sca})$.

Variable	TRO		ARO	
	Dependencies	Indep. Elem.	Dependencies	Indep. Elem.
$\mathbf{Z}$	Θ	6	ψ_{inc}, ψ_{sca}, $\Delta\omega$	16
$\mathbf{K}$	-	1	ψ_{inc}	3
$\mathbf{a}$	-	1	ψ_{inc}	2

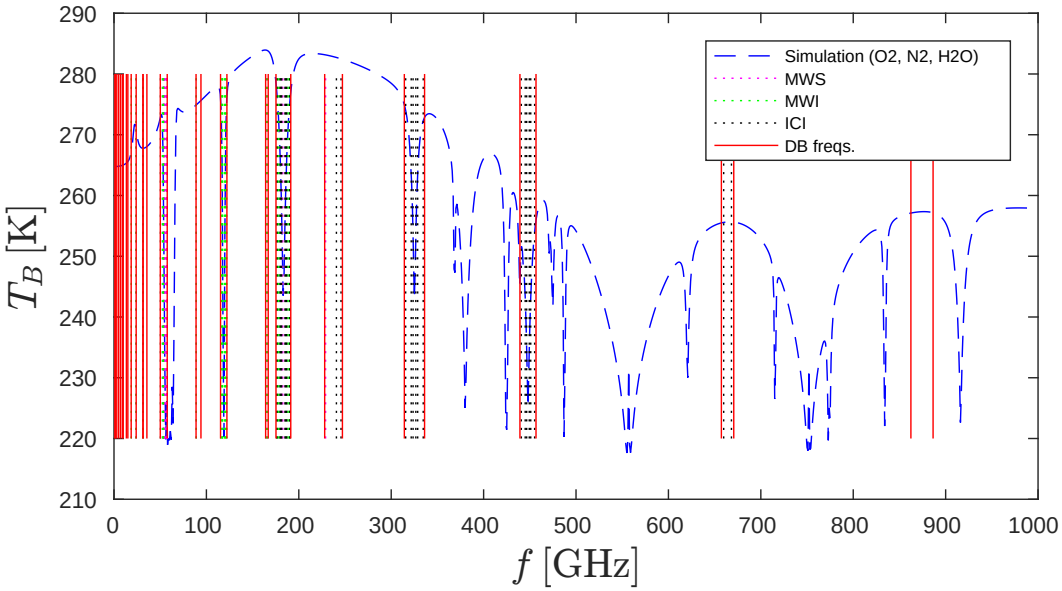

Figure 5.1.: Overview of database (DB) frequencies, along with employed ICI, MWI and MWS channels.

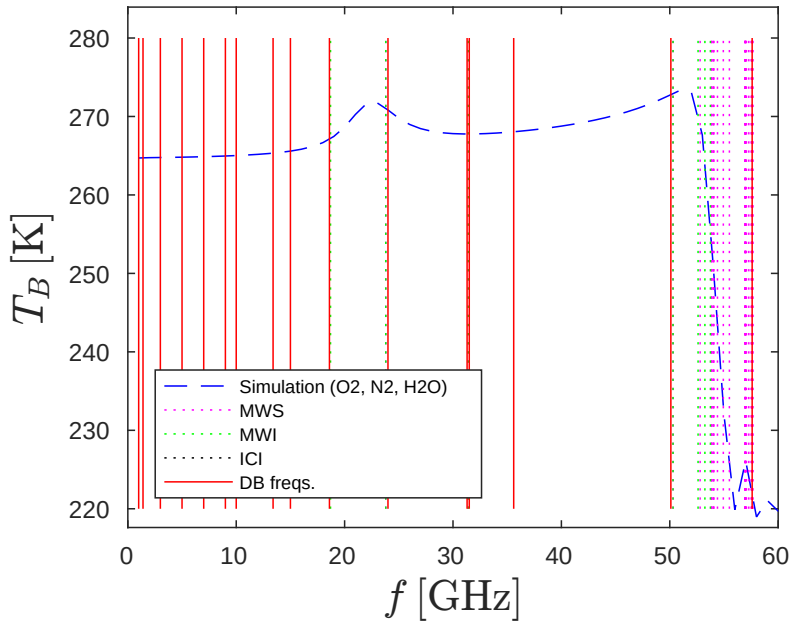

Figure 5.2.: As Fig. 5.1 but zoomed in on the lower frequency part of the database spectrum.

Table 5.8.: Database frequency set and how they cover measurement channels of target sensors.

Frequ.	18.6	31.3	50.1	88.8	115.3	164.1	175.3	228.0	314.2	439.3	657.3
(GHz)	24.0	31.5	57.6	94.1	122.2	166.9	191.3	247.2	336.1	456.7	670.7
MWS	1	2	3-16	17		18	19-23	24			
MWI	1-2	3	4-7	8	9-12	13	14-18				
ICI							1-3	4	5-7	8-10	11

Other frequencies:	
ISMAR, IceCube [GHz]:	862.4, 886.4
Geer [GHz]:	1.4, 7, 10.65
Other [GHz]:	1, 3, 5, 9, 10, 13.4, 15

5.5. Refractive index and temperature grid

The refractive index of solid and liquid water can be described accurately as a function of frequency and temperature only. Scattering data are provided on frequency and temperature grids, rather than on a refractive index grid.

The refractive index of ice is calculated using the parametrisation of *Mätzler* (2006) (using the MATLAB implementation, see Sec. 2.4) for temperatures

$$T_{\text{ice}} = [190, 230, 270]\,\text{K}. \tag{5.1}$$

For liquid water, the parametrisation by *Ellison* (2007) was chosen. The provided liquid sphere data can be used for cloud liquid droplets to drizzle and rain, i.e. requiring temperature coverage above, at and below the melting point. Since liquid water refractive indices are varying stronger with temperature than those of ice (and because SSP calculations for spheres using Mie theory are easily affordable), a finer grid has been chosen:

$$T_{\text{liq}} = [230, 250, 270, 290, 310]\,\text{K}. \tag{5.2}$$

5.6. Particle size selection

Defining a size grid is in general not as straightforward as, e.g. a frequency or temperature grid grid. This is due to that the relevance of sizes is driven by their size parameter, which in turn varies with frequency, the natural occurrence of habits at certain sizes, etc. This is furthermore due to that, depending on the tools the particle shape data is created with, the exact sizes of the particles can not be completely controlled and arbitrary sizes can not always be achieved. Hence, instead of defining one general size grid, we developed and applied general guidelines and methodologies for selecting sizes instead. These guidelines involve definition of size ranges to be covered (see Section 5.6.1) and constructing size grids following certain patterns (see Sections 5.6.2, 5.6.3 and 5.6.4 for single crystals, aggregates and external shape data habits, respectively). In addition to

that, the methodology for selecting size grids has evolved during the study resulting in some deviations form the general guidelines even for habits fully controllable by us. The number of included sizes for all habits is at least 30, but is typically 35 for aggregates and 45 for single crystals. Also, we ensure that a habit follows the size-mass relationship as given by Eq. 2.25.

5.6.1. Size ranges

When defining size ranges, we consider the parameters D_{max}, D_{veq} and x (see Section 2.5). For each of the three parameters, we have defined target size ranges, which we fulfil to as high extent as possible. In general, the target size limit that is met first determines the extend of the produced data, and if possible one size grid point equal or exceeding the limit is included.

The size ranges are different for aggregates and single crystals considering the fact that single crystals in general appear at smaller sizes than aggregates. This means that single crystals are designed with smaller maximum sizes than aggregates, while aggregates have larger minimum sizes compared to single crystals. Aggregate minimum sizes are furthermore determined by the size of their constituent crystals; the smallest aggregate can simply not be smaller then a single constituent crystal.

Table 5.9 shows the target size ranges for aggregates and single crystals, respectively. A given habit is not required to completely cover both the D_{veq} and D_{max} ranges, it is enough that one of the limits is met. For example, the habit labelled "Column type 1" (Table 5.1) does not go up to 3 mm in D_{veq}, however it does reach the D_{max} limit of 10 mm. Whether it is the D_{veq} or D_{max} limit that is reached first depends on how the particle grows with size (i.e. its α and β coefficients). Dense particles tend to be constrained by the D_{veq} range, while fluffy or high aspect-ratio particles are constrained by the D_{max} range. The size ranges for specific habits are displayed in Table 5.1.

Table 5.9.: Overview of targeted size ranges for aggregates and single crystals.

	Aggregates		Single crystals	
	min	max	min	max
D_{max}	100 μm	20 mm	10 μm	10 mm
D_{veq}	100 μm	50 mm	10 μm	30 mm
x	-	10	-	10

The scattering properties themselves are largely determined by the size parameter x, which is a function of size and frequency (see Eq. 2.23). For differing reasons, SSP for extreme x are not required (see Fig. 5.3 for an example). As particles with large x are computationally demanding, an upper limit of x is desirable. The size parameter limit was set to $x = 10$. Note that this results in frequency dependent upper limits, that is that the size ranges given in Tables 5.1 – 5.5 are filled with SSP up to different maximum sizes for different frequencies.

As a final disclaimer, there are habits for which the targeted size ranges are not met. In specific, the small constituent crystal aggregate habits (Id 17, 19, and 21 in

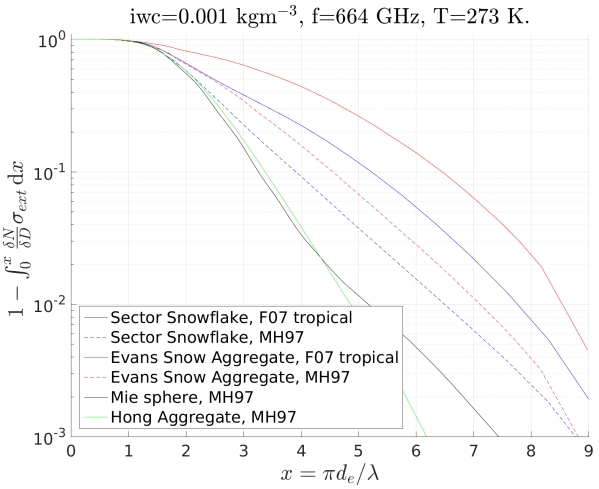

Figure 5.3: "Tail distribution" of extinction cross section weighted by particle size distribution. Frequency is 664 GHz, ice water content is 1 gm^{-3} and temperature is 273 K. The figure exemplifies the relative error if the integral giving bulk extinction is cut at a given x. For example, cutting the integral at $x = 8.5$ gives an error below 1 % for all combinations of habit and particle size distribution included.

Table 5.3), are of relatively small sizes. As discussed in Section 3.2.1, the aggregate simulations could not generate particles large enough when assuming 100 μm crystals, hence additional versions with scaled-up crystals were produced as a compensation (i.e. the large aggregate habits). However, scaling up the particles in this way means that the smallest size available for that habit also increases. Furthermore, the single crystals, with Id 12 to 16 (recreated from the database by *Liu*, 2008), do not fulfil the 3 mm D_{veq} target limit. This is due to that the target maximum $D_{\mathrm{veq}}$was only set to 2 mm in the beginning of the study, and additional sizes have not been added retroactively because of time restraints and the low priority of these habits.

5.6.2. Single crystal size grids

For single crystals we in general have a high degree of control in designing the size grid, since the habits have clear geometric definitions. We chose to use an equidistant linearly grid for D_{veq} of 10 – 100 μm with a spacing of 10 μm and a logarithmic one for $D_{\mathrm{veq}} > 100\,\mu$m.

There are some exceptions to the above. The liquid and ice sphere habits are calculated using Mie theory, hence it is inexpensive to derive their SSP for a larger number of sizes. For them, the grid was chosen to have a logarithmic spacing with 200 grid points over $D_{\mathrm{veq}} = 1\,\mu\mathrm{m} - 50\,\mathrm{mm}$.

5.6.3. Aggregate size grids

For aggregates, a logarithmic grid is used over the whole size span. Selecting a grid for aggregates is not straight-forward, since the aggregation model (see Section 3.1.1) produces shapes of arbitrary sizes. Therefore, approximate methods have to be used. Our procedure for selecting shapes given a simulation data set is as following:

1. Determine the α and β-coefficients of the set of shape data available for the habit by fitting $\log m = f(\log D_{\mathrm{max}}) = \beta \log D_{\mathrm{max}} + \log \alpha$ using linear least-squares fitting.

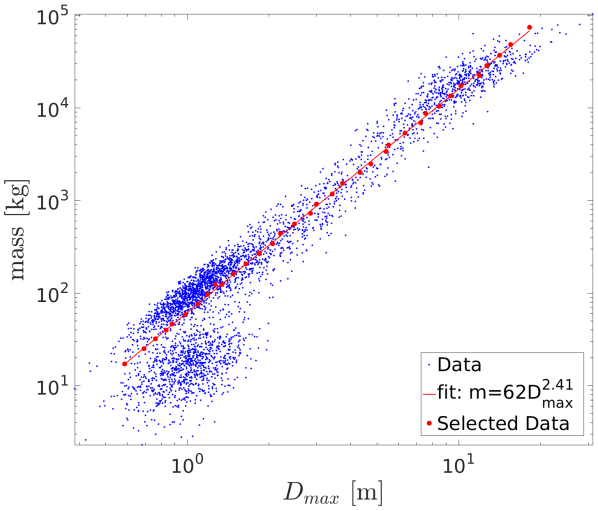

Figure 5.4: An example of the size selection procedure for aggregates. Blue dots represent output from the aggregation model, the red line a fit of the mass-size power law (axes are logarithmic). The red dots are the selected particles, 35 in total, which are both close to the line and form a logarithmic grid.

2. Select all particles that are close to this line within a certain tolerance. The tolerance used varies from case to case, but is usually not selected larger than 5 %.

3. Select N sizes from the remaining particles, such that a logarithmic grid is achieved as closely as possible. The size range used is determined by the rules presented in Section 5.6.1 and Table 5.9. Typically, $N = 35$ was chosen.

The selection procedure is visualized in Fig. 5.4.

5.6.4. External shape data size grids

For external shape data, the size ranges are determined by the sizes associated with the available shape data. We make use of the full range of sizes available. Regarding size selection, we follow the selection rules as laid out for our own aggregates. For the Evans snow aggregate, 35 out of the 95 available particles are selected forming an approximately logarithmic grid. The number of available shape models of the Tyynelä dendrite aggregate is sufficiently high, that the same selection process as for our own aggregates can and is applied, and 35 particles forming a logarithmic size grid were selected.

6. Database infrastructure

This chapter describes the internal structure of the database. This information is included for completeness. The standard user should not need to care about these details, but instead extract data using the interfaces described in the next chapter.

6.1. Data format

The netCDF4 format is used to store the scattering data. The data are sorted into separate .nc-files, one for each habit, orientation and size combination. Furthermore, there is an internal folder structure in each .nc-file, with one folder for each temperature and frequency. Table 6.1 summarizes the dimensions, variables and attribute fields included in each of the netCDF4-folders. The data are divided into three groups: `SingleScatteringData` which contains scattering variables listed in Section 5.1, `ShapeData` containing meta data regarding shape, and `CalculationData` containing log data related to the computational aspects. In Appendix B an example print-out of the data format is displayed.

As mentioned in Section 5.1, we make use of scattering matrix symmetries to reduce the amount of stored matrix elements. Same principle applies for the extinction matrix and absorption vector. For example, the scattering matrix data are stored in the variable `PhaMat_data` as an tensor with angle grids and the number matrix elements as dimensions, in total 5 dimensions (`aa_scat`, `za_scat`, `aa_inc`, `za_inc` and `phaMatElem`). For totally random orientation, there is only 6 unique and non-zero elements, i.e. length dimension `phaMatElem` = 6. To relate the stored data to the full Scattering matrix one uses the variable `phaMat_index` which is a four by four matrix, where the elements are index numbers corresponding to a stored value in `PhaMat_data`. As an example, for random orientation, the matrix is (*Mishchenko et al.*, 2002):

$$\texttt{PhaMat\_data} = \begin{pmatrix} 1 & 2 & 0 & 0 \\ 2 & 3 & 0 & 0 \\ 0 & 0 & 4 & 5 \\ 0 & 0 & -5 & 6 \end{pmatrix} \tag{6.1}$$

Negative values indicate that the element is multiplied by -1. Corresponding system applies for the absorption vector and extinction matrix.

Global:	
Attributes:	date, version
Groups:	
SingleScatteringData:	
Attributes:	orient_type.
Dimensions:	aa_scat, za_scat, aa_inc, za_inc, scatMat_row, scatMat_col, phaMatElem, extMatElem, absVecElem.
Variables:	frequency, temperature, aa_scat, za_scat, aa_inc, za_inc, phaMat_index, extMat_index, absVec_index, phaMat_data, extMat_data, absVec_data.
ShapeData:	
Attributes:	description, source, refrIndex_model, habit_file_id, habit_id, phase, refrIndex_homogenous_bool, density_homogenous_bool.
Variables:	diameter_max, diameter_vol_eq, diameter_area_eq_aerodynamical, mass, dpl, N_dipoles, refrIndex_real, refrIndex_imag, alpha, beta, gamma.
CalculationData:	
Attributes:	method, software, ADDA_version, system, n_nodes, n_cores, date_completion, ADDA_eps, ADDA_avgParam_file, ADDA_scatParam_file.

Table 6.1.: Summary of the data format for storage of SSP database entries.

6.2. Folder structure

6.2.1. Single scattering data

The levels represent the different aspect of a given SSD entry. Some of the levels are constrained to just a few allowed variants (such as phase), in which case those variants are given in below list. Other levels can vary limitlessly (such as mass), in which case there is a specific format for identification. The hierarchy order, and the allowed variants and formats are as follows:

1. Orientation

   `TotallyRandom`

   `AzimuthallyRandom`

2. Phase:

   `Ice`

Liquid

Melting

3. Aggregation level

   Aggregates

   SingleCrystals

4. Degree of riming

   Pristine

   Rimed

5. Habit type

   %s_Id%d (habit name, habit Id number)

6. Orientation

   TotallyRandom

   AzimuthallyRandom_beta%05.1fdeg (particle tilt angle β [°])

7. Particle size (data files)

   Dmax%05.0fum_Dveq%05.0fum_Mass%011.5ekg.nc (maximum diameter [μm], volume equivalent diameter [μm], mass [kg])

8. Frequency and temperature (internal netCDF folders)

   Freq%08.3fGHz_T%06.2fK (frequency, temperature)

Note that the formatting syntax is from MATLAB[1].

The orientation type occurs at both level 1 and 6. The reason for this is that the data size for the azimuthally oriented scattering data is significantly larger compared to totally randomly oriented data. The user may not be interested in the oriented particles, and can therefore choose to only import or download the random data. However, a division on orientation at level 6 is still appropriate since the tilt angle is a continuous variable. At the fifth level (Habit type), there is overview data available in several files. These are:

- report.pdf: Automatically generated documentation on the habit and SSP properties.Global:

- DataSummary.txt: Summary data available in the .txt-files for easy reading by software. One summary file is available for each orientation and habit combination.

- shape_img.png: Image depicting the specific habit.

[1] https://se.mathworks.com/help/matlab/matlab_prog/formatting-strings.html

As an example, a snapshot of the folder structure:

```
SSD
├── TotallyRandom
│   └── Ice
│       ├── Aggregates
│       │   └── Pristine
│       │       └── HongAggregate_Id8
│       │           ├── TotallyRandom
│       │           │   ├── Dmax02528um_Dveq01301um_Mass1.05758e-06kg.nc
│       │           │   └── Dmax02889um_Dveq01487um_Mass1.57881e-06kg
│       │           ├── ...
│       │           ├── report.pdf
│       │           ├── DataSummary.txt
│       │           └── shape_img.png
│       └── SingleCrystals
│           └── ...
├── AzimuthallyRandom
└── ...
```

6.2.2. Input data

The input folder contains the necessary input data to initiate the ADDA simulations available in the database. This includes shape data and ADDA specific files such as `avg_params.dat` and `scat_params.dat`. The structure at the top looks like:

```
Input
├── Shapes
│   └── Ice
│       ├── Aggregates
│       │   └── Pristine
│       │       └── HongAggregate_Id8
│       │           ├── Dmax00341um_Dveq00175um_Mass2.59444e-09kg
│       │           │   _Freq0887.000GHz.adda
│       │           └── Dmax00341um_Dveq00175um_Mass2.59444e-09kg
│       │               _Freq0887.000GHz.meta.mat
│       └── SingleCrystals
├── AddaFiles
│   ├── avg_params
│   │   ├── avg_params_eps2.dat
│   │   └── ...
│   └── scat_params
│       ├── scat_params_deg1.dat
│       └── ...
```

The shapes-folder structure is mirrored from the SSD-folder in Section 6.2.1, but with ADDA shape files and accompanying .mat-files with meta data at the bottom. The

naming format for these are

- ADDA shape file:

  `Dmax%05.0fum_Dveq%05.0fum_Mass%011.5ekg_Freq%08.3fGHz.adda` (maximum diameter [μm], volume equivalent diameter [μm], mass [kg], frequency [GHz])

- Shape meta file:

  `Dmax%05.0fum_Dveq%05.0fum_Mass%011.5ekg_Freq%08.3fGHz.mat` (maximum diameter [μm], volume equivalent diameter [μm], mass [kg], frequency [GHz])

The frequency value is here a measure of the dipole density. A value of 457 GHz means that only DDA simulations with frequencies up to 457 GHz will fulfil the standard criterion in Eq. (4.1). As stated in Section 6.2.2, 5 sampling frequencies will be used (192.0000, 337.0000, 457.0000, 671.0000 and 887.0000 GHz). The meta files includes various meta data such as D_{max} D_{veq} number of dipoles, etc.

Also stored are the rest of the ADDA files such as `avg_params.dat` and `scat_params.dat` (see Section 4.1.1).

7. Database interfaces

As described in the previous chapter, the data are stored using a multi-level folder and file structure, but users do not need to interact with this structure directly. Instead, data can be browsed, extracted, and converted to parameters and formats required for use in forward models through function sets provided with the data. Each function set is denoted as a database interface.

The main tasks of the database interfaces are to provide functionality to:

- Explore the content of the database.
- Extract selected data (habits, orientations, sizes, frequencies, etc.) from the database, and compile it into a more compact data format.
- Interpolate data in temperature, frequency, size, angles.
- Prepare habit mixes and size distribution convolved SSP.
- Conversion to SSP formats as used by forward models.

Interfaces have been implemented both in MATLAB and in Python. Core parts of these two interfaces have been designed such that functionality and usage is identical as far as possible (considering the individual design of each of these programming languages). However, the Python interface is treated as the main one, and some special features are only at hand by this interface.

Details and specifics of both interfaces are presented in Sections 7.1 and 7.2. An overview of the functions available is given in Appendix C.1. Some basic usage examples are shown in Appendix C.2. It shall be noted that functions of both interfaces use the languages' documentation infrastructure. Hence, we skip a detailed description of each individual function.

Functionality to extract SSP for use in forward models is so far restricted to the ARTS and RTTOV-SCATT models. For ARTS SSP extraction, a demo script (`demo_ssp4arts`) is available in each of the interfaces. The RTTOV-SCATT interface module is exclusively available through the Python interface. A detailed description is provided in Section 7.3.

The interface-internally used format is ARTS-like, i.e. holds the single scattering properties in the form of $\mathbf{Z}$, $\mathbf{K}$, and $\mathbf{a}$ and in dependency of frequencies and temperatures. All other SSP parameters can be and are derived from this format, and this conversion is typically part of the extraction of SSP in a forward model dedicated format (e.g. of the RTTOV-SCATT interface module).

As detailed in Section 4.1.3 and Appendix A, $\mathbf{Z}$ of azimuthally randomly oriented particles are stored in the database in the form of Spherical Harmonics. For conversion

to ARTS format, and possible other forward model SSP formats,[1] these need to be "unpacked" into the scattering matrix over discrete angle grids. This conversion is only available through the Python interface and additionally requires the SHTns library to be installed.[2]

7.1. MATLAB

The MATLAB interface to the scattering database is located in the `Matlab` subfolder of the database `DataInterfaces` folder. Following MATLAB standards, it holds each interface function in a separate MATLAB file with the same name as the function itself. For an overview and short description of the available functions see Appendix C.1.

The interface should work with any relatively recent MATLAB version. Storing data into files suitable as input to the ARTS forward model requires that the Atmlab package is installed and added to MATLAB's search path.

The above mentioned Atmlab is a collection of MATLAB functions for interaction with ARTS-2. It contains, for example, routines for reading and writing of ARTS XML files, Mie calculations, parametrisations of hydrometeor dielectric properties and particle size distributions (PSDs), atmospheric retrievals, generating atmospheric scenarios. Beside the PSD functionality, of interest for this database interface are furthermore Atmlab's functions to derive the asymmetry parameter and radar back-scattering coefficients from ARTS scattering data. We refrained from duplicating this code to add it explicitly to the database interface and instead refer the interested user to Atmlab itself. Atmlab is available from the ARTS tools webpage.[3]

7.2. Python

The Python interface to the scattering database is located in the `Python` subfolder of the database `DataInterfaces` folder. It is structured into four different modules, each residing in its own file, covering different functionality aspects:

- `utils.py` contains utility functions to access ARTS single scattering database, i.e. general database exploring and extraction functions.
- `assp.py` contains functions to produce ARTS-type SSP. This includes interpolation and merging functionalities.
- `sph.py` contains functionality for spherical harmonics transformations.

[1] Since RTTOV-SCATT can not handle polar-angle dependent extinction and absorption, i.e. can not handle any other than totally randomly oriented particles, this is not needed for RTTOV-SCATT data extraction, though.

[2] https://bitbucket.org/nschaeff/shtns, version 2.8.

[3] http://www.radiativetransfer.org/tools/

- `rttov.py` contains functions to produce sets of SSP suitable as input for RTTOV's Mie-tables module (where the derived Mie tables then can be used with RTTOV-SCATT; see also Section 7.3).

Furthermore, a script demonstrating how to extract ARTS-type SSP is provided (`demo_ssp4arts.py`). The spherical harmonics module, hence the extraction of SSP of azimuthally randomly oriented particles, as well as the RTTOV interface module are exclusive to the Python interface. Appendix C.1 gives an overview and short descriptions of all available functions in the different modules.

The interface generally works in both Python 2 and Python 3 environments, but Python 3 ($\geq$ 3.5) is suggested for full functionality. The interface (hard-)requires the following Python packages to be installed:

- `netCDF4`
- `numpy`
- `os`

Certain features have additional requirements,[4] namely (given in the form "requirement: (module) feature"):

- `typhon`, specifically the `arts` submodule: (`assp`, `demo_ssp4arts`)
  Conversion to ARTS format and writing of ARTS SSP to XML file.
- `scipy`, specifically the `interpolate` submodule: (`assp`, `sph`)
  Grid interpolations.
- `SHTns` (Fortran) library[2]: (`assp`, `sph`)
  Conversion of azimuthally random orientation $\mathbf{Z}$ from Spherical Harmonics coefficients to discrete angle grid values.
- `copy`: (`assp`)
  Creating habit mixtures.
- `pickle`: (`assp`)
  Dumping ARTS format data to a pickled Python file.
- `matplotlib`: (`utils`)
  Imaging of habit logo.

We have taken care that absence of extra packages only leads to failures when the requiring feature is actually used. Other parts of the interface can be loaded and executed with extra packages not being present.

The above mentioned `typhon` package aims to be a collection of tools for atmospheric research for Python 3 (requires Python $\geq$ 3.5). Currently, it mainly provides reading

[4] Unless noted otherwise, this refers to required Python packages.

and writing routines for ARTS XML files. Install instructions for typhon can be found on the ARTS tools webpage.[3]

Except for `netCDF4`, all other required Python packages listed above are part of standard Python distributions. The `netCDF4` is for example available with and installable through conda[5], as well as available from PyPI[6], or github[7] and installable with pip[8]. Install instructions for the `SHTns` library are included in the `README.pdf` shipped with the database.

7.3. Interface to RTTOV-SCATT

The interface to RTTOV-SCATT consists of two parts, one that belongs to the ARTS single scattering database and one that is supposed to become part of RTTOV itself, specifically of its module that creates the Mie coefficient tables.

7.3.1. ARTS SSDB-side interface

The database side part is a component of the Python database interface. It is supposed to be used to extract data from the database, prepare them on specified frequency, temperature, and particle size grids, derive the single scattering parameters that RTTOV-SCATT and its Mie coefficients module require, and write this data in tabulated form to file.

The SSP required by RTTOV-SCATT are extinction and scattering cross-sections, σ_{ext} and σ_{sca}, respectively, as well as the asymmetry parameter g. Additionally, the back-scattering cross-section σ_{bsc} is included to facilitate intended (near-)future developments in RTTOV-SCATT.

The user is able to control the frequency, temperature, and particle size grids that the data will be prepared over. The defaults is set such that no cutting of data in either frequency, temperature, or size is applied and such that data is reported on the original database grid points regarding these parameters. It might be useful, though, to apply some interpolations here (e.g. in temperature) in order to control the accuracy of the data and be more independent of the interpolations applied within RTTOV-SCATT's Mie table coefficient module.

Each habit (or more generally expressed, each particle set) has to be stored in an individual file. Each file contains the data grids (frequency, temperature, D_{max} as well as corresponding D_{veq} and mass) in the header as well as mass-size parameters α and β of the habit. This is followed by the table of σ_{ext} and σ_{sca}, g, and σ_{bsc} over frequency, temperature, and size.

The typical workflow for extracting data for one habit reads:

[5] See https://anaconda.org/anaconda/netcdf4 for the package, https://conda.io/docs/ for conda itself.
[6] https://pypi.python.org/pypi/netCDF4/1.3.0
[7] http://unidata.github.io/netcdf4-python/
[8] https://pip.pypa.io/en/stable/

```
>> S, M, mD = rttov.get_assp(habit_id=3, orientation='totally_random')
>> rssp = rttov.calc_rssp(S, M, mD)
>> rttov.write_rssp(rssp, filename='SomeHabitName.rssp',
                           dirname='Some/Folder/Name')
```

Using the database interface functionality, users are not limited by the particle habits as provided by the database, but can create own, new "habits" (or particle sets), e.g. by creating ARTS format data for habit mixes, convert the to RTTOV parameters and store to file.

7.3.2. RTTOV-side interface

The RTTOV-side interface constitutes of modifications and also some new developments of Fortran code related to the RTTOV(-SCATT) module that produces the Mie coefficient tables. Its task is to allow the user to select from available habit models (or particle sets), read the SSP data from the files produced with the database-side interface, and interpolate it to the frequency, temperature, and size grids the Mie coefficient module expects. These data are then handed over to the existing Mie coefficient module routines that derive bulk properties lookup tables (the so-called Mie coefficient tables) by applying size distribution parametrisations and other modifications. Note that frequency grids are entirely defined by the user, temperature grids are entirely defined internally as well as the number of size grid points, while the size bounds are set (in code) individually per available particle habit.

In collaboration with A. Geer (ECMWF), the existing RTTOV-side interface for digesting data from the *Liu* (2008) SSP database, has been revised and generalised, such that further external data sources can be added relatively easily in the future. The ARTS database with its database-side interface to RTTOV has been kept fairly flexible regarding the habits (or particle sets) that can be produced. This is in contrast to the *Liu* (2008) data, which are limited to the 11 habits in the original data, and where the RTTOV interface neither provides any means to produce habit mixes. Following that, the RTTOV-side interface to the ARTS SSP database has been kept as flexible as possible as well.

In general, users are not limited to a fixed set of habits from the ARTS scattering database, but can use their own datafiles. However, they have to register them in the ARTS database module file (`mod_arts.F90`) with their storage location (one common location for all files to be used), their filenames, and their associated minimum and maximum $D_{\max}$ and α and β. For the future, it is considered to make that more user-friendly, e.g. by reading the $D_{\max}$, α and β info from the file headers. However, this is left to ECMWF to implement and to ideally develop a solution that generally works for external SSP data sources.

As mentioned above, interpolation of the input SSP data to the Mie coefficient tables' grids has been implemented as part of the interface. So far this is done by tri-linear interpolation over frequency, temperature, and size in terms of $D_{\max}$with allowed extrapolation limits set in `mod_arts.F90` (in terms of grid spacing; default for frequency and temperature is half a grid spacing, while size extrapolation is practically not allowed).

Appendix C.3 contains a list of files added to and files modified from their RTTOV 11.3 counterparts.[9] It furthermore shows a snapshot of `mod_arts.F90`.

[9] No changes to the Mie coefficient module are reported for RTTOV 12, i.e. the Mie coefficient codebase should be identical for both versions.

8. Summary and user guidelines

A database of hydrometeor single scattering properties, aimed mainly at microwave and sub-millimetre frequencies, has been developed. It provides single scattering properties for a wide range of ice hydrometeors. Also liquid hydrometeors are considered, but only as perfect spheres.

Chapter 2 gives an overview of the fundamental theory surrounding the single scattering data, ultimately providing a framework for the development and description of the database. Aspects included are basic radiative transfer, relation to bulk scattering properties, refractive indices, particle orientation types, and particle shape and size parametrisation.

Particle modelling, including related software, is covered in Chapter 3. Two software packages were developed in this study with different applications in mind. The snowflake tool-kit is mainly intended to simulate and generate aggregates in a realistic manner. RimeCraft employs a more simplistic approach by growing single particles one dipole at a time. The advantage is that the growth can be almost fully controlled, resulting in particles that follow a specified mass-size parametrisation.

The scattering calculation software used, Amsterdam DDA, is described in Chapter 4 in terms of input and output. Also, the methodology for generating scattering data of azimuthally random orientation is explained (detailed information is available in Appendix A). In short, the processing involves conversion of the DDA output to the database scattering quantities, orientational averaging, and data compression using spherical harmonics.

The specifications of the database are found in Chapter 5 with an overview provided in Tables 5.1/5.3 and 5.5 for totally and azimuthally random orientation, respectively. A total of 34 habits in totally random orientation are included as well as one habit in azimuthally randomly orientation on 10 tilt angles. Different target size ranges have been defined, one for single crystals and one for aggregate type particles (Table 5.9). Most habits fulfil these ranges, but for some of habits these limits could not be met.

The frequency grid covers all channels of MWI, MWS and ICI by at least two values at edges of each band (Section 5.4). In total, 34 frequencies are included. Temperature is covered by three grid points (190-270 K) for frozen and five grid points (230-310 K) for liquid particles, making use of *Mätzler* (2006) and *Ellison* (2007) refractive index models for ice and liquid water, respectively.

Chapter 6 presents the format and infrastructure of the database. One key aspect of the data format is its generality, i.e. all secondary parameters such as asymmetry parameter can be derived from the database. Finally, Chapter 7 presents the Python and Matlab database interfaces, which provide e.g. functionality for derivation of secondary parameters. Other features include displaying of the database, interpolation and creation

of habit mixtures, and export of data for use with the ARTS and the RTTOV-SCATT RT models.

8.1. User guidelines

In order to help users to avoid pitfalls, a list of guidelines is given below, divided into items of general consideration and such rather related to usage of the data with the ARTS RT model.

General considerations

- The interfaces are not designed to be fast, i.e. are not supposed to be used on-the-run. Instead, we recommend that users create their SSP, save them, and use them further, e.g. load into their RT model, from there.
- Aggregate type particles, where the minimum available particle size is comparably large, should not be used alone, but as a habit mixture supplemented with some single crystal habit on the lower size end. This is particularly important for higher frequency SSP.
- Temperature interpolation should make use of 2nd order polynomial interpolation. The frozen hydrometeor temperature grid has been chosen to give the best compromise between memory and calculation requirements on the one, accuracy on the other hand. Deviations of 2nd order polynomial interpolated data in comparison to data on fine temperature grids was shown to be small. 2nd order polynomials were found to also produce safe results over a limited extrapolation range (few K).
- We advise against frequency interpolation between different frequency bands (or band clusters). If data outside of, but fairly close to a provided band are required, extrapolation from that band is rather recommended than interpolation between the neighbouring bands (could be achieved using data extraction with limited frequency range followed by frequency interpolation, then actually resulting in an extrapolation, or frequency extension).

ARTS specific considerations

- Temperature interpolation in ARTS by default is linear. To make better use of the produced SSP, it is suggested to derive additional temperature point SSP by 2nd order interpolation for use with ARTS. Adding the two midpoints between the three database temperatures has been proven a satisfactory improvement with acceptable memory requirement.
- Deriving data for temperatures exceeding the database range might be left to ARTS, which allows small-range extrapolation and which offers methods to ignore temperature dependence beyond the grid limits.

- ARTS format requires data to be given on regular frequency-temperature grids. The database itself does by intention not provide this over all particle sizes. Through the interfaces, particle size data can be supplemented on the grid ends with data set to zero or set (constant) from the last size point holding valid data.
- For azimuthally random orientation particles, **Z** data in ARTS is currently required on identical discrete incident and scattered polar angle grids ($\psi_{inc} = \psi_{sca}$). This is considered in the interface for producing ARTS SSP. This means, however, that some information about the angular structures of **Z** is lost (it is contained in the database, though, and can be exploited by other forward models, and hopefully by ARTS in the future).

Bibliography

Bohren, C. F., and D. R. Huffman (1998), *Absorption and scattering of light by small particles*, Wiley, New York, USA.

Côté, J., S. Gravel, A. Méthot, A. Patoine, M. Roch, and A. Staniforth (1998), The operational cmc-mrb global environmental multiscale (gem) model. part i: Design considerations and formulation, *Monthly Weather Review*, *126*(6), 1373–1395, doi:10.1175/1520-0493(1998)126⟨1373:TOCMGE⟩2.0.CO;2.

Ding, J., L. Bi, P. Yang, G. W. Kattawar, F. Weng, Q. Liu, and T. Greenwald (2016), Single-scattering properties of ice particles in the microwave regime: temperature effect on the ice refractive index with implications in remote sensing, *J. Quant. Spectrosc. Radiat. Transf.*, doi:10.1016/j.jqsrt.2016.11.026.

Ellison, W. (2006), *Thermal Microwave Radiation: Application for Remote Sensing*, *IET Electromagn. Waves Ser.*, vol. 52, chap. hwater and seawater, pp. 431–455, Inst. Eng. Technol., Stevenage, U. K.

Ellison, W. J. (2007), Permittivity of pure water, at standard atmospheric pressure, over the frequency range 0–25 THz and the temperature range 0–100°c, *Journal of Physical and Chemical Reference Data*, *36*(1), 1–18, doi:10.1063/1.2360986.

Eriksson, P., M. Jamali, J. Mendrok, and S. A. Buehler (2015), On the microwave optical properties of randomly oriented ice hydrometeors, *Atmos. Meas. Tech.*, *8*(5), 1913–1933, doi:10.5194/amt-8-1913-2015.

Evans, K. F., J. R. Wang, D. O. Starr, G. Heymsfield, L. Li, L. Tian, R. P. Lawson, A. J. Heymsfield, and A. Bansemer (2012), Ice hydrometeor profile retrieval algorithm for high-frequency microwave radiometers: application to the CoSSIR instrument during TC4, *Atmos. Meas. Tech.*, *5*(9), 2277–2306, doi:10.5194/amt-5-2277-2012.

Geer, A. J., and F. Baordo (2014), Improved scattering radiative transfer for frozen hydrometeors at microwave frequencies, *Atmos. Meas. Tech.*, 7(6), 1839–1860, doi:10.5194/amt-7-1839-2014.

Heymsfield, A. J., and L. M. Miloshevich (2003), Parameterizations for the cross-sectional area and extinction of cirrus and stratiform ice cloud particles, *J. Atmos. Sci.*, *60*(7), 936–956.

Heymsfield, A. J., S. Lewis, A. Bansemer, J. Iaquinta, L. M. Miloshevich, M. Kajikawa, C. Twohy, and M. R. Poellot (2002), A general approach for deriving the properties

of cirrus and stratiform ice cloud particles, *J. Atmos. Sci.*, *59*, 3–29, doi:10.1175/1520-0469(2002)059⟨0003:AGAFDT⟩2.0.CO;2.

Hong, G. (2007), Parameterization of scattering and absorption properties of nonspherical ice crystals at microwave frequencies, *J. Geophys. Res.*, *112*(D11), D11208, doi:10.1029/2006JD008364.

Hong, G., P. Yang, B. A. Baum, A. J. Heymsfield, F. Weng, Q. Liu, G. Heygster, and S. A. Buehler (2009), Scattering database in the millimeter and submillimeter wave range of 100-1000 ghz for nonspherical ice particles, *J. Geophys. Res.*, *114*, D06201, doi:10.1029/2008JD010451.

Iwabuchi, H., and P. Yang (2011), Temperature dependence of ice optical constants: Implications for simulating the single-scattering properties of cold ice clouds, *J. Quant. Spectrosc. Radiat. Transfer*, *112*(15), 2520–2525, doi:10.1016/j.jqsrt.2011.06.017.

Johnson, B., W. Olson, and G. Skofronick-Jackson (2016), The microwave properties of simulated melting precipitation particles: sensitivity to initial melting, *Atmos. Meas. Tech.*, *9*(1), 9–21.

Liu, G. (2008), A database of microwave single-scattering properties for nonspherical ice particles, *Bull. Amer. Met. Soc.*, *89*, 1563, doi:10.1175/2008BAMS2486.1.

Mätzler, C. (2002), Matlab functions for mie scattering and absorption, version 2, *Tech. rep.*

Mätzler, C. (2006), *Thermal Microwave Radiation: Application for Remote Sensing*, *IET Electromagn. Waves Ser.*, vol. 52, chap. 5.3 Microwave dielectric properties of ice, pp. 455–462, Inst. Eng. Technol., Stevenage, U. K.

Mishchenko, M. I., L. Travis, and A. Lacis (2002), *Scattering, absorption, and emission of light by small particles*, Cambridge University Press, Cambridge, UK.

Petty, G. W., and W. Huang (2011), The modified gamma size distribution applied to inhomogeneous and nonspherical particles: Key relationships and conversions, *J. Atmos. Sci.*, *68*, 1460–1473, doi:10.1175/2011JAS3645.1.

Rathsman, T. (2016), A software toolkit for generating ice and snow particle sharp data, Master's thesis, Msc. thesis, Earth and Space Sciences, Chalmers University of Technology, Gothenburg, Sweden.

Ray, P. S. (1972), Broadband complex refractive indices of ice and water, *Appl. Optics*, *11*, 1836–1844.

Satoh, M. (2014), Icosahedral grids, in *Atmospheric Circulation Dynamics and General Circulation Models*, Springer Praxis Books, pp. 636–660, Springer Berlin Heidelberg.

Schaeffer, N. (2013), Efficient spherical harmonic transforms aimed at pseudospectral numerical simulations, *Geochemistry, Geophysics, Geosystems*, *14*(3), 751–758, doi: 10.1002/ggge.20071.

Tsang, L., J. Kong, and K. Ding (2000), *Scattering of electromagnetic waves, Vol. 1: Theory and applications*, Wieley Interscience, New York.

Turner, D. D., S. Kneifel, and M. P. Cadeddu (2016), An improved liquid water absorption model at microwave frequencies for supercooled liquid water clouds, *J. Atmos. Oceanic Technol.*, *33*(1), 33–44, doi:10.1175/JTECH-D-15-0074.1.

Tyynelä, J., and V. Chandrasekar (2014), Characterizing falling snow using multifrequency dual-polarization measurements, *J. Geophys. Res.*, *119*(13), 8268–8283, doi: 10.1002/2013JD021369.

Warren, S. (1984), Optical constants of ice from the ultraviolet to the microwave, *Appl. Opt.*, *23*, 1206–1225, doi:10.1364/AO.23.001206.

Yurkin, M., and A. Hoekstra (2014), *User Manual for the Discrete Dipole Approximation Code ADDA 1.3b4*.

Yurkin, M. A., and A. G. Hoekstra (2011), The discrete-dipole-approximation code adda: capabilities and known limitations, *J. Quant. Spectrosc. Radiat. Transfer*, *112*(13), 2234–2247.

A. Orientation implementation

A.1. Initial particle alignment

Before any orientation averaging can be performed, the initial orientation of the particle has to be calculated. This section describes how this alignment is defined. The alignment algorithm is based mainly on aligning the principal moments of inertia axes along the Cartesian coordinate axes. Also, a number of special cases are treated in order to make the alignment consistent between particles and not dependant on small numerical differences. The result of the algorithm is that the particle fulfils the following criteria: the principal axis of the particle with the largest inertia is aligned along the z-axis, and its principal axis with the smallest inertia along the x-axis.

The algorithm involves a several steps. For particles that posses no symmetries, one step can be skipped. The algorithm operates on a coordinate grid and consists of the following steps:

1. First, the particle mass centre coordinate $\overline{\mathbf{r}}$ is calculated, according to

$$\overline{\mathbf{r}} = \sum_{i=1}^{N} m_i \mathbf{r}_i, \tag{A.1}$$

   where $\mathbf{r}_i$ is (3x1) column vector describing the coordinate of the grid point with index i, and m_i is the mass of the corresponding dipole. The dipole grid is then displaced so that the mass centre is located at the origin.

2. Next, the inertia matrix $\mathbf{I}$ relative to the origin is calculated using

$$\mathbf{I} = -\sum_{i=1}^{N} m_i [\mathbf{R}]_i^2, \tag{A.2}$$

   where $[\mathbf{R}]_i$ is the skew-symmetric matrix associated with coordinate $\mathbf{r}$, defined as

$$[\mathbf{R}] = \begin{pmatrix} 0 & -z & y \\ z & 0 & -x \\ -y & x & 0 \end{pmatrix}. \tag{A.3}$$

   $\mathbf{I}$ contains the products of inertia along the Cartesian coordinate axes, i.e.

$$\mathbf{I} = \begin{pmatrix} I_{xx} & I_{xy} & I_{xz} \\ I_{xy} & I_{yy} & I_{yz} \\ I_{xz} & I_{yz} & I_{zz} \end{pmatrix}. \tag{A.4}$$

Since $\mathbf{I}$ is real and symmetric, it can be diagonalized using eigenvector decomposition, as

$$\mathbf{\Lambda} = \mathbf{Q}\mathbf{I}\mathbf{Q}^T, \tag{A.5}$$

where $\mathbf{\Lambda}$ is a diagonal matrix with elements I_1, I_2 and I_3, which are called the principal moments of inertia. The diagonalisation is performed in such way that $I_1 \leq I_2 \leq I_3$. The columns of $\mathbf{Q}$, Q_1, Q_2 and Q_3, are the corresponding principal axes.

It follows that $\mathbf{Q}$ is a rotation matrix, which rotates the x, y and z-axes to corresponding axes of inertia. Thus, to align the particle principal axes to the coordinate axes, one has to rotate the particle grid by the inverse of $\mathbf{Q}$, i.e. $\mathbf{Q}^T$. In order to ensure that the rotation does not mirror the particle (that the rotation is pure), one has to make sure that $\det\left(\mathbf{Q}^T\right) = 1$. The rotation matrix $\mathbf{A}$ is thus calculated as

$$\mathbf{A} = \frac{\mathbf{Q}^T}{|\mathbf{Q}^T|}. \tag{A.6}$$

After the rotation, recalculation of the inertia matrix should yield

$$\mathbf{I} = \begin{pmatrix} I_{xx} & 0 & 0 \\ 0 & I_{yy} & 0 \\ 0 & 0 & I_{zz} \end{pmatrix}, \tag{A.7}$$

With

$$I_{xx} \leq I_{yy} \leq I_{zz}. \tag{A.8}$$

This criteria must always be satisfied, i.e. any of the remaining steps must make sure that it does not violate the condition.

3. If the particle contains symmetries, then two or all of the principal moments of inertia can be equal. This means that the rotation in the previous step is unambiguous, i.e. several possible orientations fulfils Eq. A.8. As an example, for hexagonal plates, $I_{xx} = I_{yy}$, meaning that its orientation in the xy-plane is unambiguous. It is desirable to remove this uncertainty, which here is done by minimizing the particle dimensions along the coordinate axes. Three cases are possible and are treated as follows:

   - $I_{xx} = I_{yy} = I_{zz}$: The particle is spherically symmetric (for example, a six bullet rosette), hence no rotation will have an impact on $\mathbf{I}$. First, the particle dimension along the z-axis is minimized by rotation around the x and y-axis. Similarly, the particle dimension along the x-axis is then maximised by rotation around the z-axis.
   - $I_{yy} = I_{zz}$: The particle is symmetric around the x-axis (a hexagonal column for example). The particle dimension along the z-axis is minimized by rotation around the x-axis.

- $I_{yy} = I_{xx}$: The particle is symmetric around the z-axis (for example, a hexagonal plate). The particle dimension along the x-axis is maximized by rotation around the z-axis

4. In the final step, it is determined whether the particle is aligned upside down or upright. First, the minimum circumsphere of the particle is calculated, with its corresponding centre. If the centre is found to be below the mass-centre of the particle (with respect to the z-axis), the the particle is said to be aligned upright. Vice versa, it is said to be aligned upside down in the case when the sphere centre is above the mass centre. In this case, the particle is rotated 180° around the x-axis to be upright.

A.2. Calculation of azimuthally oriented particles

To calculate the single scattering properties of azimuth randomly oriented particle with a specific orientation, the scattering matrix and the extinction matrix are needed. In general, the scattering matrix of a non-spherical particle depends on the incidence direction (θ_i, ϕ_i), the scattering direction (θ_s, ϕ_s) and the particle orientation described by the three Euler angles α, β and γ. If the scattering matrix $\mathbf{Z}\,(\theta_i,\, \phi_i, \theta_s,\, \phi_s,\, \alpha,\, \beta,\, \gamma)$ is known for any orientation, incidence direction, and scattering direction can be calculated. The same hold for the extinction matrix $\mathbf{K}$ except that it is independent of the scattering directions. For scattering in general, it holds that the rotation of a particle is equivalent to the inverse rotation of the incidence direction, which is the key point in our averaging approach. Therefore the particle can be kept fixed at one orientation. Every other orientation can be calculated by rotating the incidence and scattering direction according to the particle orientation. With ADDA it is only possible to calculate the scattering properties for a finite set of incidence and scattering directions. So, the scattering matrix and the extinction matrix are calculated for a set of different incidence directions and scattering directions (only scattering matrix). To reduce the computational cost one can try to exploit possible symmetries of the particle, which is explained in Section A.7. The result is a finite approximation of the scattering matrix and of the extinction matrix for finite set of incidence and scattering directions, which are fixed to the particle, see Fig. A.1, left panel.

For a specific orientation of the particle, the set of incidence and scattering directions are rotated accordingly to the orientation of the particle, see Fig. A.1 b. This approach is analogue to the analytic T-matrix method, only in a much more numerical way.

The results of an ADDA calculation are the scattering amplitude matrix and the Mueller matrix. The extinction matrix is calculated using A.38 from the scattering amplitude. Between the scattering matrix $\mathbf{Z}$ and the Mueller matrix $\mathbf{M}$ following linear relationship holds

$$\mathbf{Z}\,(\theta_i, \phi_i, \theta_s, \phi_s, \alpha, \beta, \gamma) = \frac{1}{k^2}\mathbf{L}_i\mathbf{M}\,(\theta_i, \phi_i, \theta_s', \phi_s', \alpha, \beta, \gamma)\,\mathbf{L}_s \tag{A.9}$$

with $\mathbf{L}_{i,s}$ transformation matrices, which will be defined in Sec. A.8, and k the angular wave number (*Mishchenko et al.*, 2002). The prime denotes that is not relative the

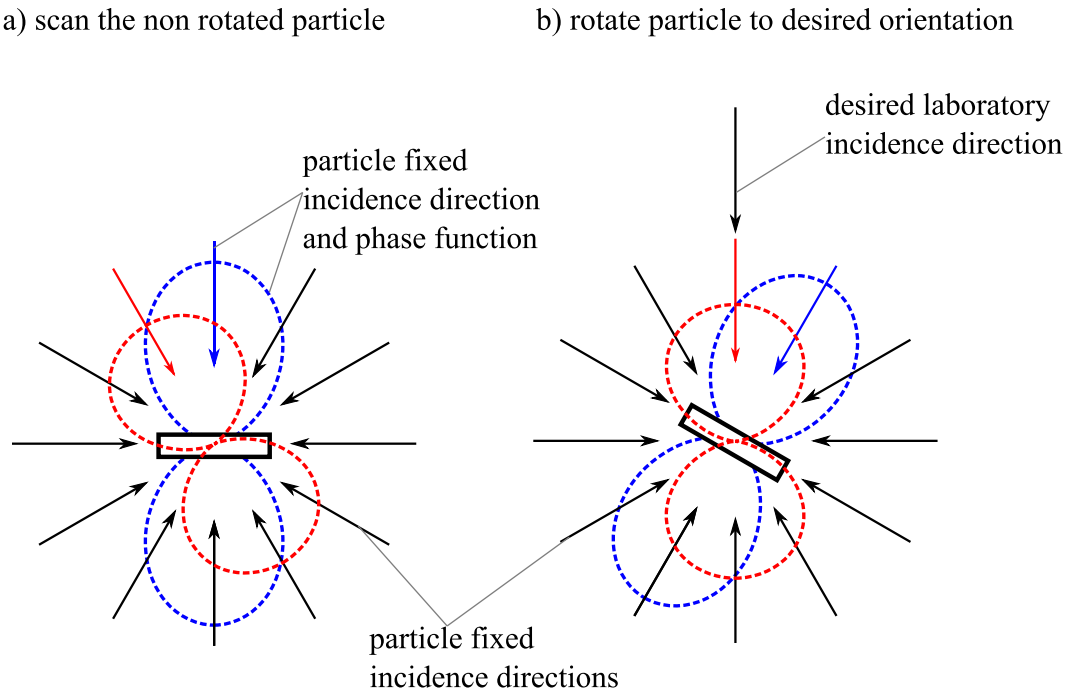

Figure A.1.: Schematic drawing of the calculation of the single scattering properties. (left) the non rotated particle with the incidence and scattering directions fixed to the particle. (right) the rotated particle and the rotated incidence and scattering directions.

laboratory system. Due to the linear relationship, it does not matter if first the Mueller matrix is transformed to a scattering matrix and the phase matrix is averaged or vice versa. Instead of transforming every calculated Mueller matrix into the scattering matrix, the averaging will be done for the Mueller matrix and at the end the averaged Mueller matrix is transformed to the scattering matrix.

For each incidence direction, ADDA automatically calculates the Mueller matrix for a given regular grid of polar angles ($\theta_{s,p}$) and azimuth angles ($\phi_{s,p}$). A regular grid of polar and azimuth angles has the property that the grid spacing is at the pole much finer than at the equator. Actually, this is advantageous for scattering, because due to the definition of the Mueller matrix the forward peak and the backward peak are located at the poles.

For the set of incidence angles, a regular grid of polar angles ($\theta_{i,p}$) and azimuth angles ($\phi_{i,p}$) are disadvantageous, because for the incidence angle an isotropic sampling is needed but the distribution of the directions of a regular grid regular grid of polar angles and azimuth angles is not isotropic. The pole directions would be sampled much higher than the equatorial directions, which is inefficient, too. Furthermore, this could induce inconsistencies, if a different fixed particle orientation is chosen. Instead of regular grid of polar angles and azimuth angles, a icosahedral grid is used. An icosahedral grid is highly isotropic. The distances between two neighbouring vertices (grid points) is everywhere the same and an icosahedral grid consist of equilateral triangles, which have all the same size. This makes the icosahedral grid convenient for grid refinement and adjusting the grid size for the needed accuracy. An icosahedral grid can be set up by recursively bisecting the edges of an icosahedron and projecting the new vertices on a sphere. Such a icosahedral grid consists of

$$N_v = 10 \cdot (2l)^2 + 2 \tag{A.10}$$

vertices and

$$N_t = 20 \cdot (2l)^2 \tag{A.11}$$

triangles with l the refinement level. The coordinates of the vertices of icosahedral grid on unit sphere are the set incidence directions. For more details on icosahedral grids, see for example *Satoh* (2014).

The actual averaging is done by approximating

$$\mathbf{X_{ao}}\left(\theta_i, \phi_i, \theta_s, \phi_s, \beta\right) = \int_0^{2\pi} \int_0^{2\pi} p_\alpha\left(\alpha\right) p_\gamma\left(\gamma\right) \mathbf{X}\left(\theta_i, \phi_i, \theta_s, \phi_s, \alpha, \beta, \gamma\right) \, \mathrm{d}\alpha \, \mathrm{d}\gamma \tag{A.12}$$

with $\mathbf{X} = (\mathbf{a}, \mathbf{K}, \mathbf{M})$ with a two fold with 16-point Gauss-Legendre quadrature. Needed interpolation is done by using a barycentric interpolation for triangles, which is explained in the next section.

A.3. Particle rotation

The incidence/scattering direction $\vec{e}_{kj,o}$ for a specific orientation is given by

$$\vec{\mathbf{e}}_{kj,o}\left(\theta_{j,o},\phi_{j,o}\right)=\mathbf{R}\left(\alpha\right)\mathbf{R}\left(\beta\right)\mathbf{R}\left(\gamma\right)\vec{\mathbf{e}}_{kj,p}\left(\theta_{j,p},\phi_{j,p}\right) \tag{A.13}$$

with α, β, and γ the Euler angles, $\vec{\mathbf{r}}_{j,p}\left(\theta_{j,p},\phi_{j,p}\right)$ the incidence/scattering direction relative to the particle and $\mathbf{R}\left(\alpha\right)\mathbf{R}\left(\beta\right)\mathbf{R}\left(\gamma\right)$ the rotation matrix (*Tsang et al.*, 2000),

$$\mathbf{R}\left(\alpha\right)\mathbf{R}\left(\beta\right)\mathbf{R}\left(\gamma\right)=\begin{pmatrix}R_{11} & R_{12} & R_{13}\\ R_{21} & R_{22} & R_{23}\\ R_{31} & R_{32} & R_{33}\end{pmatrix} \tag{A.14}$$

with

$$R_{11}=\cos(\gamma)\cos(\beta)\cos(\alpha)-\sin(\gamma)\sin(\alpha) \tag{A.15}$$

$$R_{12}=\cos(\gamma)\cos(\beta)\sin(\alpha)+\sin(\gamma)\cos(\alpha) \tag{A.16}$$

$$R_{13}=-\cos(\gamma)\sin(\beta) \tag{A.17}$$

$$R_{21}=-\sin(\gamma)\cos(\beta)\cos(\alpha)-\cos(\gamma)\sin(\alpha) \tag{A.18}$$

$$R_{22}=-\sin(\gamma)\cos(\beta)\sin(\alpha)+\cos(\gamma)\cos(\alpha) \tag{A.19}$$

$$R_{23}=\sin(\gamma)\sin(\beta) \tag{A.20}$$

$$R_{31}=\sin(\beta)\cos(\alpha) \tag{A.21}$$

$$R_{32}=\sin(\beta)\sin(\alpha) \tag{A.22}$$

$$R_{33}=\cos(\beta). \tag{A.23}$$

One important point, the polarization directions of each simulated Mueller matrix and extinction matrix are fixed to their original incidence direction. This means that the original polarization directions of the Mueller matrix and the extinction matrices change under rotation as indicated in Fig. A.2. The rotation about the laboratory Z-axis by the Euler angle α do not change the polarization, because it does not matter how big the rotation around the laboratory Z-axis the vertical polarization direction stay always in the plan spanned by incidence direction unit vector $\vec{e}_{ki}$ and the laboratory z-axis and the horizontal polarization direction stays parallel to the x-y-plane. But the combined rotations by the Euler angles β and γ do. After the combined rotation the original vertical polarization unit vector $\vec{e}_v$ is rotated out of the plane spanned by incidence direction unit vector $\vec{e}_{ki}$ and the laboratory z-axis by angle φ and original horizontal polarization unit vector $\vec{e}_h$ is rotated out of the x-y-plane by angle φ. This means after the rotation the polarization of the Mueller matrix $\mathbf{M}$ and the extinction matrix $\mathbf{K}$ need to be transformed to the laboratory polarization using the stokes rotation matrices $\mathbf{L}$ (*Mishchenko et al.*, 2002):

$$\mathbf{L}\left(\varphi\right)=\begin{pmatrix}1 & 0 & 0 & 0\\ 0 & \cos 2\varphi & -\sin 2\varphi & 0\\ 0 & \sin 2\varphi & \cos 2\varphi & 0\\ 0 & 0 & 0 & 1\end{pmatrix} \tag{A.24}$$

$$\mathbf{X} = \mathbf{L}(\varphi)\,\mathbf{X}\mathbf{L}(-\varphi) \tag{A.25}$$

with $\mathbf{X} = (\mathbf{M}, \mathbf{K})$. In the actual implementation, this leads for the Mueller matrix elements M_{ij} as they are expanded in spherical harmonics to a multiplication of the spherical harmonics coefficients by $\exp(-im\varphi)$ with m the order of the spherical harmonics coefficient. For the rotation angle φ holds

$$\varphi = \operatorname{atan2}(\vec{e}_v \cdot \vec{e}_{h,lab},\, \vec{e}_v \cdot \vec{e}_{v,lab}) \tag{A.26}$$

with the horizontal polarization unit vector in the laboratory system

$$\vec{e}_{h,lab} = \vec{e}_{v,lab} \times \vec{e}_{ki}\,, \tag{A.27}$$

the vertical polarization unit vector in the laboratory system

$$\vec{e}_{v,lab} = (\vec{e}_z \times \vec{e}_{ki}) \times \vec{e}_{ki}\,, \tag{A.28}$$

and $\vec{e}_z$ the unit vector in z-direction.

A.4. Spherical harmonics expansion of the Mueller matrix elements

Each Mueller matrix element $M_{ij}(\theta_i, \phi_i, \theta_s, \phi_s)$ is expanded in a spherical harmonics series over the scattering directions (θ_s, ϕ_s).

$$M_{ij}(\theta_i, \phi_i, \theta_s, \phi_s) = \sum_{l=0}^{l_{max}} \sum_{m=-l}^{l} C_{lm}(\theta_i, \phi_i)\, Y_{lm}(\theta_s, \phi_s) \tag{A.29}$$

with Y_{lm} the spherical harmonic function of the l-th and m-th order and with

$$C_{lm}(\theta_i, \phi_i) = \int_{\Omega_s} M_{ij}(\theta_i, \phi_i, \theta_s, \phi_s)\, Y^*_{lm}(\theta_s, \phi_s)\, \mathrm{d}\Omega_s \tag{A.30}$$

the expansion coefficients of the incidence direction (θ_i, ϕ_i). To save data space, the expansion of M_{ij} is truncated to the value l_{max}. l_{max} is defined as the lowest l for which holds, that

$$\left[\int_{\Omega_s} \left| M_{ij}(\theta_i, \phi_i, \theta_s, \phi_s) - \sum_{l=0}^{l_{max}} \sum_{m=-l}^{l} C_{lm}(\theta_i, \phi_i)\, Y_{lm}(\theta_s, \phi_s) \right|^2 \mathrm{d}\Omega_s \right]^{\frac{1}{2}} < \varepsilon_{M11}\,. \tag{A.31}$$

ε_{M11} is 0.5% of the standard deviation over the scattering directions (θ_s, ϕ_s) of the $M_{11}(\theta_i, \phi_i)$ Mueller matrix element. For the actual calculation of the spherical harmonics the SHTns library version 2.8 (*Schaeffer*, 2013) and its Python interface are used.

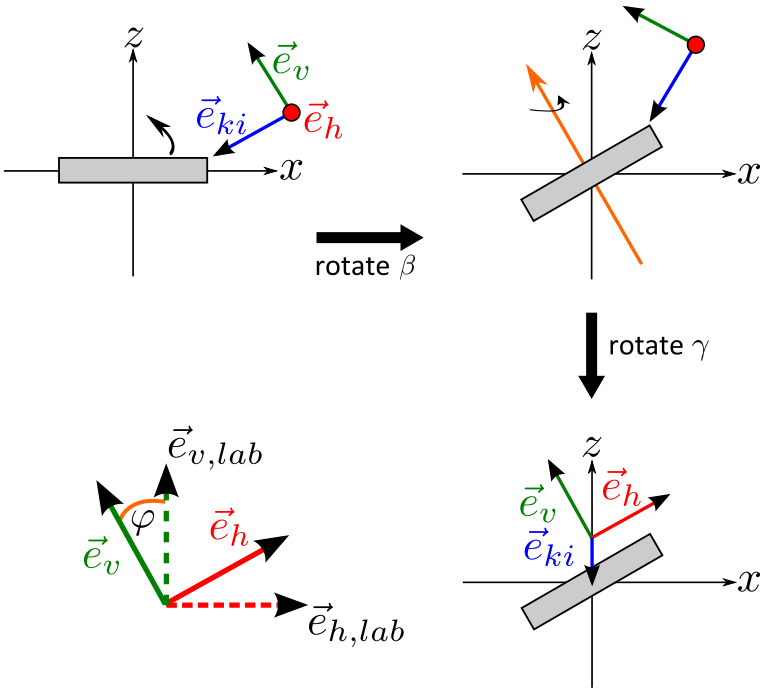

Figure A.2.: Change of the polarization directions under rotation. (top left) the incidence direction unit vector $\vec{e}_{ki}$ together with the vertical polarization unit vector $\vec{e}_v$ and the horizontal polarization unit vector $\vec{e}_h$, which are fixed to the particle, before the rotation is performed. (top right) the unit vectors after the rotation by angle β and (bottom right) after the rotation by angle γ. As indicated (bottom left) the polarization vectors after the rotation by angles β and γ are twisted by angle φ compared to the laboratory unit vectors.

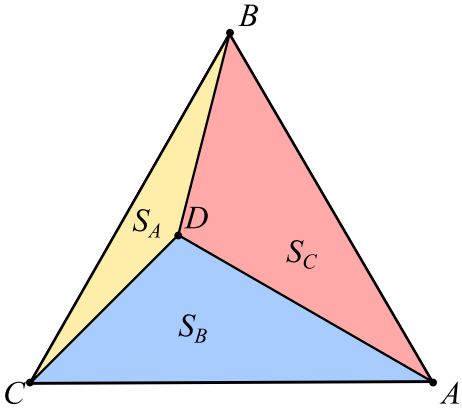

Figure A.3.: Geometry of triangular barycentric interpolation.

A.5. Barycentric interpolation

On a icosahedral grid any arbitrary point on the sphere is accompanied by three nearest points that form a equilateral triangle. Within this triangle the value at that point can be interpolated from the vertices of the triangle. A schematic of the problem is shown in Fig. A.3. The vertices A, B, and C form the equilateral triangle ABC. The point D is the evaluation point. Always two vertices and the evaluation point D form a sub-triangle. For example, the vertices B and C and the evaluation D form the triangle BCD on the opposing side of vertex A. The idea behind the barycentric interpolation is to use the ratio of the area of a sub-triangle and the area of the triangle ABC as interpolation weights. The weight belonging to vertex A is

$$w_A = \frac{S_A}{S_{ABC}} \tag{A.32}$$

with S_A the area of sub-triangle BCD and S_{ABC} the area of the triangle ABC. The weights belonging to the other two vertices are analogue to the weight of vertex A.

The area S of a triangle is using Heron's formula

$$S_i = \sqrt{s\,(s-u)\,(s-v)\,(s-w)} \tag{A.33}$$

with

$$s = \frac{u+v+w}{2} \tag{A.34}$$

and u, v, w the sides of the triangle i.

The interpolated value f_{int} at the evaluation point D is

$$f_{int}\,(D) = w_A f\,(A) + w_B f\,(B) + w_C f\,(C) \tag{A.35}$$

with $f\,(i)$ the value at a vertex i.

A.6. Mueller Matrix, scattering Matrix, extinction Matrix

The Mueller matrix is a real 4×4 matrix, that relates the incidence stokes vector to the scattering stokes vector. The Mueller matrix is dimensionless and the polarization defined relative to the scattered direction. The scattering matrix is a real 4×4 matrix, that relates the incidence stokes vector to the scattering stokes vector. In comparison to the Mueller matrix the scattering matrix has a dimension of a squared length and the polarization is defined according the incidence direction. Between the Mueller matrix $\mathbf{M}$ and the scattering matrix $\mathbf{Z}$ holds

$$\mathbf{Z} = \frac{1}{k^2}\mathbf{L}_s\mathbf{M}\mathbf{L}_i \tag{A.36}$$

with k the wave number and $\mathbf{L}_s$, $\mathbf{L}_i$ stokes rotation matrices. We will come back to them in Section A.8. The scattering matrix is the result, that we need for the scattering database. The Mueller matrix is, what results from an ADDA calculation. Because of the linearity, it does not matter if first the Mueller matrix is transformed to a scattering matrix and the scattering matrix is averaged or vice versa. Note that for totally random orientation, the rotation matrices becomes identity matrices due to the spherical symmetry. Thus, only multiplication with the factor $\frac{1}{k^2}$ is required for the conversion from $\mathbf{M}$ to $\mathbf{Z}$.

The extinction matrix describes how the radiation in forward direction is attenuated. ADDA does not calculate the extinction matrix, but the extinction matrix has to be calculated from the scattering amplitude matrix, which is calculated by ADDA. The scattering amplitude matrix is

$$\mathbf{S}\left(\theta_i, \phi_i, \theta_s, \phi_s\right) = \begin{pmatrix} S_{11} & S_{12} \\ S_{21} & S_{22} \end{pmatrix} \tag{A.37}$$

with θ_i the incidence polar angle, ϕ_i the incidence azimuth angle, θ_s the scattering polar angle and ϕ_s the scattering azimuth angle. Of course, the matrix elements S_{ij} depend on the angle, too. The extinction matrix relates on the scattering amplitude matrix for the forward direction ($\theta_i = \theta_s$, $\phi_i = \phi_s$) (*Mishchenko et al.*, 2002)

$$\mathbf{K} = \frac{2\pi}{k}\begin{pmatrix} \mathrm{Im}\left(S_{11}+S_{22}\right) & \mathrm{Im}\left(S_{11}-S_{22}\right) & -\mathrm{Im}\left(S_{12}+S_{21}\right) & \mathrm{Re}\left(S_{21}-S_{12}\right) \\ \mathrm{Im}\left(S_{11}-S_{22}\right) & \mathrm{Im}\left(S_{11}+S_{22}\right) & \mathrm{Im}\left(S_{21}-S_{12}\right) & -\mathrm{Re}\left(S_{12}+S_{21}\right) \\ -\mathrm{Im}\left(S_{12}+S_{21}\right) & -\mathrm{Im}\left(S_{21}-S_{12}\right) & \mathrm{Im}\left(S_{11}+S_{22}\right) & \mathrm{Re}\left(S_{22}-S_{11}\right) \\ \mathrm{Re}\left(S_{21}-S_{12}\right) & \mathrm{Re}\left(S_{12}+S_{21}\right) & -\mathrm{Re}\left(S_{22}-S_{11}\right) & \mathrm{Im}\left(S_{11}+S_{22}\right) \end{pmatrix} \tag{A.38}$$

with Im () and Re () denoting imaginary part and real part, respectively. For azimuthally randomly oriented particles Eq. A.38 simplifies to

$$\mathbf{K} = \frac{2\pi}{k}\begin{pmatrix} \mathrm{Im}\left(S_{11}+S_{22}\right) & \mathrm{Im}\left(S_{11}-S_{22}\right) & 0 & 0 \\ \mathrm{Im}\left(S_{11}-S_{22}\right) & \mathrm{Im}\left(S_{11}+S_{22}\right) & 0 & 0 \\ 0 & 0 & \mathrm{Im}\left(S_{11}+S_{22}\right) & \mathrm{Re}\left(S_{22}-S_{11}\right) \\ 0 & 0 & -\mathrm{Re}\left(S_{22}-S_{11}\right) & \mathrm{Im}\left(S_{11}+S_{22}\right) \end{pmatrix} \tag{A.39}$$

having only three independent matrix elements.

A.7. Symmetries

ADDA calculations cost a lot of computing power and time. To reduce computing time, we can try to use the symmetry properties of the problem. As the Mueller matrix and the scattering matrix are related by a linear equation, as given by Eq. (A.36), the Mueller matrix and the scattering matrix have the same symmetry properties. Therefore, the symmetries can be used for the Mueller matrix as for the scattering matrix. In general, if a particle has a n-fold rotation symmetry around and this axis coincide with the laboratory Z-axis, the needed azimuth angular range when sampling the particle can be constrained to $\phi_i \in \left[0, \frac{2\pi}{n}\right]$, because after a rotation of $\frac{2\pi}{n}$ the particle orientation cannot be distinguished from the non rotated orientation. Unfortunately, this does not hold in ADDA. Due to the discretisation of a particle into cubic dipoles, a particle within ADDA has at maximum a four fold symmetry. The maximum usable symmetry of a particle within ADDA is the greatest common divisor between the symmetry of ADDA and the symmetry of the particle. This has the consequence, that within ADDA for a particle with a six fold symmetry like a hexagon has only a two fold symmetry. Instead of using the rotation symmetry, mirror symmetry is used. By using the existing mirror symmetry of a particle to the X-Y-plane, X-Z-plane and/or Y-Z-plane the computational cost can be reduced at maximum by a factor of 8. For example, for the scattering matrix $\mathbf{Z}(\theta_i, \phi_i, \theta_s, \phi_s)$ of a particle, which is mirror symmetric to the X-Z-plane, holds

$$\mathbf{Z}(\theta_i, pi - \phi_i, \theta_s, \pi - \phi_s,) = \mathbf{S} \circ \mathbf{Z}(\theta_i, \phi_i, \theta_s, \phi_s) \quad \text{with} \tag{A.40}$$

with

$$\mathbf{S} = \begin{pmatrix} 1 & 1 & -1 & -1 \\ 1 & 1 & -1 & -1 \\ -1 & -1 & 1 & 1 \\ -1 & -1 & 1 & 1 \end{pmatrix} \tag{A.41}$$

and $\phi_i \leq \pi$.

The "$\circ$" stands for the Hadamard product, which is also known as entrywise product. For the derivation of $\mathbf{S}$, the behaviour of the scattering amplitude matrix under symmetry operation and the definition of the Stokes matrix was taken into account (*Mishchenko et al.*, 2002). For each used mirror symmetry the scattering matrix has to be entrywise multiplied with the matrix $\mathbf{S}$ and the number of incidence angles can be reduced by a factor of two. For the Extinction matrix the mirror symmetries hold, too.

A.8. Transform Mueller matrix to scattering matrix

As written above, one result of an ADDA simulation is the Mueller matrix. This Mueller matrix is related to incidence direction and not to the laboratory system. Furthermore, the Mueller matrix relates the polarization to the scattering direction. For the database we need the scattering matrix, which is related to the laboratory system and which relates the polarization to the incidence direction. The transformation consist of two steps:

1. Transform the Mueller from the coordinate system, that is relative to the incidence direction, to the laboratory system.

2. Transform the polarization relative to the incidence direction.

The extinction matrix do not need to be transformed, as it is defined relative to forward direction, which is the incidence direction. Therefore, we also do not need to transform the polarization and the incidence direction is already defined in the laboratory system.

A.8.1. Coordinate transformation

Within this work holds that the incidence vector is always within the X-Z-plane. Therefore, the transformation consists of a rotation around the laboratory Y-axis. We only need to transform the scattering directions, which are by definition of the Mueller matrix relative to the incidence direction, to the laboratory system, because we defined the incidence directions already in the laboratory system. First, we transform the scattering directions relative to the incidence direction from spherical coordinates to Cartesian coordinates relative to the incidence direction.

$$\vec{x}'_s = \begin{pmatrix} x'_s \\ y'_s \\ z'_s \end{pmatrix} = \begin{pmatrix} \sin\theta'_s \cos\phi'_s \\ \sin\theta'_s \sin\phi'_s \\ \cos\theta'_s \end{pmatrix} \tag{A.42}$$

Then we have to rotate them to the laboratory system. The primes indicate that the coordinates are relative to the incidence direction, whereas the unprimed coordinates indicate the laboratory system. The rotation angle is simply the polar incidence angle θ_i. For the scattering directions in the laboratory system holds

$$\vec{x} = \begin{pmatrix} x \\ y \\ z \end{pmatrix} = \begin{pmatrix} \cos\theta_i & 0 & \sin\theta_i \\ 0 & 1 & 0 \\ -\sin\theta_i & 0 & \cos\theta_i \end{pmatrix} \begin{pmatrix} x'_s \\ y'_s \\ z'_s \end{pmatrix} = R(\theta_i)\, \vec{x}'_s \,. \tag{A.43}$$

Now going back to spherical coordinates,

$$\theta_s = \arccos z \tag{A.44}$$

$$\phi_s = \operatorname{atan2}(y, x) \tag{A.45}$$

and we got scattering directions relative to laboratory system.

A.8.2. Polarization transformation

To transform the polarization basis from relative to the scattering direction to relative to incidence direction, we have to rotate the polarization basis first relatively to the scattering and then to the polarization basis relative to the incidence direction, see Fig. A.4 for the geometry of the problem. In matrix notation (*Mishchenko et al.*, 2002)

$$\mathbf{Z} = \frac{1}{k^2} \mathbf{L}_s \mathbf{M} \mathbf{L}_i \,. \tag{A.46}$$

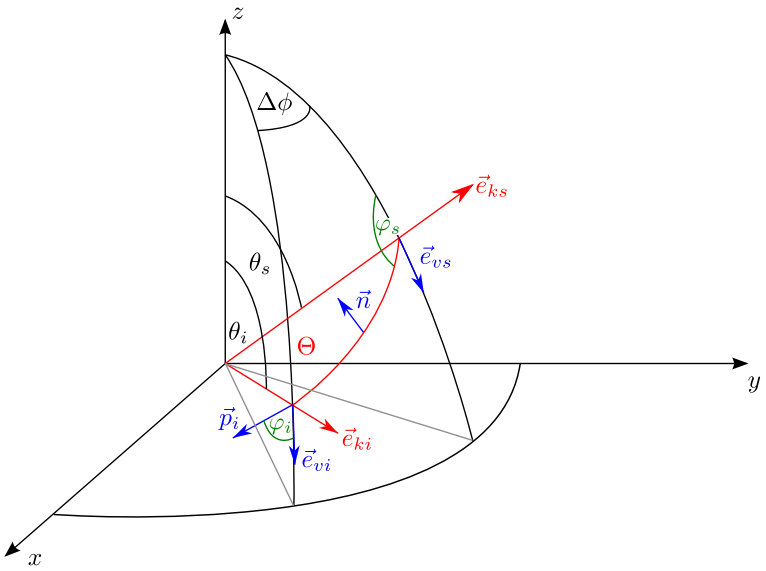

Figure A.4.: Scattering geometry in the laboratory system

The factor $\frac{1}{k^2}$ is due to the different definitions of Mueller matrix and scattering matrix. The rotations can be described by following matrices,

$$\mathbf{L}_s\left(\varphi_s\right) = \begin{pmatrix} 1 & 0 & 0 & 0 \\ 0 & \cos 2\varphi_s & \sin 2\varphi_s & 0 \\ 0 & -\sin 2\varphi_s & \cos 2\varphi_s & 0 \\ 0 & 0 & 0 & 1 \end{pmatrix} \tag{A.47}$$

describes the rotation by angle φ_s, which is the angle between the plane, that is spanned by the unit vector of the scattering direction and the laboratory Z-axis, and the scattering plane, which is the plane, that is spanned by the unit vector of the incidence direction $\vec{e}_{ki}$ and the unit vector of the scattering direction $\vec{e}_{ks}$.

$$\mathbf{L}_i\left(\varphi_i\right) = \begin{pmatrix} 1 & 0 & 0 & 0 \\ 0 & \cos 2\varphi_i & -\sin 2\varphi_i & 0 \\ 0 & \sin 2\varphi_i & \cos 2\varphi_i & 0 \\ 0 & 0 & 0 & 1 \end{pmatrix} \tag{A.48}$$

describes the rotation by angle φ_i, which is the angle between the plane, that is spanned by the unit vector of the incidence direction and the laboratory Z-axis, and the scattering plane. Before we can calculate the angles, we need first to define some quantities. The unit vector $\vec{e}_{kj}$ describing the incidence or scattering direction is

$$\vec{e}_{kj} = \begin{pmatrix} \sin\theta_j \cos\phi_j \\ \sin\theta_j \sin\phi_j \\ \cos\theta_j \end{pmatrix} \tag{A.49}$$

and the unit vector of the vertical polarisation $\vec{e}_{vj}$ for the incidence direction or the scattering direction is

$$\vec{e}_{vj} = \begin{pmatrix} \cos\theta_j \cos\phi_j \\ \cos\theta_j \sin\phi_j \\ -\sin\theta_j \end{pmatrix} \tag{A.50}$$

with $j = i$ for the incidence direction and $j = s$ for the scattering direction. The scattering angle Θ , which is the angle between the incidence direction and the scattering direction is

$$\sin\Theta = |\vec{e}_{ks} \times \vec{e}_{ki}| \tag{A.51}$$

and the normal vector $\vec{n}$, which is orthogonal to the scattering plane, is

$$\vec{n} = \frac{\vec{e}_{ks} \times \vec{e}_{ki}}{\sin\Theta} \,. \tag{A.52}$$

Furthermore, we need the vector $\vec{p}_j$, that is parallel to scattering plane and orthogonal to $\vec{e}_{kj}$

$$\vec{p}_j = \vec{n} \times \vec{e}_{kj} \,. \tag{A.53}$$

After all these definitions, for the rotation angle holds

$$\varphi_j = \begin{cases} -\arccos(\vec{e}_{vj} \cdot \vec{p}_j) & , \vec{e}_{vj} \cdot \vec{n}_j \geq 0 \\ \arccos(\vec{e}_{vj} \cdot \vec{p}_j) & , \vec{e}_{vj} \cdot \vec{n}_j < 0 \end{cases} . \tag{A.54}$$

B. Example of the data format

Below is an example of a database netCDF4 entry, printed using the MATLAB function `ncdisp` (only one internal netCDF folder is displayed):

```
/Freq0886.400GHz_T270.00K/ShapeData/
    Attributes:
               description               = 'ICON snow'
               source                    = 'location: Chalmers,
                   software: Rimecraft.'
               shape_file                = 'IconSnow_Id28/
                   Dmax00120um_Dveq00094um_\\
                   Mass3.96014e-10kg_Freq0887.000GHz.adda'
               refrIndex_model           = 'Matzler 2006'
               habit_file_id             = 'IconSnow'
               habit_id                  = 28
               phase                     = 'ice'
               refrIndex_homogenous_bool = 1
               density_homogenous_bool   = 1
    Variables:
        diameter_max
               Size:       1x1
               Dimensions:
               Datatype:   double
               Attributes:
                           _FillValue  = NaN
                           unit        = 'm'
                           description = 'Maximimum diameter,
                               calculated as the minimum
                               circumsphere diameter'
        diameter_vol_eq
               Size:       1x1
               Dimensions:
               Datatype:   double
               Attributes:
                           _FillValue  = NaN
                           unit        = 'm'
                           description = 'Volume equivalent diameter'
        diameter_area_eq_aerodynamical
```

```
        Size:       1x1
        Dimensions:
        Datatype:   double
        Attributes:
                    _FillValue = NaN
                    unit       = 'm'
mass
        Size:       1x1
        Dimensions:
        Datatype:   double
        Attributes:
                    _FillValue = NaN
                    unit       = 'kg'
dpl
        Size:       1x1
        Dimensions:
        Datatype:   int32
        Attributes:
                    _FillValue  = -1
                    description = 'Dipoles per wavelength'
N_dipoles
        Size:       1x1
        Dimensions:
        Datatype:   int32
        Attributes:
                    _FillValue  = -1
                    description = 'Number of dipoles'
refrIndex_real
        Size:       1x1
        Dimensions:
        Datatype:   double
        Attributes:
                    _FillValue  = NaN
                    description = 'Real part of refractive index'
                    note        = 'Value only given for homogenous
                        particles'
refrIndex_imag
        Size:       1x1
        Dimensions:
        Datatype:   double
        Attributes:
                    _FillValue  = NaN
                    description = 'Imaginary part of refractive
                        index'
```

```
                        note        = 'Value only given for
                            homogenous particles'
        alpha
               Size:       1x1
               Dimensions:
               Datatype:   double
               Attributes:
                           _FillValue  = NaN
                           unit        = 'degree'
                           description = 'Initial rotation angle alpha
                              (zyz-notation)'
        beta
               Size:       1x1
               Dimensions:
               Datatype:   double
               Attributes:
                           _FillValue  = NaN
                           unit        = 'degree'
                           description = 'Initial rotation angle beta
                               (zyz-notation)'
        gamma
               Size:       1x1
               Dimensions:
               Datatype:   double
               Attributes:
                           _FillValue  = NaN
                           unit        = 'degree'
                           description = 'Initial rotation angle gamma
                               (zyz-notation)'

/Freq0886.400GHz_T270.00K/CalculationData/
    Attributes:
               method              = 'DDA'
               software            = 'ADDA'
               software_version    = '1.3b4'
               system              = 'Chalmers_rss_dioptase'
               n_nodes             = ''
               n_cores             = 6
               date_completion     = 'ons 5 jul 2017 11:25:17 CEST
                                     '
               ADDA_eps            = 2
               ADDA_avgParam_file  = 'avg_params_eps2.dat'
               ADDA_scatParam_file = ''
```

C. Interface functionality

C.1. Interface functions

This appendix lists the functions available in the MATLAB and Python database interfaces and provides a short description of their purposes. The list is structured according to the main task items identified in Chapter 7. Additionally, the Python module, which the function resides in within the Python interface, is indicated in parentheses for each function. Note that in general functions with names starting with `ssdb` operate on the database content (in its native format), while functions with `assp` in their name operate on or produce data in the ARTS format.

The functions vary in relevance for the database user; some primarily serve as subfunctions to other functions and are not supposed to be called by the user. Functions of particular relevance for the user are printed in **`bold`** font, such explicitly not intended for database user usage are typeset in `grey`. Functions with purely internal purposes are not listed at all. This regards in particular the whole `sph` Python interface module.

Basic infrastructure management

`ssdb_init` (`utils`)
: Initialises the SSDB interface. Adds the interface folder to the search path and sets up the habit-folder table used by ssdb_habits.

`ssdb_habits` (`utils`)
: Keeps track on basic habit information. At first call scans the database content and keep this information in persistent variables.

Exploring database content

`ssdb_display` (`utils`)
: Explore the database content.

`ssdb_habit_logo` (`utils`)
: Displays habit logo image.

`ssdb_summary` (`utils`)
: Extracts a habit summary file. Combined call of ssdb_summary_find and ssdb_summary_read.

`ssdb_summary_find` (`utils`)
: Locates the summary file inside a habit folder.

ssdb_summary_read (utils)
: Reads a summary file.

ssdb_particle_folders (utils)
: Finds folders for individual particles. Explores the particle data of a given habit folder.

ssdb_data_files (utils)
: Finds all data files in given folder.

Importing data

ssdb_import_habit (utils)
: Reads and compiles data from the database for one habit. The data reading can be limited to specified size, frequency and temperature ranges.

ssdb_data_import (utils)
: Reads the scattering data found inside a folder.

ssdb_read_ncfile (utils)
: Reads single scattering data from a netCDF file.

get_assp (rttov)
: Get data in ARTS format over common frequency, temperature, and size grids (using assp_import_ssdb and the assp_interp_* functions).

Data manipulation

assp_interp_f (assp)
: Frequency interpolation of ARTS single scattering properties.

assp_extend_f (assp)
: Simple extension of the the frequency coverage of data. Default is to copy the data for the existing highest frequency. Setting all properties to zero is also supported.

assp_interp_t (assp)
: Temperature interpolation of ARTS single scattering properties.

assp_interp_size (assp)
: Size interpolation of ARTS single scattering properties.

assp_interp_za (assp)
: Zenith angle interpolation of ARTS single scattering properties.

assp_create_mix (assp)
: Sums up scattering data according to pre-calculated habit mix weights.

assp_bulkprops (assp)
: Calculates bulk scattering properties for a given PSD.

Format conversions

assp_import_ssdb (assp)
: As ssdb_import_habit, but additionally converts the data to ARTS format.

ssdb2assp (assp)
: Converts single scattering data from database format to the ARTS format.

calc_rssp (rttov)
: Derives single scattering properties as required for RTTOV (Cext, Csca, g, Cbsc).

assp2g (rttov)
: Derives asymmetry parameter g from ARTS-type single scattering data.

Output

assp_save (assp)
: Saves ARTS single scattering data to a MATLAB file (.mat) or Python pickled file.

assp_load (assp)
: Loads ARTS single scattering data from a MATLAB file (.mat) or Python pickled file.

ssdb_write_ncfile (utils)
: Writes single scattering data to a netCDF file.

write_rssp (rttov)
: Writes RTTOV-type single scattering data to Mie-table input file.

Note that no specific functions for ARTS XML-file output have been included in the database. For these, the user is referred to the Atmlab and typhon ARTS tools packages, respectively.

C.2. Interface usage

Here, we present some basic examples of how to use the interfaces. Unless stated otherwise, the functions discussed here reside in the utils module in the case of the Python interface. Examples are generally given in MATLAB syntax, but Python function calls look very similar as well as the screen output from both interfaces.

Initialisation A first step necessary is to initialise the interfaces, i.e. build up an internal inventory of the data available, by executing the ssdb_init function or, alternatively, the ssdb_habits function, both with the database top folder (the SSD folder in the structure as introduced in Section 6.2.1) as the single function argument.

Exploring the database: General overview As a first introduction to the interface, the database content can be explored by the function ssdb_display. Called without an argument, it prints out an overview over all habits present in the database:

```
>> ssdb_display

---------------------- ARTS single scattering data ----------------------

  The table below gives an overview of habits at hand. Thefirst three
  levels give a rough classification of each habit. Theinformation found
  in the two last levels is:

        habit id: habit name                              a         / b
          orientations
  where mass = a * Dmax^b.

  Habits marked with "(x)" are still work in progress. Use with caution.

Ice
---
 Aggregates
  Pristine
         8: HongAggregate                                 a=6.5e+01 / b=3.00
          totally_random
         1: EvansSnowAggregate                            a=2.0e-01 / b=2.39
          totally_random
        34: GemHail                                       a=5.4e+02 / b=3.02
          totally_random
        32: GemSnow                                       a=2.4e+01 / b=2.86
          totally_random
        30: IconHail                                      a=3.8e+02 / b=2.99
          totally_random
        28: IconSnow                                      a=3.1e-02 / b=1.95
          totally_random
        22: LargeBlockAggregate                           a=3.5e-01 / b=2.27
          totally_random
        18: LargeColumnAggregate                          a=2.8e-01 / b=2.44
          totally_random
        20: LargePlateAggregate                           a=2.1e-01 / b=2.26
          totally_random
        21: SmallBlockAggregate                           a=2.1e-01 / b=2.33
          totally_random
        17: SmallColumnAggregate                          a=1.4e-01 / b=2.44
          totally_random
```

```
       19: SmallPlateAggregate                    a=7.7e-02 / b=2.25
         totally_random
  (x)  26: TyynelÃ¤DendriteAggregate               a=8.1e-02 / b=2.22
         totally_random
 Rimed
       33: GemGraupel                             a=1.7e+02 / b=2.96
         totally_random
       29: IconGraupel                            a=3.9e+02 / b=3.13
         totally_random
       23: SphericalGraupel                       a=1.3e+01 / b=2.69
         totally_random
SingleCrystals
 Pristine
        2: HongBulletRosette-5b                   a=4.0e-01 / b=2.43
         totally_random
        6: HongBulletRosette-6b                   a=4.9e-01 / b=2.43
         totally_random
       12: LiuBlockColumn                         a=2.1e+02 / b=3.00
         totally_random
        7: HongColumn                             a=3.8e-02 / b=2.05
         totally_random
        5: HongBulletRosette-3b-flat              a=2.4e-01 / b=2.43
         totally_random
       11: HongBulletRosette-4b-flat              a=3.2e-01 / b=2.43
         totally_random
       31: GemCloudIce                            a=4.4e+02 / b=3.00
         totally_random
       27: IconCloudIce                           a=1.6e+00 / b=2.56
         totally_random
       14: LiuLongColumn                          a=3.4e+01 / b=3.00
         totally_random
        4: HongBulletRosette-3b-perp              a=4.4e-01 / b=2.47
         totally_random
       10: HongBulletRosette-4b-perp              a=3.2e-01 / b=2.43
         totally_random
        9: HongPlate                              a=7.6e-01 / b=2.48
         totally_random
       24: IceSphere                              a=4.8e+02 / b=3.00
         totally_random
        3: LiuSectorSnowflake                     a=8.2e-04 / b=1.44
         totally_random
       13: LiuShortColumn                         a=1.1e+02 / b=3.00
         totally_random
       15: LiuThickPlate                          a=1.1e+02 / b=3.00
```

```
         totally_random
       16: LiuThinPlate                                a=3.0e+01 / b=3.00
         totally_random
Liquid
---
 SingleCrystals
  Pristine
       25: LiquidSphere                                a=5.2e+02 / b=3.00
         totally_random

-------------------------------------------------------------------------
```

Exploring the database: Habit overview `ssdb_display` can also provide overview information for each habit included. For a specified habit id number, it can list available particle sizes, for example (output cropped):

```
>> ssdb_display(3,'totally_random')


--- 3: SectorSnowflake - totally_random ---

    a = 8.2e-04 / b = 1.44
    N = 34

    Dveq [um]   Dmax [um]   Mass [g]
    ---------   ---------   --------
        20          20      3.84e-09
        40          40      3.07e-08
        60          60      1.04e-07
        80          80      2.46e-07
       100         100      4.80e-07
       120         120      8.29e-07
       ...
```

Exploring the database: Particle overview More detailed information on available data can obtained for particles of specified size, providing the size as another input parameter, e.g. (output cropped):

```
>> ssdb_display(3,'totally_random',100e-6)

--- 3: SectorSnowflake - totally_random - 100 um ---

 Frequency [GHz]   x [-]   Temperatures [K]
 ---------------   -----   ----------------
          1.000    0.00   190.00  230.00  270.00
          3.000    0.00   190.00  230.00  270.00
          5.000    0.01   190.00  230.00  270.00
          9.000    0.01   190.00  230.00  270.00
         10.000    0.01   190.00  230.00  270.00
         ...
```

Importing data Further data locating and selection commonly works through the habit Id. For example, `ssdb_import_habit` extracts all data for a given habit, identified by the habit Id, and orientation, where the user might optionally specify and limit frequency, temperature, and size ranges:

```
>> data = ssdb_import_habit(3,'totally_random')
```

In this example, by not specifying them, default frequency, temperature, and size ranges are applied, which are set such that no data are removed from the selection. The output variable `data` will be a struct array (MATLAB) or a list of dictionary (Python), with one array/list entry per individual particle (or, particle size) and mainly holding the SSP of the particles in the database format as well as some additional auxiliary parameters (e.g. size description parameters). For example, `data(i).mass` and `data[i]['mass']` would provide the mass of particle `i` in MATLAB and Python, respectively.

The same extraction, followed by a conversion to ARTS SSP format can be achieved by `assp_import_ssdb` (in the Python interface included in the assp module) providing arrays/lists of ARTS single scattering (`S`) and scattering meta data (`M`), e.g.:

```
>> [S,M] = assp_import_ssdb(3,'totally_random')
```

where `S` and `M` then could be written to file using functions provided by the Atmlab or typhon packages.

C.3. RTTOV-SCATT changes

The following source files of the Mie coefficient table module of RTTOV-SCATT, residing in RTTOV's source subfolder `mw_scatt_coef`, have been modified (in alphabetical order):

```
density_all.F90
get_dia.F90
mie_one_temp.F90
mod_mie.F90
predict_psd_F07.F90
predict_psd.F90
rttov_scatt_make_coef.F90
scattering.F90
set_spectra.F90
```

These files have been newly created and are supposed to be added to `mw_scatt_coef` (in alphabetical order):

```
arts_scat.F90
load_arts_ssp.F90
mod_arts.F90
```

`mod_arts.F90` holds required meta information about the data available and is the place to register all data files extracted from the ARTS scattering database that shall be made known to the Mie coefficient module. Below is an example of `mod_arts.F90`:

```
module mod_arts

! Any habit from the ARTS SSP database needs to be registered here.
! That is, this module needs to be updated whenever new habits are added
! or existing ones modified.
! The order of entries in all per-habit data arrays below has to be
! identical.

use parkind1,  only: jprb, jpim, jplm
use mod_mie, only: lmax ! add whatever is needed

implicit none


!* base location of the RTTOV-SSP files from the ARTS SPP database
character(len=lmax) :: arts_folder = ''

!* total number of registered ARTS habits
integer (kind=jpim), parameter :: n_arts_habits = 2

!* maximum (allowed) f, T, D dimensions from ARTS data
integer (kind=jpim), parameter :: nf_max_arts = 34
integer (kind=jpim), parameter :: nT_max_arts =  3
integer (kind=jpim), parameter :: nD_max_arts = 45

!* maximum (allowed) extrapolation factors in f, T, D from ARTS data
real (kind=jprb), parameter :: f_extpol = 0.5
real (kind=jprb), parameter :: T_extpol = 0.5
real (kind=jprb), parameter :: D_extpol = 1e-6


!* filenames of the habits
character(len=28), dimension (n_arts_habits) :: arts_files = (/ &   ! ID
  'ID03_LiuSectorSnowflake.rssp', &                                 !  1
  'ID08_HongAggregate.rssp     ' &                                  !  2
  /)

!* Min / max diameters of the habits (Dmax [m])
real (kind=jprb), dimension (n_arts_habits) :: d_arts_min = (/ &
  2.000000e-05, &    !  1
  1.942867e-05 &     !  2
  /)
real (kind=jprb), dimension (n_arts_habits) :: d_arts_max = (/ &
  1.023801e-02, &    !  1
```

```
  9.714335e-03 &     !  2
  /)

!* Alpha and beta of mass-dimension relationship (m=a*Dmaxˆb) (for m [kg]
!* and Dmax [m])
real (kind=jprb), dimension (n_arts_habits) :: alpha_arts = (/ &
  8.17711e-04, &  !  1
  6.54480e+01 &   !  2
  /)
real (kind=jprb), dimension (n_arts_habits) :: beta_arts = (/ &
  1.44387e+00, &  !  1
  3.00000e+00 &   !  2
  /)

end module mod_arts
```

D. Habit reports

SSP Data Summary

Plate Type 1

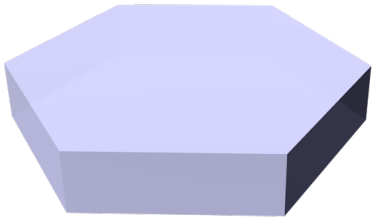

Publication date 20-Nov-2017 22:08:31

Chapter 1. Habit Specifications

Table 1.1. Habit description

Description	Hexagonal plate, using Hong parametrization (Hong 2007).
Source	location: Chalmers, software: Snowflake-toolkit (Rathsman 2016), parameterization: Hong 2007.
Comment	Note that values of alpha and beta are calculated for the upper end of d_max.

Figure 1.1. Shape rendering.

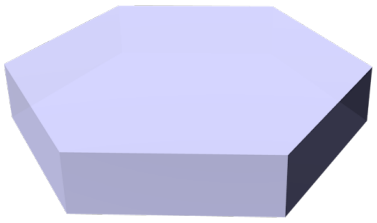

Rendering of a selected shape using Blender (https://www.blender.org/).

Table 1.2. Size parameters

	min	max	# of sizes
D_max [um]	13	8933	44
D_e [um]	10	2365	

Table 1.3. Shape parameters

α	0.7570
β	2.4770

Figure 1.2. Mass-size relationship

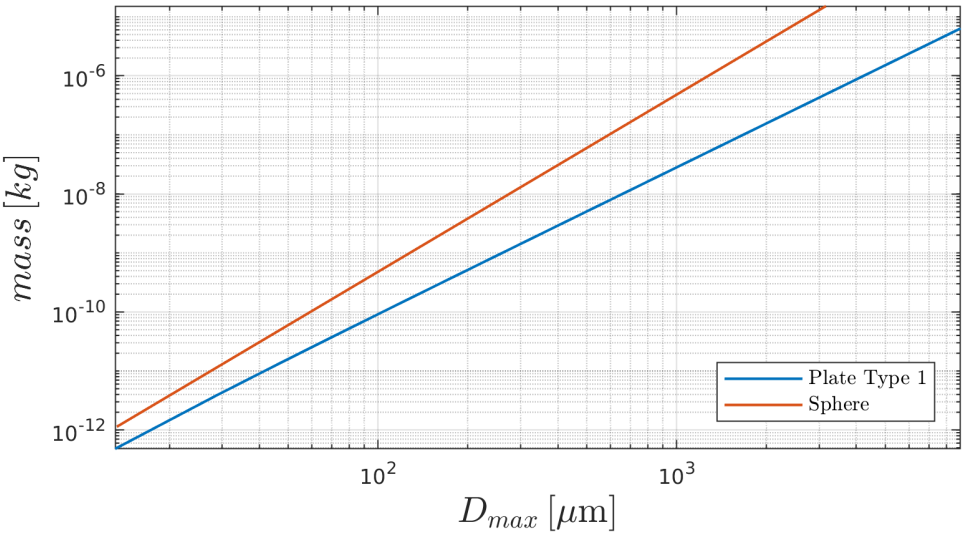

Mass as a function of D_max. Sphere included as a reference. Ice density assumed.

Chapter 2. Single Scattering Properties

Table 2.1. SSP description

Source	ADDA (Yurkin 2011)
Format	ARTS SSP format v.3
Orientation	totally_random
Density [kg/m³]	ice (916.70)
Refractive index	Matzler 2006

Table 2.2. SSP grid

frequency [GHz]	1, 1, 3, 5, 7, 9, 10, 13, 15, 19, 24, 31, 32, 36, 50, 58, 89, 94, 115, 122, 164, 167, 175, 191, 228, 247, 314, 336, 439, 457, 657, 671, 862, 886,
Temperature [K]	190, 230, 270,

Figure 2.1. Extinction

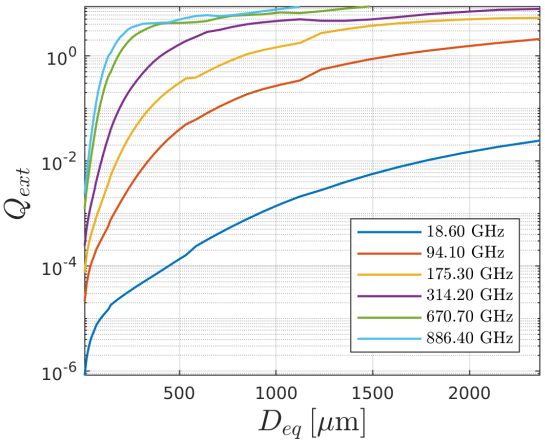

Extinction efficiency as a function of volume volume equivalent diameter, for a selection of six frequencies. Temperature is 230 K.

Figure 2.2. Assymetry parameter

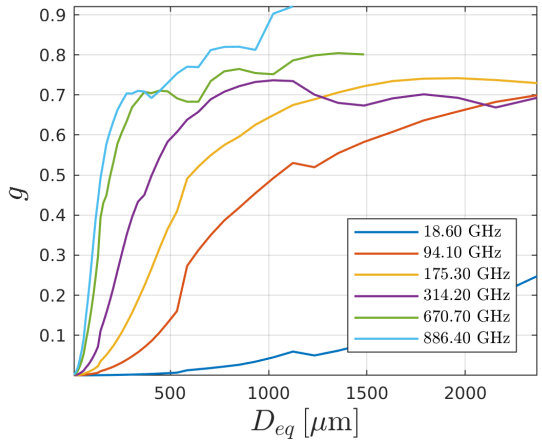

Assymetry parameter as a function of volume equivalent diameter, for a selection of six frequencies. Temperature is 230 K.

Figure 2.3. Single scattering albedo

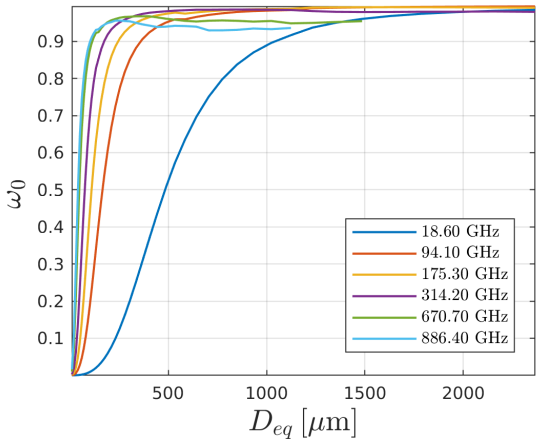

Single scattering albedo as a function of volume volume equivalent diameter, for a selection of six frequencies. Temperature is 230 K.

SSP Data Summary

Column Type 1

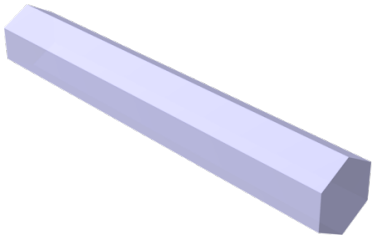

Publication date 20-Nov-2017 22:06:43

Chapter 1. Habit Specifications

Table 1.1. Habit description

Description	Hexagonal column, using Hong parametrization (Hong 2007).
Source	location: Chalmers, software: Snowflake-toolkit (Rathsman 2016), parameterization: Hong 2007.
Comment	Note that values of alpha and beta are calculated for the upper end of d_max.

Figure 1.1. Shape rendering.

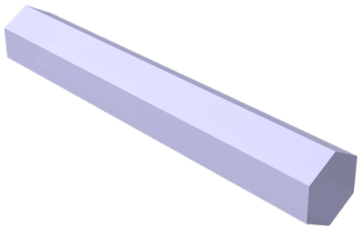

Rendering of a selected shape using Blender (https://www.blender.org/).

Table 1.2. Size parameters

	min	max	# of sizes
D_max [um]	14	8835	44
D_e [um]	10	1671	

Table 1.3. Shape parameters

α	0.0380
β	2.0511

Figure 1.2. Mass-size relationship

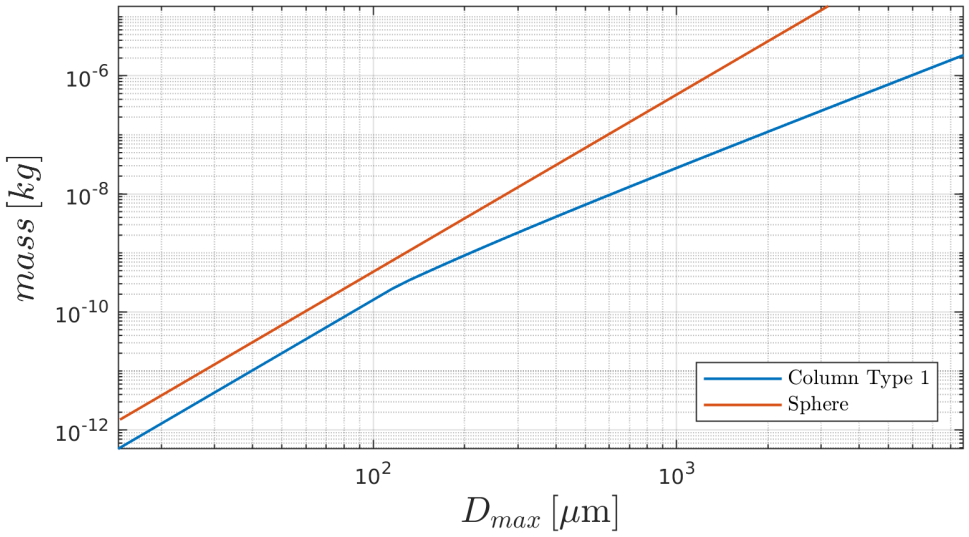

Mass as a function of D_max. Sphere included as a reference. Ice density assumed.

Chapter 2. Single Scattering Properties

Table 2.1. SSP description

Source	ADDA (Yurkin 2011)
Format	ARTS SSP format v.3
Orientation	totally_random
Density [kg/m³]	ice (916.70)
Refractive index	Matzler 2006

Table 2.2. SSP grid

frequency [GHz]	1, 1, 3, 5, 7, 9, 10, 13, 15, 19, 24, 31, 32, 36, 50, 58, 89, 94, 115, 122, 164, 167, 175, 191, 228, 247, 314, 336, 439, 457, 657, 671, 862, 886,
Temperature [K]	190, 230, 270,

Figure 2.1. Extinction

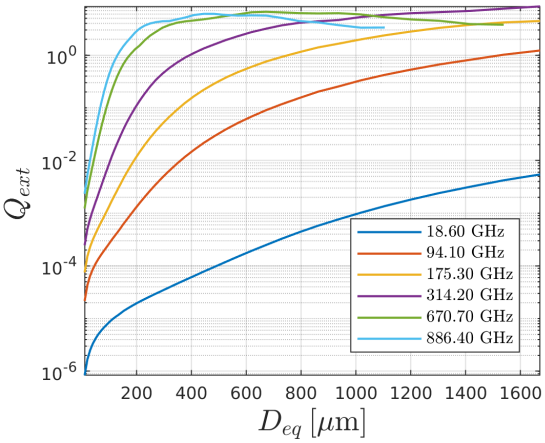

Extinction efficiency as a function of volume volume equivalent diameter, for a selection of six frequencies. Temperature is 230 K.

Figure 2.2. Assymetry parameter

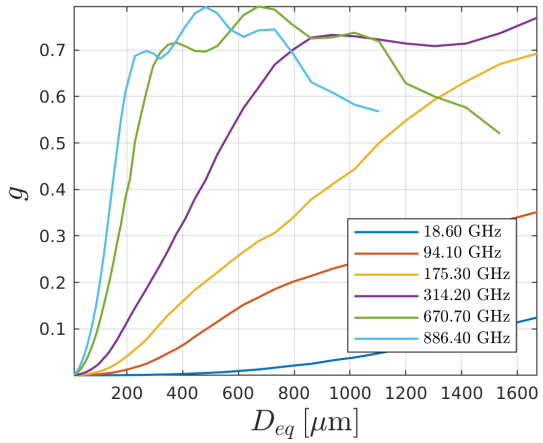

Assymetry parameter as a function of volume equivalent diameter, for a selection of six frequencies. Temperature is 230 K.

Figure 2.3. Single scattering albedo

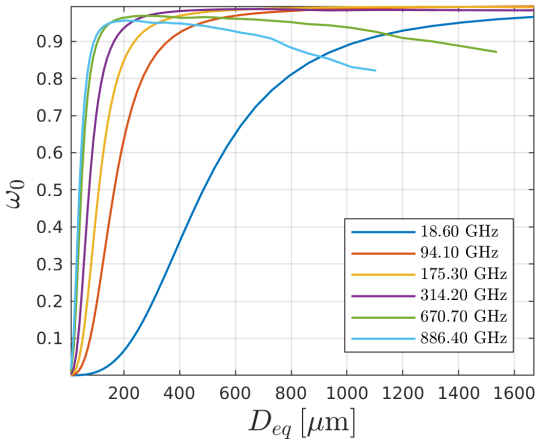

Single scattering albedo as a function of volume volume equivalent diameter, for a selection of six frequencies. Temperature is 230 K.

SSP Data Summary

Thin Plate

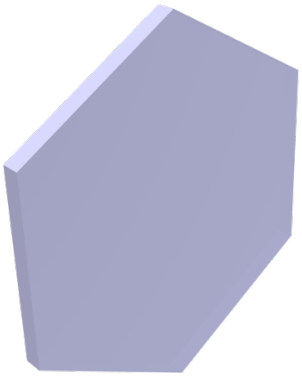

Publication date 20-Nov-2017 22:14:12

Chapter 1. Habit Specifications

Table 1.1. Habit description

Description	Hexagonal thin plate, using Liu parametrization (Liu 2008).
Source	location: Chalmers, software: Snowflake-toolkit (Rathsman 2016), parameterization: Liu 2008.
Comment	Note that aspect ratio is constant.

Figure 1.1. Shape rendering.

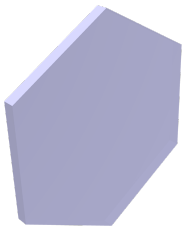

Rendering of a selected shape using Blender (https://www.blender.org/).

Table 1.2. Size parameters

	min	max	# of sizes
D_max [um]	25	4490	34
D_e [um]	10	1775	

Table 1.3. Shape parameters

α	29.6594
β	3

Figure 1.2. Mass-size relationship

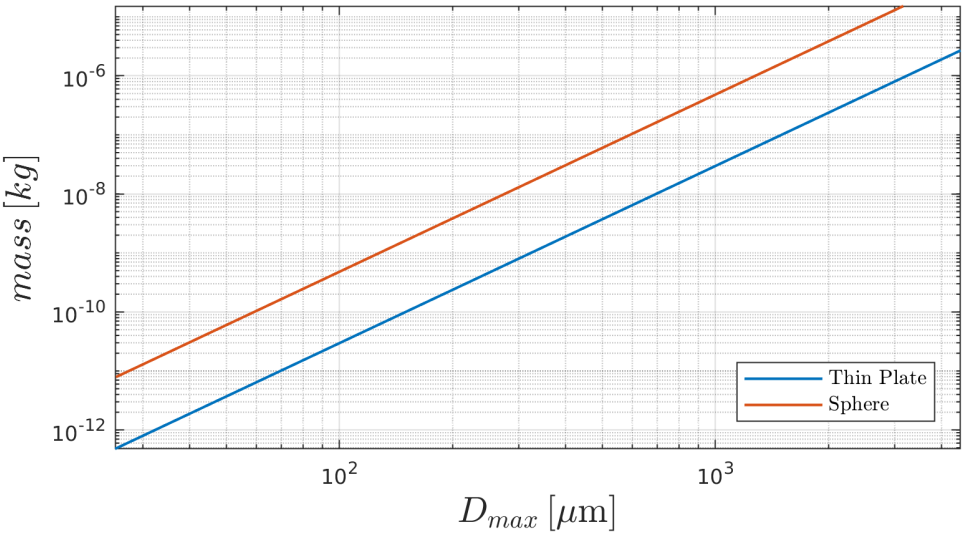

Mass as a function of D_max. Sphere included as a reference. Ice density assumed.

Chapter 2. Single Scattering Properties

Table 2.1. SSP description

Source	ADDA (Yurkin 2011)
Format	ARTS SSP format v.3
Orientation	totally_random
Density [kg/m³]	ice (916.70)
Refractive index	Matzler 2006

Table 2.2. SSP grid

frequency [GHz]	1, 1, 3, 5, 7, 9, 10, 13, 15, 19, 24, 31, 32, 36, 50, 58, 89, 94, 115, 122, 164, 167, 175, 191, 228, 247, 314, 336, 439, 457, 657, 671, 862, 886,
Temperature [K]	190, 230, 270,

Figure 2.1. Extinction

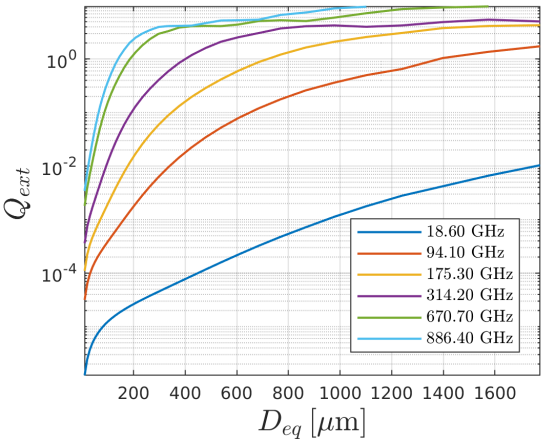

Extinction efficiency as a function of volume volume equivalent diameter, for a selection of six frequencies. Temperature is 230 K.

Figure 2.2. Assymetry parameter

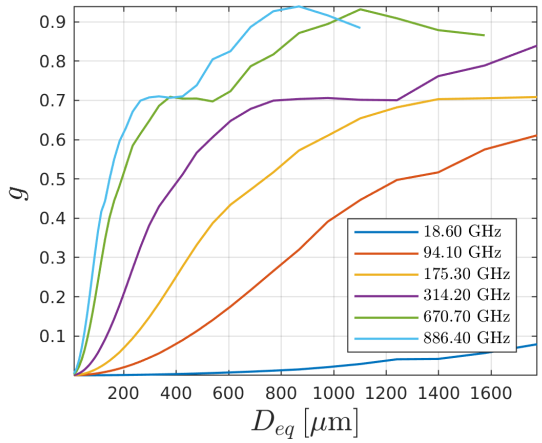

Assymetry parameter as a function of volume equivalent diameter, for a selection of six frequencies. Temperature is 230 K.

Figure 2.3. Single scattering albedo

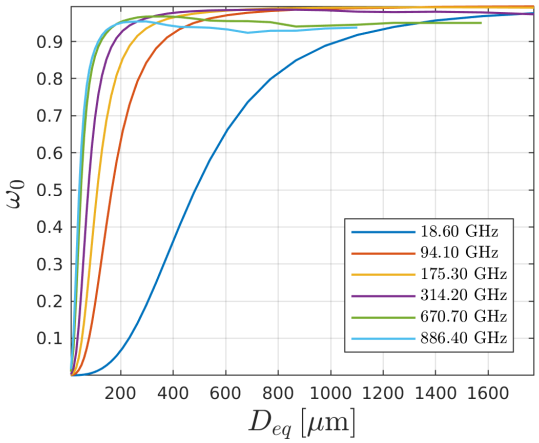

Single scattering albedo as a function of volume volume equivalent diameter, for a selection of six frequencies. Temperature is 230 K.

SSP Data Summary

Thick Plate

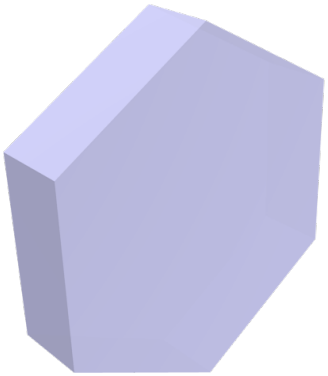

Publication date 20-Nov-2017 22:13:28

Chapter 1. Habit Specifications

Table 1.1. Habit description

Description	Hexagonal thick plate, using Liu parametrization (Liu 2008).
Source	location: Chalmers, software: Snowflake-toolkit (Rathsman 2016), parameterization: Liu 2008.
Comment	Note that aspect ratio is constant.

Figure 1.1. Shape rendering.

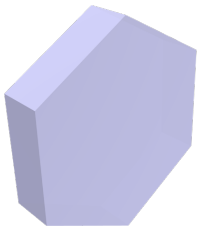

Rendering of a selected shape using Blender (https://www.blender.org/).

Table 1.2. Size parameters

	min	max	# of sizes
D_max [um]	16	2881	34
D_e [um]	10	1775	

Table 1.3. Shape parameters

α	112.2791
β	3.0000

Figure 1.2. Mass-size relationship

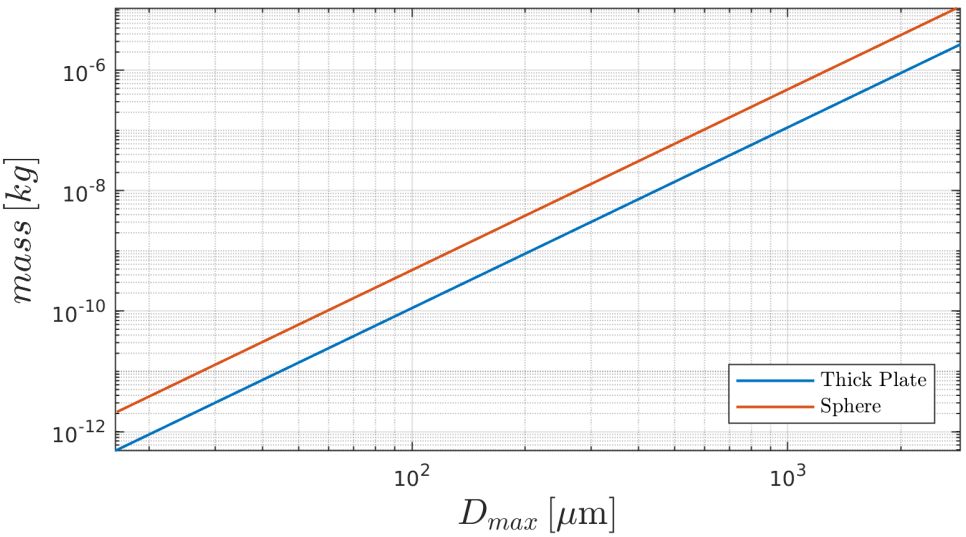

Mass as a function of D_max. Sphere included as a reference. Ice density assumed.

Chapter 2. Single Scattering Properties

Table 2.1. SSP description

Source	ADDA (Yurkin 2011)
Format	ARTS SSP format v.3
Orientation	totally_random
Density [kg/m³]	ice (916.70)
Refractive index	Matzler 2006

Table 2.2. SSP grid

frequency [GHz]	1, 1, 3, 5, 7, 9, 10, 13, 15, 19, 24, 31, 32, 36, 50, 58, 89, 94, 115, 122, 164, 167, 175, 191, 228, 247, 314, 336, 439, 457, 657, 671, 862, 886,
Temperature [K]	190, 230, 270,

Figure 2.1. Extinction

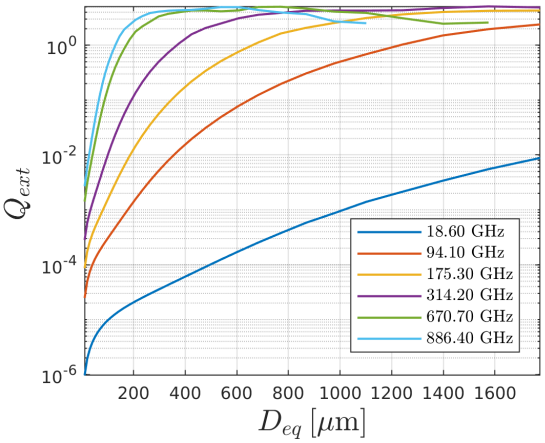

Extinction efficiency as a function of volume volume equivalent diameter, for a selection of six frequencies. Temperature is 230 K.

Figure 2.2. Assymetry parameter

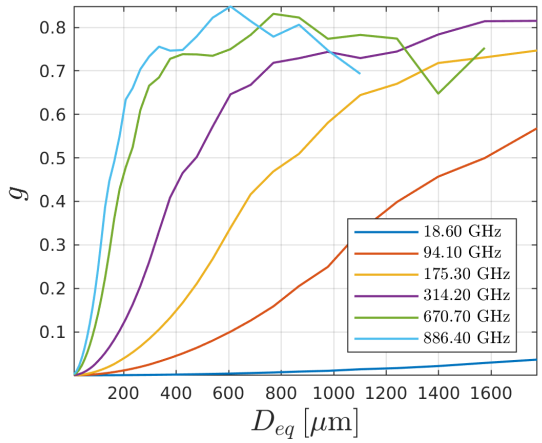

Assymetry parameter as a function of volume equivalent diameter, for a selection of six frequencies. Temperature is 230 K.

Figure 2.3. Single scattering albedo

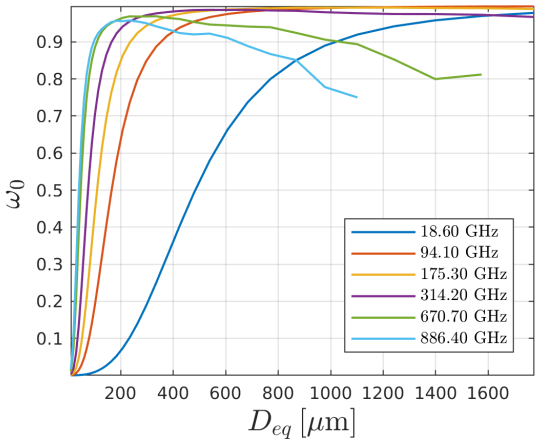

Single scattering albedo as a function of volume volume equivalent diameter, for a selection of six frequencies. Temperature is 230 K.

SSP Data Summary

Block Column

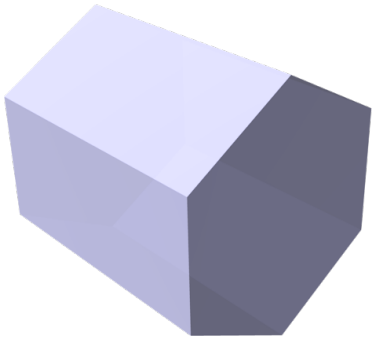

Publication date 20-Nov-2017 22:10:59

Chapter 1. Habit Specifications

Table 1.1. Habit description

Description	Hexagonal block column, using Liu parametrization (Liu 2008).
Source	location: Chalmers, software: Snowflake-toolkit (Rathsman 2016), parameterization: Liu 2008.
Comment	Note that aspect ratio is constant.

Figure 1.1. Shape rendering.

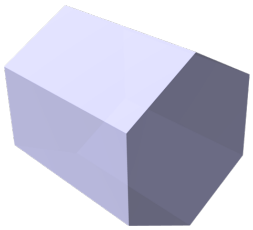

Rendering of a selected shape using Blender (https://www.blender.org/).

Table 1.2. Size parameters

	min	max	# of sizes
D_max [um]	13	2336	34
D_e [um]	10	1775	

Table 1.3. Shape parameters

α	210.5107
β	3.0000

Figure 1.2. Mass-size relationship

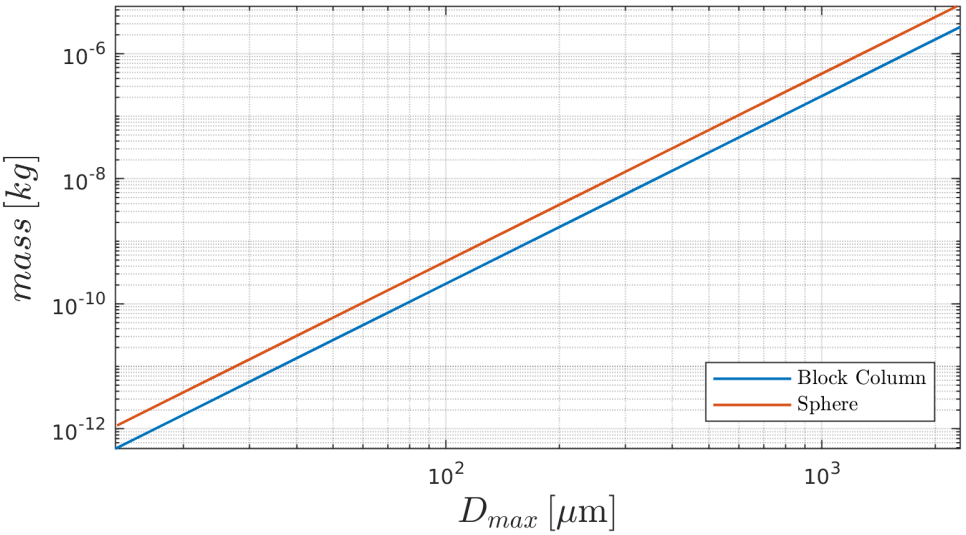

Mass as a function of D_max. Sphere included as a reference. Ice density assumed.

Chapter 2. Single Scattering Properties

Table 2.1. SSP description

Source	ADDA (Yurkin 2011)
Format	ARTS SSP format v.3
Orientation	totally_random
Density [kg/m³]	ice (916.70)
Refractive index	Matzler 2006

Table 2.2. SSP grid

frequency [GHz]	1, 1, 3, 5, 7, 9, 10, 13, 15, 19, 24, 31, 32, 36, 50, 58, 89, 94, 115, 122, 164, 167, 175, 191, 228, 247, 314, 336, 439, 457, 657, 671, 862, 886,
Temperature [K]	190, 230, 270,

Figure 2.1. Extinction

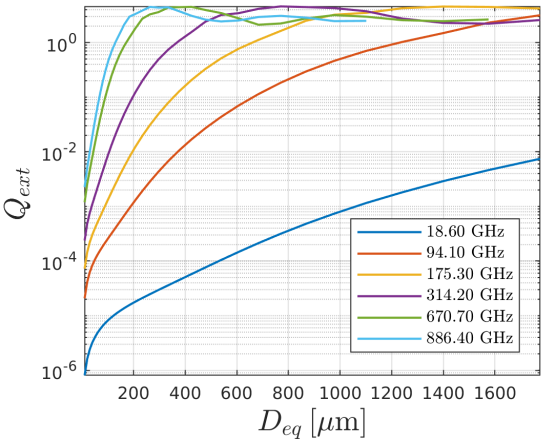

Extinction efficiency as a function of volume volume equivalent diameter, for a selection of six frequencies. Temperature is 230 K.

Figure 2.2. Assymetry parameter

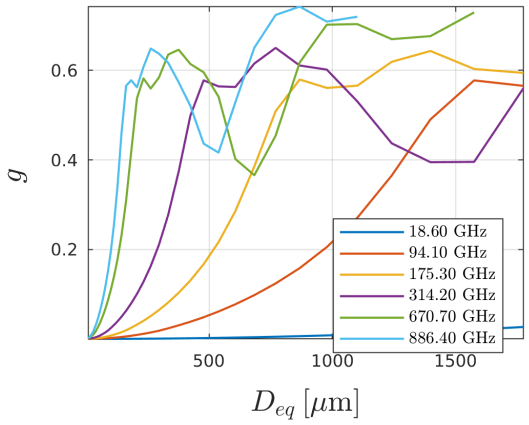

Assymetry parameter as a function of volume equivalent diameter, for a selection of six frequencies. Temperature is 230 K.

Figure 2.3. Single scattering albedo

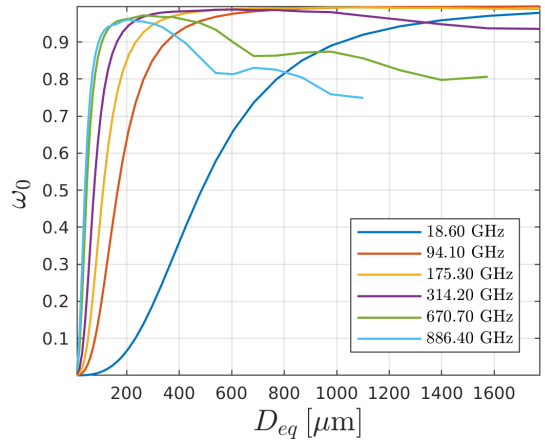

Single scattering albedo as a function of volume volume equivalent diameter, for a selection of six frequencies. Temperature is 230 K.

SSP Data Summary

Short Column

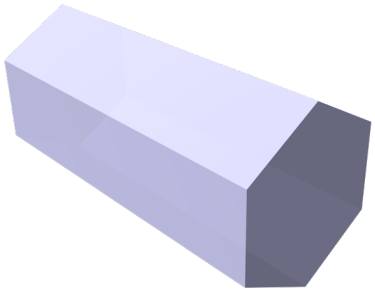

Publication date 20-Nov-2017 22:11:47

Chapter 1. Habit Specifications

Table 1.1. Habit description

Description	Hexagonal short column, using Liu parametrization (Liu 2008).
Source	location: Chalmers, software: Snowflake-toolkit (Rathsman 2016), parameterization: Liu 2008.
Comment	Note that aspect ratio is constant.

Figure 1.1. Shape rendering.

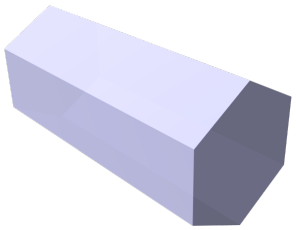

Rendering of a selected shape using Blender (https://www.blender.org/).

Table 1.2. Size parameters

	min	max	# of sizes
D_max [um]	17	2932	34
D_e [um]	10	1775	

Table 1.3. Shape parameters

α	106.5109
β	3.0000

Figure 1.2. Mass-size relationship

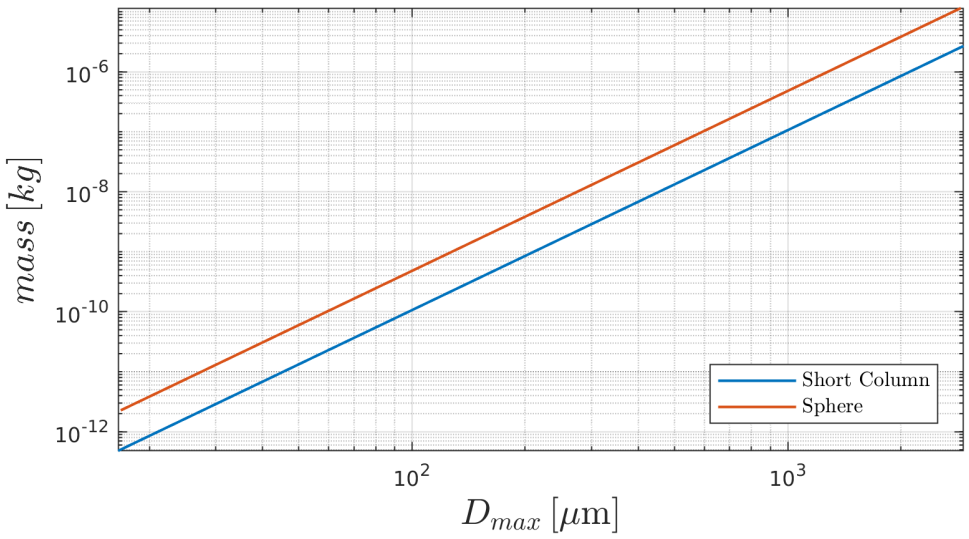

Mass as a function of D_max. Sphere included as a reference. Ice density assumed.

Chapter 2. Single Scattering Properties

Table 2.1. SSP description

Source	ADDA (Yurkin 2011)
Format	ARTS SSP format v.3
Orientation	totally_random
Density [kg/m³]	ice (916.70)
Refractive index	Matzler 2006

Table 2.2. SSP grid

frequency [GHz]	1, 1, 3, 5, 7, 9, 10, 13, 15, 19, 24, 31, 32, 36, 50, 58, 89, 94, 115, 122, 164, 167, 175, 191, 228, 247, 314, 336, 439, 457, 657, 671, 862, 886,
Temperature [K]	190, 230, 270,

Figure 2.1. Extinction

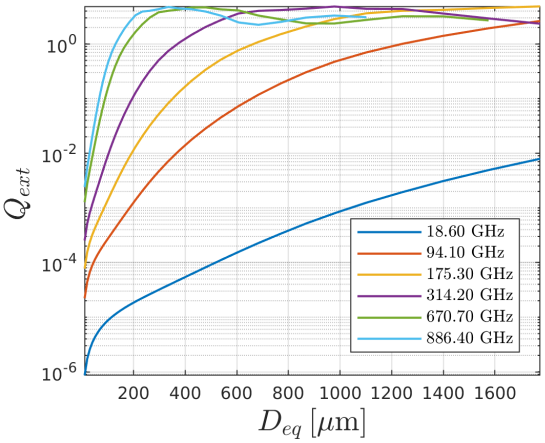

Extinction efficiency as a function of volume volume equivalent diameter, for a selection of six frequencies. Temperature is 230 K.

Figure 2.2. Assymetry parameter

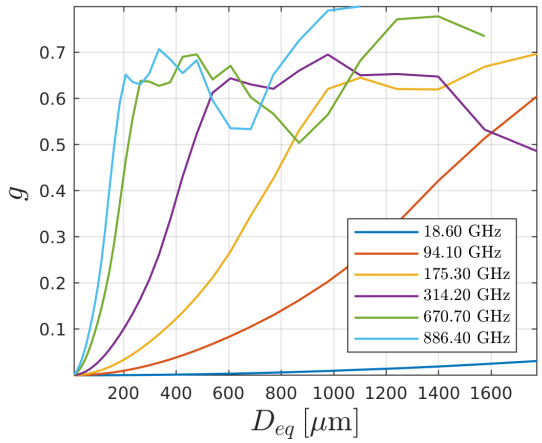

Assymetry parameter as a function of volume equivalent diameter, for a selection of six frequencies. Temperature is 230 K.

Figure 2.3. Single scattering albedo

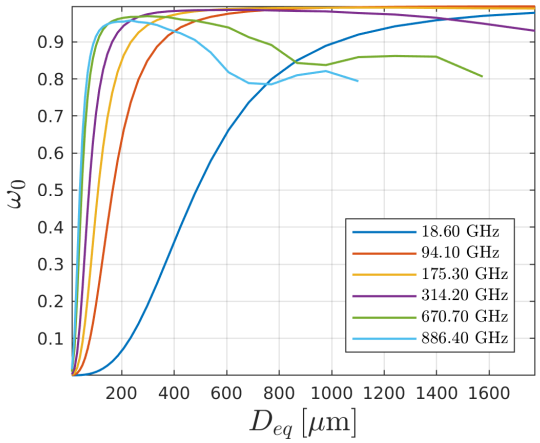

Single scattering albedo as a function of volume volume equivalent diameter, for a selection of six frequencies. Temperature is 230 K.

SSP Data Summary

Long Column

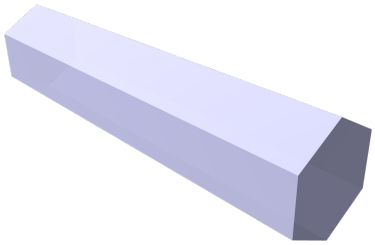

Publication date 20-Nov-2017 22:12:30

Chapter 1. Habit Specifications

Table 1.1. Habit description

Description	Hexagonal long column, using Liu parametrization (Liu 2008).
Source	location: Chalmers, software: Snowflake-toolkit (Rathsman 2016), parameterization: Liu 2008.
Comment	Note that aspect ratio is constant.

Figure 1.1. Shape rendering.

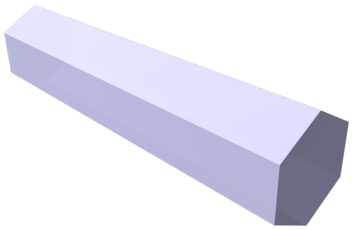

Rendering of a selected shape using Blender (https://www.blender.org/).

Table 1.2. Size parameters

	min	max	# of sizes
D_max [um]	24	4291	34
D_e [um]	10	1775	

Table 1.3. Shape parameters

α	33.9786
β	3.0000

Figure 1.2. Mass-size relationship

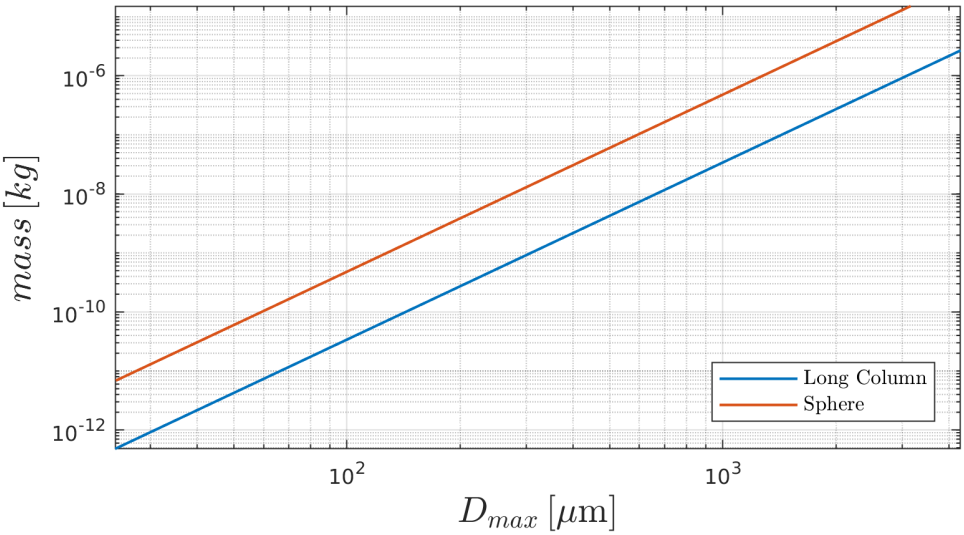

Mass as a function of D_max. Sphere included as a reference. Ice density assumed.

Chapter 2. Single Scattering Properties

Table 2.1. SSP description

Source	ADDA (Yurkin 2011)
Format	ARTS SSP format v.3
Orientation	totally_random
Density [kg/m³]	ice (916.70)
Refractive index	Matzler 2006

Table 2.2. SSP grid

frequency [GHz]	1, 1, 3, 5, 7, 9, 10, 13, 15, 19, 24, 31, 32, 36, 50, 58, 89, 94, 115, 122, 164, 167, 175, 191, 228, 247, 314, 336, 439, 457, 657, 671, 862, 886,
Temperature [K]	190, 230, 270,

Figure 2.1. Extinction

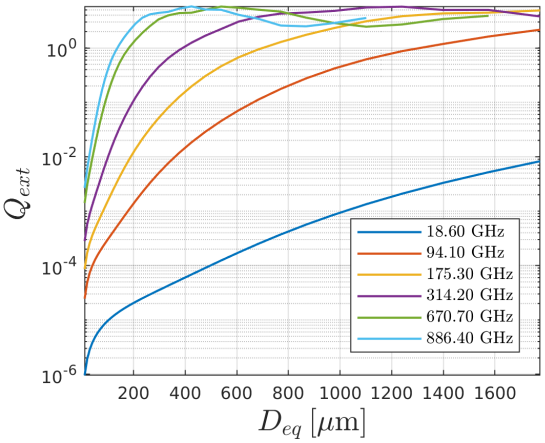

Extinction efficiency as a function of volume volume equivalent diameter, for a selection of six frequencies. Temperature is 230 K.

Figure 2.2. Assymetry parameter

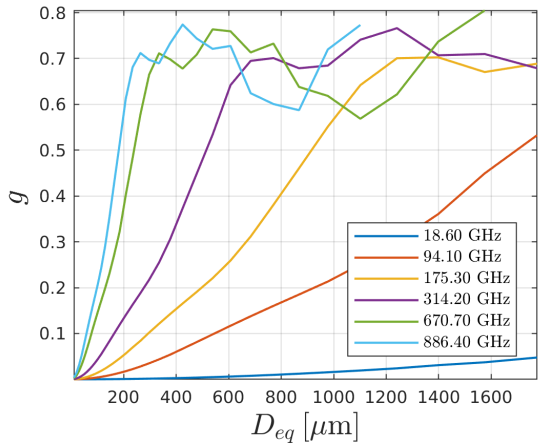

Assymetry parameter as a function of volume equivalent diameter, for a selection of six frequencies. Temperature is 230 K.

Figure 2.3. Single scattering albedo

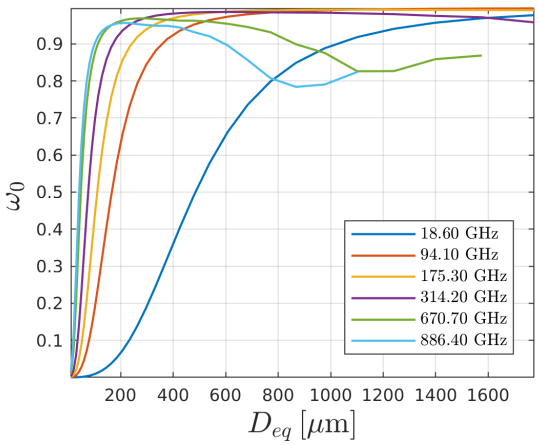

Single scattering albedo as a function of volume volume equivalent diameter, for a selection of six frequencies. Temperature is 230 K.

SSP Data Summary

Sector Snowflake

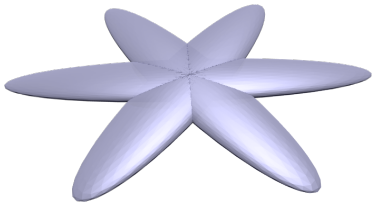

Publication date 20-Nov-2017 22:03:53

Chapter 1. Habit Specifications

Table 1.1. Habit description

Description	Sector snowflake, using Liu parametrization (Liu 2008).
Source	location: Chalmers, software: Snowflake-toolkit (Rathsman 2016), parameterization: Liu 2008.
Comment	Note that the alpha and beta values are calculated for the upper end of d_max, since the shape transitions to spheroidal in the lower end of d_max.

Figure 1.1. Shape rendering.

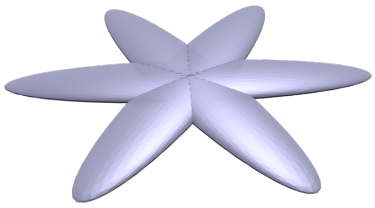

Rendering of a selected shape using Blender (https://www.blender.org/).

Table 1.2. Size parameters

	min	max	# of sizes
D_max [um]	20	8735	33
D_e [um]	20	1216	

Table 1.3. Shape parameters

α	8.2226e-04
β	1.4446

Figure 1.2. Mass-size relationship

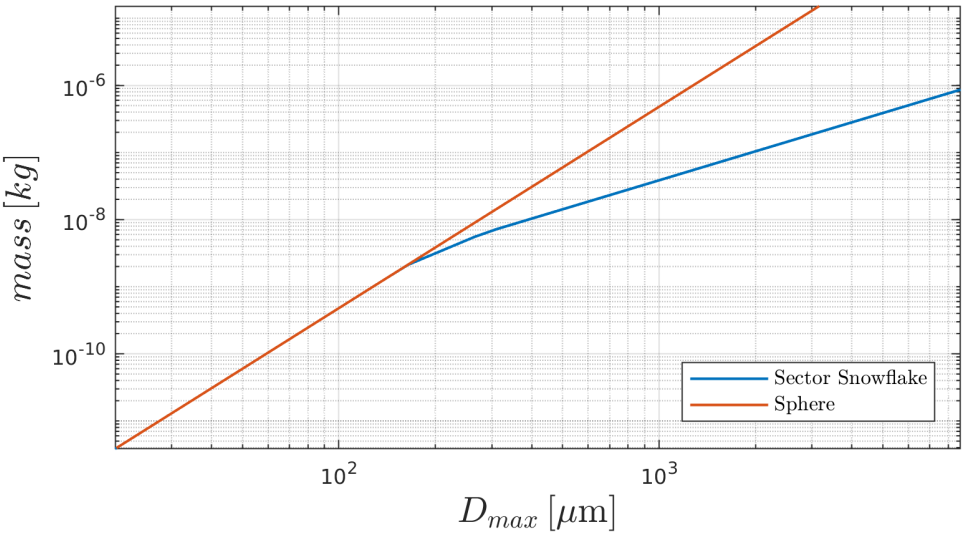

Mass as a function of D_max. Sphere included as a reference. Ice density assumed.

Chapter 2. Single Scattering Properties

Table 2.1. SSP description

Source	ADDA (Yurkin 2011)
Format	ARTS SSP format v.3
Orientation	totally_random
Density [kg/m³]	ice (916.70)
Refractive index	Matzler 2006

Table 2.2. SSP grid

frequency [GHz]	1, 1, 3, 5, 7, 9, 10, 13, 15, 19, 24, 31, 32, 36, 50, 58, 89, 94, 115, 122, 164, 167, 175, 191, 228, 247, 314, 336, 439, 457, 657, 671, 862, 886,
Temperature [K]	190, 230, 270,

Figure 2.1. Extinction

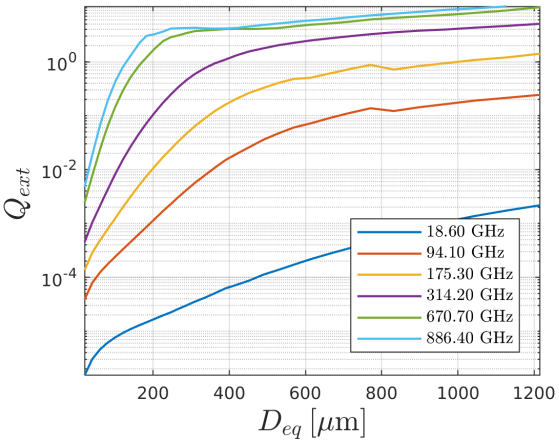

Extinction efficiency as a function of volume volume equivalent diameter, for a selection of six frequencies. Temperature is 230 K.

Figure 2.2. Assymetry parameter

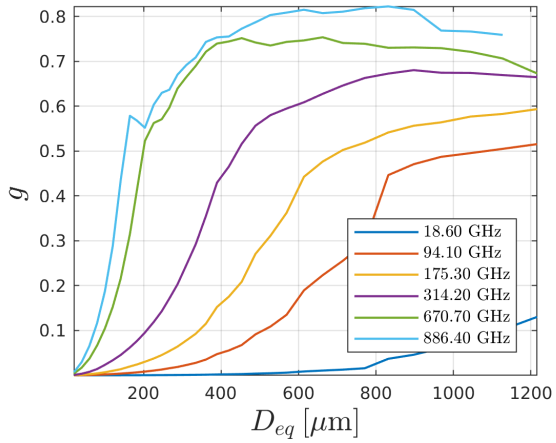

Assymetry parameter as a function of volume equivalent diameter, for a selection of six frequencies. Temperature is 230 K.

Figure 2.3. Single scattering albedo

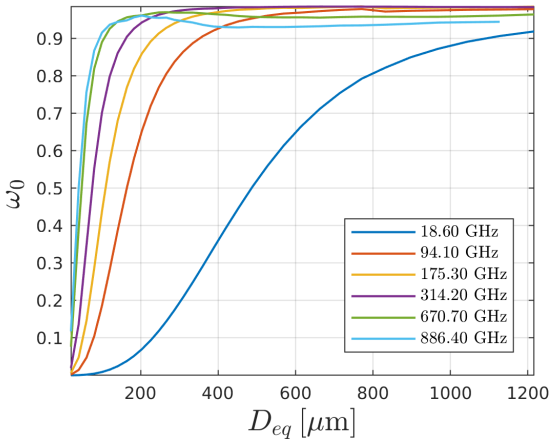

Single scattering albedo as a function of volume volume equivalent diameter, for a selection of six frequencies. Temperature is 230 K.

SSP Data Summary

Ice Sphere

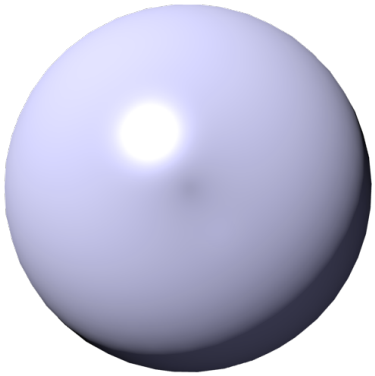

Robin Ekelund

Publication date 25-Oct-2017 21:36:10

Chapter 1. Habit Specifications

Table 1.1. Habit description

Description	Ice sphere
Source	location: Chalmers
Comment	

Figure 1.1. Shape rendering.

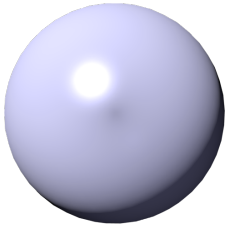

Rendering of a selected shape using Blender (https://www.blender.org/).

Table 1.2. Size parameters

	min	max	# of sizes
D_max [um]	1	47354	199
D_e [um]	1	47354	

Table 1.3. Shape parameters

α	479.9830
β	3.0000

Figure 1.2. Mass-size relationship

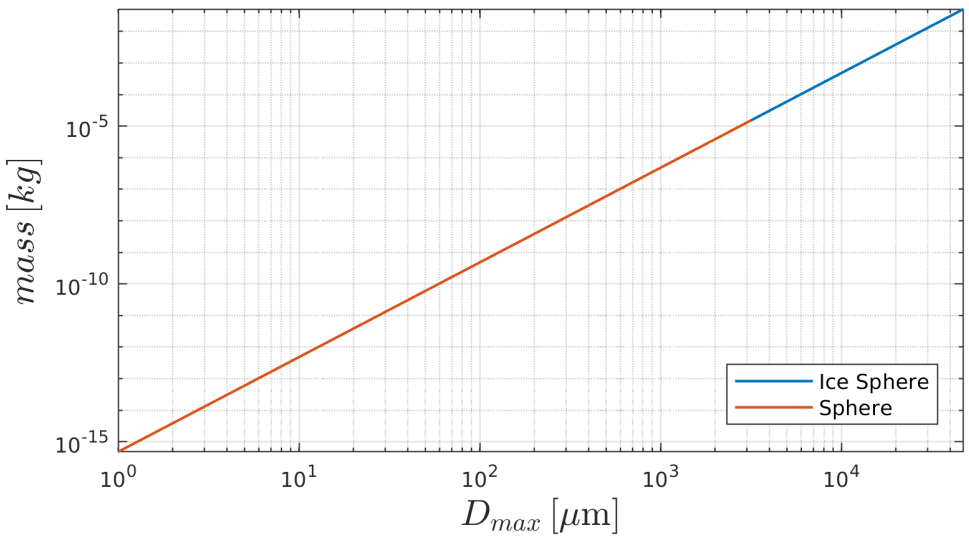

Mass as a function of D_max. Sphere included as a reference. Ice density assumed.

Chapter 2. Single Scattering Properties

Table 2.1. SSP description

Source	ADDA (Yurkin 2011)
Format	ARTS SSP format v.3
Orientation	totally_random
Density [kg/m³]	ice (405.54)
Refractive index	Matzler 2006

Table 2.2. SSP grid

frequency [GHz]	1, 1, 3, 5, 7, 9, 10, 13, 15, 19, 24, 31, 32, 36, 50, 58, 89, 94, 115, 122, 164, 167, 175, 191, 228, 247, 314, 336, 439, 457, 657, 671, 862, 886,
Temperature [K]	190, 230, 270,

Figure 2.1. Extinction

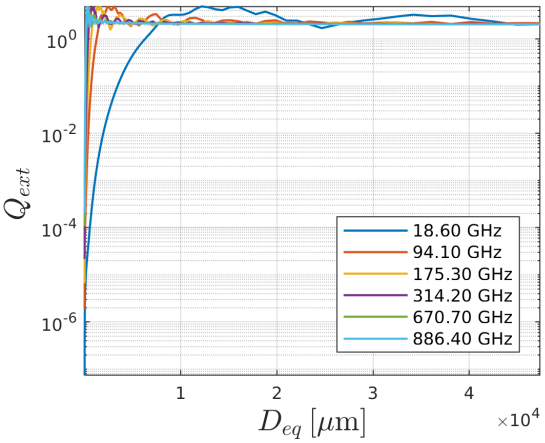

Extinction efficiency as a function of volume volume equivalent diameter, for a selection of six frequencies. Temperature is 230 K.

Figure 2.2. Assymetry parameter

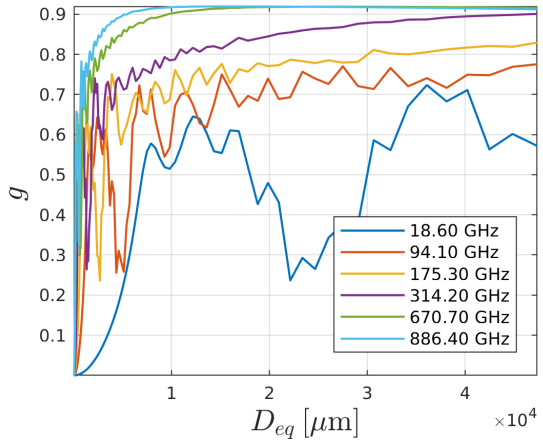

Assymetry parameter as a function of volume equivalent diameter, for a selection of six frequencies. Temperature is 230 K.

Figure 2.3. Single scattering albedo

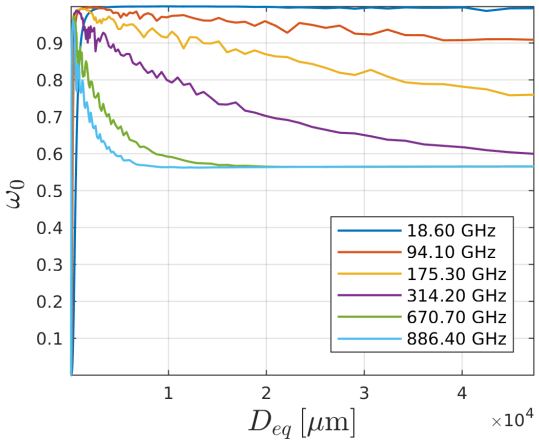

Single scattering albedo as a function of volume volume equivalent diameter, for a selection of six frequencies. Temperature is 230 K.

SSP Data Summary

ICON Cloud Ice

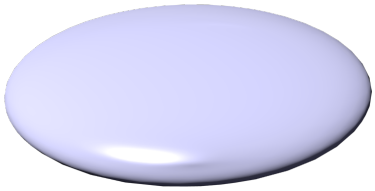

Publication date 20-Nov-2017 22:20:21

Chapter 1. Habit Specifications

Table 1.1. Habit description

Description	ICON cloud ice
Source	location: Chalmers, software: Rimecraft.
Comment	

Figure 1.1. Shape rendering.

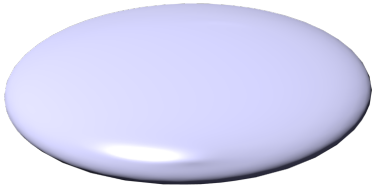

Rendering of a selected shape using Blender (https://www.blender.org/).

Table 1.2. Size parameters

	min	max	# of sizes
D_max [um]	13	8931	44
D_e [um]	10	2660	

Table 1.3. Shape parameters

α	1.5900
β	2.5600

Figure 1.2. Mass-size relationship

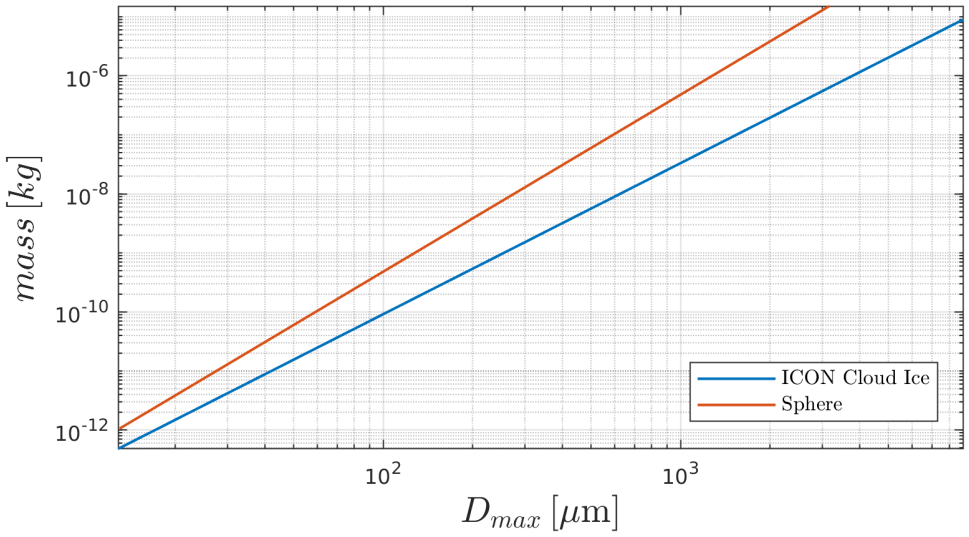

Mass as a function of D_max. Sphere included as a reference. Ice density assumed.

Chapter 2. Single Scattering Properties

Table 2.1. SSP description

Source	ADDA (Yurkin 2011)
Format	ARTS SSP format v.3
Orientation	totally_random
Density [kg/m³]	ice (916.70)
Refractive index	Matzler 2006

Table 2.2. SSP grid

frequency [GHz]	1, 1, 3, 5, 7, 9, 10, 13, 15, 19, 24, 31, 32, 36, 50, 58, 89, 94, 115, 122, 164, 167, 175, 191, 228, 247, 314, 336, 439, 457, 657, 671, 862, 886,
Temperature [K]	190, 230, 270,

Figure 2.1. Extinction

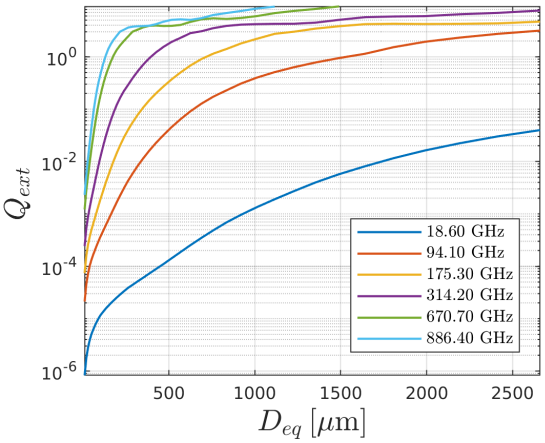

Extinction efficiency as a function of volume volume equivalent diameter, for a selection of six frequencies. Temperature is 230 K.

Figure 2.2. Assymetry parameter

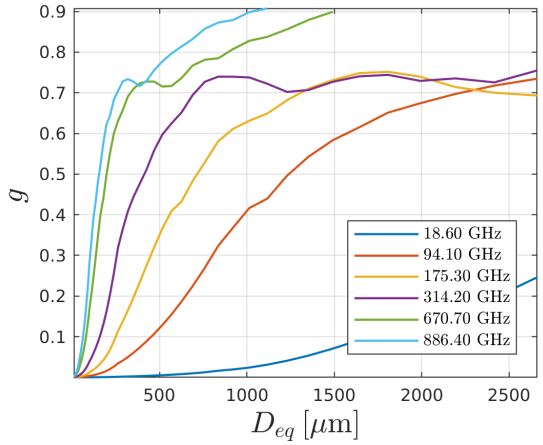

Assymetry parameter as a function of volume equivalent diameter, for a selection of six frequencies. Temperature is 230 K.

Figure 2.3. Single scattering albedo

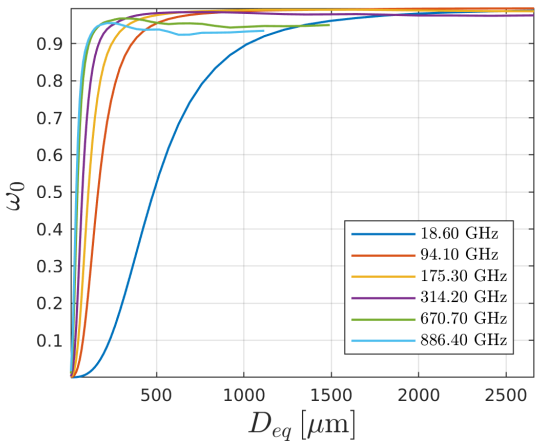

Single scattering albedo as a function of volume volume equivalent diameter, for a selection of six frequencies. Temperature is 230 K.

SSP Data Summary

GEM Cloud Ice

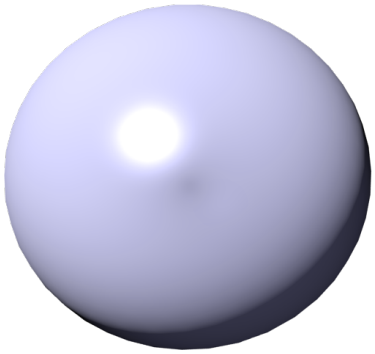

Publication date 20-Nov-2017 22:51:53

Chapter 1. Habit Specifications

Table 1.1. Habit description

Description	GEM cloud ice
Source	location: Chalmers, software: Rimecraft.
Comment	

Figure 1.1. Shape rendering.

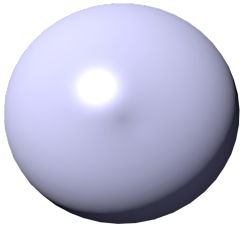

Rendering of a selected shape using Blender (https://www.blender.org/).

Table 1.2. Size parameters

	min	max	# of sizes
D_max [um]	10	2802	44
D_e [um]	10	2722	

Table 1.3. Shape parameters

α	440.0000
β	3.0000

Figure 1.2. Mass-size relationship

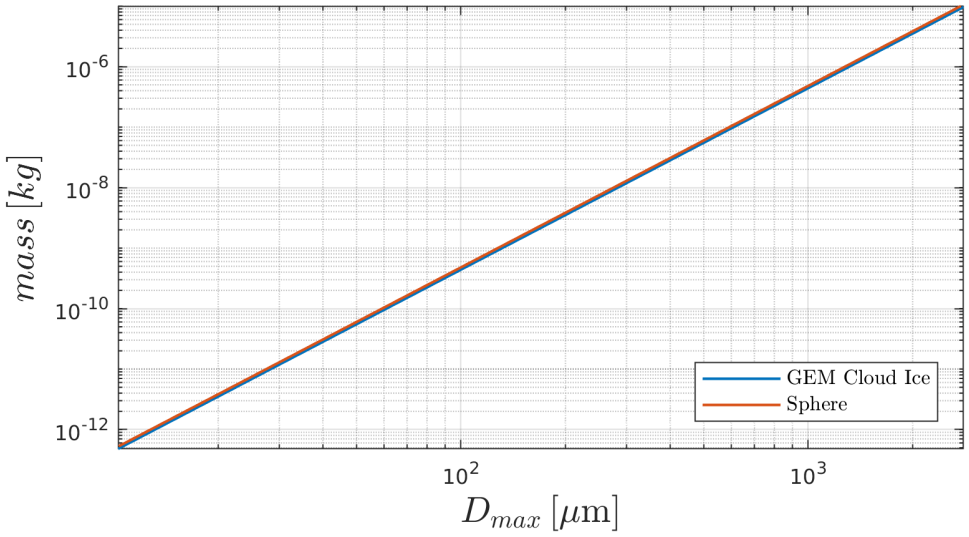

Mass as a function of D_max. Sphere included as a reference. Ice density assumed.

Chapter 2. Single Scattering Properties

Table 2.1. SSP description

Source	ADDA (Yurkin 2011)
Format	ARTS SSP format v.3
Orientation	totally_random
Density [kg/m³]	ice (916.70)
Refractive index	Matzler 2006

Table 2.2. SSP grid

frequency [GHz]	1, 1, 3, 5, 7, 9, 10, 13, 15, 19, 24, 31, 32, 36, 50, 58, 89, 94, 115, 122, 164, 167, 175, 191, 228, 247, 314, 336, 439, 457, 657, 671, 862, 886,
Temperature [K]	190, 230, 270,

Figure 2.1. Extinction

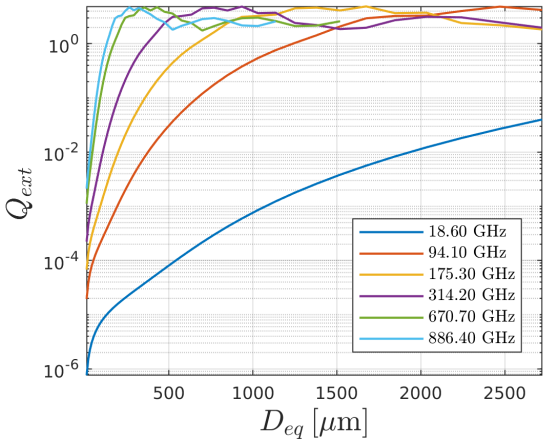

Extinction efficiency as a function of volume volume equivalent diameter, for a selection of six frequencies. Temperature is 230 K.

Figure 2.2. Assymetry parameter

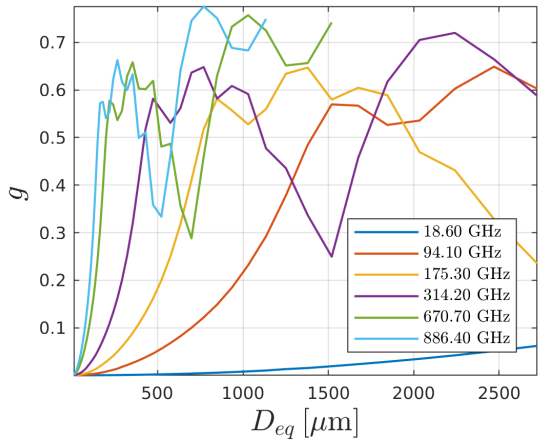

Assymetry parameter as a function of volume equivalent diameter, for a selection of six frequencies. Temperature is 230 K.

Figure 2.3. Single scattering albedo

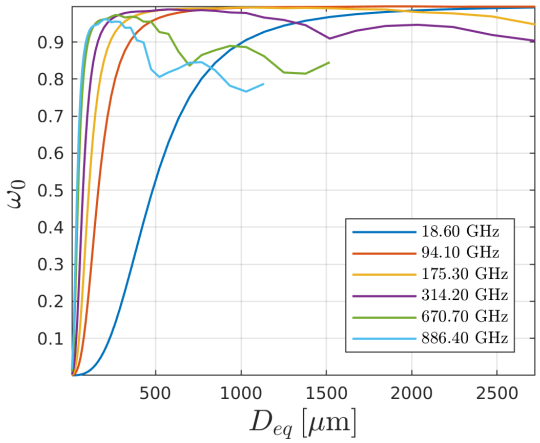

Single scattering albedo as a function of volume volume equivalent diameter, for a selection of six frequencies. Temperature is 230 K.

SSP Data Summary

6-Bullet Rosette

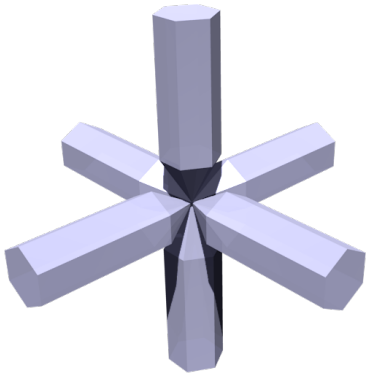

Publication date 20-Nov-2017 22:06:00

Chapter 1. Habit Specifications

Table 1.1. Habit description

Description	Hexagonal 6-bullet rosette, using Hong parametrization (Hong 2007).
Source	location: Chalmers, software: Snowflake-toolkit (Rathsman 2016), parameterization: Hong 2007.
Comment	-

Figure 1.1. Shape rendering.

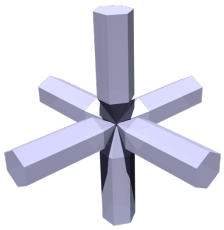

Rendering of a selected shape using Blender (https://www.blender.org/).

Table 1.2. Size parameters

	min	max	# of sizes
D_max [um]	16	8905	44
D_e [um]	10	2166	

Table 1.3. Shape parameters

α	0.4927
β	2.4278

Figure 1.2. Mass-size relationship

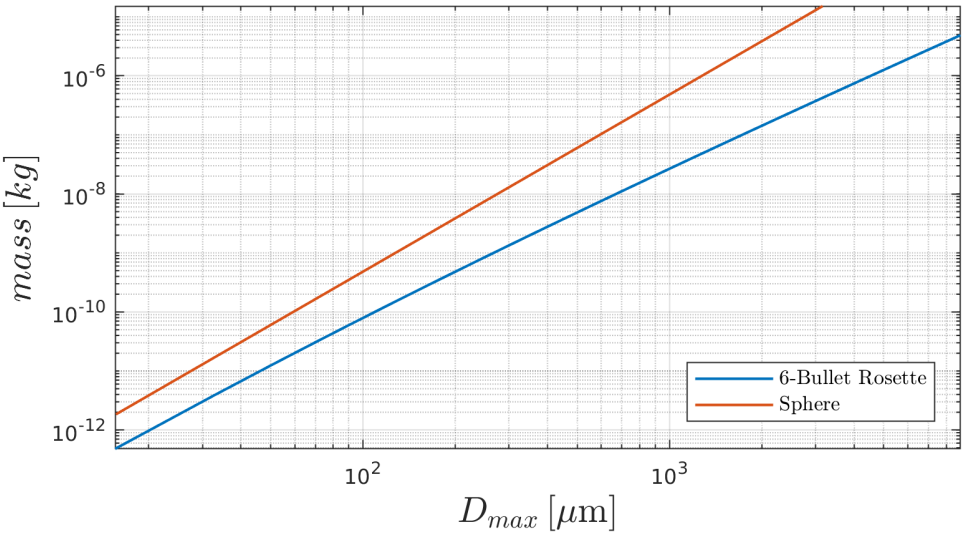

Mass as a function of D_max. Sphere included as a reference. Ice density assumed.

Chapter 2. Single Scattering Properties

Table 2.1. SSP description

Source	ADDA (Yurkin 2011)
Format	ARTS SSP format v.3
Orientation	totally_random
Density [kg/m³]	ice (916.70)
Refractive index	Matzler 2006

Table 2.2. SSP grid

frequency [GHz]	1, 1, 3, 5, 7, 9, 10, 13, 15, 19, 24, 31, 32, 36, 50, 58, 89, 94, 115, 122, 164, 167, 175, 191, 228, 247, 314, 336, 439, 457, 657, 671, 862, 886,
Temperature [K]	190, 230, 270,

Figure 2.1. Extinction

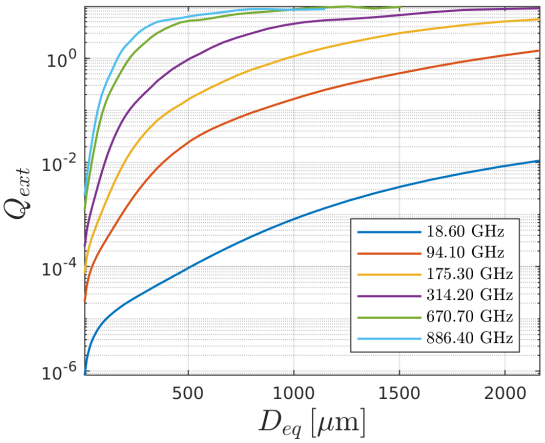

Extinction efficiency as a function of volume volume equivalent diameter, for a selection of six frequencies. Temperature is 230 K.

Figure 2.2. Assymetry parameter

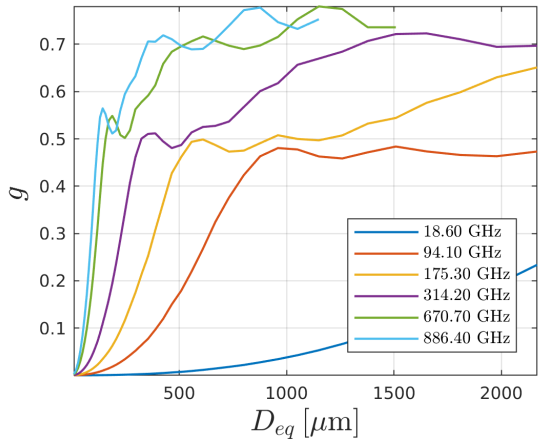

Assymetry parameter as a function of volume equivalent diameter, for a selection of six frequencies. Temperature is 230 K.

Figure 2.3. Single scattering albedo

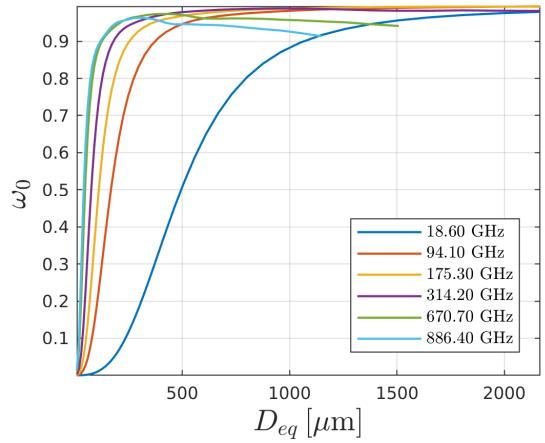

Single scattering albedo as a function of volume volume equivalent diameter, for a selection of six frequencies. Temperature is 230 K.

SSP Data Summary

5-bullet Rosette

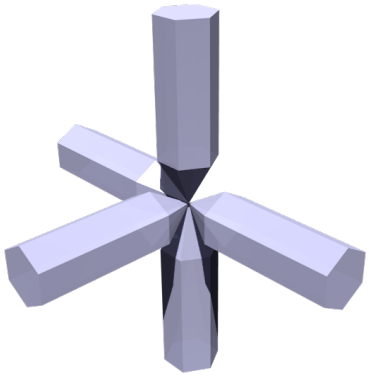

Publication date 20-Nov-2017 22:03:19

Chapter 1. Habit Specifications

Table 1.1. Habit description

Description	Hexagonal 5-bullet rosette. The bullets have the same dimensions as in the Hong bullet rosette (Hong 2007).
Source	location: Chalmers, software: Snowflake-toolkit (Rathsman 2016), parameterization: Hong 2007.
Comment	-

Figure 1.1. Shape rendering.

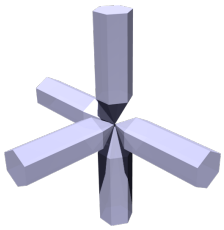

Rendering of a selected shape using Blender (https://www.blender.org/).

Table 1.2. Size parameters

	min	max	# of sizes
D_max [um]	17	8924	44
D_e [um]	10	2042	

Table 1.3. Shape parameters

α	0.4047
β	2.4254

Figure 1.2. Mass-size relationship

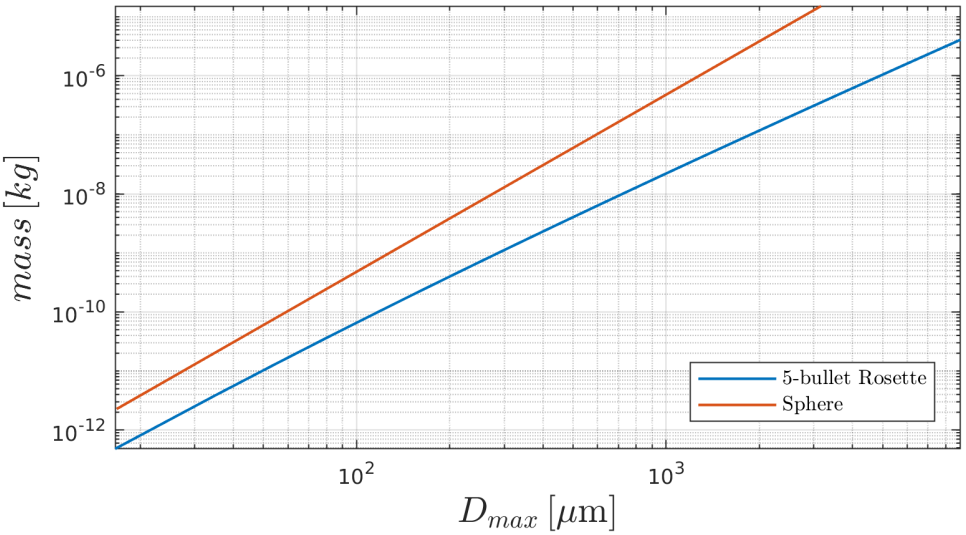

Mass as a function of D_max. Sphere included as a reference. Ice density assumed.

Chapter 2. Single Scattering Properties

Table 2.1. SSP description

Source	ADDA (Yurkin 2011)
Format	ARTS SSP format v.3
Orientation	totally_random
Density [kg/m³]	ice (916.70)
Refractive index	Matzler 2006

Table 2.2. SSP grid

frequency [GHz]	1, 1, 3, 5, 7, 9, 10, 13, 15, 19, 24, 31, 32, 36, 50, 58, 89, 94, 115, 122, 164, 167, 175, 191, 228, 247, 314, 336, 439, 457, 657, 671, 862, 886,
Temperature [K]	190, 230, 270,

Figure 2.1. Extinction

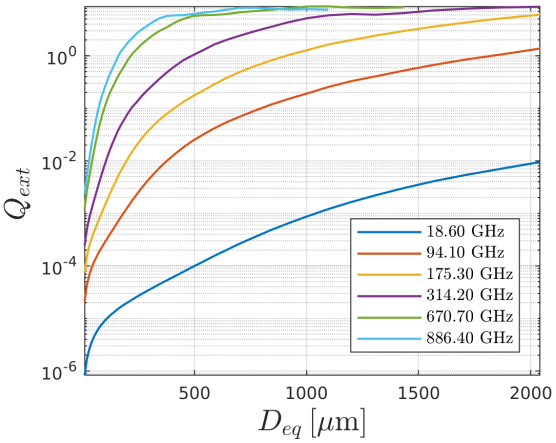

Extinction efficiency as a function of volume volume equivalent diameter, for a selection of six frequencies. Temperature is 230 K.

Figure 2.2. Assymetry parameter

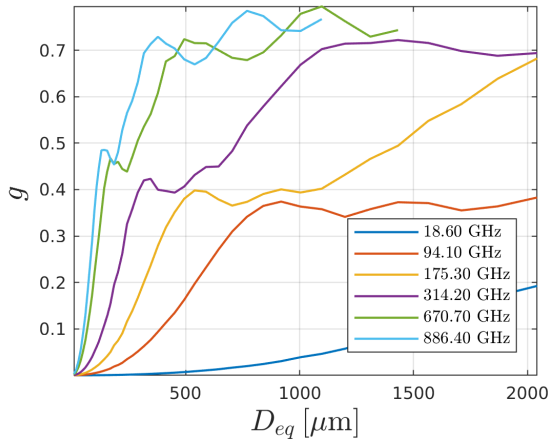

Assymetry parameter as a function of volume equivalent diameter, for a selection of six frequencies. Temperature is 230 K.

Figure 2.3. Single scattering albedo

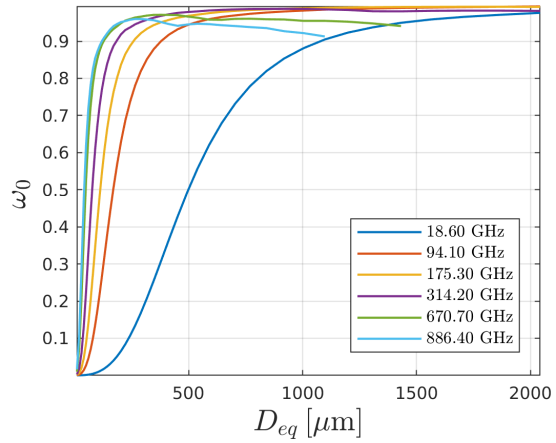

Single scattering albedo as a function of volume volume equivalent diameter, for a selection of six frequencies. Temperature is 230 K.

SSP Data Summary

Perpendicular 4-Bullet Rosette

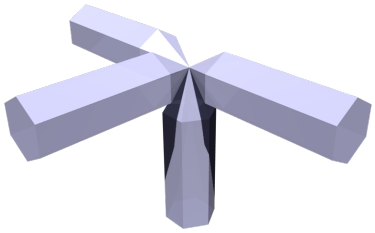

Publication date 20-Nov-2017 22:09:26

Chapter 1. Habit Specifications

Table 1.1. Habit description

Description	Perpendicular hexagonal 4-bullet rosette. The bullets have the same dimensions as in the Hong bullet rosette (Hong 2007).
Source	location: Chalmers, software: Snowflake-toolkit (Rathsman 2016), parameterization: Hong 2007.
Comment	-

Figure 1.1. Shape rendering.

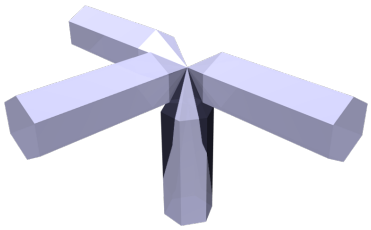

Rendering of a selected shape using Blender (https://www.blender.org/).

Table 1.2. Size parameters

	min	max	# of sizes
D_max [um]	18	8949	44
D_e [um]	10	1899	

Table 1.3. Shape parameters

α	0.3248
β	2.4259

Figure 1.2. Mass-size relationship

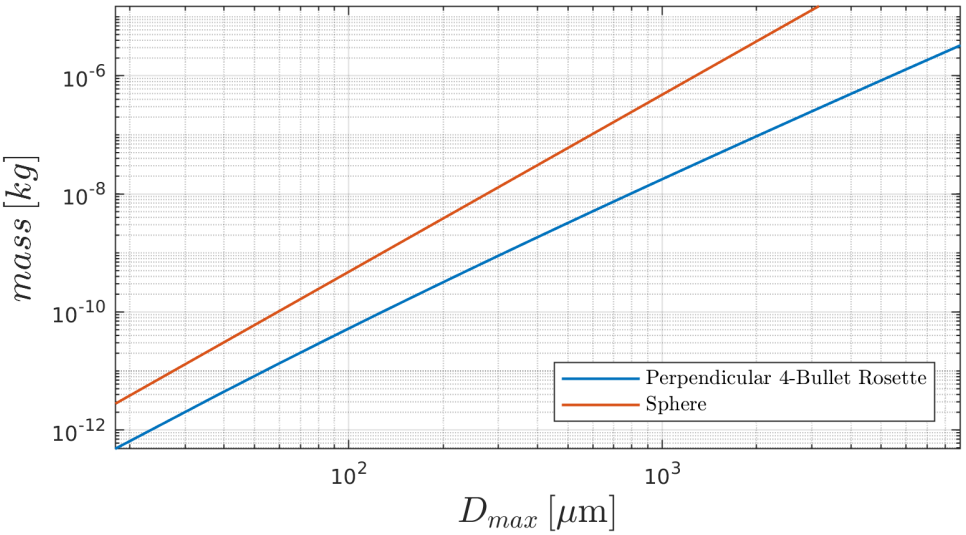

Mass as a function of D_max. Sphere included as a reference. Ice density assumed.

Chapter 2. Single Scattering Properties

Table 2.1. SSP description

Source	ADDA (Yurkin 2011)
Format	ARTS SSP format v.3
Orientation	totally_random
Density [kg/m³]	ice (916.70)
Refractive index	Matzler 2006

Table 2.2. SSP grid

frequency [GHz]	1, 1, 3, 5, 7, 9, 10, 13, 15, 19, 24, 31, 32, 36, 50, 58, 89, 94, 115, 122, 164, 167, 175, 191, 228, 247, 314, 336, 439, 457, 657, 671, 862, 886,
Temperature [K]	190, 230, 270,

Figure 2.1. Extinction

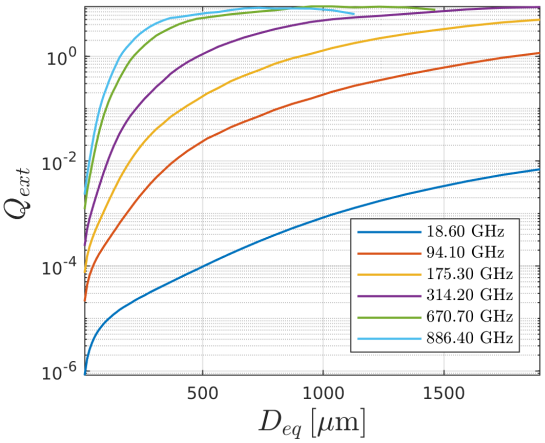

Extinction efficiency as a function of volume volume equivalent diameter, for a selection of six frequencies. Temperature is 230 K.

Figure 2.2. Assymetry parameter

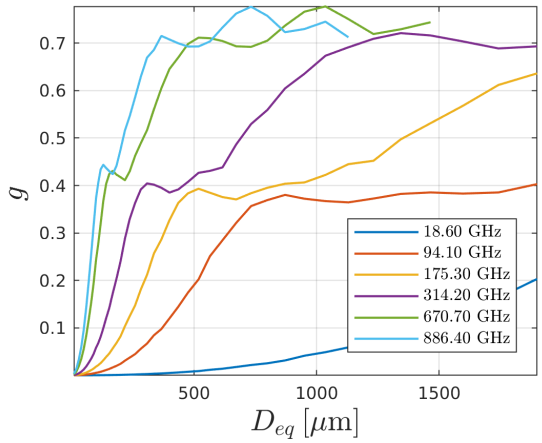

Assymetry parameter as a function of volume equivalent diameter, for a selection of six frequencies. Temperature is 230 K.

Figure 2.3. Single scattering albedo

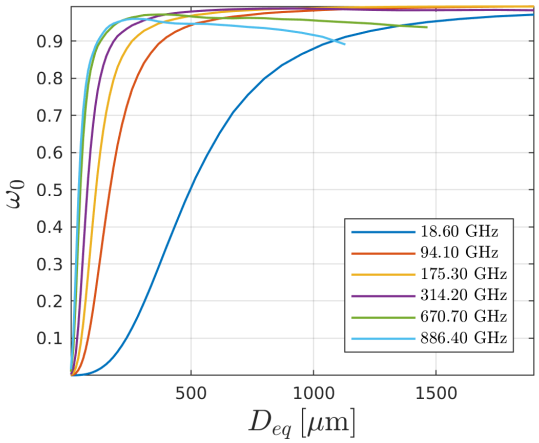

Single scattering albedo as a function of volume volume equivalent diameter, for a selection of six frequencies. Temperature is 230 K.

SSP Data Summary

Flat 4-Bullet Rosette

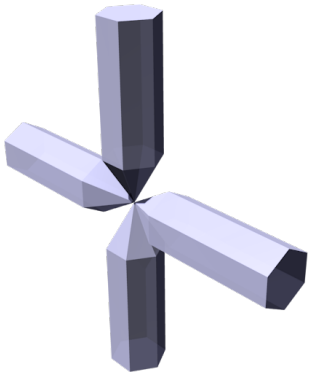

Publication date 20-Nov-2017 22:10:18

Chapter 1. Habit Specifications

Table 1.1. Habit description

Description	Flat hexagonal 4-bullet rosette. The bullets have the same dimensions as in the Hong bullet rosette (Hong 2007).
Source	location: Chalmers, software: Snowflake-toolkit (Rathsman 2016), parameterization: Hong 2007.
Comment	-

Figure 1.1. Shape rendering.

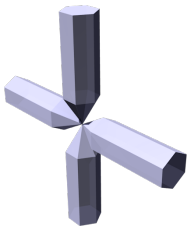

Rendering of a selected shape using Blender (https://www.blender.org/).

Table 1.2. Size parameters

	min	max	# of sizes
D_max [um]	18	8949	44
D_e [um]	10	1899	

Table 1.3. Shape parameters

α	0.3248
β	2.4259

Figure 1.2. Mass-size relationship

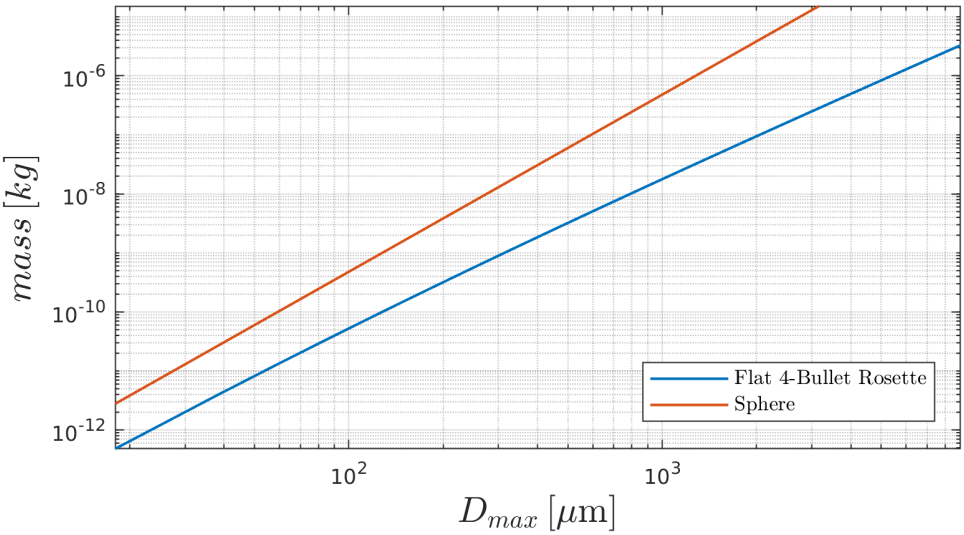

Mass as a function of D_max. Sphere included as a reference. Ice density assumed.

Chapter 2. Single Scattering Properties

Table 2.1. SSP description

Source	ADDA (Yurkin 2011)
Format	ARTS SSP format v.3
Orientation	totally_random
Density [kg/m³]	ice (916.70)
Refractive index	Matzler 2006

Table 2.2. SSP grid

frequency [GHz]	1, 1, 3, 5, 7, 9, 10, 13, 15, 19, 24, 31, 32, 36, 50, 58, 89, 94, 115, 122, 164, 167, 175, 191, 228, 247, 314, 336, 439, 457, 657, 671, 862, 886,
Temperature [K]	190, 230, 270,

Figure 2.1. Extinction

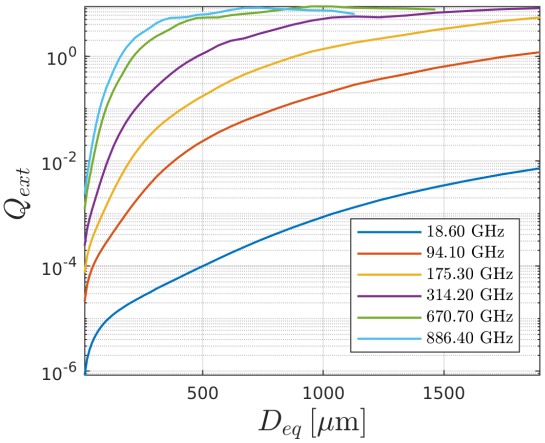

Extinction efficiency as a function of volume volume equivalent diameter, for a selection of six frequencies. Temperature is 230 K.

Figure 2.2. Assymetry parameter

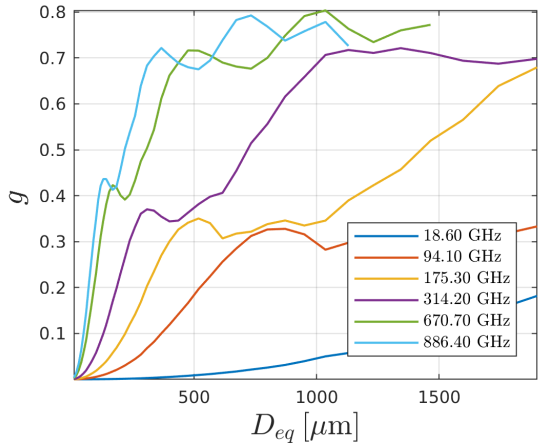

Assymetry parameter as a function of volume equivalent diameter, for a selection of six frequencies. Temperature is 230 K.

Figure 2.3. Single scattering albedo

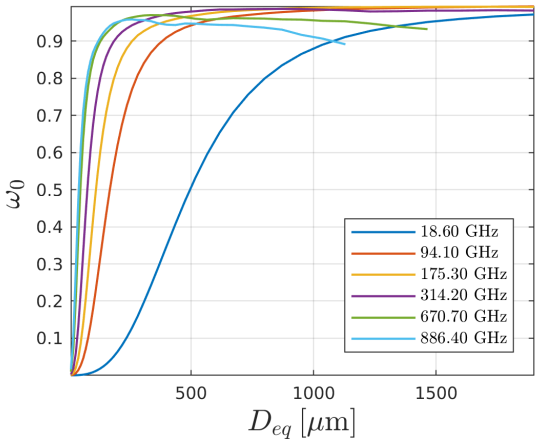

Single scattering albedo as a function of volume volume equivalent diameter, for a selection of six frequencies. Temperature is 230 K.

SSP Data Summary

Perpendicular 3-Bullet Rosette

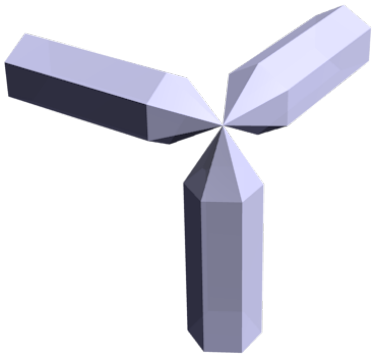

Publication date 20-Nov-2017 22:04:35

Chapter 1. Habit Specifications

Table 1.1. Habit description

Description	Perpendicular hexagonal 3-bullet rosette. The bullets have the same dimensions as in the Hong bullet rosette (Hong 2007).
Source	location: Chalmers, software: Snowflake-toolkit (Rathsman 2016), parameterization: Hong 2007.
Comment	-

Figure 1.1. Shape rendering.

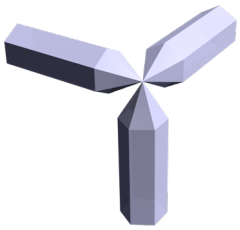

Rendering of a selected shape using Blender (https://www.blender.org/).

Table 1.2. Size parameters

	min	max	# of sizes
D_max [um]	19	8949	44
D_e [um]	10	1958	

Table 1.3. Shape parameters

α	0.4373
β	2.4675

Figure 1.2. Mass-size relationship

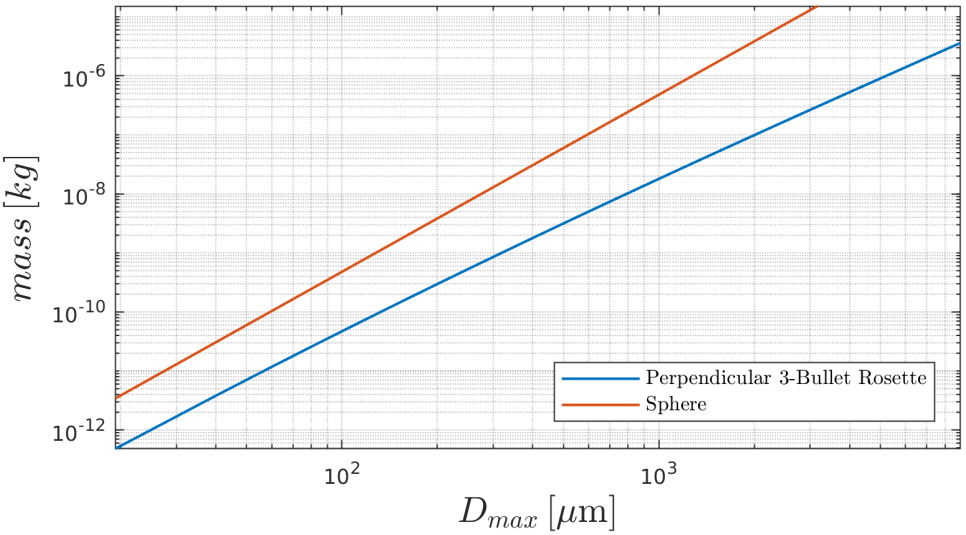

Mass as a function of D_max. Sphere included as a reference. Ice density assumed.

Chapter 2. Single Scattering Properties

Table 2.1. SSP description

Source	ADDA (Yurkin 2011)
Format	ARTS SSP format v.3
Orientation	totally_random
Density [kg/m³]	ice (916.70)
Refractive index	Matzler 2006

Table 2.2. SSP grid

frequency [GHz]	1, 1, 3, 5, 7, 9, 10, 13, 15, 19, 24, 31, 32, 36, 50, 58, 89, 94, 115, 122, 164, 167, 175, 191, 228, 247, 314, 336, 439, 457, 657, 671, 862, 886,
Temperature [K]	190, 230, 270,

Figure 2.1. Extinction

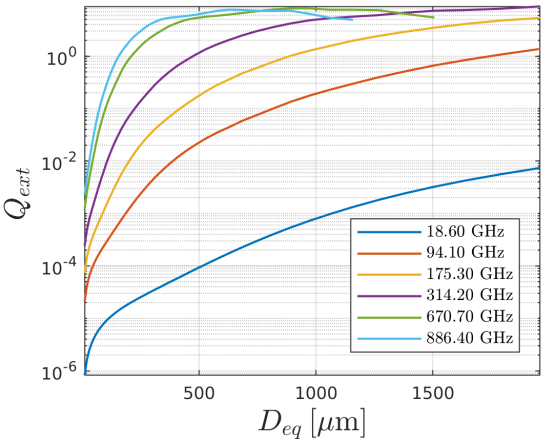

Extinction efficiency as a function of volume volume equivalent diameter, for a selection of six frequencies. Temperature is 230 K.

Figure 2.2. Assymetry parameter

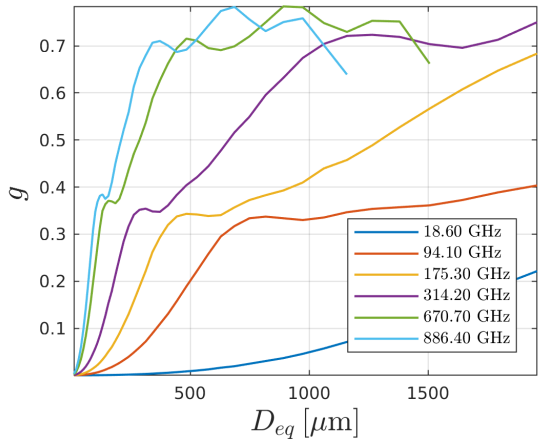

Assymetry parameter as a function of volume equivalent diameter, for a selection of six frequencies. Temperature is 230 K.

Figure 2.3. Single scattering albedo

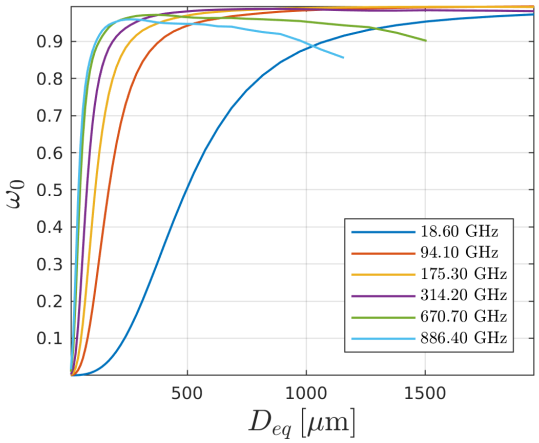

Single scattering albedo as a function of volume volume equivalent diameter, for a selection of six frequencies. Temperature is 230 K.

SSP Data Summary

Flat 3-Bullet Rosette

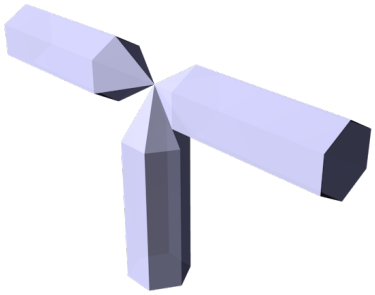

Publication date 20-Nov-2017 22:05:17

Chapter 1. Habit Specifications

Table 1.1. Habit description

Description	Flat hexagonal 3-bullet rosette. The bullets have the same dimensions as in the Hong bullet rosette (Hong 2007).
Source	location: Chalmers, software: Snowflake-toolkit (Rathsman 2016), parameterization: Hong 2007.
Comment	-

Figure 1.1. Shape rendering.

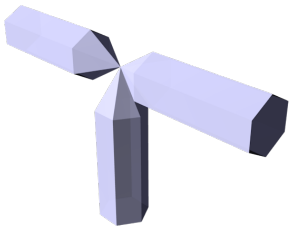

Rendering of a selected shape using Blender (https://www.blender.org/).

Table 1.2. Size parameters

	min	max	# of sizes
D_max [um]	20	8980	44
D_e [um]	10	1730	

Table 1.3. Shape parameters

α	0.2433
β	2.4257

Figure 1.2. Mass-size relationship

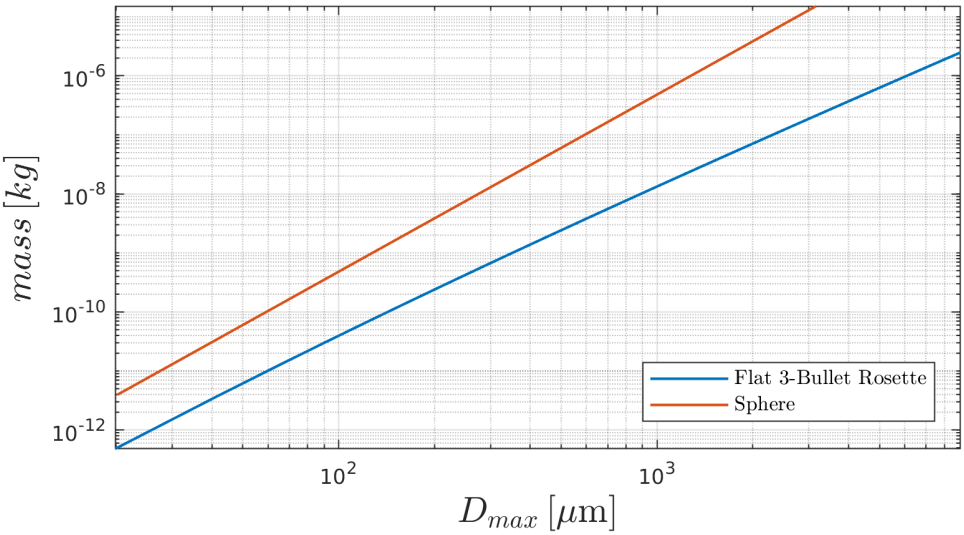

Mass as a function of D_max. Sphere included as a reference. Ice density assumed.

Chapter 2. Single Scattering Properties

Table 2.1. SSP description

Source	ADDA (Yurkin 2011)
Format	ARTS SSP format v.3
Orientation	totally_random
Density [kg/m³]	ice (916.70)
Refractive index	Matzler 2006

Table 2.2. SSP grid

frequency [GHz]	1, 1, 3, 5, 7, 9, 10, 13, 15, 19, 24, 31, 32, 36, 50, 58, 89, 94, 115, 122, 164, 167, 175, 191, 228, 247, 314, 336, 439, 457, 657, 671, 862, 886,
Temperature [K]	190, 230, 270,

Figure 2.1. Extinction

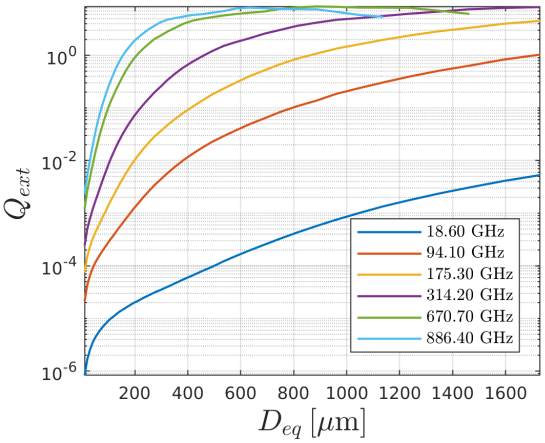

Extinction efficiency as a function of volume volume equivalent diameter, for a selection of six frequencies. Temperature is 230 K.

Figure 2.2. Assymetry parameter

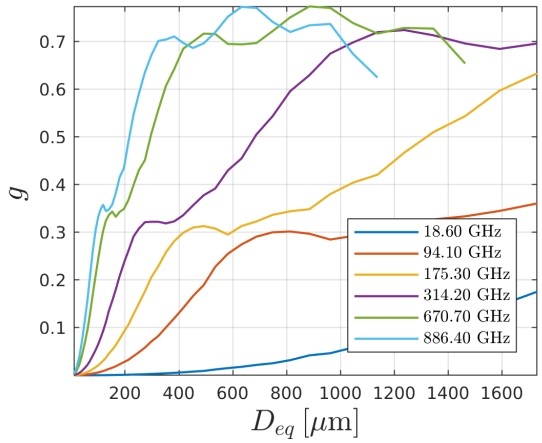

Assymetry parameter as a function of volume equivalent diameter, for a selection of six frequencies. Temperature is 230 K.

Figure 2.3. Single scattering albedo

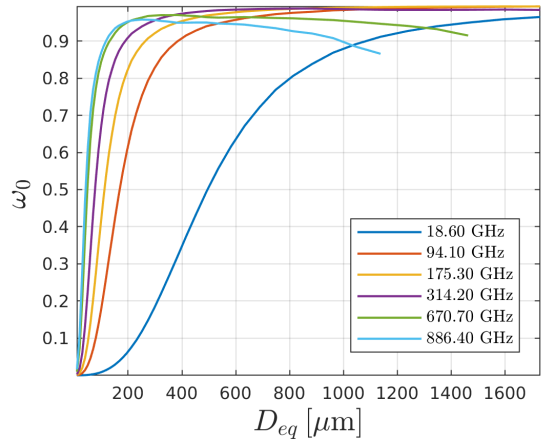

Single scattering albedo as a function of volume volume equivalent diameter, for a selection of six frequencies. Temperature is 230 K.

SSP Data Summary

Evans Snow Aggregate

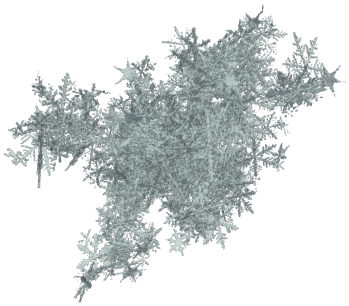

Publication date 07-Dec-2017 18:15:05

Chapter 1. Habit Specifications

Table 1.1. Habit description

Description	Snowflake aggregate, shape files from Evans 2012
Source	Evans 2012.
Comment	

Figure 1.1. Shape rendering.

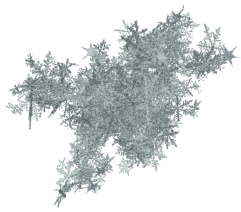

Rendering of a selected shape using Blender (https://www.blender.org/).

Table 1.2. Size parameters

	min	max	# of sizes
D_max [um]	32	9483	34
D_e [um]	50	2109	

Table 1.3. Shape parameters

α	0.1963
β	2.3861

Figure 1.2. Mass-size relationship

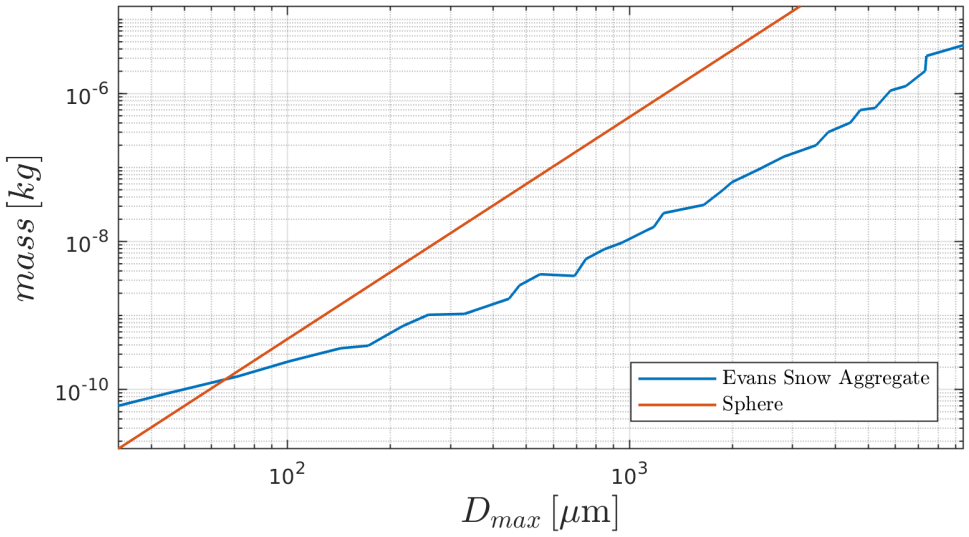

Mass as a function of D_max. Sphere included as a reference. Ice density assumed.

Chapter 2. Single Scattering Properties

Table 2.1. SSP description

Source	ADDA (Yurkin 2011)
Format	ARTS SSP format v.3
Orientation	totally_random
Density [kg/m³]	ice (916.70)
Refractive index	Matzler 2006

Table 2.2. SSP grid

frequency [GHz]	1, 1, 3, 5, 7, 9, 10, 13, 15, 19, 24, 31, 32, 36, 50, 58, 89, 94, 115, 122, 164, 167, 175, 191, 228, 247, 314, 336, 439, 457, 657, 671, 862, 886,
Temperature [K]	190, 230, 270,

Figure 2.1. Extinction

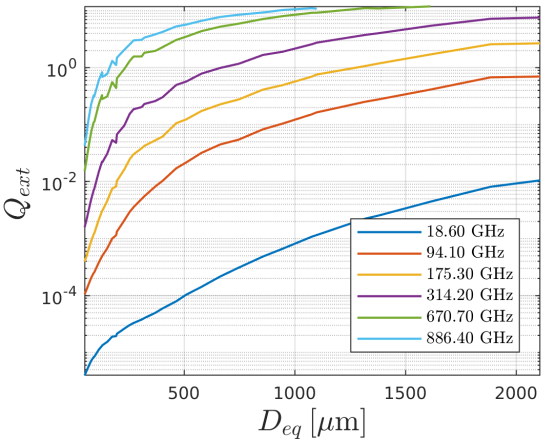

Extinction efficiency as a function of volume volume equivalent diameter, for a selection of six frequencies. Temperature is 230 K.

Figure 2.2. Assymetry parameter

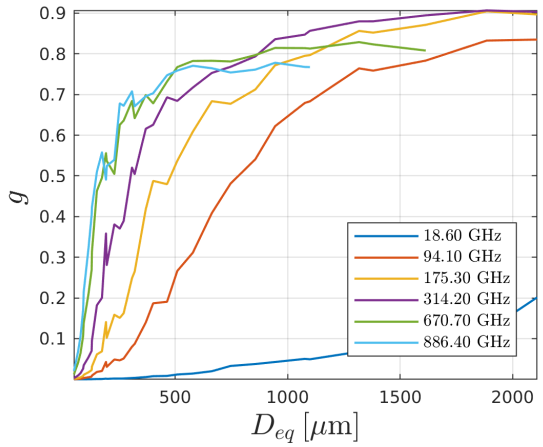

Assymetry parameter as a function of volume equivalent diameter, for a selection of six frequencies. Temperature is 230 K.

Figure 2.3. Single scattering albedo

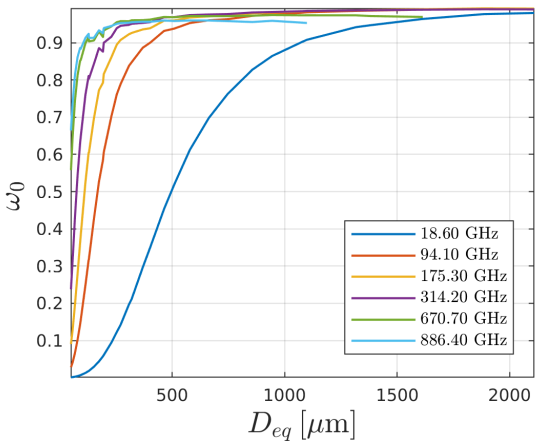

Single scattering albedo as a function of volume volume equivalent diameter, for a selection of six frequencies. Temperature is 230 K.

SSP Data Summary

Tyynela Dendrite Aggregate

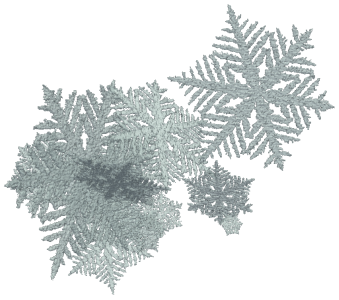

Publication date 07-Dec-2017 18:15:48

Chapter 1. Habit Specifications

Table 1.1. Habit description

Description	Aggregate of fernlike dendrites.
Source	Tyynela and Chandrasekar 2014.
Comment	

Figure 1.1. Shape rendering.

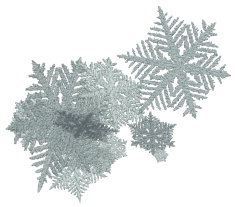

Rendering of a selected shape using Blender (https://www.blender.org/).

Table 1.2. Size parameters

	min	max	# of sizes
D_max [um]	595	12845	27
D_e [um]	228	2254	

Table 1.3. Shape parameters

α	0.0970
β	2.2428

Figure 1.2. Mass-size relationship

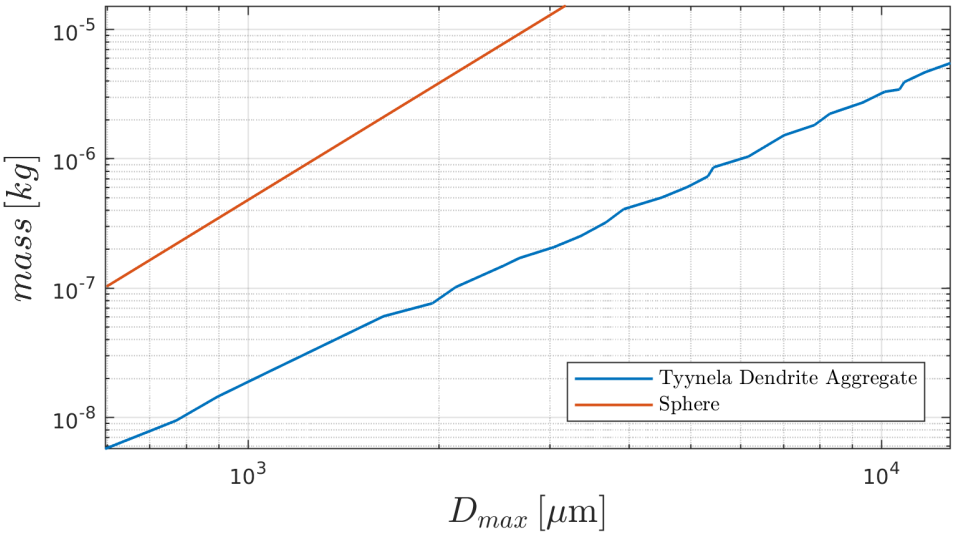

Mass as a function of D_max. Sphere included as a reference. Ice density assumed.

Chapter 2. Single Scattering Properties

Table 2.1. SSP description

Source	ADDA (Yurkin 2011)
Format	ARTS SSP format v.3
Orientation	totally_random
Density [kg/m³]	ice (916.70)
Refractive index	Matzler 2006

Table 2.2. SSP grid

frequency [GHz]	1, 1, 3, 5, 7, 9, 10, 13, 15, 19, 24, 31, 32, 36, 50, 58, 89, 94, 115, 122, 164, 167, 175, 191, 228, 247, 314, 336, 439, 457, 657, 671, 862, 886,
Temperature [K]	190, 230, 270,

Figure 2.1. Extinction

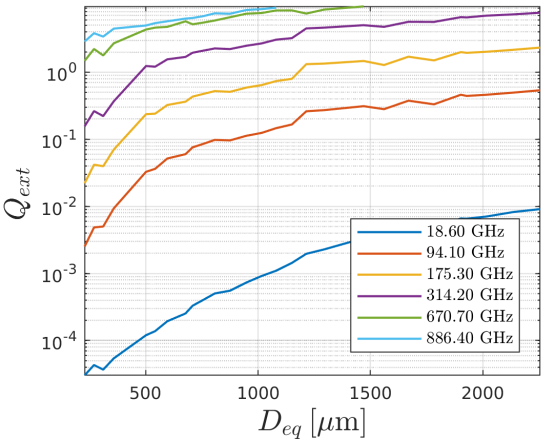

Extinction efficiency as a function of volume volume equivalent diameter, for a selection of six frequencies. Temperature is 230 K.

Figure 2.2. Assymetry parameter

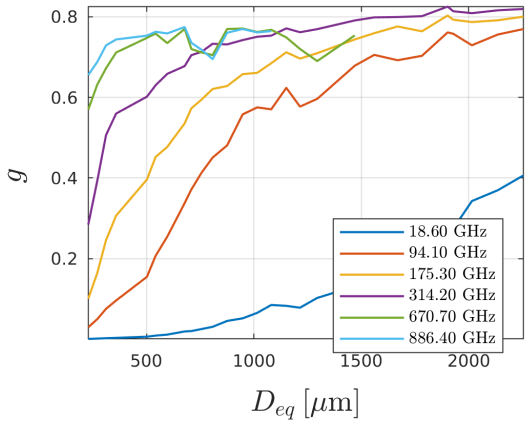

Assymetry parameter as a function of volume equivalent diameter, for a selection of six frequencies. Temperature is 230 K.

Figure 2.3. Single scattering albedo

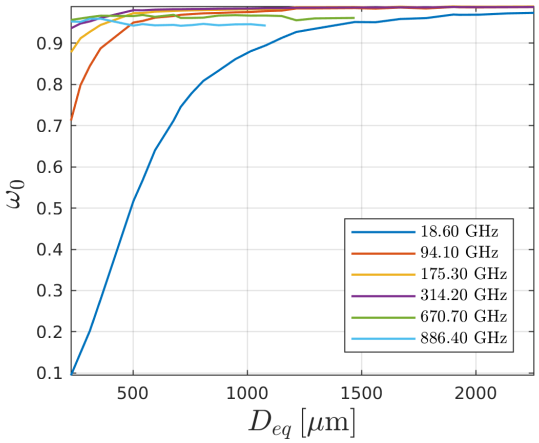

Single scattering albedo as a function of volume volume equivalent diameter, for a selection of six frequencies. Temperature is 230 K.

SSP Data Summary

8-Column Aggregate

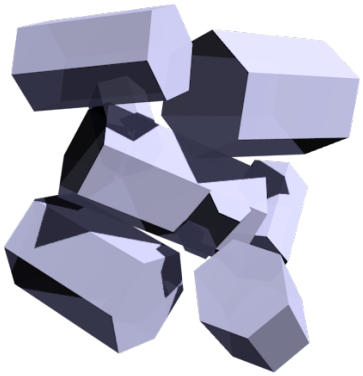

Publication date 20-Nov-2017 22:07:24

Chapter 1. Habit Specifications

Table 1.1. Habit description

Description	Hexagonal column aggregate, using Hong parametrization (Hong 2007).
Source	location: Chalmers, software: Snowflake-toolkit (Rathsman 2016), parameterization: Hong 2007.
Comment	Note that shape and proportions are constant with size, resulting in beta=3.

Figure 1.1. Shape rendering.

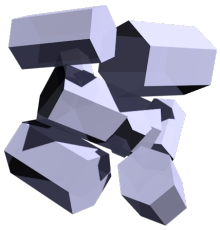

Rendering of a selected shape using Blender (https://www.blender.org/).

Table 1.2. Size parameters

	min	max	# of sizes
D_max [um]	19	8478	38
D_e [um]	10	4363	

Table 1.3. Shape parameters

α	65.4480
β	3.0000

Figure 1.2. Mass-size relationship

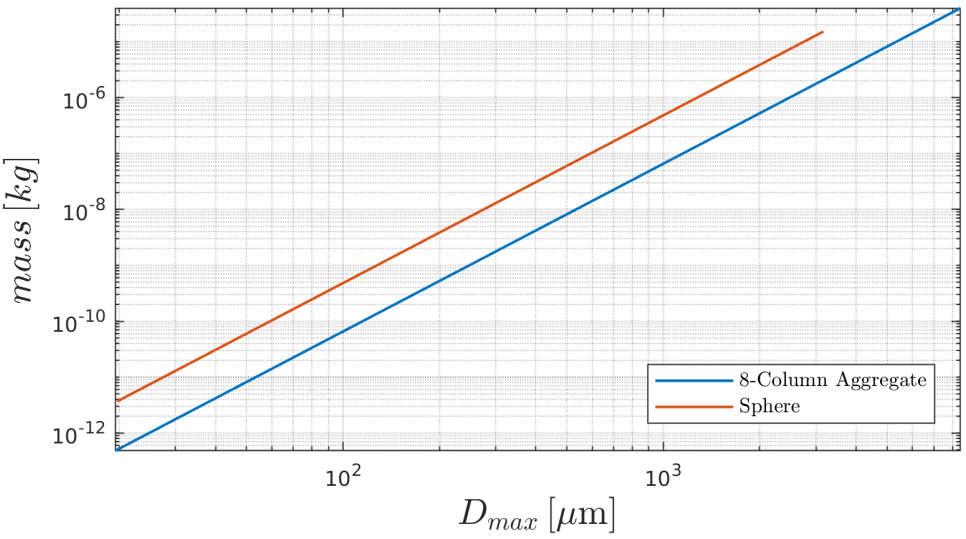

Mass as a function of D_max. Sphere included as a reference. Ice density assumed.

Chapter 2. Single Scattering Properties

Table 2.1. SSP description

Source	ADDA (Yurkin 2011)
Format	ARTS SSP format v.3
Orientation	totally_random
Density [kg/m³]	ice (916.70)
Refractive index	Matzler 2006

Table 2.2. SSP grid

frequency [GHz]	1, 1, 3, 5, 7, 9, 10, 13, 15, 19, 24, 31, 32, 36, 50, 58, 89, 94, 115, 122, 164, 167, 175, 191, 228, 247, 314, 336, 439, 457, 657, 671, 862, 886,
Temperature [K]	190, 230, 270,

Figure 2.1. Extinction

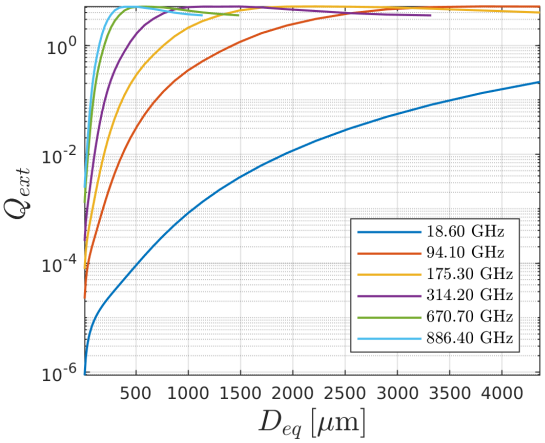

Extinction efficiency as a function of volume volume equivalent diameter, for a selection of six frequencies. Temperature is 230 K.

Figure 2.2. Assymetry parameter

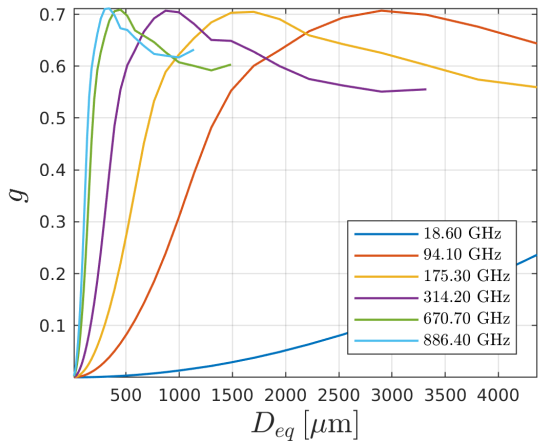

Assymetry parameter as a function of volume equivalent diameter, for a selection of six frequencies. Temperature is 230 K.

Figure 2.3. Single scattering albedo

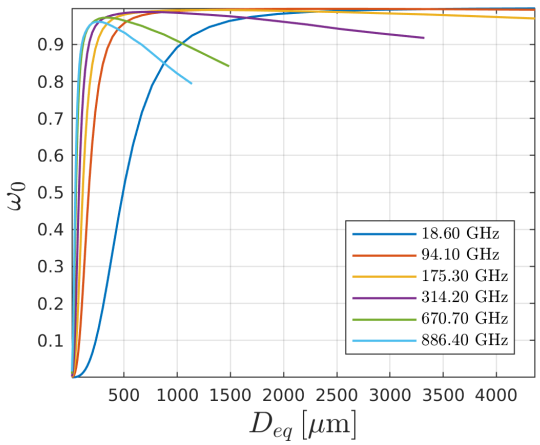

Single scattering albedo as a function of volume volume equivalent diameter, for a selection of six frequencies. Temperature is 230 K.

SSP Data Summary

Small Column Aggregate

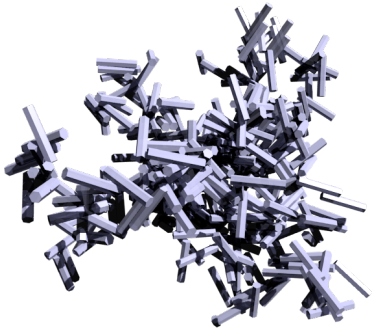

Publication date 20-Nov-2017 22:14:54

Chapter 1. Habit Specifications

Table 1.1. Habit description

Description	Hexagonal column aggregates, mean aspect ratio = 5. Prototype crystal d_max=100 um.
Source	location: Chalmers, software: Snowflake-toolkit (Rathsman 2016).
Comment	

Figure 1.1. Shape rendering.

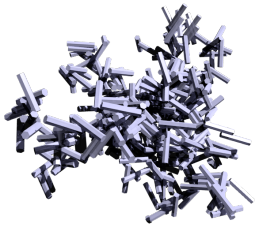

Rendering of a selected shape using Blender (https://www.blender.org/).

Table 1.2. Size parameters

	min	max	# of sizes
D_max [um]	105	3624	34
D_e [um]	37	690	

Table 1.3. Shape parameters

α	0.1376
β	2.4438

Figure 1.2. Mass-size relationship

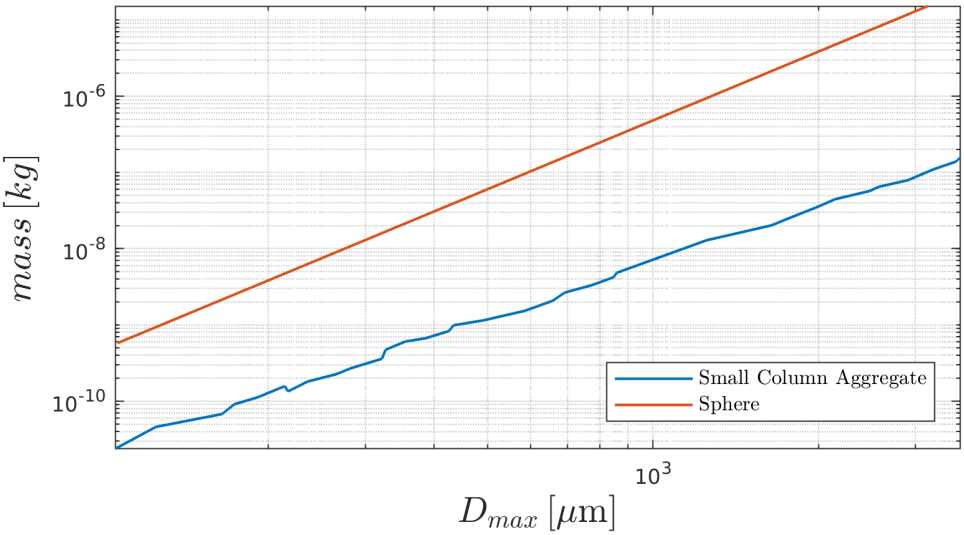

Mass as a function of D_max. Sphere included as a reference. Ice density assumed.

Chapter 2. Single Scattering Properties

Table 2.1. SSP description

Source	ADDA (Yurkin 2011)
Format	ARTS SSP format v.3
Orientation	totally_random
Density [kg/m³]	ice (916.70)
Refractive index	Matzler 2006

Table 2.2. SSP grid

frequency [GHz]	1, 1, 3, 5, 7, 9, 10, 13, 15, 19, 24, 31, 32, 36, 50, 58, 89, 94, 115, 122, 164, 167, 175, 191, 228, 247, 314, 336, 439, 457, 657, 671, 862, 886,
Temperature [K]	190, 230, 270,

Figure 2.1. Extinction

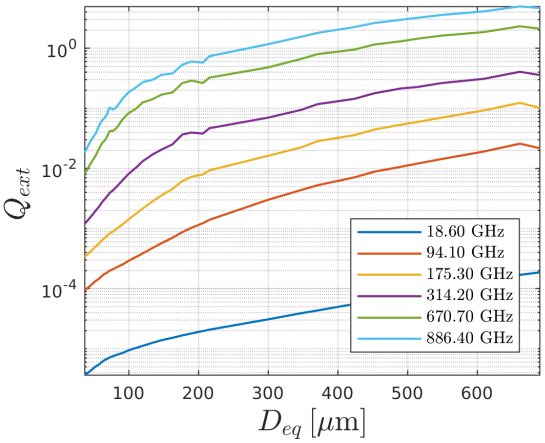

Extinction efficiency as a function of volume volume equivalent diameter, for a selection of six frequencies. Temperature is 230 K.

Figure 2.2. Assymetry parameter

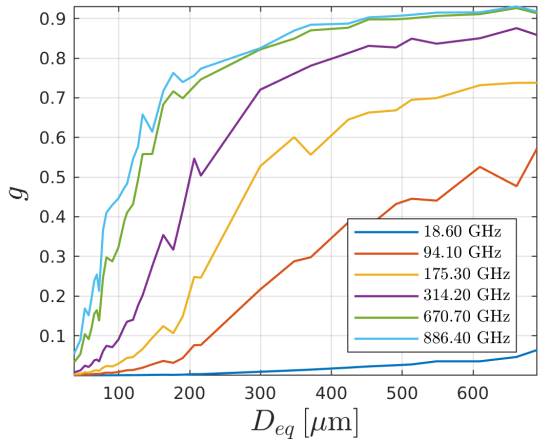

Assymetry parameter as a function of volume equivalent diameter, for a selection of six frequencies. Temperature is 230 K.

Figure 2.3. Single scattering albedo

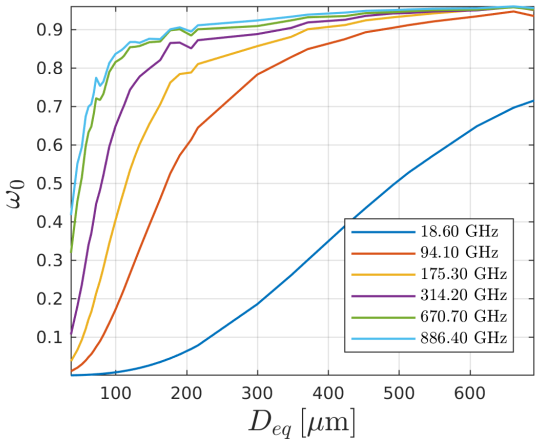

Single scattering albedo as a function of volume volume equivalent diameter, for a selection of six frequencies. Temperature is 230 K.

SSP Data Summary

Large Column Aggregate

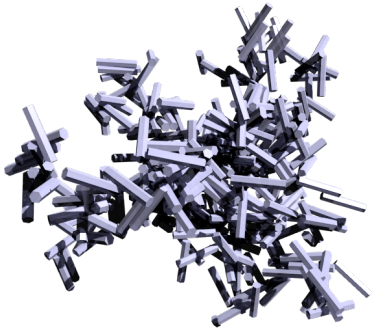

Publication date 20-Nov-2017 22:15:35

Chapter 1. Habit Specifications

Table 1.1. Habit description

Description	Hexagonal column aggregates, mean aspect ratio = 5. Prototype crystal d_max=350 um.
Source	location: Chalmers, software: Snowflake-toolkit (Rathsman 2016).
Comment	

Figure 1.1. Shape rendering.

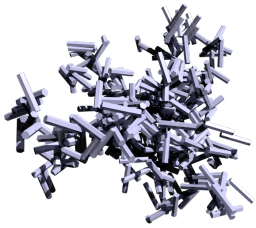

Rendering of a selected shape using Blender (https://www.blender.org/).

Table 1.2. Size parameters

	min	max	# of sizes
D_max [um]	368	15602	34
D_e [um]	128	2689	

Table 1.3. Shape parameters

α	0.2758
β	2.4440

Figure 1.2. Mass-size relationship

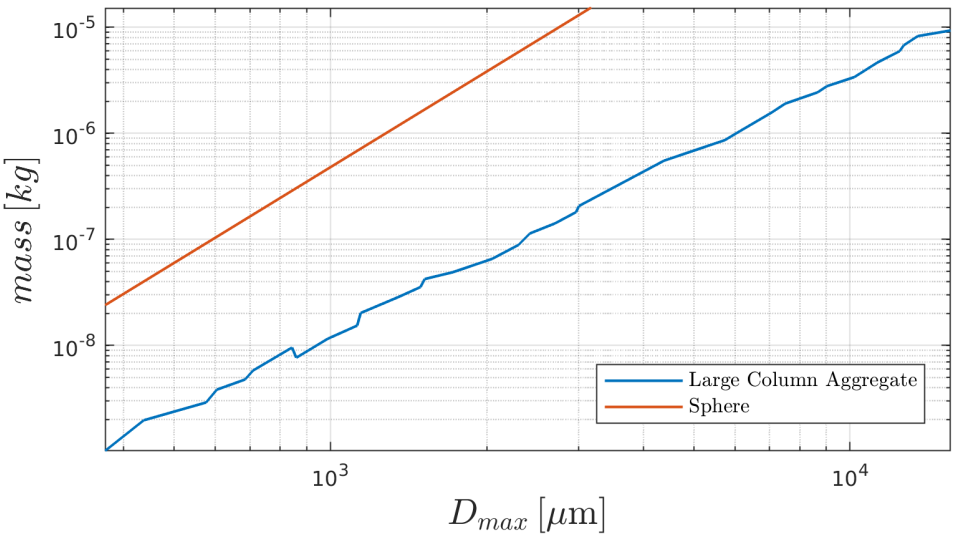

Mass as a function of D_max. Sphere included as a reference. Ice density assumed.

Chapter 2. Single Scattering Properties

Table 2.1. SSP description

Source	ADDA (Yurkin 2011)
Format	ARTS SSP format v.3
Orientation	totally_random
Density [kg/m³]	ice (916.70)
Refractive index	Matzler 2006

Table 2.2. SSP grid

frequency [GHz]	1, 1, 3, 5, 7, 9, 10, 13, 15, 19, 24, 31, 32, 36, 50, 58, 89, 94, 115, 122, 164, 167, 175, 191, 228, 247, 314, 336, 439, 457, 657, 671, 862, 886,
Temperature [K]	190, 230, 270,

Figure 2.1. Extinction

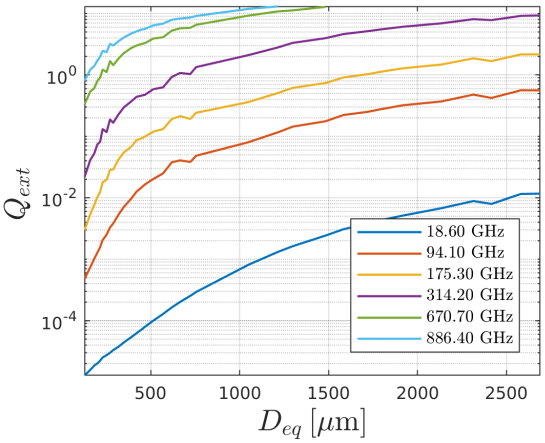

Extinction efficiency as a function of volume volume equivalent diameter, for a selection of six frequencies. Temperature is 230 K.

Figure 2.2. Assymetry parameter

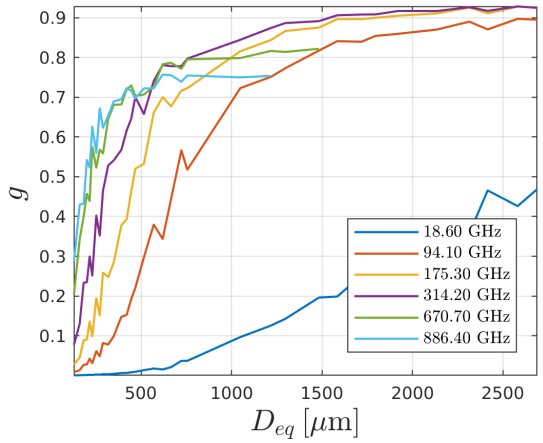

Assymetry parameter as a function of volume equivalent diameter, for a selection of six frequencies. Temperature is 230 K.

Figure 2.3. Single scattering albedo

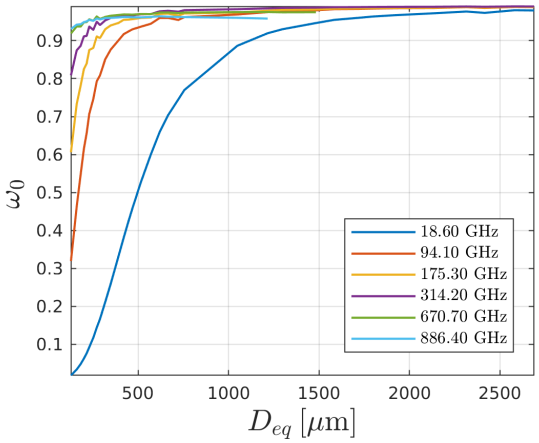

Single scattering albedo as a function of volume volume equivalent diameter, for a selection of six frequencies. Temperature is 230 K.

SSP Data Summary

Small Block Aggregate

Publication date 20-Nov-2017 22:17:44

Chapter 1. Habit Specifications

Table 1.1. Habit description

Description	Hexagonal column aggregates, mean aspect ratio = 1.25. Prototype crystal d_max=100 um.
Source	location: Chalmers, software: Snowflake-toolkit (Rathsman 2016).
Comment	

Figure 1.1. Shape rendering.

Rendering of a selected shape using Blender (https://www.blender.org/).

Table 1.2. Size parameters

	min	max	# of sizes
D_max [um]	100	6891	34
D_e [um]	72	1533	

Table 1.3. Shape parameters

α	0.2137
β	2.3327

Figure 1.2. Mass-size relationship

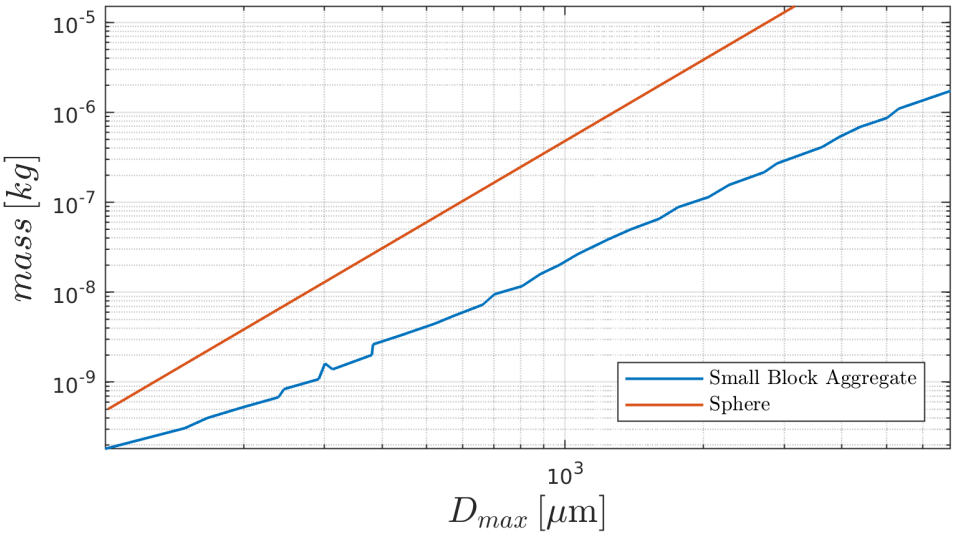

Mass as a function of D_max. Sphere included as a reference. Ice density assumed.

Chapter 2. Single Scattering Properties

Table 2.1. SSP description

Source	ADDA (Yurkin 2011)
Format	ARTS SSP format v.3
Orientation	totally_random
Density [kg/m³]	ice (916.70)
Refractive index	Matzler 2006

Table 2.2. SSP grid

frequency [GHz]	1, 1, 3, 5, 7, 9, 10, 13, 15, 19, 24, 31, 32, 36, 50, 58, 89, 94, 115, 122, 164, 167, 175, 191, 228, 247, 314, 336, 439, 457, 657, 671, 862, 886,
Temperature [K]	190, 230, 270,

Figure 2.1. Extinction

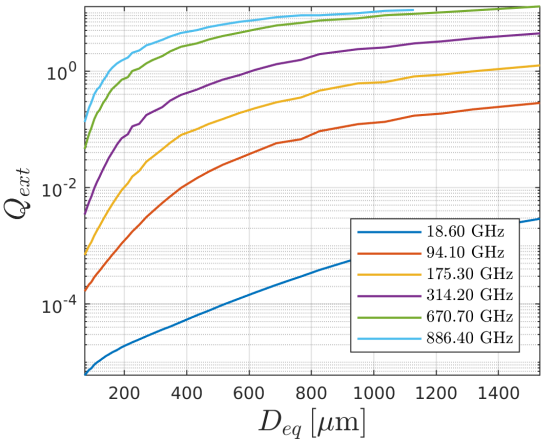

Extinction efficiency as a function of volume volume equivalent diameter, for a selection of six frequencies. Temperature is 230 K.

Figure 2.2. Assymetry parameter

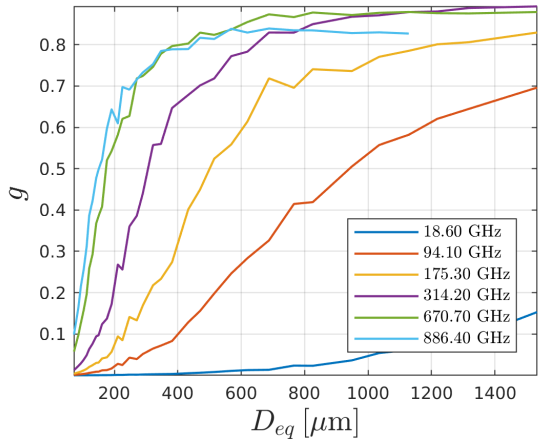

Assymetry parameter as a function of volume equivalent diameter, for a selection of six frequencies. Temperature is 230 K.

Figure 2.3. Single scattering albedo

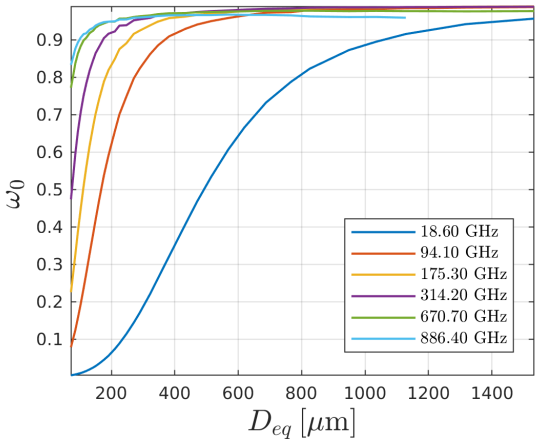

Single scattering albedo as a function of volume volume equivalent diameter, for a selection of six frequencies. Temperature is 230 K.

SSP Data Summary

Large Block Aggregate

Publication date 20-Nov-2017 22:18:26

Chapter 1. Habit Specifications

Table 1.1. Habit description

Description	Hexagonal column aggregates, mean aspect ratio = 1.25. Prototype crystal d_max=350 um.
Source	location: Chalmers, software: Snowflake-toolkit (Rathsman 2016).
Comment	

Figure 1.1. Shape rendering.

Rendering of a selected shape using Blender (https://www.blender.org/).

Table 1.2. Size parameters

	min	max	# of sizes
D_max [um]	349	17437	34
D_e [um]	253	4321	

Table 1.3. Shape parameters

α	0.3499
β	2.2657

Figure 1.2. Mass-size relationship

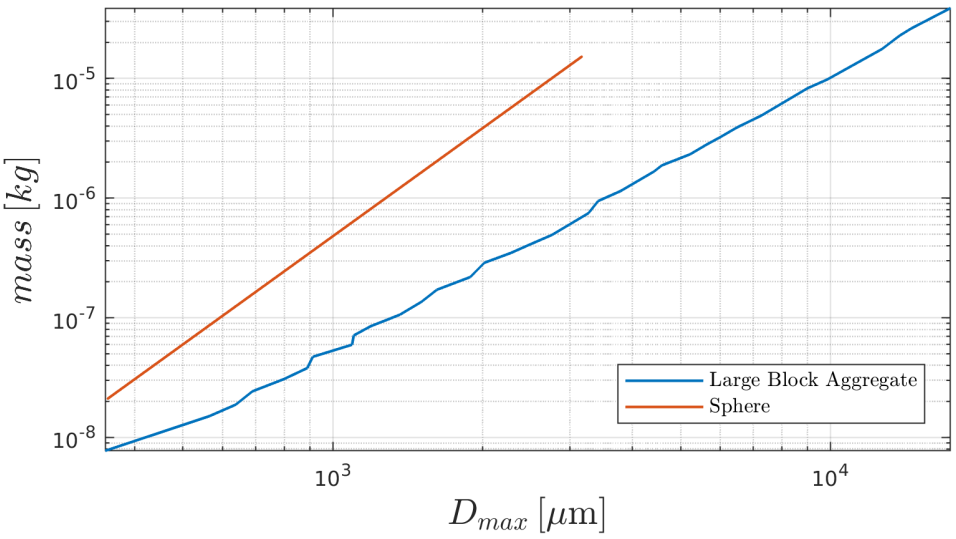

Mass as a function of D_max. Sphere included as a reference. Ice density assumed.

Chapter 2. Single Scattering Properties

Table 2.1. SSP description

Source	ADDA (Yurkin 2011)
Format	ARTS SSP format v.3
Orientation	totally_random
Density [kg/m³]	ice (916.70)
Refractive index	Matzler 2006

Table 2.2. SSP grid

frequency [GHz]	1, 1, 3, 5, 7, 9, 10, 13, 15, 19, 24, 31, 32, 36, 50, 58, 89, 94, 115, 122, 164, 167, 175, 191, 228, 247, 314, 336, 439, 457, 657, 671, 862, 886,
Temperature [K]	190, 230, 270,

Figure 2.1. Extinction

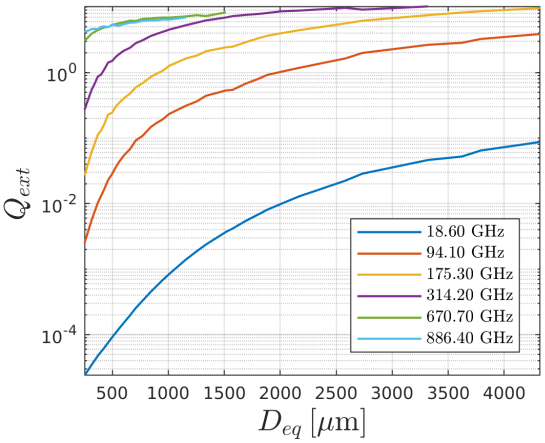

Extinction efficiency as a function of volume volume equivalent diameter, for a selection of six frequencies. Temperature is 230 K.

Figure 2.2. Assymetry parameter

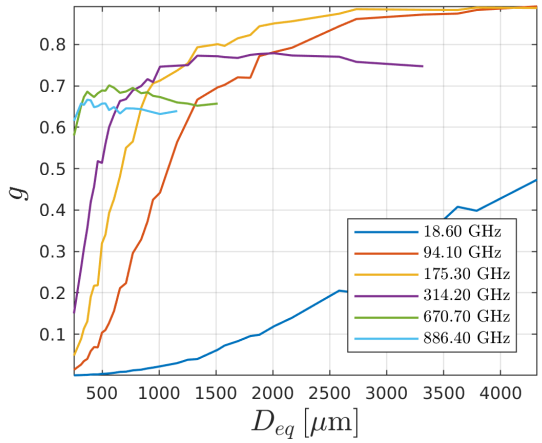

Assymetry parameter as a function of volume equivalent diameter, for a selection of six frequencies. Temperature is 230 K.

Figure 2.3. Single scattering albedo

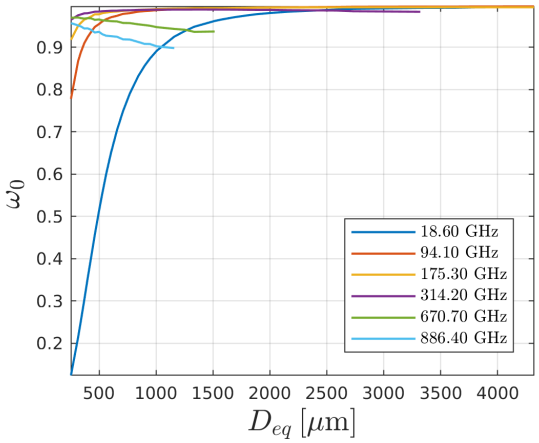

Single scattering albedo as a function of volume volume equivalent diameter, for a selection of six frequencies. Temperature is 230 K.

SSP Data Summary

Small Plate Aggregate

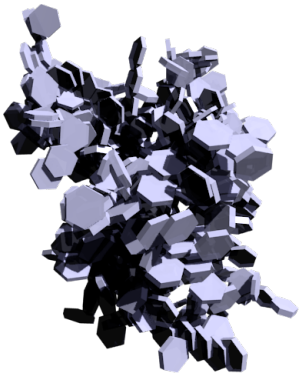

Publication date 20-Nov-2017 22:16:18

Chapter 1. Habit Specifications

Table 1.1. Habit description

Description	Hexagonal plate aggregates, mean aspect ratio = 6. Prototype crystal d_max=100 um.
Source	location: Chalmers, software: Snowflake-toolkit (Rathsman 2016).
Comment	

Figure 1.1. Shape rendering.

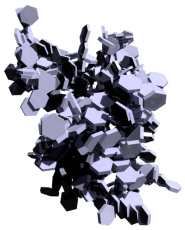

Rendering of a selected shape using Blender (https://www.blender.org/).

Table 1.2. Size parameters

	min	max	# of sizes
D_max [um]	99	5378	34
D_e [um]	53	1048	

Table 1.3. Shape parameters

α	0.0772
β	2.2470

Figure 1.2. Mass-size relationship

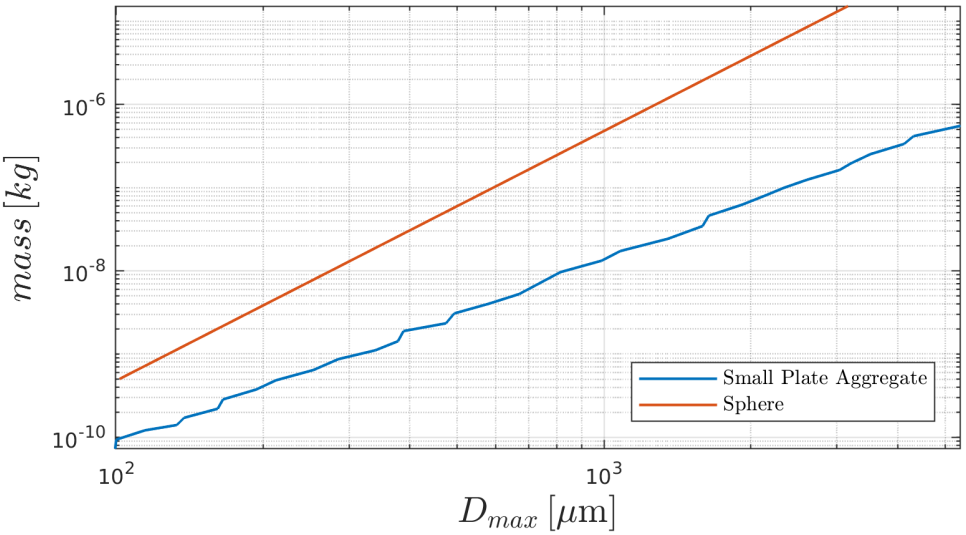

Mass as a function of D_max. Sphere included as a reference. Ice density assumed.

Chapter 2. Single Scattering Properties

Table 2.1. SSP description

Source	ADDA (Yurkin 2011)
Format	ARTS SSP format v.3
Orientation	totally_random
Density [kg/m³]	ice (916.70)
Refractive index	Matzler 2006

Table 2.2. SSP grid

frequency [GHz]	1, 1, 3, 5, 7, 9, 10, 13, 15, 19, 24, 31, 32, 36, 50, 58, 89, 94, 115, 122, 164, 167, 175, 191, 228, 247, 314, 336, 439, 457, 657, 671, 862, 886,
Temperature [K]	190, 230, 270,

Figure 2.1. Extinction

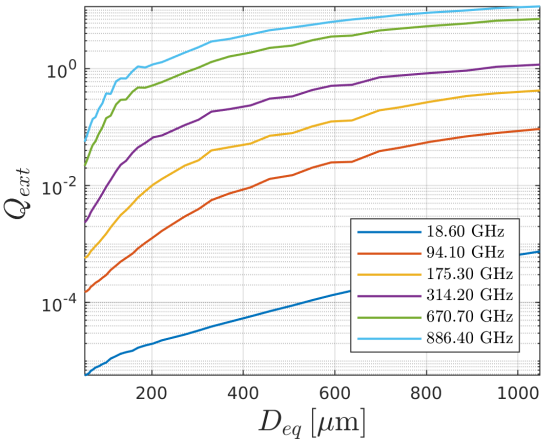

Extinction efficiency as a function of volume volume equivalent diameter, for a selection of six frequencies. Temperature is 230 K.

Figure 2.2. Assymetry parameter

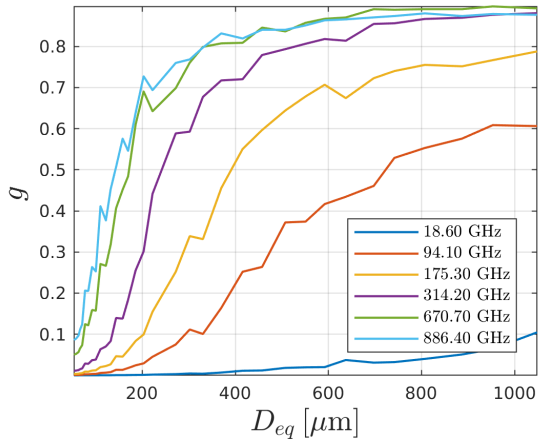

Assymetry parameter as a function of volume equivalent diameter, for a selection of six frequencies. Temperature is 230 K.

Figure 2.3. Single scattering albedo

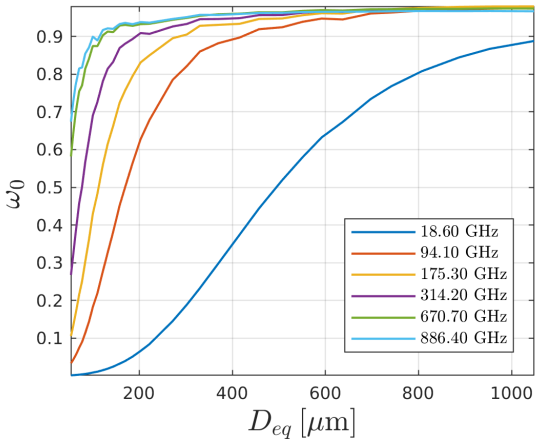

Single scattering albedo as a function of volume volume equivalent diameter, for a selection of six frequencies. Temperature is 230 K.

SSP Data Summary

Large Plate Aggregate

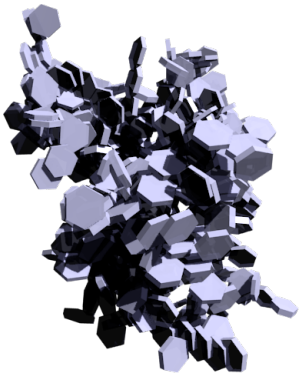

Publication date 20-Nov-2017 22:17:01

Chapter 1. Habit Specifications

Table 1.1. Habit description

Description	Hexagonal plate aggregates, mean aspect ratio = 6. Prototype crystal d_max=350 um.
Source	location: Chalmers, software: Snowflake-toolkit (Rathsman 2016).
Comment	

Figure 1.1. Shape rendering.

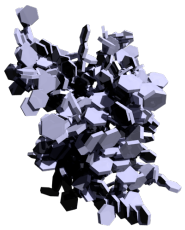

Rendering of a selected shape using Blender (https://www.blender.org/).

Table 1.2. Size parameters

	min	max	# of sizes
D_max [um]	349	18824	33
D_e [um]	197	3669	

Table 1.3. Shape parameters

α	0.2085
β	2.2571

Figure 1.2. Mass-size relationship

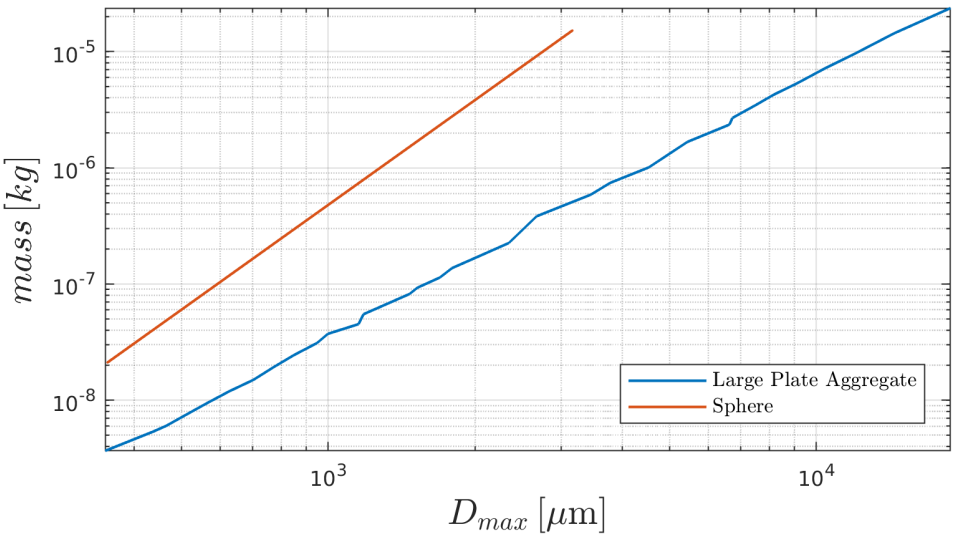

Mass as a function of D_max. Sphere included as a reference. Ice density assumed.

Chapter 2. Single Scattering Properties

Table 2.1. SSP description

Source	ADDA (Yurkin 2011)
Format	ARTS SSP format v.3
Orientation	totally_random
Density [kg/m³]	ice (916.70)
Refractive index	Matzler 2006

Table 2.2. SSP grid

frequency [GHz]	1, 1, 3, 5, 7, 9, 10, 13, 15, 19, 24, 31, 32, 36, 50, 58, 89, 94, 115, 122, 164, 167, 175, 191, 228, 247, 314, 336, 439, 457, 657, 671, 862, 886,
Temperature [K]	190, 230, 270,

Figure 2.1. Extinction

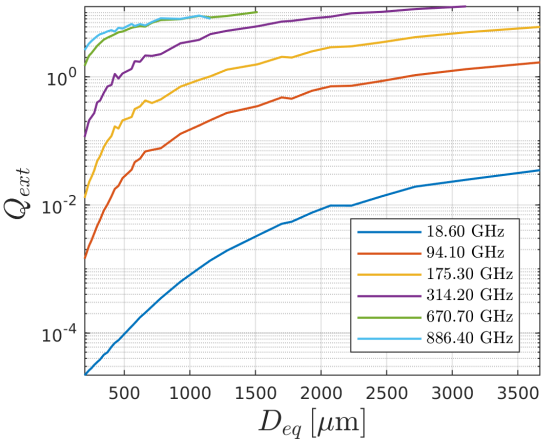

Extinction efficiency as a function of volume volume equivalent diameter, for a selection of six frequencies. Temperature is 230 K.

Figure 2.2. Assymetry parameter

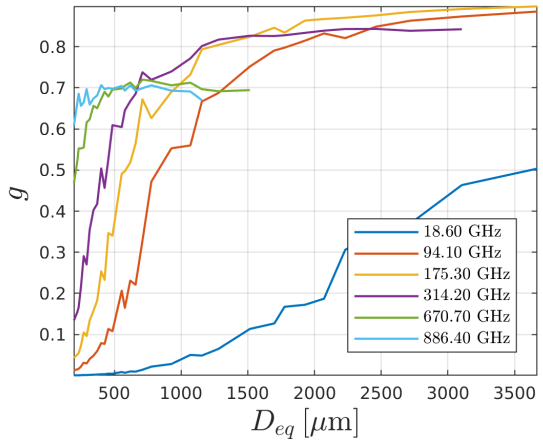

Assymetry parameter as a function of volume equivalent diameter, for a selection of six frequencies. Temperature is 230 K.

Figure 2.3. Single scattering albedo

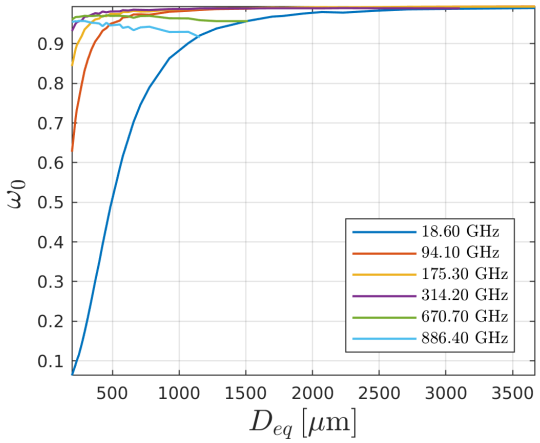

Single scattering albedo as a function of volume volume equivalent diameter, for a selection of six frequencies. Temperature is 230 K.

SSP Data Summary

ICON Hail

Publication date 07-Dec-2017 18:17:46

Chapter 1. Habit Specifications

Table 1.1. Habit description

Description	ICON hail
Source	location: Chalmers, software: Rimecraft.
Comment	

Figure 1.1. Shape rendering.

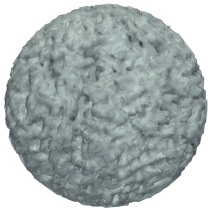

Rendering of a selected shape using Blender (https://www.blender.org/).

Table 1.2. Size parameters

	min	max	# of sizes
D_max [um]	120	4759	30
D_e [um]	94	4457	

Table 1.3. Shape parameters

α	383.5055
β	2.9942

Figure 1.2. Mass-size relationship

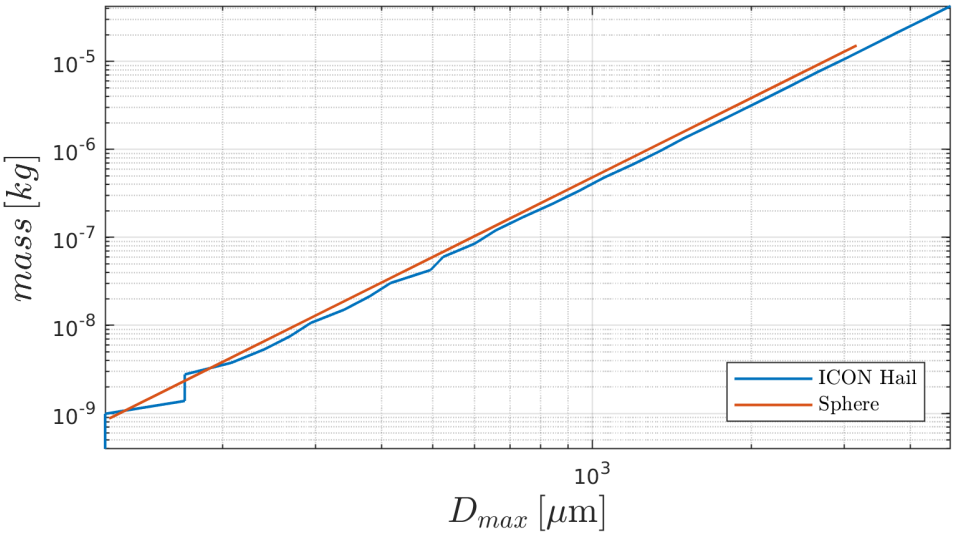

Mass as a function of D_max. Sphere included as a reference. Ice density assumed.

Chapter 2. Single Scattering Properties

Table 2.1. SSP description

Source	ADDA (Yurkin 2011)
Format	ARTS SSP format v.3
Orientation	totally_random
Density [kg/m³]	ice (916.70)
Refractive index	Matzler 2006

Table 2.2. SSP grid

frequency [GHz]	1, 1, 3, 5, 7, 9, 10, 13, 15, 19, 24, 31, 32, 36, 50, 58, 89, 94, 115, 122, 164, 167, 175, 191, 228, 247, 314, 336, 439, 457, 657, 671, 862, 886,
Temperature [K]	190, 230, 270,

Figure 2.1. Extinction

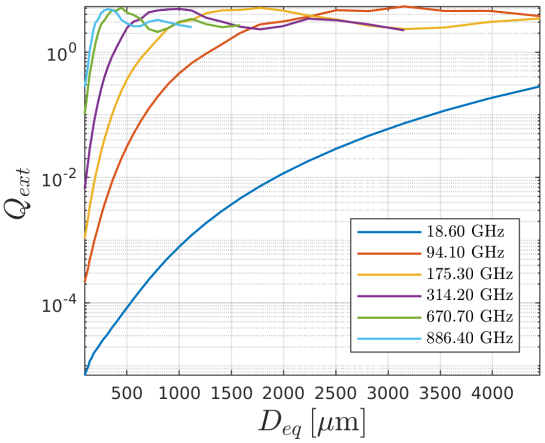

Extinction efficiency as a function of volume volume equivalent diameter, for a selection of six frequencies. Temperature is 230 K.

Figure 2.2. Assymetry parameter

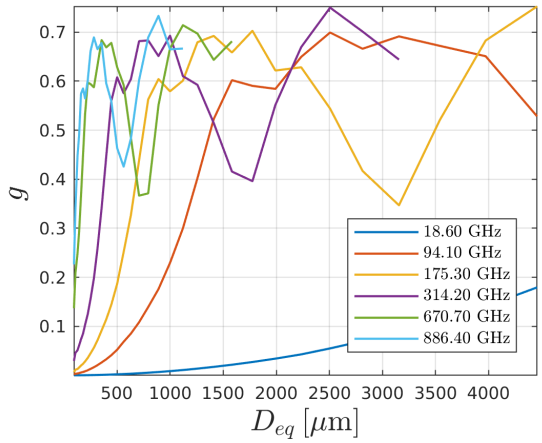

Assymetry parameter as a function of volume equivalent diameter, for a selection of six frequencies. Temperature is 230 K.

Figure 2.3. Single scattering albedo

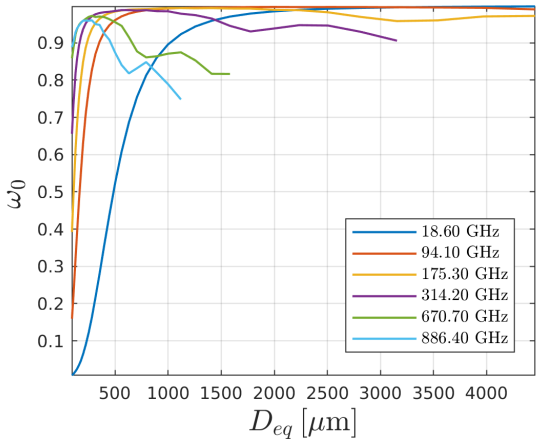

Single scattering albedo as a function of volume volume equivalent diameter, for a selection of six frequencies. Temperature is 230 K.

SSP Data Summary

ICON Snow

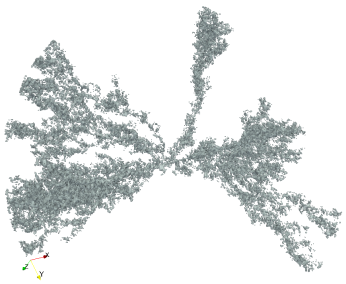

Publication date 07-Dec-2017 18:16:25

Chapter 1. Habit Specifications

Table 1.1. Habit description

Description	ICON snow
Source	location: Chalmers, software: Rimecraft.
Comment	

Figure 1.1. Shape rendering.

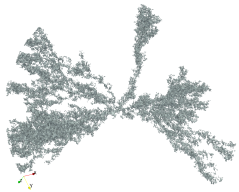

Rendering of a selected shape using Blender (https://www.blender.org/).

Table 1.2. Size parameters

	min	max	# of sizes
D_max [um]	120	17153	30
D_e [um]	94	2906	

Table 1.3. Shape parameters

α	0.0311
β	1.9486

Figure 1.2. Mass-size relationship

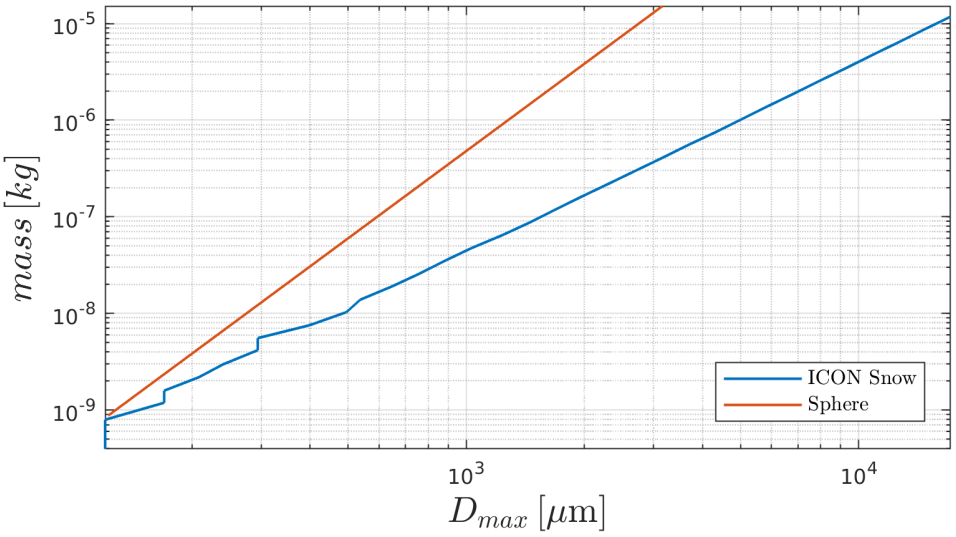

Mass as a function of D_max. Sphere included as a reference. Ice density assumed.

Chapter 2. Single Scattering Properties

Table 2.1. SSP description

Source	ADDA (Yurkin 2011)
Format	ARTS SSP format v.3
Orientation	totally_random
Density [kg/m³]	ice (916.70)
Refractive index	Matzler 2006

Table 2.2. SSP grid

frequency [GHz]	1, 1, 3, 5, 7, 9, 10, 13, 15, 19, 24, 31, 32, 36, 50, 58, 89, 94, 115, 122, 164, 167, 175, 191, 228, 247, 314, 336, 439, 457, 657, 671, 862, 886,
Temperature [K]	190, 230, 270,

Figure 2.1. Extinction

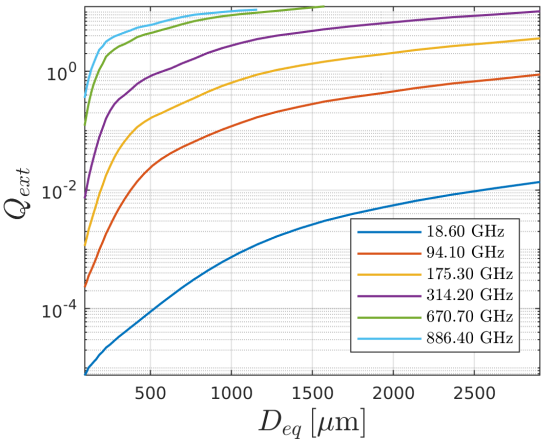

Extinction efficiency as a function of volume volume equivalent diameter, for a selection of six frequencies. Temperature is 230 K.

Figure 2.2. Assymetry parameter

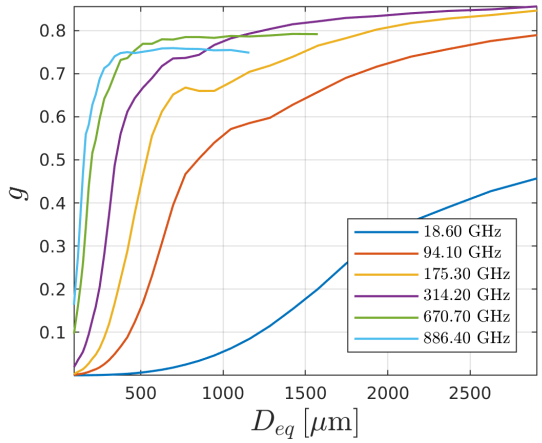

Assymetry parameter as a function of volume equivalent diameter, for a selection of six frequencies. Temperature is 230 K.

Figure 2.3. Single scattering albedo

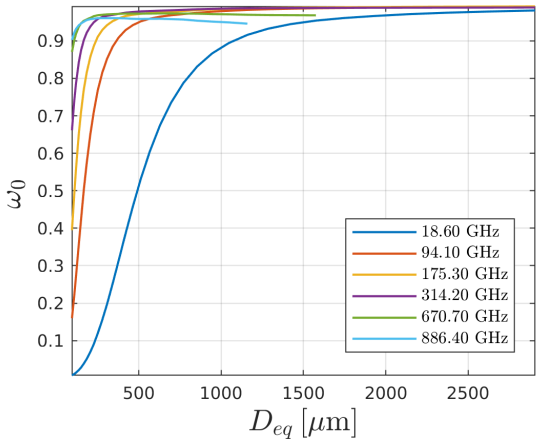

Single scattering albedo as a function of volume volume equivalent diameter, for a selection of six frequencies. Temperature is 230 K.

SSP Data Summary

GEM Hail

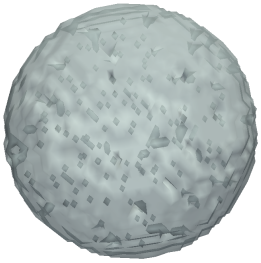

Publication date 07-Dec-2017 18:19:35

Chapter 1. Habit Specifications

Table 1.1. Habit description

Description	GEM hail
Source	location: Chalmers, software: Rimecraft.
Comment	

Figure 1.1. Shape rendering.

Rendering of a selected shape using Blender (https://www.blender.org/).

Table 1.2. Size parameters

	min	max	# of sizes
D_max [um]	120	4482	29
D_e [um]	94	4457	

Table 1.3. Shape parameters

α	535.4203
β	3.0187

Figure 1.2. Mass-size relationship

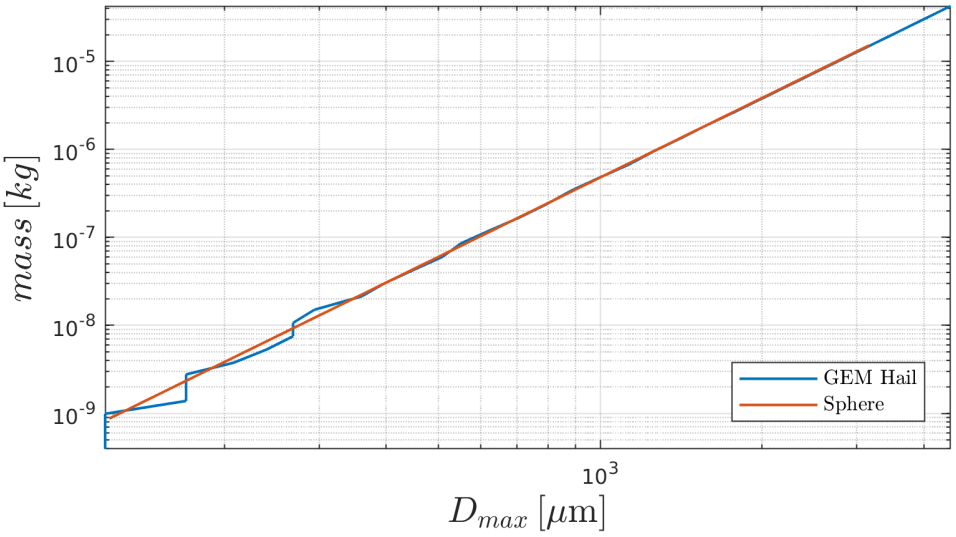

Mass as a function of D_max. Sphere included as a reference. Ice density assumed.

Chapter 2. Single Scattering Properties

Table 2.1. SSP description

Source	ADDA (Yurkin 2011)
Format	ARTS SSP format v.3
Orientation	totally_random
Density [kg/m³]	ice (916.70)
Refractive index	Matzler 2006

Table 2.2. SSP grid

frequency [GHz]	1, 1, 3, 5, 7, 9, 10, 13, 15, 19, 24, 31, 32, 36, 50, 58, 89, 94, 115, 122, 164, 167, 175, 191, 228, 247, 314, 336, 439, 457, 657, 671, 862, 886,
Temperature [K]	190, 230, 270,

Figure 2.1. Extinction

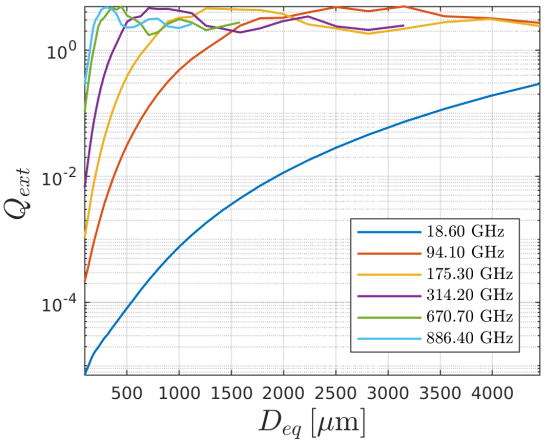

Extinction efficiency as a function of volume volume equivalent diameter, for a selection of six frequencies. Temperature is 230 K.

Figure 2.2. Assymetry parameter

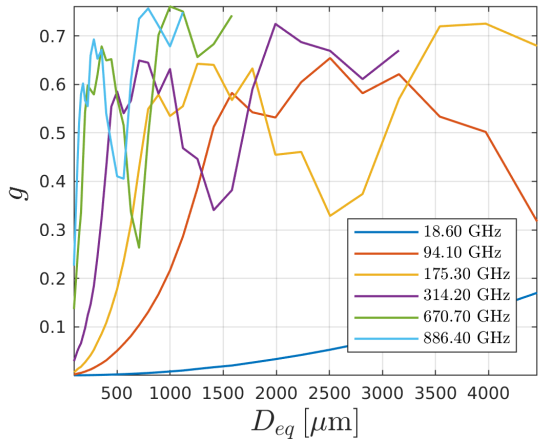

Assymetry parameter as a function of volume equivalent diameter, for a selection of six frequencies. Temperature is 230 K.

Figure 2.3. Single scattering albedo

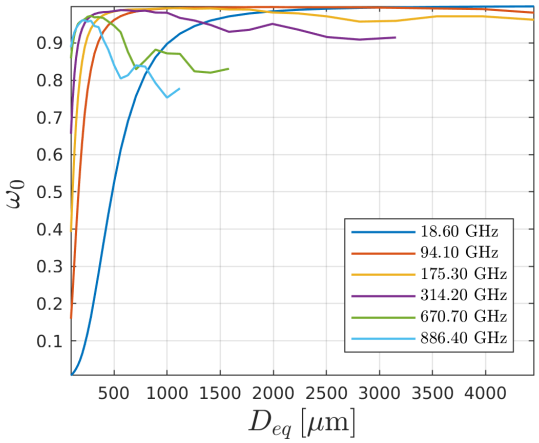

Single scattering albedo as a function of volume volume equivalent diameter, for a selection of six frequencies. Temperature is 230 K.

SSP Data Summary

GEM Snow

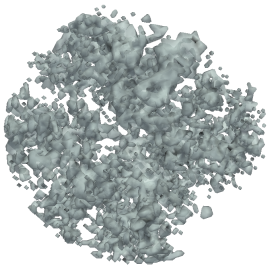

Publication date 07-Dec-2017 18:18:22

Chapter 1. Habit Specifications

Table 1.1. Habit description

Description	GEM snow
Source	location: Chalmers, software: Rimecraft.
Comment	

Figure 1.1. Shape rendering.

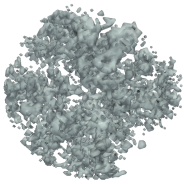

Rendering of a selected shape using Blender (https://www.blender.org/).

Table 1.2. Size parameters

	min	max	# of sizes
D_max [um]	170	9309	31
D_e [um]	94	4457	

Table 1.3. Shape parameters

α	24.0072
β	2.8571

Figure 1.2. Mass-size relationship

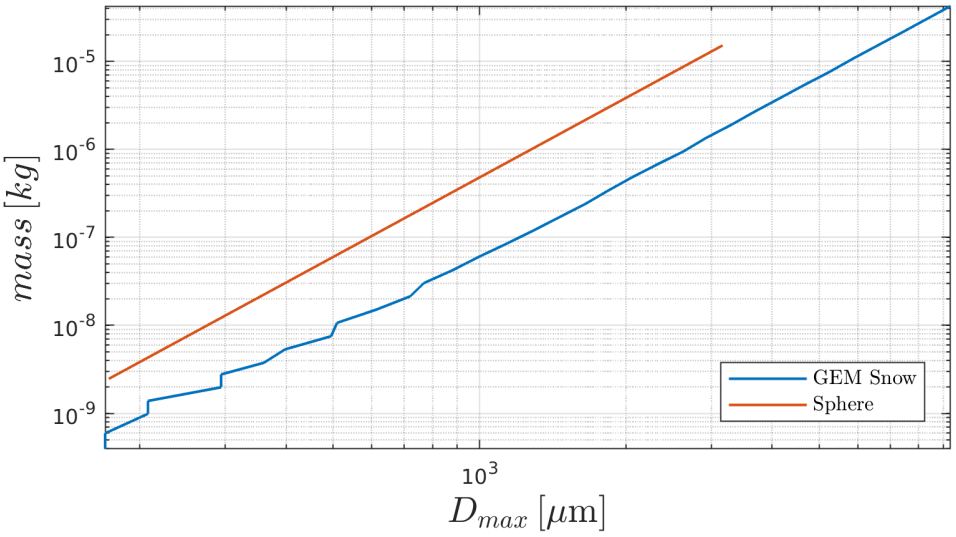

Mass as a function of D_max. Sphere included as a reference. Ice density assumed.

Chapter 2. Single Scattering Properties

Table 2.1. SSP description

Source	ADDA (Yurkin 2011)
Format	ARTS SSP format v.3
Orientation	totally_random
Density [kg/m³]	ice (916.70)
Refractive index	Matzler 2006

Table 2.2. SSP grid

frequency [GHz]	1, 1, 3, 5, 7, 9, 10, 13, 15, 19, 24, 31, 32, 36, 50, 58, 89, 94, 115, 122, 164, 167, 175, 191, 228, 247, 314, 336, 439, 457, 657, 671, 862, 886,
Temperature [K]	190, 230, 270,

Figure 2.1. Extinction

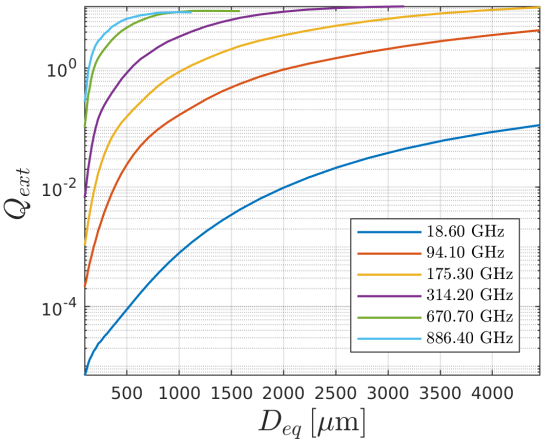

Extinction efficiency as a function of volume volume equivalent diameter, for a selection of six frequencies. Temperature is 230 K.

Figure 2.2. Assymetry parameter

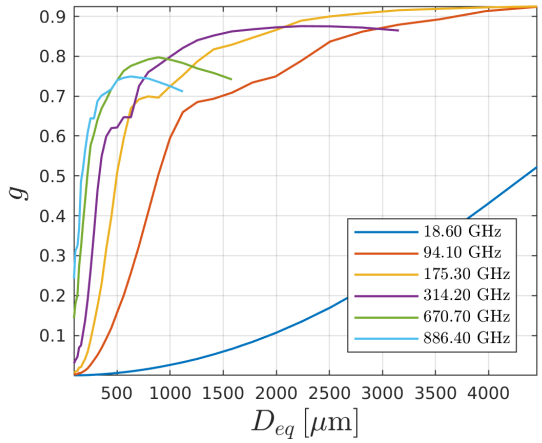

Assymetry parameter as a function of volume equivalent diameter, for a selection of six frequencies. Temperature is 230 K.

Figure 2.3. Single scattering albedo

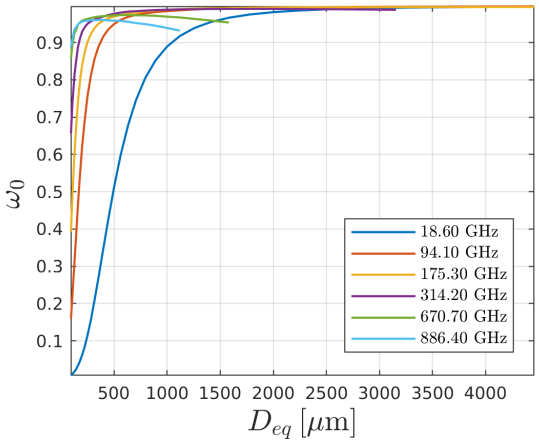

Single scattering albedo as a function of volume volume equivalent diameter, for a selection of six frequencies. Temperature is 230 K.

SSP Data Summary

Spherical Graupel

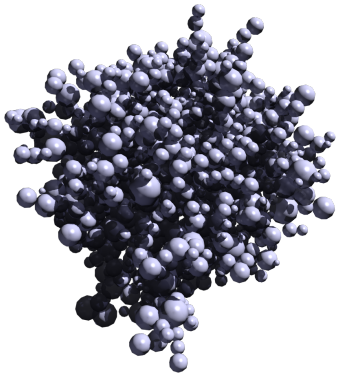

Publication date 20-Nov-2017 22:19:01

Chapter 1. Habit Specifications

Table 1.1. Habit description

Description	Spherical graupel
Source	location: Chalmers, software: Snowflake-toolkit (Rathsman 2016).
Comment	

Figure 1.1. Shape rendering.

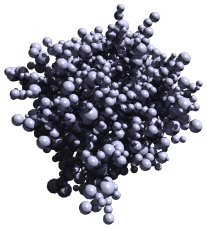

Rendering of a selected shape using Blender (https://www.blender.org/).

Table 1.2. Size parameters

	min	max	# of sizes
D_max [um]	622	8308	29
D_e [um]	454	4528	

Table 1.3. Shape parameters

α	13.2741
β	2.6862

Figure 1.2. Mass-size relationship

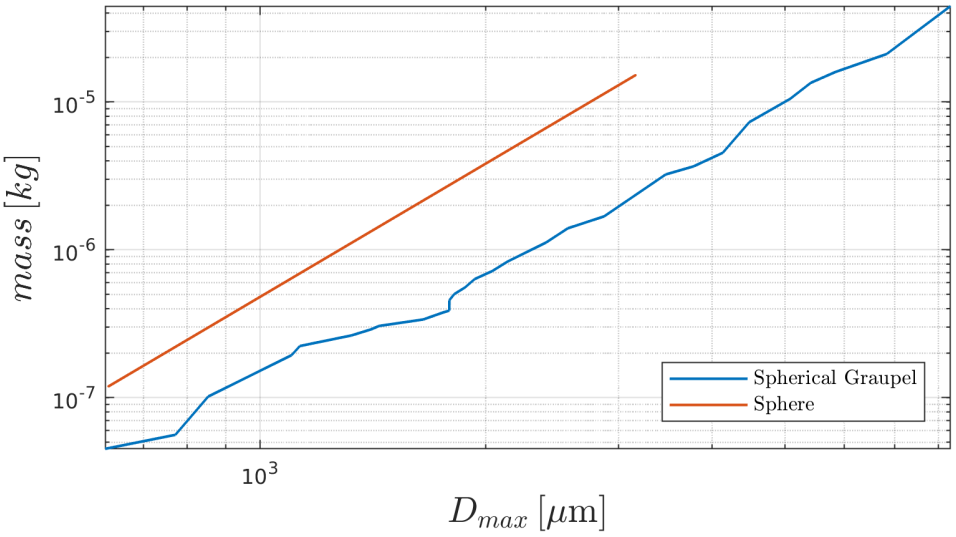

Mass as a function of D_max. Sphere included as a reference. Ice density assumed.

Chapter 2. Single Scattering Properties

Table 2.1. SSP description

Source	ADDA (Yurkin 2011)
Format	ARTS SSP format v.3
Orientation	totally_random
Density [kg/m³]	ice (916.70)
Refractive index	Matzler 2006

Table 2.2. SSP grid

frequency [GHz]	1, 1, 3, 5, 7, 9, 10, 13, 15, 19, 24, 31, 32, 36, 50, 58, 89, 94, 115, 122, 164, 167, 175, 191, 228, 247, 314, 336, 439, 457, 657, 671, 862, 886,
Temperature [K]	190, 230, 270,

Figure 2.1. Extinction

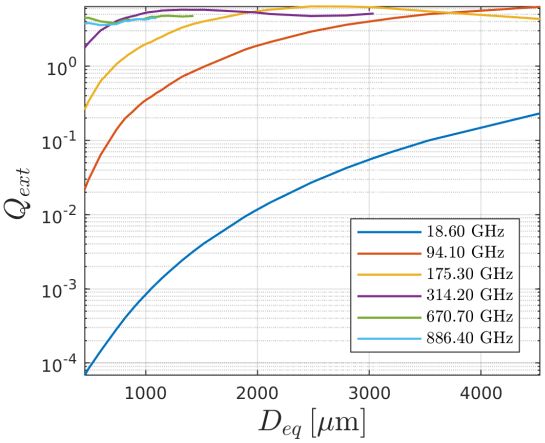

Extinction efficiency as a function of volume volume equivalent diameter, for a selection of six frequencies. Temperature is 230 K.

Figure 2.2. Assymetry parameter

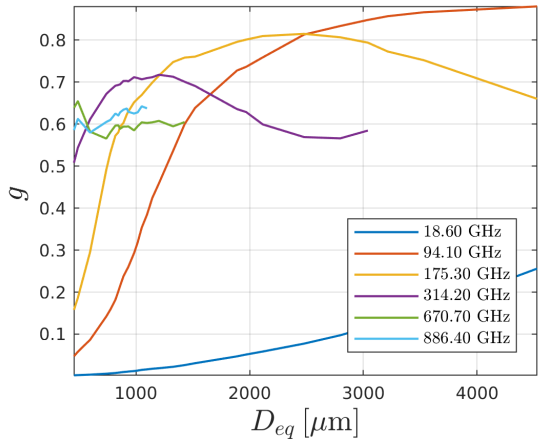

Assymetry parameter as a function of volume equivalent diameter, for a selection of six frequencies. Temperature is 230 K.

Figure 2.3. Single scattering albedo

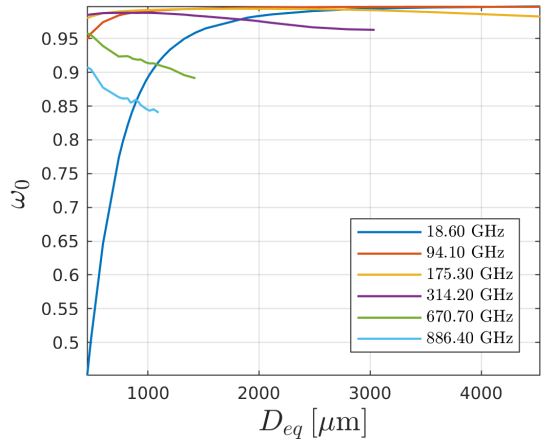

Single scattering albedo as a function of volume volume equivalent diameter, for a selection of six frequencies. Temperature is 230 K.

SSP Data Summary

ICON Graupel

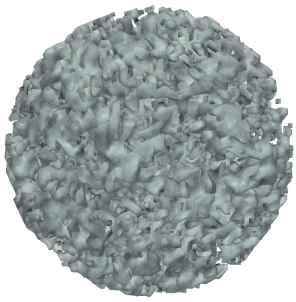

Publication date 07-Dec-2017 18:17:06

Chapter 1. Habit Specifications

Table 1.1. Habit description

Description	ICON graupel
Source	location: Chalmers, software: Rimecraft.
Comment	

Figure 1.1. Shape rendering.

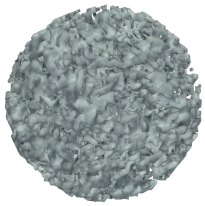

Rendering of a selected shape using Blender (https://www.blender.org/).

Table 1.2. Size parameters

	min	max	# of sizes
D_max [um]	170	5969	31
D_e [um]	94	4457	

Table 1.3. Shape parameters

α	394.8402
β	3.1345

Figure 1.2. Mass-size relationship

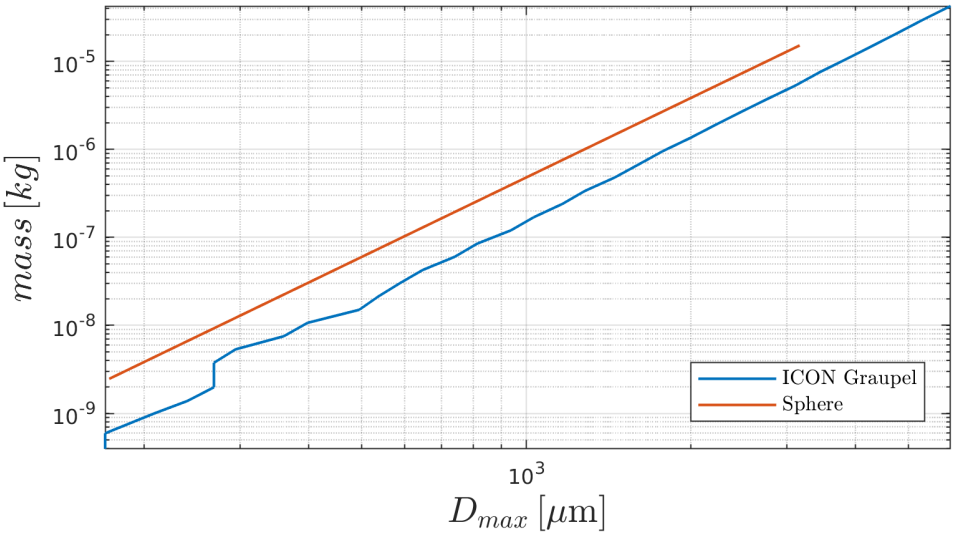

Mass as a function of D_max. Sphere included as a reference. Ice density assumed.

Chapter 2. Single Scattering Properties

Table 2.1. SSP description

Source	ADDA (Yurkin 2011)
Format	ARTS SSP format v.3
Orientation	totally_random
Density [kg/m³]	ice (916.70)
Refractive index	Matzler 2006

Table 2.2. SSP grid

frequency [GHz]	1, 1, 3, 5, 7, 9, 10, 13, 15, 19, 24, 31, 32, 36, 50, 58, 89, 94, 115, 122, 164, 167, 175, 191, 228, 247, 314, 336, 439, 457, 657, 671, 862, 886,
Temperature [K]	190, 230, 270,

Figure 2.1. Extinction

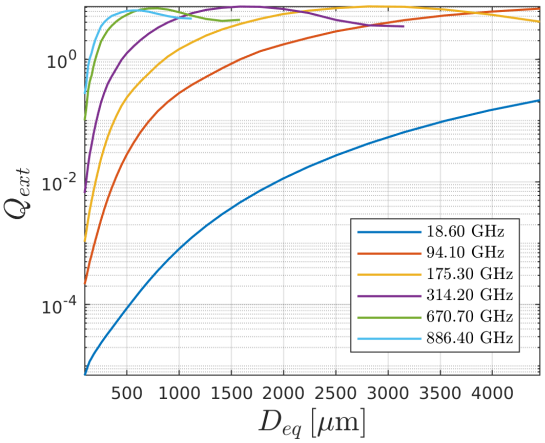

Extinction efficiency as a function of volume volume equivalent diameter, for a selection of six frequencies. Temperature is 230 K.

Figure 2.2. Assymetry parameter

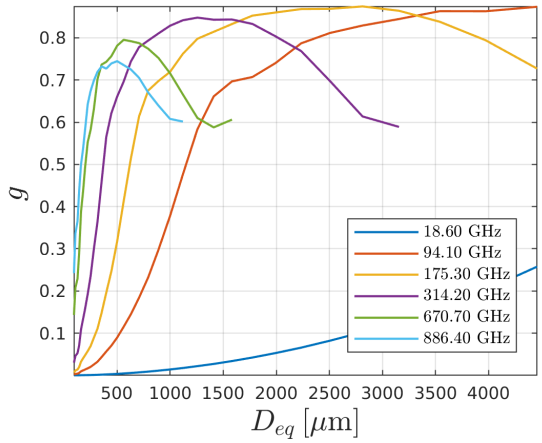

Assymetry parameter as a function of volume equivalent diameter, for a selection of six frequencies. Temperature is 230 K.

Figure 2.3. Single scattering albedo

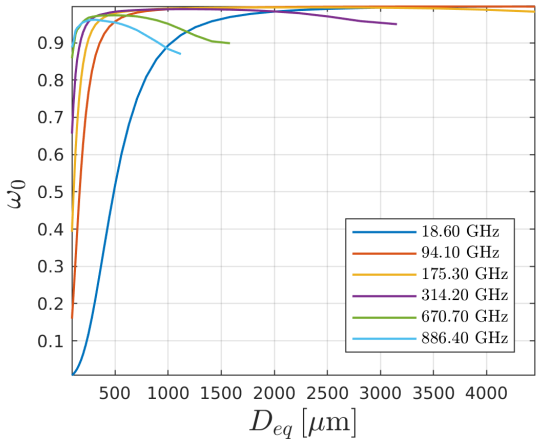

Single scattering albedo as a function of volume volume equivalent diameter, for a selection of six frequencies. Temperature is 230 K.

SSP Data Summary

GEM Graupel

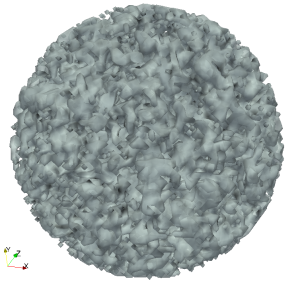

Publication date 07-Dec-2017 18:18:59

Chapter 1. Habit Specifications

Table 1.1. Habit description

Description	GEM graupel
Source	location: Chalmers, software: Rimecraft.
Comment	

Figure 1.1. Shape rendering.

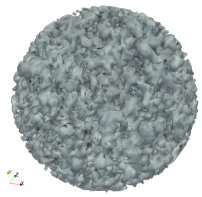

Rendering of a selected shape using Blender (https://www.blender.org/).

Table 1.2. Size parameters

	min	max	# of sizes
D_max [um]	120	5871	31
D_e [um]	94	4457	

Table 1.3. Shape parameters

α	172.7527
β	2.9646

Figure 1.2. Mass-size relationship

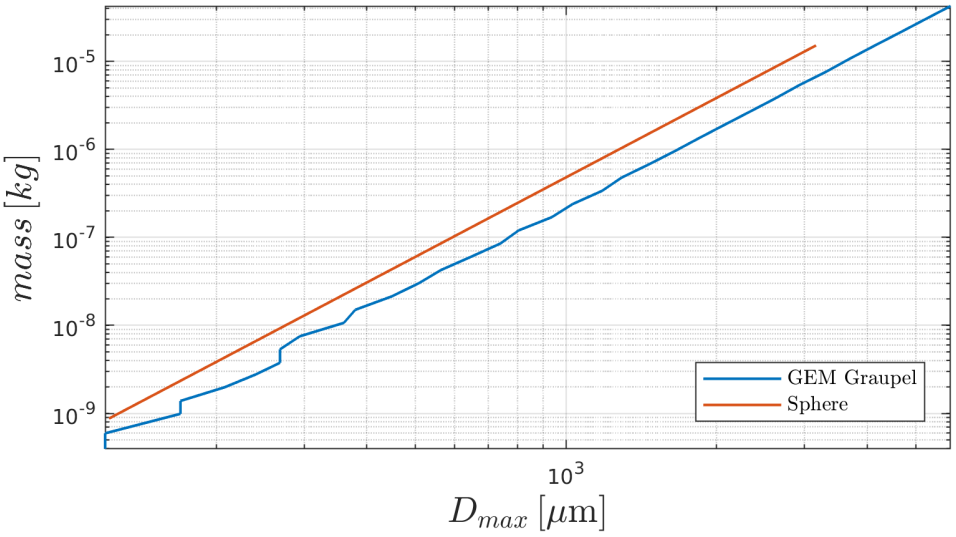

Mass as a function of D_max. Sphere included as a reference. Ice density assumed.

Chapter 2. Single Scattering Properties

Table 2.1. SSP description

Source	ADDA (Yurkin 2011)
Format	ARTS SSP format v.3
Orientation	totally_random
Density [kg/m³]	ice (916.70)
Refractive index	Matzler 2006

Table 2.2. SSP grid

frequency [GHz]	1, 1, 3, 5, 7, 9, 10, 13, 15, 19, 24, 31, 32, 36, 50, 58, 89, 94, 115, 122, 164, 167, 175, 191, 228, 247, 314, 336, 439, 457, 657, 671, 862, 886,
Temperature [K]	190, 230, 270,

Figure 2.1. Extinction

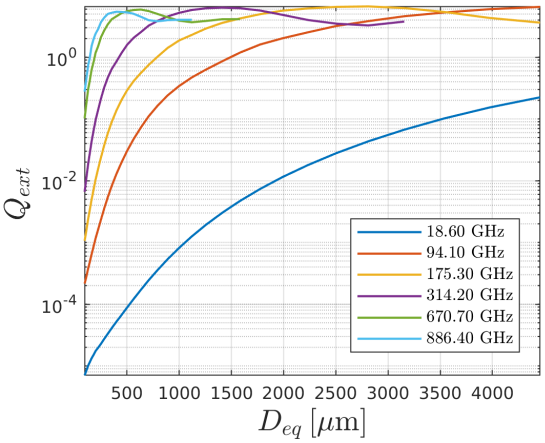

Extinction efficiency as a function of volume volume equivalent diameter, for a selection of six frequencies. Temperature is 230 K.

Figure 2.2. Assymetry parameter

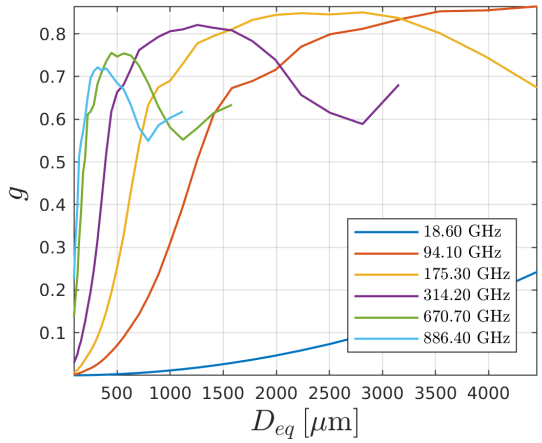

Assymetry parameter as a function of volume equivalent diameter, for a selection of six frequencies. Temperature is 230 K.

Figure 2.3. Single scattering albedo

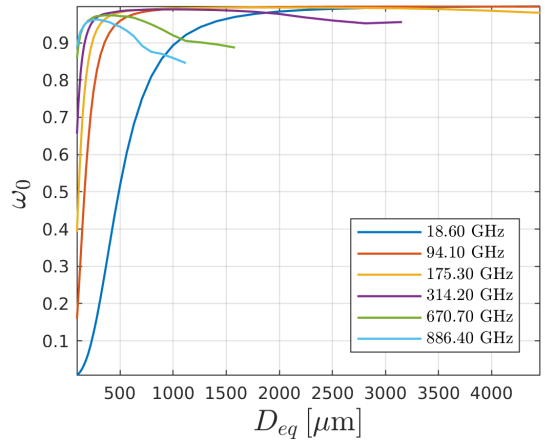

Single scattering albedo as a function of volume volume equivalent diameter, for a selection of six frequencies. Temperature is 230 K.

SSP Data Summary

Liquid Sphere

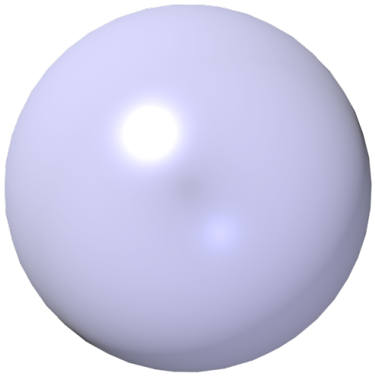

Robin Ekelund

Publication date 25-Oct-2017 21:45:27

Chapter 1. Habit Specifications

Table 1.1. Habit description

Description	Liquid sphere
Source	location: Chalmers
Comment	

Figure 1.1. Shape rendering.

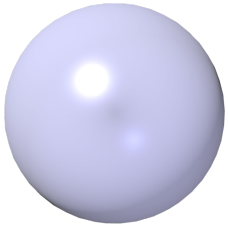

Rendering of a selected shape using Blender (https://www.blender.org/).

Table 1.2. Size parameters

	min	max	# of sizes
D_max [um]	1	47354	199
D_e [um]	1	47354	

Table 1.3. Shape parameters

α	523.5988
β	3.0000

Figure 1.2. Mass-size relationship

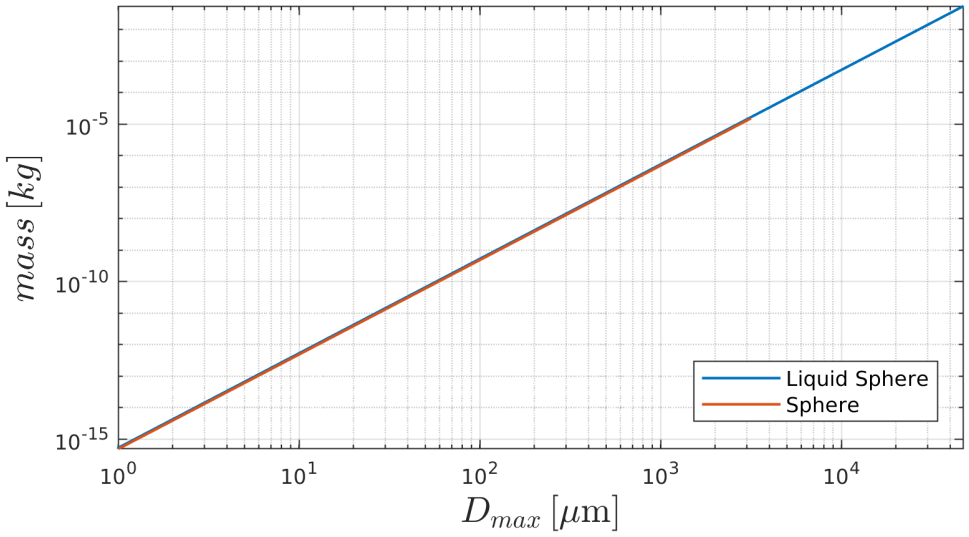

Mass as a function of D_max. Sphere included as a reference. Ice density assumed.

Chapter 2. Single Scattering Properties

Table 2.1. SSP description

Source	ADDA (Yurkin 2011)
Format	ARTS SSP format v.3
Orientation	totally_random
Density [kg/m³]	ice (520.77)
Refractive index	water_ellison07

Table 2.2. SSP grid

frequency [GHz]	1, 1, 3, 5, 7, 9, 10, 13, 15, 19, 24, 31, 32, 36, 50, 58, 89, 94, 115, 122, 164, 167, 175, 191, 228, 247, 314, 336, 439, 457, 657, 671, 862, 886,
Temperature [K]	230, 250, 270, 290, 310,

Figure 2.1. Extinction

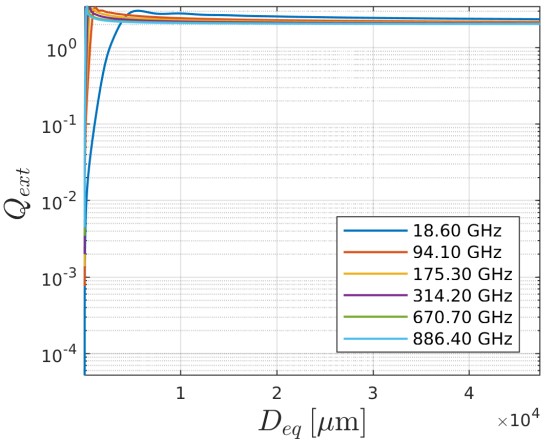

Extinction efficiency as a function of volume volume equivalent diameter, for a selection of six frequencies. Temperature is 270 K.

Figure 2.2. Assymetry parameter

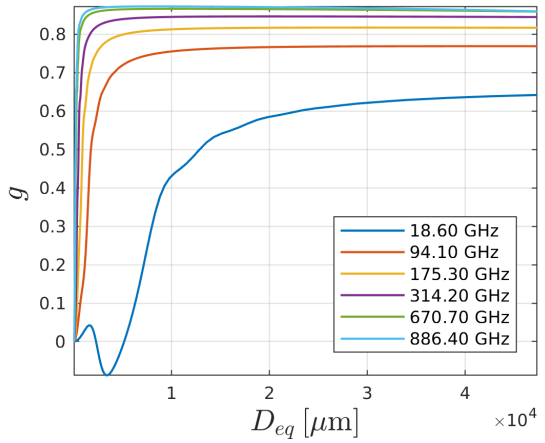

Assymetry parameter as a function of volume equivalent diameter, for a selection of six frequencies. Temperature is 270 K.

Figure 2.3. Single scattering albedo

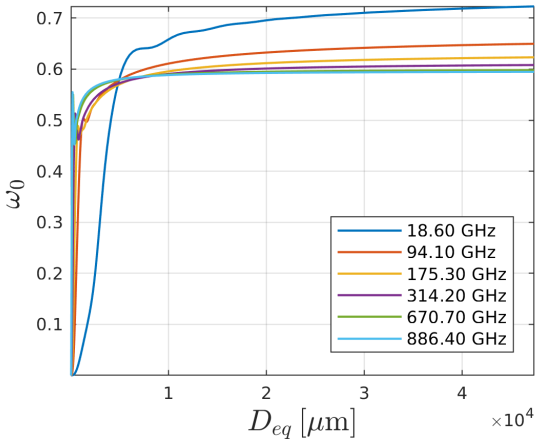

Single scattering albedo as a function of volume volume equivalent diameter, for a selection of six frequencies. Temperature is 270 K.